Microfibrous Entrapped Catalysts for Low Temperature CO Oxidation in Humid Air

by

Shirish Shriram Punde

A dissertation submitted to the Graduate Faculty of
Auburn University
in partial fulfillment of the
requirements for the Degree of
Doctor of Philosophy

Auburn, Alabama
August 03, 2013

Keywords: CO Oxidation, Platinum, Ceria, Catalyst, Microfibrous Entrapment, Kinetics

Approved by

Bruce J Tatarchuk, Chair and Professor of Chemical Engineering
Yoon Y Lee, Professor of Chemical Engineering
Mario Eden, Professor of Chemical Engineering
Bart Prorok, Professor of Materials Engineering

Abstract

CO oxidation at ambient conditions poses a major challenge due to CO self-poisoning at low temperature as well as passivation of the catalyst in the presence of moisture. A highly active novel catalyst has been developed for CO oxidation at ambient conditions. The use of ceria as a promoter for supported noble metal catalysts was investigated. A ceria promoted catalyst was found to be highly active, yielding more than 99% conversion at low (<500 ppm) as well as high (>2500 ppm) CO concentrations. Further, the impact of the ceria deposition method and the type of catalyst support on catalytic activity was also studied. Activity measurements as well as O_2 – H_2 titration studies revealed that ceria deposition by incipient wetness impregnation resulted in close association of ceria and Pt which resulted in better activity of the catalyst. Pt – CeO_2/SiO_2 catalysts with Pt > 2.5% (w/w) and CeO_2 > 15% (w/w) were found to be highly active (conversion ≥99%) and stable at 10-90% relative humidity (RH) at ambient temperature.

The catalyst was further optimized experimentally by varying the catalyst preparation variables such as the type of silica support, the type of Pt precursor, and the drying and calcination conditions of Pt and ceria precursors. Further, the catalytic activity was correlated with surface characteristics using characterization techniques such as TPR, TEM, H_2 and CO chemisorption and BET surface area, pore volume and pore size measurements. The Pt precursor with neutral metal ion species in solution resulted in a catalyst (TOF: 0.12 s^{-1}) that

was more than 10 times better active compared to a catalyst prepared with acidic Pt precursor (TOF: 0.01 s^{-1}). Also, the drying and calcination conditions for both Pt and ceria precursors had a major impact on the dispersion and/or the distribution profile of metal (oxide) on the support.

With the composition and preparation procedure for the preparation of the Pt-CeO2/SiO2 catalyst established, the catalysts entrapment in the nickel microfibrers was carried out. The microfibrous entrapped catalysts (MFEC) were highly active and outperformed the packed bed as well as diluted packed bed. MFEC's unique structure with uniform voidage: (a) minimized axial dispersion; (b) reduced flow maldistributions and improved radial dispersion. Further, MFECs made of metal fibers (MF) showed many advantages: (a) improved heat conduction in the catalyst bed, due to micron sized MF matrix; (b) uniform temperature profile, minimized cold spots in the reactor bed. MFECs were highly active and more stable in comparison with packed bed. This experimental observation was also confirmed with a one dimensional pseudo-homogeneous reactor model that was solved by commercial software COMSOL®. The MFECs with their high activity and great stability could be used in various CO removal applications such as fire escape emergency face masks, advanced filtration units, and the like.

Acknowledgments

This dissertation is a result of collaboration and support of a lot of people. I would like to acknowledge the guidance and encouragement of my advisor Prof. Bruce Tatarchuk. I would like to express my sincere gratitude to Dr. Yoon Lee, Dr. Mario Eden and Dr. Bart Prorok for serving on my committee and to Dr. Orlando Acevedo for being an outside dissertation reader. I would also like to thank my colleagues at the Center for Microfibrous Materials Manufacturing, especially Dwight Cahela, Dr. Don Cahela, Megan Schumacher, Kimberly Dennis, Ranjeeth Kalluri, Amogh Karwa, Abhijeeth Phalle, Dr Hongyun Yang, Robert Henderson and Ryan Sothen among many others. I am also grateful to Sue Allen Abner and Karen Cochran for their administrative support. I am also indebted to Ms Carol Lovvorn for her administrative support during my tenure at Auburn University. Special thanks are due to my best friends in Auburn, Sachin Nair, Jins Alexander, Nitin Yogi and Payal Agarwal for their enormous help and support throughout my graduate studies.

I am greatly indebted to my parents and my brother for their unwavering support, constant love, encouragement and motivation throughout my life. Finally, I would like to thank my wife Bhakti for supporting me in all the good and the difficult times, without whom it is impossible for me to visualize my life. With an immense gratification, I would like to dedicate this work to my parents and my wife.

Table of Contents

List of Tables

List of Figures

I. Introduction and Literature Review

I.1 Motivation

Atmospheric carbon monoxide (CO), even in trace amounts is harmful to humans as well as the environment. CO mitigation at high temperature is well studied and the solutions such as a catalytic converter and the like are efficient at high temperature, however CO removal at low temperature still poses a problem. Due to its low boiling point and critical temperature, adequate adsorption at room temperature is not possible. Its very low solubility in almost all solvents makes it impossible to be removed by physical absorption. Hence, the only means to remove CO is to oxidize CO to CO_2. Removal of CO by oxidation to CO_2 at low temperature poses a major challenge because of the slow surface kinetics and CO self-poisoning of the catalyst. CO oxidation catalyst that is highly active in the presence of moisture is required as most of the applications demand removal of CO from humid air.

Most of the transition metal based catalysts that are active at higher temperature for CO oxidation are inactive at room temperature. Further, some of the catalysts such as CuO based catalysts, which work well even at room temperature; however are inhibited by the presence of moisture. For example, supported nano-gold catalysts are highly active for CO oxidation even below 0^0C, but they become inactive in the presence of moisture. Considering the problems associated with the available catalysts for the applications, and the opportunity to solve these problems, task for developing a new catalyst was undertaken.

It was important that the catalyst be active at low temperature and in the presence of moisture. The catalyst so developed was compared with commercially available catalysts, and was analyzed for various operating conditions. Further, it was important to optimize the catalyst preparation recipe with the help of experimental results and surface characterization results. The knowledge of chemical composition, surface characteristics and reaction data would help in optimizing the catalyst and the catalytic application systems.

CO oxidation at room temperature was found to be a diffusion controlled reaction; therefore, the use of small catalyst particles was essential for optimum utilization of the catalyst. However, the use of small particles in a packed bed poses problems such as bed channeling, flow maldistributions and the like. Therefore, one of the goals of this research was to develop a filter media that would incorporate small catalyst particles and thereby minimize bed channeling, flow maldistributions and reduce the pressure drop. Keeping this in mind the catalysts were entrapped in microfibers and studied for this application. Finally, to understand the greater performance of the microfibrous entrapped catalysts, a reactor model was developed to describe the system.

There are many applications involving CO removal at room temperature in the presence of moisture. For example, emergency escape products, exhaust gas treatment during cold start-up, cathode air filter for fuel cells, advanced filtration units and the like. Most of the applications demand low temperature CO removal in the presence of moisture, with minimal pressure drop at lower costs. Considering the problems associated with the existing catalytic systems, the goal of this work was to develop a highly active and stable catalytic system that offers lower pressure drop and is cheap.

I.2 Introduction

Carbon monoxide (CO) is generated due to partial combustion of transportation fuels, coal and by incomplete burning of carbonaceous materials during fire. CO from fuel combustion alone accounts for 89% of total CO emissions from anthropogenic sources in developed countries [1]. Atmospheric CO, even in trace amounts is harmful to humans as well as the environment. Exposure to CO concentration of 10 ppmv for 8 – hr has adverse effects on the human nervous system. In humans, CO toxicity appears to result from a combination of tissue hypoxia and direct CO–mediated damage at the cellular level [2]. In the United States alone CO poisoning accounts for 3500 to 4000 deaths annually [3]. CO influences atmospheric chemistry as well and affects global climate in general. CO reacts with hydroxyl radicals in the troposphere, depleting OH radical concentration, which in turn affects the photo-chemistry of troposphere. Hydroxyl radicals act as a sink for many atmospheric gases with relatively low water solubilities, such as NOx, SO_2, ozone and all the volatile hydrocarbons. Therefore, growth in the tropospheric CO concentration would result in enhancing the concentrations and lifetimes of these greenhouse gases in the troposphere. Additionally, a greater transfer of CO to the stratosphere could result in depletion of ozone, due to reaction with CO [4].

In light of the impact of atmospheric CO on humans and environment, removal of CO has been extensively studied over last three decades. CO removal by adsorption or absorption is inadequate, while catalytic oxidation to CO_2 is the most viable option. There are two approaches to mitigate problems associated with atmospheric CO: (a) minimize CO emissions at source, to minimize impact on environment; (b) purification of breathing air by catalytic filter, to prevent harmful effects of CO on humans. Vehicle exhausts are the main source of CO emissions; however, use of catalytic converters has reduced CO emissions from vehicle exhaust [5]. But, significant amount of CO is emitted during cold-start up due to low activity of three-way catalysts at low or near ambient temperatures. Also, in the case

of a fire emergency or a mining accident, purification of breathing air requires use of a catalytic filter that is highly active at ambient temperatures. Hence, there is a need for a highly active CO oxidation catalyst that maintains its higher activity over a wide range of temperature, CO concentration and is stable in the presence of moisture.

Low temperature CO oxidation is a difficult task, since it is characterized by slow surface kinetics and strong CO self-poisoning of the catalyst which compete with each other. Additionally, presence of moisture might favor or mar a catalyst depending upon surface chemistry or reaction mechanism on the catalyst. CO concentration is also one of the important factors affecting activity; some catalysts get ignited at higher CO concentration (>2500 ppm CO) by exploiting high exothermicity of CO oxidation reaction, while others get deactivated or CO self – poisoned at high CO concentration. While at low CO concentrations (<500 ppm CO), some catalysts would not work in the absence of significant heat of reaction and others might work due to low CO self-poisoning. CO oxidation is also characterized by chaotic oscillations, periodic or a-periodic self sustaining oscillations. These oscillations could arise due to concentration, temperature, moisture, or oxygen variation at the surface level. These complexities make it difficult to design a CO oxidation catalyst which would work in a broader (low – high) temperature and concentration range in the presence of moisture.

In the case of larger catalyst particles diffusional resistances affect reaction kinetics, leading to greater rates of CO self-poisoning causing deactivation of the catalyst. However, conventional packed bed (PB) of smaller particles poses problems such as high pressure drop, packing issues, bed channeling, flow maldistributions, and dead zones in the reactor bed, which result in poor inter-phase heat and mass transfer rates. Most of these problems are related to poor packaging of smaller particles, strongly suggesting the need for immobilization of small particles. In most of the catalytic applications, foam structures or honeycomb structure or a monolith are used for better contacting efficiency when the use

of smaller catalyst particles is of importance. However, in the case of CO oxidation at low temperature, the performance of the catalyst is dependent on the adiabatic temperature rise of the catalyst bed, and the presence of an inert thermal mass in the form of honeycomb structure or foam, would reduce the adiabatic temperature rise and hence the activity of the catalyst. Also, the maximum amount of catalyst loading in these contacting systems is limited to not more than 15% by volume, thus demanding a larger footprint of the catalytic application system and increased cost. Therefore, a novel heterogeneous contacting system was needed for the utilization of the CO oxidation catalyst in smaller particle sizes that can overcome the drawbacks of the traditional packed beds.

I.3 Catalysts for CO Oxidation

Since 1920s, a mixture of copper and manganese oxides, known as Hopcalite [6] has been used as a CO oxidation catalyst. Hopcalite is highly active at low temperature; however, undergoes deactivation in the presence of moisture [7, 8]. Apart from manganese oxide, cobalt oxide can act as a good low temperature catalyst [9]; however, it undergoes deactivation with time even in the absence of moisture [10, 11]. Although, a mixture of metal oxides is favorable because of cost benefits, their inability to maintain stability and activity for a longer duration, demanded exploring the activity of noble metal catalysts for the application. The discovery of nano-dispersed gold particles and their higher activity towards CO oxidation by Haruta et al [12], generated a lot of interest in nano-gold catalysts. It was found that gold catalysts with crystallites smaller than 5 nm were highly active [13]. However, the preparation of nano – gold crystallites by deposition precipitation method gave rise to scale up problems, whereas preparation by incipient wetness impregnation method resulted in a small fraction of deposited gold as a metallic gold, and that too in the form of large crystallites [14]. Further, the presence of moisture has also been found detrimental to the activity of gold based catalysts [15]. Also, one of the issues concerning gold catalysts is the low melting point of nano-gold particles, 573K for 2-nm

gold crystallites due to quantum size effects, making the gold catalysts unsuitable for using in a wide-range of temperature for CO oxidation.

Supported noble metal (Pt, Pd, Rh, Ru) catalysts have long been used for CO oxidation [16-18]. However, the activity of platinum based catalysts was found to be better compared to other Pt group metals [19]. Further, it was also found out that activity was dependent on nature of support [20]. Platinum based catalysts were highly active at low temperatures when supported on TiO_2, SnO_x, and CeO_2 [14, 21, 22]. Catalytic activity of supported Pt catalysts have also been shown to improve significantly by addition of a transition metal oxide co-promoter, for example, CoOx, MnOx, and FeOx [23-25]. Some of these promoted Pt catalysts, however, deactivated over time in the presence of moisture. With this background in mind, we took up the task of developing a highly active and stable catalyst applicable in a wide – temperature range while maintaining its activity in the presence of moisture.

I.4 Tin Oxide Containing Catalysts

Modified tin oxide on its own has been reported to be active at elevated temperatures for CO oxidation [26]. It was believed that lattice oxygen of SnO_2 was consumed during reaction and then repopulated with O_2 from the gas phase. Tin oxide also has been used as a dopant for catalyzed oxidation reaction, wherein SnO_2 greatly increased the oxidation potential[27, 28].

Further, tin oxide supported noble metal catalysts have also been used for low temperature CO oxidation [29, 30]. However, the amount of noble metal used in these catalysts was of the order of 15-20% w/w of noble metal, making them highly expensive. Use of SnO_2 as a promoter for supported noble metal catalysts has also been investigated, for instance, alumina supported Pt catalysts promoted with SnO_2 have been reported to be active at low temperature[31].

During this work, a SnO_2 promoted Pt catalyst has been proposed. This catalyst thrives in room temperature under humid conditions. The catalyst preparation variables were optimized based on experimental results and the catalyst was characterized in detail.

I.5 Ceria Promoted Catalysts

Ceria supported metal oxide catalysts have been studied in detail for the CO oxidation [32-35]. Further, ceria supported noble metal catalysts have also been investigated for catalytic CO oxidation [36-38]. Ceria can act as an oxygen reservoir and provide lattice oxygen for CO oxidation, additionally the presence of ceria can stabilize the noble metal dispersion [38]. In the case of Au/ceria catalysts, it has been found that the morphology of ceria support played a crucial role in the activity of the catalyst [39]. Further, a study of CO oxidation using the ceria supported noble metal catalysts found that the oxidation mechanism involved a reaction between a lattice oxygen from ceria and a CO adsorbed on the noble metal [40]. Furthermore, noble metal deposition on the ceria could increase the oxygen storage capacity of the ceria [41]. Also, ceria showed a superior reducibility at nano scale compared to the bulk ceria [42].

However, ceria as a support provides significantly low surface area for noble metal deposition. Furthermore, the superior reducibility of nano-ceria crystallites could not be harnesses when ceria is used as a support. In light of these observations, during this work, the effect of ceria as a promoter for silica supported Pt catalysts for CO oxidation was studied in detail. During this work, it was found out that the ceria promoted Pt catalyst was highly active for CO oxidation at ambient temperature in the presence of moisture (10-90% RH). Further, it was also found that the use of silica (TOF: 0.067 s^{-1}) instead of alumina (TOF: 0.015 s^{-1}) as a support for ceria promoted Pt catalyst was highly beneficial to the catalytic activity.

The close association of Pt-ceria was determined to be the crucial factor for the catalytic activity. The preparation of the catalysts by the successive incipient wetness impregnation method was observed to result in the most active catalyst. The various catalyst preparation variables such as type of support, type of ceria deposition method, type of Pt precursor and the drying and calcination conditions of the precursors were investigated in detail during this study.

I.6 Microfibrous Entrapped Catalysts

A new class of micro-structured materials consisting of sorbents/catalysts entrapped in metal, ceramic, or polymer microfibers (MFES/MFEC) has been developed at Auburn University [43-45]. These materials immobilize the small particles by sinter-locking them in fiber mesh, also these materials are flexible and pleatable. The immobilization of particles results in better heterogeneous contacting efficiency. Additional studies with entrapped sorbents have shown that high voidages and structural uniformity of MFES lowered flow maldistributions, eliminated the peaking flows between particles, and helped achieve better radial dispersion [46].

A typical micrograph of MFECs is shown in Figure I.1. The catalyst particles are sinter-locked in a mesh of microfibers. The MFECs are also flexible and pleatable as shown in Figure I.2. During this study, application of MFECs was investigated. The preparation process for MFECs is mentioned later.

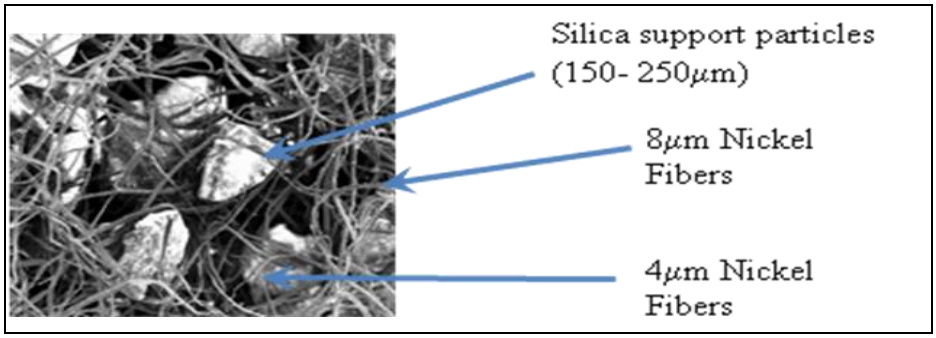

Figure I.1. SEM Micrograph of Microfibrous Entrapped Catalysts (MFEC)

Figure I.2. Image of Rolled MFEC

I.7 Comparison with Commercial Catalysts

It was important to know the activity of the newly developed catalysts. However, it was more important to know how these catalysts behave under different operating conditions, and how these catalysts compare with the commercially available catalysts. During this work, the ceria promoted and tin oxide promoted Pt catalysts were developed and tested at different operating conditions such as different levels of humidity, CO concentrations, temperature, particle size and face velocities. Further, the commercially available catalysts such as 3M NanAuCat®, Aurolite®, and Carulite® (a mixture of copper and manganese oxides) were tested and compared with these novel catalysts. The hysteresis effect of the operating conditions was also studied on the novel catalysts as well as the commercial catalysts.

Finally, the MFECs were compared with the commercial catalysts for the desired application conditions such as the fire escape mask application, advanced filtration conditions and the cathode air filter (for PEM fuel cell) test conditions.

I.8 Reactor Modeling

To help design the catalytic systems and to understand the significant activity improvement offered by the MFECs, a reactor model was developed. The kinetic data was fitted to various reaction mechanisms and a reasonable fit was obtained. Using that mechanism a reactor model was developed. The mathematical model was solved by commercially available software COMSOL® multiphysics. The details of the modeling and the solving procedure are mentioned later.

There are two possible reasons for the difference in the activity of powder catalyst and MFECs, namely: reduced axial dispersion and increased thermal dispersion due to introduction of metal microfibers in the MFECs. These hypotheses were evaluated in detail. Additionally the progression of reaction in the reactor was also investigated using the transient reactor model.

II Experimental Details

The purpose of this chapter is to give a basic overview of the experimental and characterization methods used as well as the materials/conditions used during this work. The preparation conditions used during the optimization of catalyst preparation variables for SnO_2 or CeO_2 promoted Pt catalysts are mentioned in the relevant sections in the next chapters.

II.1 Catalyst Preparation Methods and Materials

II.1.1 Silica Supported Mixed Oxide Catalysts

The catalysts were prepared by the incipient wetness impregnation method. Supported mixed oxide catalysts were prepared using either the co-impregnation method (denoted by: -A) or the successive impregnation method (denoted by: -B). In the case of the mixed oxide catalysts, transition metal precursors were dried at 100^0 C overnight and calcined at 300^0 C for 2 hours in air. Copper (II) nitrate hydrate, cobalt (II) nitrate hexahydrate, and manganese (II) nitrate hydrate (Puratronic® 99.999% metal basis, Alfa Aesar) were used as precursors for CuOx, CoOx, and MnOx respectively. For SnOx, tin (IV) acetate (Sigma Aldrich) was used as a precursor. High surface area silica (Davisil® 645, Sigma Aldrich) was used as a catalyst support.

II.1.2 Promoted Noble Metal Catalysts

During this study, most of the catalysts were prepared by using the successive incipient wetness impregnation method (successive IN method) on silica or an alumina support. High surface area silica

(Davisil® 645, Davisil® 644, Merck® 10180, Merck® 10184, silica Grade 7734, Sigma Aldrich) and Davisil® LC 250 (Grace Davison) and γ – alumina (catalyst support, Alfa Aesar) were used as catalyst supports. The steps followed during the catalyst preparation by incipient wetness impregnation method were: (a) impregnation of a promoter precursor on the silica support followed by drying and calcination, (b) impregnation of a Pt precursor on the promoter-silica support followed by drying and calcination. The ceria precursor used was cerium (III) nitrate hexahydrate (REacton® 99.99%, Alfa Aesar). The Pt precursors differing in acidity were used, namely: (a) diammine dinitro platinum (DADNP) (8.2% w/w in dil. NH_4OH, Strem Chemicals); (b) tetraammineplatinum (II) hydroxide hydrate (TAPH) (Sigma Aldrich); (c) tetraammineplatinum (II) nitrate (TAPN) (99.99%, Sigma Aldrich); and (d) chloroplatinic acid (8wt% in H_2O, Sigma Aldrich). Potassium stannate (97%, Aldrich), Tin acetate (99%, Aldrich), and Stannic chloride (97%, Aldrich) were used for the preparation of tin oxide based catalysts.

Pd based catalysts were prepared with two different precursors, palladium nitrate (PdN, Sigma Aldrich) and diammine dinitro palladium (DPdN, (8.2% w/w in NH_4OH, Strem Chemicals)). In the case of the co-impregnated Pd-promoter catalyst, the precursors were dried at 100^0 C overnight and calcined at 300^0 C for 2 hours in air. In the case of Pt or Pd catalysts (-B-PdN, and -B-DPdN) prepared by successive impregnation, the Pt or Pd precursors were dried at 100^0 C overnight and calcined at 400^0 C for 3 hours in air.

The drying and calcination conditions used for the catalyst optimization studies were: (A) drying conditions: (a) vacuum drying at 40^0C for 6 hours; (b) overnight drying at 75^0C; and (c) drying for 4 hours at 125^0C; (B) calcination temperature: 200-600^0C; (C) calcination time: 1-6 hrs.

The effects of various ceria deposition methods were studied by preparing Pt-CeO_2/SiO_2 catalysts using three different ceria deposition methods, namely incipient wetness impregnation

(denoted by: -IN-), deposition precipitation (denoted by: -DP-) and grafting (denoted by: -GR-). During the preparation of ceria/silica by IN, silica support was impregnated with a cerium (III) nitrate hexahydrate (REacton® 99.99%, Alfa Aesar) solution, then dried overnight at 100^0 C and calcined at 300^0 C for two hours in air. The preparation of ceria/silica by the DP method was carried out as given by Reddy et al [47], briefly: cerium (III) ammonium nitrate (99.9%, Sigma Aldrich), DI water, and silica were mixed together and aq. NH_4OH was added drop wise with stirring until pH = 8. The resulting product was then filtered and washed with DI water followed by drying overnight at 100^0 C and calcination at 300^0 C in air for 2 hours. The preparation of ceria/silica by grafting (GR) was carried out according to the procedure given by Bensalem et al. [48], briefly: a suspension of silica in a benzene solution of cerium (III) acetylacetonate (Sigma Aldrich) was heated at 60^0 C with reflux for two hours. The resulting products were filtered and dried overnight at 100^0 C and then calcined in air at 300^0 C for two hours. The CeO_2/SiO_2 prepared by these different methods were then impregnated with the Pt precursor (DADNP) and were then dried at 100^0 C overnight and calcined at 400^0 C for 3 hours.

In the case of tin oxide promoted noble metal catalysts, the preparation method used for SnO_2 deposition was as follows: (a) potassium stannate (97%, Aldrich) was impregnated into SiO_2(Davisil Grade 645) using the incipient wetness impregnation method, (b) impregnation was followed by drying, (c) a stoichiometric equivalent of sulfuric acid was added, (d) the sample was dried again, (e) the resultant was washed with DI water, and (f) dried a final time. The sample of SnO_2/silica such prepared was then calcined at followed by Pt impregnation of the Pt precursor which was then dried and calcined.

II.1.3 Microfibrous Entrapped Catalysts Preparation

The microfibrous media were prepared using nickel fibers (2, 4, 8, and 12 μm), obtained from Intra-micron. Common procedure for the preparation of the MFECs is described here in brief. The raw materials used in this process were: (a) microfibers: nickel fibers (2, 4, 8, and 12 μm); (b) catalyst

support: silica or alumina; (c) cellulose fibers. The method for the preparation of the MFECs involved mainly four steps: (a) pre-form preparation, (b) pre-oxidation, (c) sintering, and (d) active metal/promoter deposition.

The first step of MFECs preparation involved the pre-form preparation which was done by wet-lay method. During this step a suspension of metal microfibers and cellulose fibers of desired weight and volume was prepared using a high sheer blender and water as a solution. This suspension was then added to a head box and the suspension was continuously stirred. Then the desired amount of catalyst support was added to the head box while stirring the suspension and a uniform mix of catalyst support particles and fibers was obtained in the head box. Finally the excess water was drained and a uniform media that entraps the catalyst support particles in the mesh of metal and cellulose fibers was obtained. Thin sheets of pre-forms are thus obtained on the bottom screen of the head box during the wet-lay method. These performs were then dried in oven at 100^0C overnight to get rid of excess water and moisture inside the catalyst support particles.

During the pre-oxidation step of the MFEC preparation, the dried pre-forms were cut to the desired sizes and the cellulose fibers in the pre-forms were oxidized/burned. The conditions used for the pre-oxidation steps were calcining the pre-forms at 400^0C for 30 minutes in air diluted with N_2. A modified pre-oxidation condition was used during this study which involved carrying out the pre-oxidation in three steps namely: (a) calcining at 400^0C for 15 minutes in air diluted with N_2, (b) calcining at 450^0C for 10 minutes in air diluted with N_2, and finally (c) calcining at 475^0C for 10 minutes in air diluted with N_2. The structure of the pre-forms at the end of pre-oxidation step was extremely weak due to absence of cellulose fibers.

During sintering step for MFEC preparation, the pre-oxidized sheets were sintered in diluted hydrogen atmospheres at about 900-1000 ^{0}C. During sintering, the metal microfibers bond with each other and form a sinter-locked mesh of fibers that entraps the catalyst particles. Since the high temperature treatment can cause decrease in the surface area for the high surface area silica support, extreme care was taken during the sintering and the time of sintering was optimized so that the effect on the catalyst support particles was minimum. During this work the sintering of the nickel microfibers was carried out at 950^{0}C for 30 minutes. The resulting samples were analyzed by Quantachrome AS1 instrument to study the effect of high temperature sintering on surface area and the reduction in the surface area was not more than 10% at the maximum.

The final step in the MFEC preparation was the deposition of the active metal/promoter on the entrapped catalyst support. The procedure was carried out by incipient wetness impregnation method and the drying and calcination conditions were as mentioned already for the promoter as well as the active metal.

II.2 Catalyst Testing and the Experimental Set-up

The challenge gas used for the experimental studies was in the range of 50-10000 ppm of CO in air, with a relative humidity of 0-90%. Air and CO in Nitrogen flow were measured and controlled prior to mixing using mass flow controllers. The resulting gaseous mixture was passed through a water saturator for introducing water vapor in the stream. The relative humidity of the resulting gas was detected using a RH detector. The concentration of the challenge gas was measured using Agilant® gas chromatogram. Calibration curves for various CO concentrations were obtained for the determination of CO concentration. However, for low CO concentrations, the electrochemical sensor was used for the detection of inlet CO concentration. Outlet CO concentration was measured using an electrochemical sensor (detection limit: 0.1 ppm CO). The electrochemical sensor assembly, Q-Rae Plus, also had a data-

logging option. The electrochemical sensor was calibrated every week with a calibration gas obtained from Rae Systems. The reactor used for the experiments was a tubular Pyrex reactor, various reactor diameters were used for the experimentation such as one inch, ¾ inch, ½ inch, and the like. The reactors were custom made at glass blowing shop at Auburn University Science Center. The catalyst powder or entrapped catalysts were supported with a glass-frit support, or a quartz wool support. In order to get a uniform flow in the catalyst bed, the inlet gas was first flown through a thin layer of quartz wool before letting to the catalyst bed. Precautions were taken so that the outlet of the reactor containing CO was vented out of the room via the fume hood exhaust.

Briefly the experimental conditions are given below: (a) all the tests conducted for CO oxidation in air, i.e. excess oxygen, (b) operating temperature: 20-150°C; operating pressure: atmospheric, (c) face velocity: 10-150 cm/sec; (d) humidity: 0-95% RH; and (e) Detection limit of the electrochemical sensor: 1.0 ppm CO. The schematic for the experimental set-up used for the CO oxidation activity tests is shown below in Figure II.1.

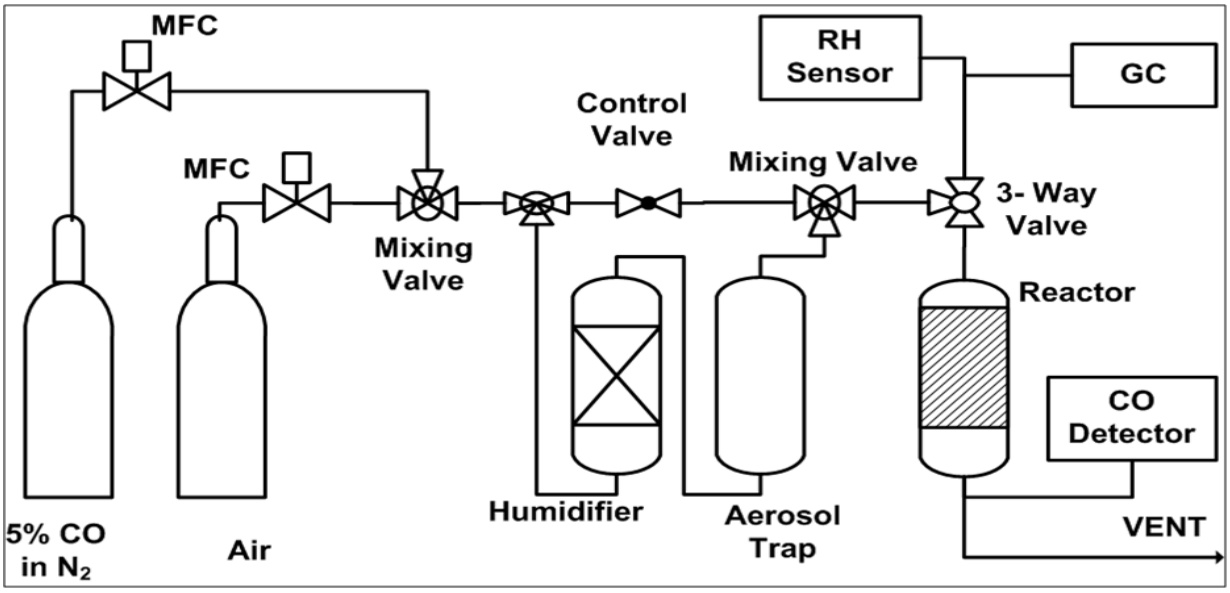

Figure II.1. Schematic of Experimental set-up

II.3 Characterization Techniques

II.3.1 Powder X-Ray Diffraction

Powder XRD was carried out on samples of the catalysts, to study the effect of various preparation variables on the crystallite sizes of the promoters used in the catalysts. Specifically for ceria promoted catalysts, presence of Platinum was not detected by XRD; however for tin oxide promoted catalysts, the presence of Platinum was detected. Powder XRD was carried out using a Rigaku MIniflex with a Cu source at 30 KV/15mA. The XRD spectra were obtained at 0.5 (2theta) /min. The catalyst samples were manually ground. The crystallite sizes were calculated by Scherrer equation from the observed spectra using the Jade software.

II.3.2 BET Surface Area and Pore Size Analysis

Total surface area of a catalyst support is one of the most important parameters in catalyst performance. The surface area of the support dictates the dispersion of the active metal/promoter in the catalyst. If the surface area of the catalyst support is significantly higher, then the number of active sites available for the deposition of the active metal/promoter is greater and therefore the dispersion of the active metal is better. The most common method for estimating the surface area of the catalyst support is that developed by Brunauer, Emmett and Teller (BET) in 1938. This method of surface area estimation involves principles of physical adsorption. The underlying assumption of this method is that under the conditions of measurement, the adsorbate forms a monolayer over the support surface, and by measuring the amount of adsorbate taken by the support (uptake) the surface area of the support can be determined.

Brunauer-Emmet-Teller (BET) method was used for measuring surface areas, in which the adsorbate gas (nitrogen) is weakly and non-specifically adsorbed on all surfaces. BET surface areas, pore

volumes (PVs), average pore size (APS) and pore size distributions were obtained using a Quantachrome AS1 Surface area and pore size analyzer using nitrogen adsorption at 77K. BET surface area analysis employed three or five point adsorption, while the calculations of the surface area and the pore sizes were done by using the AS1 Win software based on the data obtained with the AS1 instrument. The average pore sizes (APS) of the samples were estimated using a cylindrical pore model and the PV and APS were estimated at a relative pressure of 0.995.

II.3.3 Chemisorption

During the BET surface area measurement, the adsorbate adsorbs on the surface weakly and non-specifically. During chemisorption, however, the adsorbate strongly attaches to the metallic surface and based on the volume of the adsorbate uptake by the catalyst sample, the active SA (metal surface area) of the catalyst can be estimated. Chemisorption is simple and well established method for metals characterization [49, 50]. During chemisorption, the uptake of the adsorbate is plotted at different pressures, known as an isotherm that basically indicates the metal atoms accessible to the gas. Since, the amount of metal loading for a given sample is known beforehand, thus chemisorption enables the measurement of the ratio of surface metal atoms to the total metal atoms in a sample. This ratio is also known as dispersion.

To enable the estimation of the number of active metal sites, it is important to know the stoichiometry of adsorption for the given system of gas and metal. These stoichiometries are determined by extensive experimentation with the given gas and highly pure metal samples. For reproducible results and accurate estimation of the active surface areas, the chemisorption technique requires a highly clean metal surface [51]. Typically, the cleaning of the surface is carried out by removing the weakly adsorbed species on the surface by applying high vacuum at higher temperatures such as 300^0C. Then the metal surface is cleaned in a reducing atmosphere to convert all the possible

oxide species into metallic form, followed by applying vacuum to remove the reducing species that may get adsorbed on the surface, followed by cooling in inert atmosphere. During this work the static volumetric method of chemisorption was used.

During this work, three adsorbates were used for the measurement of the dispersion/active surface area of the active metal or promoter. In order to measure the ceria surface area, oxygen chemisorption was carried out, whereas, for the measurement of Platinum active surface area, CO and Hydrogen chemisorption was employed.

The preferred gases to measure active metal surface area are O_2, H_2, and CO. However, H_2 and CO are preferred for chemisorption on Platinum. Monolayer of hydrogen with a stoichiometry of one hydrogen atom to one platinum atom has been reported by several researchers between room temperature and 100^{o}C. Monolayer of CO with a stoichiometry of one CO molecule to one platinum atom (sometimes 0.7 to 1.25) has also been reported by several researchers between room temperature and 100^{o}C. A clean platinum surface was obtained for reproducible chemisorptions measurements by following a series of in-situ pretreatment steps as reported later. The primary step is an evacuation step in order to remove moisture as well as adsorbed organic molecules on the surface. Subsequent hydrogen reduction has been reported to be essential for reproducible hydrogen or CO uptakes on the platinum surfaces. Measurement of CO/H_2 uptake at 30^{0}C was observed to provide reproducible isotherms. The equilibration time was chosen to be 5 min as suggested by other researchers.

The chemisorption was carried out using the Quantachrome AS1 instrument operated in the automated mode. The ceria SAs were estimated by O_2 chemisorption and the Pt SAs were estimated from CO and H_2 chemisorptions. A stoichiometry of (1:1) was assumed for (CO: Pt) and (H: Pt) for

chemisorption at 30^0C. For O_2 chemisorption on ceria at 30^0C, adsorption of 2µmol O_2/m^2 ceria was assumed [52]. In order to get reproducible isotherms of CO/H_2 from Pt chemisorption, the pre-treatment sequence followed was: (a) cleaning (200^0C, 1 hr, He), (b) evacuation (200^0C, 2hr, vacuum), (c) reduction (300^0C, 1 hr, H_2) and (d) adsorbed H_2 removal (300^0C, 2 hr, vacuum). Since the H_2 treatment at 300^0C reduces most of the surface ceria [52], for O_2 chemisorption on ceria the same pre-treatment sequence was followed.

II.3.4 Oxygen Hydrogen Titration

Hydrogen reacts stoichiometrically with the adsorbed oxygen layer on the Platinum surface at room temperature. This stoichiometric reaction between hydrogen and oxygen provides a lot of advantages, such as, increased sensitivity, rapid equilibration, and the like for the estimation of the Pt surface area. In the case of ceria promoted platinum catalysts, the oxygen-hydrogen titration can be used in a unique way to find out total ceria surface area, total platinum surface area, as well as the ceria surface area in contact with platinum. This unique protocol was developed by Salasc, et al [52].

According to this protocol, initially the oxygen chemisorption (OC) is carried out on ceria promoted platinum catalyst, which gives combined uptake of oxygen on ceria and platinum. Then, titration by hydrogen (HT) is carried out. Further, titration by oxygen (OT) is carried out at room temperature, which gives the total uptake of oxygen on platinum as well as ceria in contact with platinum. Finally, hydrogen chemisorption (HC) is carried out to determine the platinum active surface area. When, this hydrogen uptake (HC) considering the stoichiometry is subtracted from the earlier two oxygen uptakes (OC and OT), the resultant O_2 uptake would enable the estimation of total ceria surface area and ceria surface area in contact with platinum. The schematic of the reactions occurring at the surface is given in Figure II.2, Figure II.3, and Figure II.4.

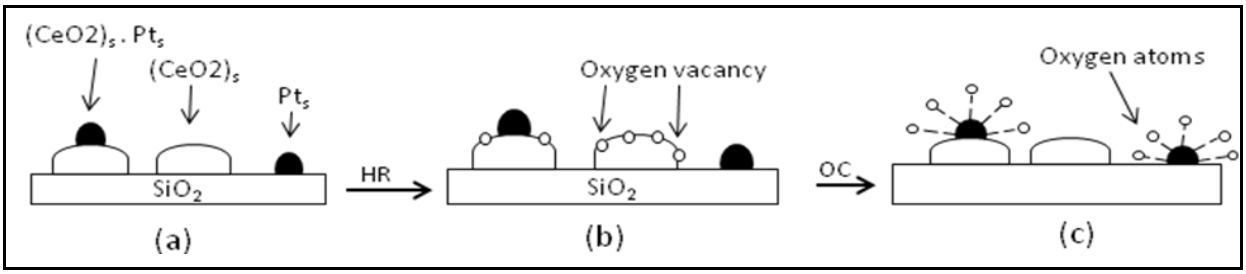

Figure II.2. O_2-H_2 Titration on Pt-Ceria/Silica catalyst –O_2 chemisorption

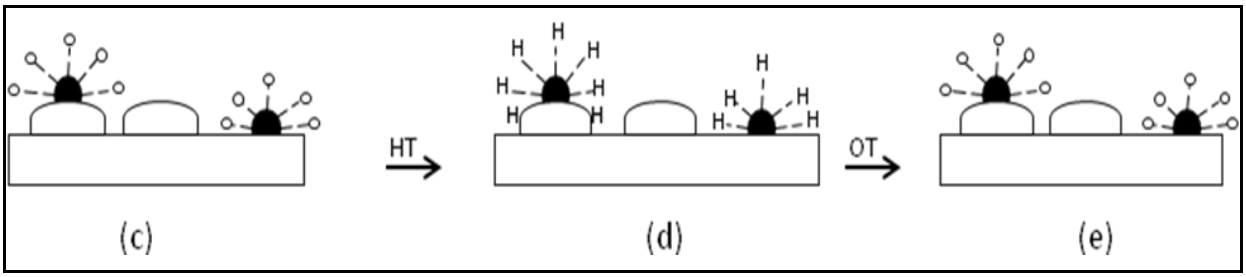

Figure II.3. O_2-H_2 Titration on Pt-Ceria/Silica catalyst – H_2 Titration and O_2 Titration

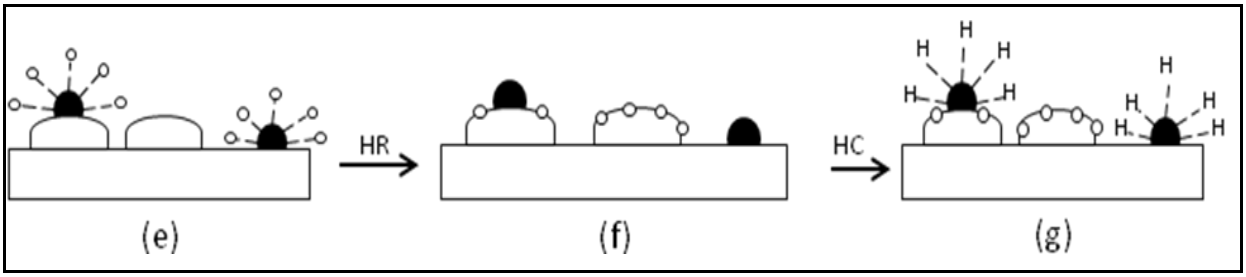

Figure II.4. O_2-H_2 Titration on Pt-Ceria/Silica catalyst – H_2 reduction and H_2 Chemisorption

Note 1: Pt_S:surface Pt; $(CeO2)_S$: surface CeO_2; $(CeO_2)_S.Pt_S$: surface ceria in contact with surface Pt.

Note 2: (a) catalyst surface, (b) catalyst surface after hydrogen reduction (HR), (c) catalyst surface after oxygen chemisorption (OC) , (d) catalyst surface after hydrogen titration (HT), (e) catalyst surface after oxygen titration (OT), (f) catalyst surface after hydrogen reduction (HR), (g) catalyst surface after hydrogen chemisorption (HC)

The reactions occurring at the surface are given below in Table II.1. The stoichiometry can be estimated from these reactions as proposed by salasc et al [52]. In order to get a clean surface for hydrogen chemisorption, the samples were reduced in hydrogen (HR) before HC. This HR step is carried out at elevated temperatures to remove all the adsorbed moisture as well. The final hydrogen chemisorption step however is carried out at room temperature.

Table II.1. Reactions Occurring at the Catalyst Surface During O2-H2 Titration

Operation	**Reaction(s)**	**Explanation**
O_2 Chemisorption (OC)	$Pt_S + (Ce_2O_3)_S + O_{2(g)} = Pt_S\text{-}O_{ads} + (2CeO_2)_S$	O_2 chemisorption: Pt and Ce_2O_3
H_2 Titration (HT)	$Pt_S – O_{ads} + 1½\ H_{2(g)} = Pt_S – H_{ads} + H_2O$ $((2CeO_2)_S.Pt_S) + H_{2(g)} = ((2CeO_2)_s.\ Pt_S)$**HH**	Reaction of H_2 with adsorbed O H_2 spillover to ceria adjacent to Pt
O_2 Titration (OT)	$Pt_S – H + ¾\ O_{2(g)} = Pt_S – O_{ads} + ½\ H_2O$ $((2CeO_2)_S.Pt_S)$**HH** $+ ½\ O_{2(g)} = ((2CeO_2)_S.$ $Pt_S) + H_2O$	Reaction of O_2 with adsorbed H O_2 reacts with spilled over H_2
H_2 Chemisorption (HC)	$Pt_S + ½\ H_{2(g)} = Pt_S – H_{ads}$	H_2 chemisorption on surface Pt

*All the reactions are occurring on surface species (Pt: Pt_S, (CeO_2): $(CeO_2)_S$, and (Ce_2O_3): $(Ce_2O_3)_S$)

In the case of ceria, hydrogen reduction at T > 470 – 570K would reduce the surface of the ceria; however, in the presence of noble metal the reduction of the ceria surface could be carried out even at room temperature. This could happen due to the migration of hydrogen from metallic particles to the ceria support. Also, magnetic balance studies indicated that only the ceria surface (in the absence of noble metal) can get reduced at 573K whereas the bulk reduction of ceria took place at significantly higher temperatures [53]. Based on the redox properties of ceria and the H2 spillover in the presence of noble metals, this protocol was developed by Salasc et al.

For estimation of the total ceria surface area as well as the ceria surface area in contact with the noble metal, the estimation of noble metal surface area is crucial. So if the oxygen uptake during O_2 chemisorption is measured, then by subtracting the hydrogen uptake during hydrogen chemisorption, one could obtain the total ceria surface area [52]. Additionally, based on the oxygen uptake during oxygen titration, from the stoichiometric equations given in Table II.1, it would be possible to estimate the ceria surface area in contact with noble metal [52].

During this work, this oxygen – hydrogen titration protocol developed by Salasc et al [52] was used to determine the ceria surface area in contact with Pt. During this work, Quantachrome AS1 instrument was used in batch mode for carrying out the O_2-H_2 titration on the Pt-ceria/silica catalyst.

II.3.5 Electron Microscopy

TEM was used to image the powder samples. The powder was crushed and a suspension was prepared using sonication, which was then dispersed on a copper 300 mesh specimen grid coated with formvar carbon. Instrument used was ZEISS EM10, with 60kV, and 160K or 200K magnification. MFECs were imaged using ZEISS EVO 50 VP SEM to study the fibrous structure of fibrous matrix.

II.3.6 Temperature Programmed Reduction (TPR)

Temperature Programmed Reduction (TPR) of the catalyst samples (0.2g) was carried out using 15sccm of 5% H_2 in Argon in the temperature range of 293 – 1023 K at heating rate of 10K/min. In order to get reproducible results from TPR, a sequence of pre-treatment similar to that reported by Rocchini et al [54] was employed: (a) pre-treatment in 5% O_2 in Argon for 2 hours at 400^0C, and (b) flow Ar at 500^0C for one hour. The H_2 consumption was estimated from the changes in thermal conductivity (measured by TCD detector), and calibrated using copper oxide standard (*Alfa Aesar*).

III Catalyst Screening

III.1 Introduction

During this work, a number of catalysts were screened for CO oxidation at ambient conditions ($T<50^0C$, RH: 10-90%). Commercial catalysts, catalyst formulations reported in scientific literature were screened initially. Later, conventional as well as novel transition metal oxide catalysts, supported noble metal catalysts with and without promoter were prepared and tested.

Commercially available hopcalite type of catalysts (mixture of CuOx and MnOx) such as Carulite® and Moleculite® were tested in humid and dry conditions over a wide range of CO concentrations at 25^0C. These catalysts were highly in dry conditions at high CO concentration (>2500 ppm). However, these catalysts deactivated in the presence of moisture. Also, these catalysts were less active or inactive (conversion <5%) at low CO (CO <500ppm).

CO oxidation is exothermic with an adiabatic temperature rise of 1^0C per 100ppm CO reacted. Considering the activity results of Carulite catalysts, it could be concluded that these TM oxide catalysts showed activity at higher CO by exploiting the exothermicity of the reaction. Due to exothermic CO oxidation, some catalysts may appear active at low temperature at high CO. The objective of this study was to develop a CO oxidation catalyst that is highly active in humid air (RH: 10-90%), over a wide range of temperature and CO, and specifically active at room temperature.

So, the screening tests were done at ambient conditions at low CO (CO<500 ppm; $\Delta T<5°C$).

III.2 Non-Noble Metal Catalysts

Review of scientific literature on catalytic CO oxidation with non-noble metal catalysts revealed following potential candidates for this application: CuOx, CoOx, MnOx, AgOx, CeOx and the mixtures thereof. During this study, activity of silica (Davisil 645; SA: 300m^2/g) supported TM oxides and their mixture was investigated. The catalysts were prepared by either co – impregnation (-A) or successive impregnation (-B) followed by drying overnight at 120^{0}C and calcining at 300^{0}C for 3 hours in air.

Although a large number of catalysts were screened, a selected few results are given in this section. The composition and activity of these non-noble metal catalysts is given in Table III.1.

Table III.1. Composition and Activity of the Non-noble Metal Catalysts

No.	Catalyst	Conv. (25^{0}C; 50% RH)	Conv. (0% RH)
1	**5-15%CuOx/SiO_2**	NA	NA (T≤200^{0}C)
2	**5-15%CeOx/SiO_2**	NA	NA (T≤200^{0}C)
3	**5-15%MnOx/SiO_2**	NA	NA (T≤200^{0}C)
4	**5% CuOx – 15%CeOx/SiO_2 –A**	NA	40% (T = 150^{0}C)
5	**5% CuOx – 15%CeOx/SiO_2 – B**	NA	NA (T≤200^{0}C)
6	**5%AgOx – 15% CeOx/SiO_2 – B**	NA	NA (T≤200^{0}C)
7	**15%CoOx/SiO_2**	NA	10% (T = 100^{0}C)
8	**5%CuOx – 15% CoOx/SiO_2 – B**	NA	15% (T = 75^{0}C)
9	**5%CeOx – 15% CoOx/SiO_2 – B**	NA	25% (T = 75^{0}C)
10	**5%CoOx – 15% CeOx/SiO_2 – B**	NA	10% (T = 125^{0}C)

Test Conditions: CO: 250 ppm in air, SV: 360000 hr^{-1}; Particle size: 150 – 250 µm; Reactor ID: ¾"

CuOx/alumina [55] and CuOx/titania [56] have been reported to be active at T≥150°C. During this study, silica supported CuOx (up to 15%) was found to be inactive at T≤200^{0}C in dry and humid conditions. Manganese oxide based catalysts were reportedly active for CO oxidation at T ≤100^{0}C [57]; however, MnOx/SiO_2 catalysts screened during this work were inactive at T≤200^{0}C. Surface CuOx and MnOx layer could react with moisture to form inactive metal hydroxide layer; therefore, CuOx or MnOx promoted catalysts would be inactive in moist conditions. Also, silica supported ceria catalysts (15% CeOx/SiO_2) were inactive for T≤200^{0}C in both moist and dry conditions.

Ceria doped with La and Cu showed CO oxidation activity in dry conditions at T≥100^{0}C [58, 59], also 6%CuO/CeO2 showed activity at T≤ 100^{0}C [33]. During catalyst screening, CuOx-CeOx/SiO2 catalysts were tested and found to be inactive in humid conditions. However, the catalysts prepared by co-impregnation were active at T≥150^{0}C (CO conv. > 40%) in dry conditions. Catalysts prepared by successive impregnation were however inactive, indicating a possibility of formation of a mixed oxide surface species during co-impregnation which might be responsible for activity.

AgOx based catalysts were highly active for selective CO oxidation in the presence of hydrogen, at T≤50^{0}C [60], also silver doped ceria showed enhanced redox properties and greater [61]. In order to exploit the symbiotic relationship between AgOx and ceria, AgOx/silica catalysts with ceria as a promoter were prepared and tested. The catalysts were found to be inactive at T≤ 200^{0}C. 10% CoOx/SiO_2 catalyst was active in dry conditions at T≥100^{0}C, but the activity decreased with time. Unsupported cobalt oxide has been reported to be active due to presence of active surface oxygen species [62], and the activity decay could be explained by loss these oxygen species due to reduction of active CoOx with CO [11]. The catalyst was inactive for humid conditions at T≤200^{0}C.

A mixture of CuOx and CoOx supported on alumina has been reported to be active at room temperature and was more active than monoxide catalysts [63]. During this study, silica supported mixed oxides catalysts were found to be more active (conv.: 15% at 75°C) than monoxides (conv.: 10% at 100°C) in dry conditions. This observation certainly indicated a synergistic behavior of the copper and cobalt oxides, as reported earlier. However, the catalyst activity decreased over time, similar to that of non-promoted $CoOx/SiO_2$ catalyst. Addition of CuOx would create crystal defects which would certainly increase surface oxygen species of CoOx which were believed to provide active sites for CO oxidation. However, the mixed oxide catalysts were active in moist conditions.

Presence of ceria would enhance the activity of CoOx as ceria could act as an oxygen reservoir and replenish the surface oxygen species of CoOx, the active sites for CO oxidation. Many researchers have reported the CO oxidation activity enhancement due to doping of cobalt oxide with ceria [32, 64]. Ceria supported CoOx catalyst has shown activity at $T>100^0C$ [65] and mesoporous cobalt ceria oxides were active at 100^0C [66]. During this study, silica supported mixed CeOx and CoOx catalysts were prepared and screened. Ceria doped (1-5%) CoOx (15-25%) catalysts were active (Conv.: 25% at 75°C) in dry conditions. The CoOx doped (1-5%) ceria (15-25%) catalysts showed lower activity (Conv.: 10% at 125°C) compared to $5\%CeOx\text{-}15\%CoOx/SiO_2$ catalyst. If surface oxygen species in CoOx provide the active sites for CO oxidation, addition of CuOx or CeOx as dopant would enhance activity by creating crystal defects in CoOx. However, these catalysts were inactive in the presence of moisture.

Ceria (5%) doped CoOx (15%) catalyst showed the highest activity amongst all the non-noble metal catalysts and was also stable under dry conditions. None of the TM oxide catalysts were active in the presence of moisture at T<200°C. Also, TM oxide catalysts were not active over a wide range of CO concentration. TM oxide catalysts show CO oxidation activity at low temperatures under dry conditions only at higher CO concentrations by exploiting the exothermicity of the reaction.

III.3 Noble – Metal Catalysts

Cobalt and manganese oxides have been reported as beneficial promoters for Pt catalysts [23, 24], whereas tin oxide and ceria were found as promising supports for Pt catalysts [21, 22]. Hence, the effect of CoOx, MnOx, SnOx, ZrO_2, and CeO_2 as promoter for silica or alumina supported Pt (or Pd) catalysts was investigated during this study.

Catalysts were prepared by incipient wetness impregnation (co-impregnation (-A) or successive impregnation (-B)). The sequence of impregnation was promoter followed by noble metal. Promoter precursors were dried overnight at 110^0C followed by calcination at 300^0C for two hours in air. Pt or Pd precursors were dried overnight at 100^0C, followed by calcination at 400^0C for three hours in air. Activity results for these catalysts are given in Table III.2.

Table III.2: Activity comparison of Noble – metal catalysts

No.	Catalyst	% Conv.*	No.	Catalyst	%Conv.*
1	5%Pt/SiO_2	40.0	**10**	5% Pt-15%SnOx/γ-Al_2O_3-B	55.0
2	5%Pt/γ - Al_2O_3	33.0	**11**	5% Pd-15%SnOx/SiO_2 –B	15.0
3	5%Pd/SiO_2	7.0	**12**	5% Pt-20%ZrO_2/SiO_2-DP-B	38.0
4	5%Pd/ γ - Al_2O_3	<5.0	**13**	5% Pt-20%ZrO_2/SiO_2-Gr-B	42.0
5	5%Pt – 15% CoOx/SiO_2 –B	26.0	**14**	5%Pd-16%CeO_2 /SiO_2 –B	36.0
6	5%Pt -15% CoOx/ γ-Al_2O_3-B	31.0	**15**	5%Pd-16%CeO_2/SiO_2-PN-A	10.0
7	5%Pt – 15%MnOx/SiO_2 –B	28.0	**16**	5%Pd-16%CeO_2/SiO_2-PN-B	22.0
8	5%Pt –15%MnOx/ γ-Al_2O_3-B	25.0	**17**	2.5% Pt-16%CeO_2/SiO_2-B	**99.0**
9	5% Pt – 15%SnOx/SiO_2 –B	70.0			

*Conversion values reported after 2 hours

Test Conditions: 250 ppm CO in air, Catalyst bed thickness: 2.5mm; Face Velocity: 45 cm/sec; Particle size: 200 µm; Reactor ID: ¾"; Humidity: 50% RH; Temperature: 25^{0}C

Pt/SiO_2 catalyst and CoOx or MnOx promoted Pt/SiO_2 catalysts have been reportedly active for CO oxidation [67] and promoted catalysts showed better activity [68]. Pt/alumina catalysts also showed improved activity with addition of MnOx [69, 70]. During this study, although promoted Pt/SiO_2 or Pt/alumina catalysts were found to be more active than unpromoted catalyst initially, the CoOx and MnOx promoted catalysts declined in activity over time. Non-promoted Pt catalysts performed better than Pd based catalysts. Further, Pt/Alumina was less active compared to Pt/Silica catalyst.

15% Pt/SnO_2 catalyst [29, 71] and SnO2 promoted Pt/alumina [30, 31]have been reported to be active for CO oxidation in humid conditions. During this study, SnOx promoted Pt/SiO_2 and Pt/alumina catalysts were prepared and tested for activity. Silica supported Pt/SnOx catalyst was highly active (Conv.: 70%) for CO oxidation at room temperature in humid air. Pt-SnOx/alumina (Conv.: 55%) catalyst was less active in comparison with Pt-SnOx/Silica. Also, Pd-SnOx/Silica catalyst was less active (CO conversion: 15%) compared to Pt based catalysts (70% conversion). Pt-SnO_2 interfacial area was found to be responsible for the activity of Pt/SnO_2 catalyst and the CO oxidation mechanism involved transfer of lattice oxygen from SnOx to the interfacial active sites [30]. Silica support probably provided better Pt-SnO_2 interfacial area compared to alumina support resulting in greater activity.

Pt/ZrO_2 has shown CO oxidation activity at T≥150^{0}C [72]. Zirconia is known to act as an oxygen reservoir and the ability of zirconia to undergo redox cycles at lower temperatures improved with decreased crystallite size. To exploit the redox properties of nano-scale zirconia, 5%Pt/SiO2 catalysts with zirconia promoter (20% w/w) were investigated during this study. Zirconia deposition on silica was carried out by deposition precipitation (DP) method (process by *Dijs., et al* [73]) or by grafting (GR)

method (process by *Seo., et al* [74]). Catalyst prepared with ZrO_2 deposited by GR method performed better (42% conversion) compared to ZrO_2 deposited by DP method (38% conversion). Zirconia promoter was certainly better than CoOx and MnOx promoters and the zirconia promoted catalysts were highly stable for CO oxidation at room temperature under humid conditions.

Pt/ceria catalysts have been reported to be active for CO oxidation [40, 75]. Ceria is known for its ability to store oxygen and undergo redox cycles even at room temperatures, which makes ceria a promising promoter for oxidation catalysts. Further, CO oxidation mechanism on Pt/ceria involved reaction of lattice oxygen on ceria with CO adsorbed on Pt [40].

During this study, ceria promoted Pt and Pd catalysts supported on silica were tested. Pd based catalysts were prepared using two different precursors: (a) diammine dinitro palladium (II) (DADNPd) by successive impregnation (-B); (b) palladium nitrate – by co-impregnation (-PN-A) and successive impregnation (-PN-B). Pd-ceria/silica prepared by DADNPd was more active compared to catalysts prepared with palladium nitrate. Also, preparation with palladium nitrate by co-impregnation resulted in a less active catalyst compared preparation by successive impregnation. If Pd were to provide active sites for CO oxidation, co-impregnation of ceria and Pd could result in less active catalyst by forming the PdOx – CeOx mixed oxide. Pt based catalysts were highly active compared to Pd based catalysts as well.

III.4 Ceria Promoted Noble Metal Catalysts

Ceria promoted 2.5%Pt/silica catalysts were the most active (Conv.: 99%) for CO oxidation in humid conditions giving more than 99% conversion. Although Pt was preferred, feasibility of using Pd in combination with Pt was studied to assess the cost reduction potential (price ratio: Pt:Pd≈4). The catalysts were prepared by successive impregnation. The ceria precursor was impregnated first followed by drying overnight at 120^0C and calcination at 300^0C for two hours. The deposition of noble metals was

carried out in a single step. The Pt or Pd precursor alone or a mixture of both precursors as per the desired noble metal weight loading was used for impregnation. The impregnated support was dried overnight at 120^0C and then calcined at 400^0C for 3 hours in air. The ceria precursor used was cerium (III) nitrate hexahydrate, the Pt precursor used was diammine dinitro Platinum (II) in dilute NH_4OH and the Pd precursor used was diammine dinitro Palladium (II) in dilute NH_4OH. These ceria promoted noble metal catalysts were tested for CO oxidation at room temperature in humid air and the results are given in Table III.3.

Pt based catalysts were highly active in comparison to Pd based catalyst. Further, addition of Pd to Pt did not improve the activity of the catalyst. Based on these results, Pt was chosen as the active metal for the ceria promoted catalysts.

Table III.3: Activity of Ceria Promoted Noble Metal Catalysts

No.	Catalyst	Reaction Rate (µmol/g/s)
1	**5% Pd-16%CeO_2/SiO_2-B**	2.24
2	**2.5% Pd-16%CeO_2/SiO_2-B**	1.45
3	**2.5% Pd - 2.5% Pt-16%CeO_2/SiO_2-B**	3.30
4	**1.25% Pd - 1.25% Pt-16%CeO_2/SiO_2-B**	2.38
5	**2.5% Pt-16%CeO_2/SiO_2-B**	5.88

Test Conditions: Face velocity: 60 cm/sec; Humidity: 50% RH; Temperature: 25^0C; Reactor: 0. 75" ID; Catalyst bed depth: 3.2mm (with 50% inert); Particle Size: 150-250 µm; Inlet CO Concentration: 500ppm

III.5 Conclusions

From the catalyst screening tests, it was observed that the supported mixed oxide catalysts were not active for room temperature CO oxidation in the presence of moisture. The catalyst screening also revealed that the use of cobalt oxide or manganese oxide as a promoter for the noble metal catalyst was although beneficial, these catalysts deactivated over time in the presence of moisture. Tin oxide promoted Pt catalyst and ceria promoted Pt catalysts were highly active and stable for CO oxidation at room temperature in the presence of moisture.

The tin oxide and ceria promoted Pt catalysts were investigated in detail. The effect of various preparation conditions on the catalyst performance was studied experimentally and was correlated to the surface characterization results. A path finding exercise to optimize these catalysts was carried out and the results are given in subsequent chapters.

IV Synthesis and Optimization of Tin Oxide Promoted Pt Catalyst

IV.1 Introduction

During catalyst screening, tin oxide promoted Pt catalyst showed greater activity for CO oxidation at low temperature in the presence of water vapor. The activity of the Pt/SnO2 catalyst has also been attributed to the formation of surface hydroxyl groups on the tin oxide surface, which react with CO adsorbed on Pt [76]. The performance of the catalyst is a function of catalyst composition as well as the preparation conditions used.

During this study, the optimization of the tin oxide promoted Pt catalyst was carried out by studying the effect of catalyst composition on the catalyst activity. Further, the preparation conditions were optimized based on the experimental results and were correlated with surface characterization. Further, the performance of the catalyst at different testing conditions was verified. Finally, the activity maintenance of the catalyst at desired CO removal application conditions was studied.

IV.2 Experimental Details

IV.2.1 Catalyst Preparation Processes and Methods

IV.2.1.1 Tin Oxide Deposition Method

For this study, different types of tin oxide deposition methods were used to prepare 5% Pt – 25% SnO_2/SiO_2 catalysts. Tin oxide promoter can be deposited on silica support by different methods as outlined below: (A) prepare slurry of tin metal and silica, which oxidizes tin to metastannic acid, which

coats silica. Metastannic acid after drying gives tin oxide [77]; (B) deposition precipitation by tin chloride hydrolysis: impregnate silica with tin chloride followed by hydrolysis by ammonium hydroxide, which yields tin hydroxide. After washing with dilute alkali to remove excess chloride ions and drying at 100°C overnight, SnO_2/SiO_2 was obtained; (C) impregnation of tin acetate (*Alfa Aesar*) followed by drying overnight at 100°C and calcining at 300°C for three hours; (D) deposition by potassium stannate (*Sigma Aldrich*) hydrolysis with sulfuric acid. Catalyst support was impregnated with potassium stannate followed by drying followed by impregnation with stoichiometric amount of sulfuric acid. After washing to remove potassium sulfate and drying of tin hydroxide SnO_2/SiO_2 was obtained.

Organometallic compound of tin such as Tetrabutyltin, Tin Isopropoxide, and Tin tert-butoxide have a boiling point in the range of 200-250°C and they decompose at T>250°C. Also, high pressure decomposition results into coke formation. Further, oxidation of these compounds using powerful oxidizing agents could be carried out at temperatures below their boiling or decomposition temperatures; however, the process is highly unstable, explosive and unsafe for scale up. Also, greater loadings (>15% w/w) of SnO_2 could not be obtained using these compounds. So, the use of organometallic compounds other than tin acetate for incipient wetness impregnation was not pursued.

Once the tin oxide was deposited on the silica support, the Pt deposition was carried out by incipient wetness impregnation. For the Pt deposition, the Pt precursor used was diammine dinitro platinum (II) (DADNP, 8% w/w in dilute NH_4OH, *Strem Chemicals*). The Pt precursor was impregnated on SnO_2/SiO_2 support followed by drying at 125^0C overnight and calcining at 400^0C for three hours in air.

IV.2.1.2 Catalyst Support Selection

Four supports were considered for this study: silica, γ-alumina, activated carbon and titania. Due to the requirements of the preparation conditions such as Pt precursor calcination temperature, high PV

and SA of the support, only silica (Davisil® 645, *Sigma Aldrich*) and γ-alumina (catalyst support*, Alfa Aesar*) were selected for the study. The selected supports had similar SA (300m^2/g) and pore structures (PV: 1.10-1.15 cc/g; APS: 145-150 Å). Pt (3.5%) and SnO_2 (25%) loadings were kept same.

The tin oxide deposition was carried out by the potassium stannate – sulfuric acid route. K_2SnO_3 impregnation on support was followed by drying, followed by impregnation of H_2SO_4 and drying and washing with DI water followed by final drying step. All the drying steps were carried out in vacuum at 40^0C. The Pt deposition was carried out by using the Pt precursor (DADNP), followed by drying at 120^0C overnight and calcination at 400^0C for three hours in air.

IV.2.1.3 Type of Silica Support

For this study, four types of silica with different SA and porous structures were selected and 2.5%Pt-25%SnO_2/SiO_2 catalysts were prepared. Silica supports used were (Sigma Aldrich): Merck® 10180 (750 m2/g; 0.66cc/g; 40 Å), Merck® 60 (500 m2/g; 0.8cc/g; 60 Å), Merck® 10184 (300 m2/g; 1.0cc/g; 100 Å), and Davisil® (645+644) (750 m2/g; 0.66cc/g; 40 Å). The tin oxide deposition was carried out by the potassium stannate – sulfuric acid route (as described in previous section). All the drying steps were carried out in vacuum at 40^0C. Pt deposition was carried out by using the Pt precursor (DADNP), followed by drying at 120^0C overnight and calcination at 400^0C for three hours in air.

IV.2.1.4 Effect of Drying Conditions during Tin Oxide Deposition

The preferred tin oxide deposition method was deposition by hydrolysis of potassium stannate with sulfuric acid. The process has already been mentioned earlier. Briefly, the process was as follows: (i) impregnate silica with potassium stannate solution; (ii) dry the impregnated silica; (iii) impregnate dried silica with stoichiometric amount of sulfuric acid in water; (iv) dry sample; (v) wash with DI water to remove potassium sulfate; (vi) dry sample to get SnO_2/SiO_2. There were three drying steps in the process.

So, the effect of different drying conditions on activity was studied by preparing catalyst with same composition (5%Pt - 15%SnO_2/SiO_2) differing only in the drying conditions used during preparation. Two types of drying conditions were evaluated: drying under vacuum at 40°C (V); drying at 125^0C in oven for 3 hours (D). In total eight different catalysts were prepared, each denoted by three letters indicating the type of drying condition used for 3 different drying steps during process. For example: VDV would indicate (a) drying under vacuum after potassium stannate impregnation; (b) high temperature drying after sulfuric acid hydrolysis; and (c) drying under vacuum after washing with DI water.

The Pt precursor used for this study was DADNP, and the drying of the Pt precursor was carried out at 120^0C overnight and the Pt precursor was calcined at 400^0C for three hours.

IV.2.1.5 Effect of SnO_2/SiO_2 Calcination during Tin Oxide Deposition

Tin oxide has been known to decorate Pt crystallites during high temperature processing. If tin oxide were to be subjected to a high temperature treatment prior to Pt deposition, the decoration of Pt crystallites during Pt precursor calcination could be avoided. So, the impact of calcination of 25%SnO_2/SiO_2 on activity was investigated. Tin oxide deposition was carried out by potassium stannate-sulfuric acid route and all the drying steps were carried out under vacuum at 40°C. Pt (3.5%) deposition was carried out using DADNP by drying overnight at 125^0C and calcining at 500^0C for three hours. After the tin oxide deposition step, the resulting SnO_2/SiO_2 powder was subjected to different calcination temperatures (125°C, 400°C, and 600°C) for two hours in air.

IV.2.1.6 Effect of SnO_2 Loading

Impact of SnO_2 promoter content on activity was investigated by varying the SnO_2 content (5-30% w/w) while maintaining the Pt (5% w/w), silica support (Davisil® 645) and other preparation conditions

same. The tin oxide deposition was carried out by the potassium stannate – sulfuric acid route and all of the drying steps were carried out under vacuum at 40^0C. The resulting SnO2/SiO2 was not calcined and DADNP was used for Pt deposition, by drying overnight at 120^0C and calcining at 400^0C for 3 hours in air. The deposition of tin oxide was carried out in single step and different potassium stannate solutions corresponding to different SnO_2 loadings were used for impregnation.

IV.2.1.7 Pt Precursor & Calcination Conditions Selection Study

The effect of the Pt precursor on Pt dispersion and the catalytic activity was studied by preparing 5%Pt – 25%SnO_2/SiO_2 catalysts using four different Pt precursors, namely: (a) diammine dintro platinum (II) (DADNP Strem Chemicals), (b) chloroplatinic Acid (8% w/w in H2O, *Sigma Aldrich*), (c) tetraammine platinum (II) hydroxide (TAPH, 99%, *Sigma Aldrich*), and (d) tetraammine platinum (II) nitrate (TAPN, 99%, *Sigma Aldrich*). All of the Pt precursors were dried in oven at 125^0C for 4 hours; and all of the Pt precursors were calcined at 300^0C, 400^0C, 500^0C, and 600^0C for 4 hours in air. The other preparation conditions were: (a) SnO_2 deposition route: potassium stannate – sulfuric acid route, and all drying steps were carried out in vacuum at 40^0C for six hours, and (b) SnO_2/SiO_2 calcination at 600^0C for two hours in air.

Platinum acetyl acetonate (Pt – acac) is one of the commonly used Pt precursor during catalyst preparation. However, Pt-acac was not studied during this study, due to its low solubility (<1.5% w/v) in all the major solvents such as water, toluene, acetone, THF, and iso-propyl alcohol. Lower solubility of a platinum salt meant higher number of successive impregnation steps to get the required Platinum loading, which could result in contamination. Therefore, in the best interest, Pt-acac was not studied.

For calcination time studies, 5%Pt – 25%SnO_2/SiO_2 catalysts were prepared with DADNP precursor and calcining at 500°C in air for (a) one hour, (b) two hours, (c) three hours, or (d) six hours.

IV.2.1.8 Pt Precursor Drying Condition Selection Study

Since drying rate could affect activity, its impact was investigated by comparing the activity of 5% Pt – 25% SnO_2/SiO_2 prepared using three different drying conditions: (a) drying at room temperature under vacuum, (b) drying overnight at 100^0C, or (c) drying at 125^0C for 4 hours. The other preparation conditions were: (a) SnO_2 deposition route: potassium stannate – sulfuric acid route, and all drying steps were carried out in vacuum at 40^0C for six hours, and (b) SnO_2/SiO_2 calcination at 600^0C for two hours in air. Pt precursor (DADNP) was calcined at 500°C in air for three hours.

IV.2.1.9 Pt Loading

The effect of Pt weight loading was investigated for (X% Pt – 25%SnO_2/SiO_2) catalyst by varying the Pt content from 1.25% to 7.5%. All other preparation conditions were maintained the same: tin oxide deposition route (potassium stannate – sulfuric acid route, and all drying steps were carried out in vacuum at 40^0C for six hours), the drying (125°C for 4 hours) and calcination conditions (500°C in air for three hours) of DADNP precursor.

IV.2.2 Catalyst Characterization

Catalysts were characterized using BET SA analyzer, powder XRD, and CO chemisorption at 30°C. The details for these techniques such as the instruments used during this study and the steps for the analysis are given in the 'experimental details' chapter. In the case of tin oxide promoted catalysts, the tin oxide crystallite sizes were estimated from the XRD spectra using the Jade software employing the Scherrer equation for observed peak at 2theta: 35 ° (111).

IV.3 Results and Discussions

IV.3.1 Tin Oxide Deposition Method

5% Pt – 25% SnO_2/SiO_2 catalysts prepared by four different tin oxide deposition methods were tested for CO activity and the results are given in Figure IV.1. These catalysts were also characterized by BET SA analyzer, XRD and CO chemisorption and the results are given in Table IV.1.

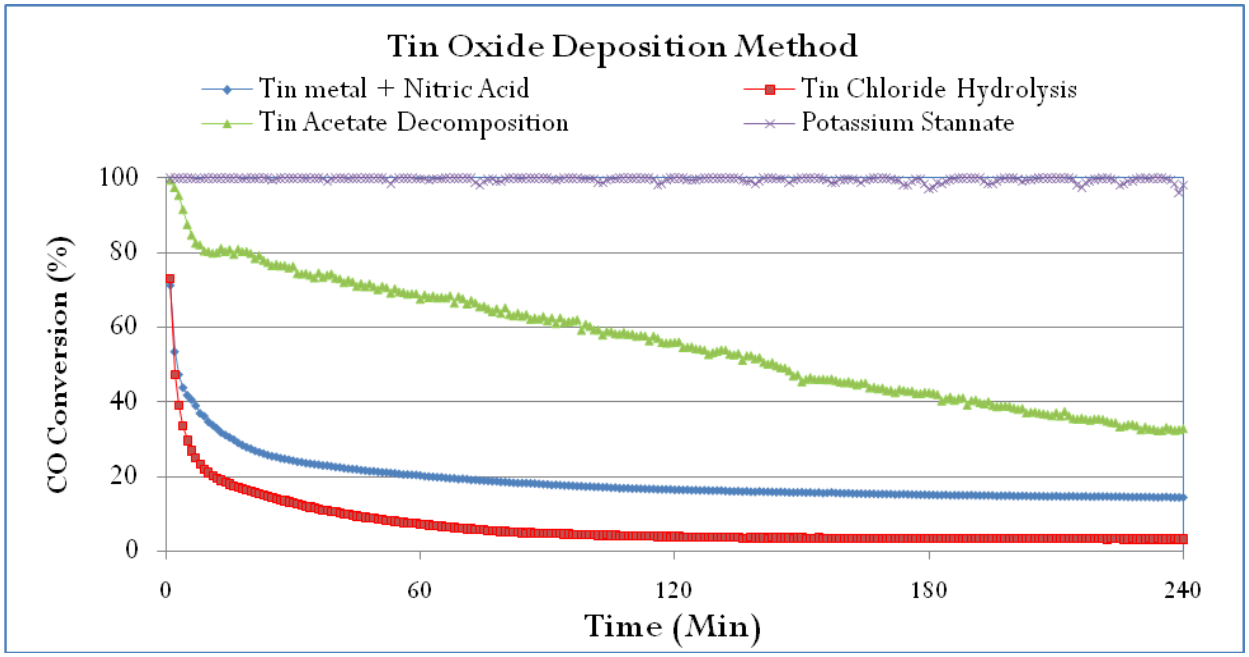

Figure IV.1. The Effect of Tin Oxide Deposition Method on Catalyst Performance

Test Conditions: Face velocity: 30 cm/sec; Humidity: 50% RH; Temperature: 25^{0}C; Particle size: 150-250µm; Reactor ID: 0.75"; Catalyst bed Ht: 3.5 mm; Inlet CO: 275ppm in air.

Tin oxide deposition method had a significant effect on the catalytic activity with catalyst prepared by deposition of tin oxide by the potassium stannate route performing better than other catalysts. The surface characterization by XRD revealed that the SnO_2 deposition had a significant impact on SnO_2 dispersion and deposition by the potassium stannate – sulfuric acid route yielded better SnO_2

dispersion. From the activity data, it could be said that the activity was directly proportional to SnO_2 dispersion, except for the tin chloride route, wherein the presence of chloride ions might have decreased activity. Even though deposition by tin acetate route yielded better Pt dispersion, the activity was less compared to potassium stannate route, indicating that the dispersion of SnO_2 was more important than Pt.

Table IV.1. Effect of SnO_2 Deposition Method on Activity, SnO_2 and Pt Dispersion

SnO_2 Deposition Method	**BET SA (m^2/g)**	**SnO_2 Crystallite Size (nm)**	**Pt Crystallite Size (nm)**	**Reaction Rate* (µmol/g·s)**
$K_2SnO_3 + H_2SO_4$ route	227	4.80	6.28	3.11
$Sn + HNO_3$ route	255	22.6	6.82	0.47
$SnCl_4$ + NaOH route	293	11.3	9.44	0.16
Tin Acetate	283	10.7	5.62	0.99

**Test Conditions: Face velocity: 30 cm/sec; Humidity: 50% RH; Temperature: 25^{0}C; Particle size: 150-250µm; Reactor ID: 0.75"; Catalyst bed Ht: 3.5 mm; Inlet CO: 275ppm in air.*

The preparation method by tin metal and nitric acid route was highly dependent on the size of tin powder and metastannic acid formed by reaction coated silica before decomposing to SnO_2. So it could not take advantage of SA of silica and yielded poor SnO2 dispersion, confirmed by XRD. The presence of excess chloride ions would always be an issue for preparation by tin chloride route. Preparation by tin acetate route produced second best catalyst. Tin acetate was an expensive precursor and the tin oxide dispersion obtained was very poor as well. So, SnO_2 deposition by the potassium stannate – sulfuric acid route was chosen as the preferred method and investigated in detail.

IV.3.2 Catalyst Support Selection

The effects of support were investigated by preparing 3.5%Pt-25%SnO_2/support catalysts on silica and alumina supports and were tested for CO activity and the activity results along with the surface characterization results are given in Table IV.2.

Table IV.2. **Effect of Support on Activity, SnO_2 and Pt Dispersion**

Support (3.5% Pt-25%SnO_2)	BET SA (m^2/g)	SnO_2 Crystallite Size XRD (nm)*	CO Chemisorption on Pt		Reaction Rate* (µmol/g·s)
			%D	Dp(nm)	
SiO_2	231	4.80	15.2	7.44	3.11
γ-$Al2O_3$	224	13.2	30.8	3.70	0.31

**Test Conditions: Face velocity: 30 cm/sec; Humidity: 50% RH; Temperature: 25^{0}C; Particle size: 150-250µm; Reactor: 0.75" ID; Catalyst bed Ht: 3.5 mm; Inlet CO: 275ppm in air.*

From the XRD analysis, it was observed that the tin oxide deposition on silica resulted in smaller SnO_2 crystallites (4.8nm) compared to the tin oxide deposition on γ-alumina (13.2nm). The similarity between the silica and tin oxide crystal structure could have resulted in a better dispersion of tin oxide on silica support in comparison with the alumina support. Pt dispersion however was better for alumina supported catalyst.

During this study, the pH of the Pt precursor solutions was in the range of 7-8, and the surface of silica was negatively charged with IEP of 1.7 – 3.5, whereas the surface of tin oxide promoter was neutral in charge with an IEP of 6.0 – 8.0 [78] and alumina was also neutral in charge with IEP of 6-8. The DADNP precursor resulted in a neutral Pt species. A neutral Pt species in the precursor solution would

have a weak interaction with silica surface. However, the presence of NH_4OH in the precursor solution would result in NH_4^+ ions in solution which would block the negatively charged silica surface. So the neutrally charged tin oxide surface (IEP: 6.0-8.0) would provide the anchoring sites for the neutral Pt species to weakly adsorb on the tin oxide surface. However, the deposition of Pt on alumina supported SnO_2 would be non-preferential and use of any Pt precursor would result in the same result as the IEP of SnO_2 and alumina were similar. Based on the IEP of the support and promoter and the precursors used, silica would result in close association of Pt-SnO_2 and would yield greater Pt-SnO_2 interfacial area. Although the Pt dispersion obtained by using alumina was better than that of silica supported catalyst, the location of Pt crystallites was important. If Pt crystallites were deposited on SnO_2, then only they would be highly active and the presence of Pt on support would not yield a highly active catalyst.

Silica supported catalyst was almost ten times as active as γ-alumina supported catalyst. Based on these experimental and characterization results, silica was selected as the preferred support for the tin oxide promoted Pt catalyst.

IV.3.3 Type of Silica Support Selection Study

Support structure could play a crucial role in determining the dispersion of promoter or active metal. In order to investigate the impact of silica support structure on the activity, four different silica types that had different SA, PV and APS (details in Table IV.3) were used to prepare 2.5%-25%SnO_2/SiO_2 catalysts. These catalysts were tested for CO activity at room temperature in the presence of moisture and the activity results are given in Table IV.3.

High SA support can provide greater number of nucleation sites, yielding better dispersion. However, higher SA supports have smaller pore openings and greater tortuosity, which decreases the

effective diffusivity of the reactants in the catalyst. The effective diffusivity of CO for all of the supports was estimated and is tabulated in Table IV.3.

Table IV.3. Effect of Type of Silica Support on Catalytic Activity and CO Effective Diffusivity

(2.5%-25%SnO_2/SiO_2) Silica Type	BET SA (m^2/g)	PV (cc/g)	Avg. Pore size (Å)	Reaction rate* (μmol/g/s)	Effective Diffusivity (x10^3) cm2/s
Merck 10180	750	0.66	40	0.15	1.23
Merck 60	500	0.80	60	0.30	1.81
Merck 10184	300	1.0	100	0.87	2.94
Davisil 645 + Davisil 644#	300	1.15	150	1.61	4.25

**Test Conditions: Face velocity: 30 cm/sec; 50% RH; 25^{0}C; Particle size: 63-200μm; Reactor: 0.75" ID; Catalyst bed Ht: 6.0 mm; Inlet CO: 250ppm in air; # Two supports mixed to get the required particle size.*

Initially, the mean free path of CO was calculated [79] and the mean free path for CO at room temperature is: 6.5×10^{-8} (in m). Since, for ($l/d_{pore} > 10$), the diffusion is mainly Knudsen diffusion[79], for supports with APS ≤ 60 Å, the diffusion was assumed to be Knudsen diffusion. For other supports, the diffusion was assumed to be a combined bulk and Knudsen diffusion. The Knudsen diffusion coefficient was estimated based on the APS of support [79], then the effective Knudsen diffusivity was estimated. Although, the tortuosity and particle porosity would be different for these supports, due to lack of experimental data, ($\tau = 3$), and ($\varepsilon_P = 0.6$) was assumed for all supports. The bulk diffusivity(D_B) was estimated using Chapman-Enskog kinetic theory [80]. The effective bulk diffusivity was estimated assuming the same tortuosity and porosity values for all the supports.

High SA supports could improve dispersion but decrease effective diffusivity; therefore, it was necessary to see the trade-off between the increase in dispersion and decrease in mass transfer rate to the active sites. From Table IV.3, it could be seen that the porous structure had a significant impact on effective diffusivity even with the assumption of equal tortuosity and porosity. Comparing the effective diffusivity values, the Davisil support (150 Å) had almost 3.5 times effective diffusivity that of Merck 10180 (40Å). By comparing the CO activity data, it could be concluded that the disadvantages of increase in mass transfer resistance outweighed the benefits of better dispersion.

The support pore size had a major impact on catalytic activity and supports with wider pores performed better due to better effective diffusivity of CO in those catalysts. Based on the experimental observations and estimated effective diffusivity values, the reaction was mostly diffusion controlled at room temperature.

Considering these observations, the silica support with high surface area and wider pore openings, Davisil 645 (SA: 300m^2/g; PV: 1.15 cc/g; APS: 150 Å) was selected for further studies.

IV.3.4 Effect of Tin Oxide Loading

CO oxidation on Pt/SnO_2 involved reaction between CO adsorbed on Pt and OH adsorbed on tin oxide and the interfacial Pt-SnO2 area provided active sites for CO oxidation [76]. In the case of SnO_2 promoted catalysts, Pt-SnO_2 area, SnO_2 dispersion and Pt dispersion would be a function of tin oxide loading. The effect of SnO_2 loading was studied by preparing catalysts with 5% Pt (w/w) differing only in the SnO_2 loading (5-30% w/w). The activity and surface characterization results are given in Table IV.4.

Increased SnO_2 loading significantly increased catalytic activity from 5% to 25% SnO_2 loading. However, further increase in the SnO_2 loading from 25% to 30% resulted in decreased catalytic activity.

The CO chemisorption results showed that there was no trend in Pt dispersion with respect to tin oxide loading. Pt crystallite sizes obtained were in the range of 6-7.5 nm for the catalysts studied.

Table IV.4. The Effect of Tin Oxide Loading on Catalytic Activity, SnO_2 and Pt Dispersion

Catalyst	BET SA (m^2/g) (No Pt)/(With Pt)	SnO_2 Crystallite Size (nm)	Pt %D	Reaction Rate*(µmol/g·s)
5% Pt – 5% SnO_2/SiO_2	(272)/(256)	3.2	18	0.91
5% Pt – 10% SnO_2/SiO_2	(269)/(250)	3.7	16	1.70
5% Pt – 15% SnO_2/SiO_2	(243)/(232)	3.9	17	2.98
5% Pt – 20% SnO_2/SiO_2	(240)/(231)	4.3	15	4.27
5% Pt – 25% SnO_2/SiO_2	(227)/(224)	4.8	16	5.43
5% Pt – 30% SnO_2/SiO_2	(204)/(199)	5.1	19	4.21

**Test Conditions: Humidity: 50% RH, Temperature: 25^{0}C, Reactor ID: ¾", Particle Size: 200 µm, Cat. Wt: 0.50g, (a) Face velocity: 45 cm/sec, CO Conc.: 400ppm in air*

XRD analysis indicated that increased tin oxide loading increased tin oxide crystallite size. Increasing SnO_2 loading from 20% to 30% increased crystallite size from 4.3nm to 5.1nm. Also, the BET SA analysis indicated that increased SnO_2 loading significantly decreased the SA of catalyst.

Increased SnO_2 loading from 5% to 25% certainly increased the Pt-SnO_2 interfacial area thereby improving the catalytic activity. However, further increase in the SnO_2 loading resulted in lower SnO_2 dispersion thereby lower Pt-SnO_2 interfacial area and lower activity. Also, increased SnO_2 loading resulted in lower SA and bigger SnO_2 crystallites would cause pore blocking and or pore narrowing, leading to decreased effective diffusivity. Thus, SnO_2 loading greater than 25% resulted in lower activity.

Considering these activity and surface characterization results, the optimum SnO_2 loading was in the range of 20-25% w/w for the Pt-SnO_2/SiO_2 catalyst.

IV.3.5 Effect of Drying Conditions during Tin Oxide Deposition

The effect of different drying conditions on activity was studied by preparing catalyst with same composition (5%Pt - 15%SnO_2/SiO_2) differing only in the drying conditions used during preparation. These catalysts were tested for CO oxidation activity and the activity results along with the surface characterization results are given in Table IV.5.

Table IV.5. **Effect of Drying Conditions on Catalytic Activity and SnO2 and Pt Dispersion**

Drying Conditions	BET SA (m^2/g)	SnO_2 Dp (nm)	Pt %D	Reaction Rate (µmol/g·s)*
VVV	286	ND	18	2.7
VVD	225	ND	20	2.8
VDV	239	ND	19	2.8
VDD	236	ND	18	2.7
DVV	171	4.1	19	1.1
DVD	193	4.3	20	1.0
DDV	217	4.4	19	0.2
DDD	223	4.6	20	0.1

**Test Conditions: Humidity: 50% RH, Temperature: 25^{0}C, Reactor ID: ¾", Particle Size: 200 µm, Cat. Wt: 0.50g, (a) Face velocity: 45 cm/sec, CO Conc.: 400ppm in air;*

The first drying step had a profound effect on the catalytic activity. When the first drying step was vacuum drying, the catalysts performed at least two times better than other catalysts. Estimated Pt dispersion values from CO chemisorption indicated that Pt dispersion was not affected by drying conditions used during SnO_2 deposition. XRD analysis indicated that initial drying step had a significant impact on SnO_2 dispersion and initial vacuum drying resulted in SnO_2 crystallites of less than 3 nm, whereas high temperature drying resulted in crystallites greater than 4 nm. BET SA analysis showed that the decrease in SA was significantly lower if first drying step was vacuum drying.

CO oxidation mechanism would involve reaction of adsorbed CO on Pt with either OH adsorbed on SnO_2 or lattice oxygen from SnO_2 adjacent to Pt. Greater SnO_2 SA would mean higher Pt-SnO_2 interfacial area for equivalent Pt loading and dispersion; therefore, resulting in better activity. From experimental and characterization results, the catalyst prepared by drying under vacuum for all steps during SnO_2 deposition outperformed all the other catalysts.

Therefore, the preferred method of drying during tin oxide deposition was chosen to be VVV method (all steps performed by vacuum drying at 40^0C for six hours).

IV.3.6 Effect of SnO_2/SiO_2 Calcination

Tin oxide could decorate Pt crystallites during Pt precursor calcination at 500^0C, which could affect the active surface area for CO oxidation. If SnO_2/SiO_2 was calcined prior to Pt deposition, the decoration of Pt crystallites could be avoided. In order to study the effect of SnO_2/SiO_2 calcination, four catalysts with same composition (3.5%Pt-25% SnO_2/SiO_2) differing only in the SnO_2/SiO_2 calcination temperature were prepared and the activity and surface characterization results are given in Table IV.6.

Increased SnO2/SiO2 calcination temperature improved catalytic activity. The Pt precursor was calcined at 500°C. The catalyst prepared by calcining SnO_2/SiO_2 at a temperature (600°C) greater than

the Pt precursor calcination temperature resulted in the highest activity. As expected, the XRD results showed the negative effect of high temperature calcination on SnO_2 dispersion.

Table IV.6. Effect of SnO_2/SiO_2 Calcination on Catalytic Activity and SnO_2 and Pt Dispersion

SnO_2/SiO_2 Calcination Temperature	SnO_2 Dp (nm)#	CO Chemisorption on Pt @ 30^0C			Reaction Rate* (µmol/g·s)
		SA(m^2/g)	%D	Dp(nm)	
40^0C	ND	1.25	16.9	6.69	3.05
125^0C	4.1	1.38	18.6	6.06	3.22
400^0C	4.5	1.4	18.8	6.02	3.67
600^0C	5.0	1.39	18.9	5.98	4.69

**Test Conditions: Humidity: 50% RH, Temperature: 25^0C, Reactor ID: ¾", Particle Size: 200 µm, Cat. Wt: 0.50g, Face velocity: 30 cm/sec, CO Conc.: 500ppm in air; #XRD analysis prior to Pt deposition*

However, the most interesting results were the estimate Pt dispersion values from CO chemisorption, which showed improved Pt dispersion with increased SnO_2/SiO_2 calcination temperature. Therefore, the characterization and experimental results qualitatively proved the decoration of Pt crystallites by SnO_2 during Pt precursor calcination. When SnO_2 was calcined at higher temperature, the structural stability minimized decoration of Pt during Pt precursor calcination.

Therefore, calcination of SnO_2/SiO_2 at a temperature higher than Pt precursor calcination temperature resulted in better Pt dispersion and better activity due to minimized Pt decoration by SnO_2.

IV.3.7 Platinum Precursor Selection Study

The nature of precursor (acidic or basic) and the nature of support play crucial role in determining the dispersion as well as distribution profile of the active metal (oxide) in the catalyst. The Pt precursor can affect the catalytic activity mainly in three ways: (a) Pt dispersion; (b) block or inhibit

access to the active sites by formation of strongly adsorbed residual surface species, e.g. chloride ions adsorbed on the support; and (c) dictating the metal distribution profile on the support, via the interaction with the support (tin oxide on silica). During this study, the effect of Pt precursor on Pt dispersion and activity was studied by preparing 5%Pt – 25%SnO_2/SiO_2 catalysts using four different Pt precursors as mentioned earlier. These catalysts were then tested for CO oxidation activity and the results are given in Table IV.7.

Table IV.7. Effect of Pt Precursor and Calcination Temperature on Catalytic Activity

Catalyst: 5%Pt – 25%SnO_2/SiO_2 Pt Precursor	**Rate of Reaction (µmol/g/s)**				**Pt (%D)****	**TOF (x100)**
	300°C	**400°C**	**500°C**	**600°C**		
Chloroplatinic Acid	**0.21**	0.13	0.10	0.08	14.2	0.58
Tetraammine platinum hydroxide (TAPH)	0.45	0.58	**0.66**	0.52	16.9	1.51
Tetraammine platinum nitrate (TAPN)	0.47	0.52	**0.94**	0.84	18.8	1.91
Diammine dinitro platinum (DADNP)	2.62	2.76	**3.62**	1.81	19.3	4.36

**Estimated Pt Dispersion from CO chemisorption for best performing catalyst of every Pt precursor

**Test Conditions: Humidity: 50% RH, Temperature: 25^{0}C, Reactor ID: ¾", Particle Size: 200 µm, Cat. Wt: 0.80g, Face velocity: 45 cm/sec, CO Conc.: 400ppm in air;*

Catalysts prepared with DADNP precursor outperformed all the other catalysts. Comparing the estimated Pt dispersion values, the catalysts prepared using DADNP and TAPN resulted in better Pt dispersion compared to other catalysts. Also, the TOF for catalyst prepared by DADNP was significantly greater.

Use of chloroplantinic acid yielded the least active catalyst, probably due to presence of PtO_xCl_y surface species on the catalyst. Since no reduction of catalyst samples was performed to activity

measurement, the PtO_xCl_y species might have resulted in less activity. TAPH and TAPN have been reported to form PtO_x species during calcination which may result in lower activity. During CO chemisorption, the pretreatment steps would reduce those PtOx species, so the impact of PtOx could only be seen from the experimental activity results. However, the huge difference in the activity of the catalysts prepared using TAPN and DADNP was not clear from CO chemisorption results.

The difference in the activity could be explained based on the interaction of these precursors with either SnO_2 or SiO_2. The effect of type of Pt precursor on Pt dispersion has been studied extensively [81-86]. The support characteristics, specifically iso – electric point (IEP) of the support, and the ionic species formed by the Pt precursor would determine the type of interaction (repulsive, attractive, and neutral) between the support and the Pt precursor [87]. If the pH of the precursor solution is below the IEP of the support then the anionic species of the precursor could easily chemisorb on the support surfaces with a positive charge. In contrast, cationic species easily chemisorb on the support surfaces with a negative charge if the pH of the precursor solution is over the IEP of the support [87]. In the case of Pt/SiO_2 catalysts, it has been reported that the nature of the ionic species of the Pt precursor played a crucial role in the final dispersion of the Pt on the silica support [86].

During this study, the pH of the non-chlorinated Pt precursor solutions was in the range of 7-8, and the surface of silica was negatively charged with IEP of 1.7 – 3.5, whereas the surface of tin oxide promoter was neutral in charge with an IEP of 6.0 – 8.0 [78]. Among the Pt precursors used, TAPH ($(NH3)_4Pt^+$) and TAPN ($(NH3)_4Pt^+$) had positively charged ionic species, whereas the DADNP precursor resulted in a neutral Pt species. So, in the case of the TAPH and the TAPN precursors, a strong interaction would exist between the metal cation in the Pt precursor solution and the negatively charged silica surface. In the case of DADNP, a neutral Pt species in the precursor solution would have a

weak interaction with silica surface. However the neutrally charged tin oxide surface (IEP: 6.0-8.0) could have provided the anchoring sites for the neutral Pt species to weakly adsorb on the tin oxide surface.

Based on the IEP of the support and promoter and the precursors used, DADNP would result in close association of Pt-SnO2 and would yield greater Pt-SnO2 interfacial area. Although the Pt dispersion obtained by using DADNP and TAPN was almost similar, the location of Pt crystallites was crucial in determining the activity of the catalysts. If Pt crystallites were deposited on SnO_2, then only they would be highly active and the presence of Pt on support would not yield a highly active catalyst.

In other words, the better Pt dispersion obtained for the DADNP precursor could be a result of the Pt deposition not only on the silica but also on tin oxide. In the case of the chloroplatinic acid precursor, the pH of the impregnating solution was in the range of 5-6, and the precursor resulted in a negatively charged ionic species $(PtCl_6)^{2-}$. Therefore there was no strong interaction between the Pt species with either the silica or ceria, resulting in a poor Pt dispersion.

Based on these experimental results, it was concluded that the neutral charged DANDP precursor yielded the best performing catalyst in the case of tin oxide promoted Pt catalysts and was chosen as the preferred Pt precursor.

IV.3.8 Selection of Pt Precursor Calcination Conditions

The calcination process has three important variables, namely: (a) calcination temperature, (b) calcination time, and (c) calcination atmosphere. During this study, the effect of these various calcination process conditions was studied experimentally and an effort has been made to correlate the activity of the catalysts to the surface characterization.

IV.3.8.1 Effect of Calcination Temperature

The activity results for the effect of calcination temperature of different Pt precursors are given in Table IV.7. The composition of the catalyst was maintained at 5%Pt – 25%SnO_2/SiO_2. As seen from the activity data and explained earlier, the catalysts prepared by using DADNP precursor resulted in greater activity. Therefore, the effect of calcination temperature on the Pt dispersion was studied only for the catalysts prepared by DADNP precursor. The results of CO chemisorption are given in Table IV.8.

In the case of the catalysts prepared using chloroplatinic acid as precursor, the activity decreased with increased calcination temperature. For the non-chlorinated Pt precursors such as TAPH, TAPN, and DADNP a volcano type of profile was obtained for catalytic activity with respect to calcination temperature. The catalytic activity increased with increased calcination temperature from 300°C to 500°C and further increase in the calcination temperature resulted in decreased activity.

Table IV.8. **Effect of Pt Precursor Calcination Temperature on Activity and Pt Dispersion**

Calcination Temperature	CO Chemisorption at 30^0C			Rate of Reaction (µmol/g/s)*
	SA (m^2/g)	%D	Dp (nm)	
300^0C	1.56	21.1	5.38	2.62
400^0C	1.47	19.8	5.71	2.76
500^0C	1.39	18.8	6.02	3.62
600^0C	1.13	15.4	7.36	1.81

**Test Conditions: Humidity: 50% RH, Temperature: 25^0C, Reactor ID: ¾", Particle Size: 200 µm, Cat. Wt: 0.80g, Face velocity: 45 cm/sec, CO Conc.: 400ppm in air;*

As expected, the Pt dispersion decreased with increased calcination temperature. Reduction in the Pt dispersion could be explained by two factors: (a) surface diffusion of Pt to form bigger crystallites, and (b) decoration of Pt crystallites by SnO_2. If the reduction in dispersion was caused by surface

diffusion of Pt, then the overall active surface area would be lower resulting in lower catalytic activity. If however, the reduction in Pt dispersion was caused by the decoration of Pt by SnO_2, the Pt-SnO_2 interfacial area would increase, believed to be responsible for activity, thus resulting in greater activity.

The catalytic activity increased with increased calcination temperature till 500°C, which was most probably a result of decoration of Pt crystallites by tin oxide. However, calcination at 600°C probably reduced Pt dispersion by surface diffusion of Pt, thereby reducing the overall active SA and thus resulting in lower activity.

Therefore, a trade-off existed between the decoration of Pt by SnO2 and surface diffusion of Pt with respect to temperature and these two factors had opposing effects on activity. The balance of these two factors resulted in a peak activity at 500°C. Therefore, calcination temperature of 500^0C was selected for further studies.

IV.3.8.2 Effect of Calcination Time & Calcination Atmosphere

Both the decoration of Pt with SnO2 and surface diffusion of Pt to form bigger crystallites are functions of calcination temperature and calcination time. Therefore, the time of calcination would have a great impact on the final metal dispersion and ultimately the catalytic activity. During this study, the effect of calcination time on activity of the catalyst (5%Pt – 25%SnO_2/SiO_2) was studied by varying the calcination time (1,2,3 and 6 hrs) during catalyst preparation. These catalysts were tested for CO oxidation activity and the activity and surface characterization results are given in Table IV.9

As expected, the Pt dispersion decreased with increased calcination time. Impact on Pt dispersion was quite significant. However, the catalytic activity showed a volcano profile with respect to calcination time similar to that of calcination temperature and the activity was optimum at calcination time of 3 hours.

Table IV.9. Effect of Calcination Time on Catalytic Activity and Pt Dispersion

Calcination Time	CO Chemisorption at 30^0C			Rate of Reaction (µmol/g/s)
	SA (m^2/g)	%D	Dp (nm)	
One hour	1.79	24.2	4.67	1.13
Two hours	1.37	18.5	6.12	1.23
Three hours	1.33	18.0	6.29	1.57
Six hours	1.23	16.6	6.82	0.63

Test Conditions: Humidity: 50% RH, Temperature: 25^{0}C, Reactor ID: ¾", Particle Size: 200 µm, Cat. Wt: 0.80g, Face velocity: 30 cm/sec, CO Conc.: 250ppm in air;

The volcano type of activity profile could be explained on the similar lines of calcination temperature effect. Lower calcination time would result in lesser decoration of Pt by SnO_2 and higher calcination times would result in significant decoration. Also, there would be an optimum value for the extent of Pt decoration, as less decoration would yield lower Pt-SnO_2 area and greater decoration would yield significantly lower Pt SA. The initial increase in the activity with increased calcination time was probably due to formation of Pt-SnO_2 active sites due to decoration of Pt crystallites by SnO_2. However, increase in the calcination time after three hours may have resulted in over-decorated Pt crystallites resulting in lower Pt SA and thus lower activity.

Therefore, calcination time of 3 hours was chosen for the DADNP precursor.

The effect of calcination atmosphere on the catalytic activity was studied by varying the calcination atmosphere during the DADNP precursor calcination. The different calcination atmospheres

used for this study were: (a) air, (b) humid air, (c) inert gas (N_2), and (d) no flow condition. Other preparation conditions were maintained the same during catalyst (5%Pt – 25%SnO_2/SiO_2) preparation. When these catalysts were tested for CO oxidation activity, no significant effect of the calcination atmosphere was observed on the catalytic activity. Catalysts calcined in humid air; however, yielded poor activity (rate: 1.4 μmol/g.s) compared to catalysts calcined in air (rate: 1.6 μmol/g.s).

Therefore no further investigation was done and calcination in air was chosen for preparation.

IV.3.9 Effect of Platinum Precursor Drying Condition

The drying conditions used during preparation are critical in determining the dispersion and distribution of the precursor salt on the support. During the drying step, the solvent is evaporated and the remaining precursor salt from the impregnating solution crystallizes to form crystallites on the support. These salts on thermal treatment yield the active metal/metal oxide on the support; therefore, the crystallite size of the precursor salt is important. During drying step, the surface area of the support and the concentration of the precursor salt would determine the nucleation and the crystallization rates. This ratio of nucleation of the precursor crystallites and growth rate of these crystallites would ultimately determine the crystallite size of the precursor salt and that of the final active metal/ metal oxide in the catalyst [88]. If the surface area is greater, the rate of nucleation would be greater and the crystallite size would be smaller. The drying conditions used would affect the rate of nucleation as well as the rate of crystal growth. Therefore, the rate of drying is crucial in determining the dispersion in the catalyst.

The precursor could interact with the support in mainly three ways: (a) strong interaction, (b) weak interaction and (c) no interaction – neutral. Based on the type of interaction that exists between the precursor and the support, the adsorption equilibrium could change. [89]. The impact of drying

conditions is greater when the interaction between the solute and support is weak or when the concentration of the precursor is high [89].

The drying rate used during the precursor drying could be classified into three main categories, namely: (a) constant, (b) falling or (c) accelerated. During the evaporation of the solvent, the solvent vapors are transported to the opening of the pores in the support and the remaining solution would also get transported to the interiors, so there are two transport processes that are occurring simultaneously, namely: (a) solution transport and (b) solvent vapor transport. The solvent vapor transport is characterized by two processes: (a) capillary flow and (b) solvent vapor diffusion [90-92]. Depending on the rate of drying used and the type of interaction that exists between the precursor and the support, two possible conditions might exist, namely: (a) fast drying and (b) slow drying. During fast drying, the rate of vapor diffusion is much faster than the capillary flow; therefore, the evaporation is continuous. During slow drying, the capillary flow is faster than the vapor removal; therefore, the evaporation takes place initially at the external surface and then moves inward in a discontinuous manner [90]. The solution transport is mainly governed by the pore size and pore size distribution of the catalyst support. When the solvent is evaporated, the remaining solution has increased precursor salt concentration, therefore concentration gradients get created within the solution inside the pores [90]. Obviously due to the concentration gradients, the diffusion of the precursor salts would take place. Depending on the rate of diffusion and the rate of solvent removal, the crystallization process of the precursor salt would get affected [90]. This process of solute diffusion and solvent removal would also dictate the crystallite size and crystallite distribution inside the pores.

For a catalyst, the active metal distribution within the catalyst could be mainly visualized as one of the four profiles: (a) homogeneous, (b) egg-shell, (c) egg-white, and (d) egg-yolk. These four profiles are shown in Figure IV.2 [93, 94]. This active metal distribution profile is a function of drying conditions.

As stated above, since the rate of drying depending on the interaction between the solute-support and rates of drying would eventually determine the crystallite size and crystallite distribution on the support, and these crystallites on calcination would yield the active metal/metal oxide.

For a system with weak interaction between the solute-support a faster drying rate would essentially result in a profile that is somewhat similar to egg-shell profile [93]. However, if the drying rate is slow, then a distribution profile close to the homogeneous profile could be obtained. On the other hand for the systems with a strong interaction between the precursor and the support, the drying rate has negligible effect on the metal distribution profile [93]. However, the effect was pronounced in systems with weaker interactions [95].

Based on the above discussion on the effect of drying condition on the metal distribution, briefly there are two important factors [96]: (a) type of interaction between the precursor and the support, and (b) rate of drying. In the case of strong interaction between the support and the precursor, the rate of drying does not affect the active metal distribution as long as the precursor concentration is not high. In the case of weak interaction; however, the rate of drying strongly impacts the final catalyst distribution in the catalyst, as follows: (a) faster drying rate yields egg-shell profiles, (b) slower drying rate yield homogeneous profiles [95].

Figure IV.2. Metal Distribution Profiles within a Support

During this study, three different drying rates were considered, drying at room temperature under vacuum, drying overnight at 100^{0}C, and drying at 125^{0}C for 4 hours. These catalysts were tested for CO activity and the results are shown in Figure IV.3.

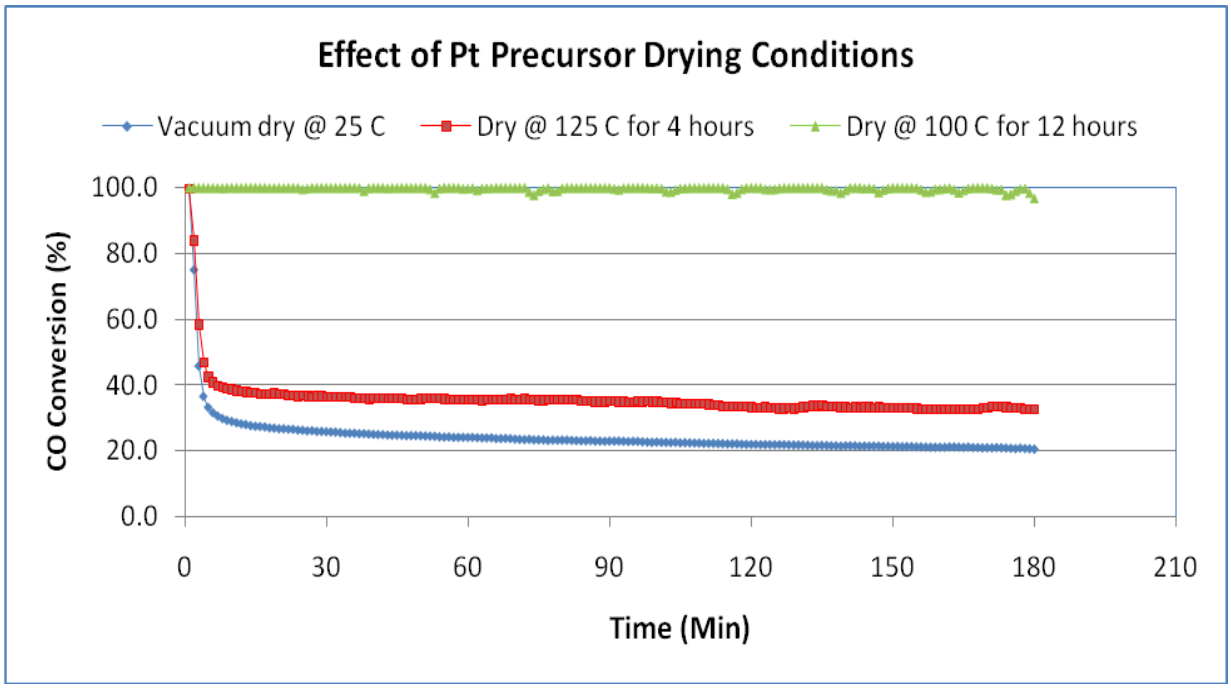

Figure IV.3. Effect of Pt Precursor Drying Condition on Catalytic Activity

Test Conditions: Face velocity: 30 cm/sec; Humidity: 50% RH; Temperature: 25^{0}C; Particle size: 150-250µm; Reactor: 0.75" ID; Catalyst bed Ht: 3.5 mm; Inlet CO: 275ppm in air

The catalyst dried at 100^{0}C overnight performed the best. It could be said that the resulting metal profile within the support might be somewhere between egg-shell and homogeneous. It should also be noted that the drying rate had a major impact during the tin oxide deposition as well. Further, since the mechanism demands presence of tin oxide and platinum active sites adjacent to each other, it would be possible that during the tin oxide deposition process, there was a homogeneous distribution profile of tin oxide on silica support, whereas during the platinum deposition process, the profile could either be egg-shell, homogeneous, or egg-white. The suitable metal profile would also depend on the

type of reaction, in other words, if the reaction is diffusion controlled, then an egg-shell profile would be preferred, whereas for a reaction-controlled process, a homogeneous profile is more suitable. In this case, as it would be discussed in subsequent chapters, the reaction being diffusion controlled, an egg-shell or an egg-white profile would be preferred.

Additionally, the drying rate would have an impact on Pt dispersion as well, for example, a homogeneous metal profile would result in better dispersion compared to egg-shell profile, as the number of nucleation sites is greater in homogeneous profile, and the crystallite size would be smaller. The estimated Pt dispersion values from CO chemisorption are given in Table IV.10. The drying conditions indeed had an impact on the Pt dispersion. The high temperature drying (drying at 125^0C for four hours) resulted in poor Pt dispersion compared to drying at lower temperatures.

Table IV.10. Effect of Pt Precursor Drying Conditions on Catalytic Activity and Pt Dispersion

Drying Condition	Pt SA (m^2/g)	Pt (%D)	Pt Dp (nm)	Rate of Reaction* (µmol/g/s)
Vacuum Dry, T: 25^0C	1.61	21.7	5.21	0.621
T: 100°C; 12 hours	1.67	22.4	5.04	3.11
T: 125°C; 4 hours	1.20	15.4	7.29	0.99

**Test Conditions: Face velocity: 30 cm/sec; Humidity: 50% RH; Temperature: 25^0C; Particle size: 150-250µm; Reactor: 0.75" ID; Catalyst bed Ht: 3.5 mm; Inlet CO: 275ppm in air*

The difference in the Pt dispersions for the catalysts prepared by vacuum drying and drying at 100^0C for 12 hours was within the instrumentation error range (2%). So, the effect of drying conditions was mainly on the distribution profile on Pt on the catalyst. Since DADNP precursor had weak interaction with SnO2 as explained before, drying at higher temperature could have resulted in egg-shell profile yielding poor Pt dispersion.

Consequently, drying at vacuum drying at 25° would result in close to homogeneous distribution of Pt and intermediate drying rates like drying at 100°C would result in distribution profiles that are close to egg-white or close to egg-shell. Not only the Pt dispersion but the SnO_2 location was also important. Considering the amount of SnO_2 loaded (25%) and the crystallite sizes obtained by XRD (<4nm), the SnO_2 could be assumed to have a close to homogeneous profile. If the Pt distribution were to be egg-shell then the Pt-SnO_2 interfacial area would be lower. Although a homogeneous profile of Pt would be favorable for Pt-SnO_2 interfacial area, the reaction being diffusion controlled would result in lesser amount of Pt utilization. Therefore, the drying condition at 100°C would balance the trade-off between the Pt-SnO_2 interfacial area and Pt utilization due to diffusion controlled reaction.

So, the Pt precursor drying condition was selected as drying at 100^0C for 12 hours.

IV.3.10 Effect of Pt Loading

Increased Pt loading would increase Pt SA and would obviously result in highly active catalyst; however, increased Pt loading would also cause decreased Pt dispersion. So a trade-off exists between the crystallite size and active surface area. During this study, the effect of Pt loading was investigated by preparing the catalyst (X% Pt – 25%SnO_2/SiO_2) by maintaining same preparation conditions. The activity results and the CO chemisorption results for these catalysts are given in Table IV.11.

The activity increased with increasing Pt loading till Pt loading of 5 wt% and further increase in the Pt loading resulted in declined catalytic activity. From the CO chemisorption results it was observed that the Pt dispersion decreased with increased Pt loading. The decrease in the Pt dispersion was quite significant (D: 51% (1.25% Pt); D: 12% (7.5% Pt)). From TOF values, it could be seen that the activity was not directly proportional to Pt SA. Increased Pt loading would improve the Pt-SnO2 interfacial area which was responsible for CO activity. Also, lower Pt loading may have resulted in lower activity due to

CO poisoning, as the reaction was conducted in a close to differential reactor, so as to get accurate TOF values. It was found out that the increase in Platinum loading after 5% caused a significant decrease in the dispersion of Pt and decrease in the catalytic activity per Pt atom.

Table IV.11. Effect of Pt Loading on Catalytic Activity and Pt Dispersion

Pt (w/w)	Pt SA (m^2/g)	Pt %D	Pt Dp (nm)	TOF (x100)	Rate of Reaction (µmol/g/s)*
1.25%	1.59	51.7	2.19	4.09	1.32
2.5%	1.95	31.6	3.58	5.63	2.25
3.75%	2.26	24.4	4.64	6.59	3.01
5.00%	2.29	18.5	6.11	7.18	3.45
7.50%	2.28	12.4	9.14	6.60	3.12

**Test Conditions: Face velocity: 45 cm/sec; Humidity: 50% RH; Temperature: 25^{0}C; Particle size: 150-250µm; Reactor: 0.75" ID; Catalyst bed Ht: 3.0 mm (inert: 66%); Inlet CO: 500ppm in air*

Therefore, Pt loading of 3.75% to 5.0% was chosen to be optimum for Pt-SnO_2/SiO_2 catalysts.

IV.3.11 Effect of Hydrogen Reduction

During the Pt precursor calcination, there was a possibility of formation of PtOx species; therefore, the effect of hydrogen reduction on catalytic activity was investigated. The catalyst (3% Pt – 25%SnO_2/SiO_2) was subjected to H_2 reduction (H_2: 30% v/v, in N_2) at two different temperatures 150^{0}C and 200^{0}C (reduction temperature had to be below 250^{0}C, otherwise reduction of SnO2 to Sn was possible). The resulting catalysts were tested for CO activity.

When compared with un-reduced catalyst (rate: 2.18 µmol/g.s), no effect of H_2 reduction was observed on the CO activity (rate: 2.20 µmol/g.s). Either the amount of PtOx formed was insignificant or the H2 reduction temperature was insufficient to reduce those PtOx species.

IV.3.12 Bimetallic Noble Metal Catalysts Promoted with Tin Oxide

In order to investigate the possibility of optimizing the cost of catalyst, the possibility of substituting Pt with Pd or Ru in part or completely was investigated. For the preparation of Pt-Ru bimetallic catalysts acetyl acetonate salts of Pt and Ru were used and for the preparation of Pt – Pd bimetallic catalysts, di – ammine dintro salts of Pt and Pd were used.

IV.3.12.1 Pt-Ru Catalyst Promoted with Tin Oxide

The Pt – Ru catalysts were prepared by co – impregnation method. The SnO_2/SiO_2 was prepared by potassium stannate route with all the drying steps carried out under vacuum at 40°C. The resulting SnO_2/SiO_2 was not calcined at 600°C, because Pt-acac and Ru-acac precursors were calcined at 160°C. The SnO_2/SiO_2 was impregnated with Pt-acac and/or Ru-acac precursor solution in toluene followed by vacuum drying at 40°C followed by calcination at 160°C for 2 hours in air. Depending on the desired loading of Pt and Ru *(Pt: Ru = 5:2.5; 5:5; all in w/w%)*, the Pt-acac and Ru-acac solution in Toluene was prepared for impregnation. The catalysts such prepared were tested for the CO oxidation activity at room temperature and the results are given in Table IV.12.

Table IV.12. SiO_2 Supported Pt-Ru Catalysts Promoted with SnO_2 for CO Oxidation

Catalyst	**CO Conversion (%)***
5% Pt – 25% SnO_2-SiO_2 – DADNP Precursor method*	99.0
5% Pt – 2.5% Ru – 25% SnO_2-SiO_2	60.0
5% Pt – 5% Ru – 25% SnO_2-SiO_2	50.0

**Test Conditions: Face velocity: 30 cm/sec; Humidity: 50% RH; Temperature: 25^0C; Particle size: 150-250µm; Reactor: 0.75" ID; Catalyst bed Ht: 3.5 mm; Inlet CO: 250ppm in air*

The bimetallic catalysts, Pt – Ru, performed poorly in comparison with the Pt-SnO_2/SiO_2 catalyst prepared by the DADNP precursor method. Co-impregnation could result in Pt-Ru species which might not be active for CO oxidation, thereby decreasing the overall utilization of Pt. As seen from the results, increased Ru content decreased activity even though the amount of Pt was the same. Further, the preparation procedure demanded the use of Pt-acac and Ru-acac solution which had low solubility and required greater number of impregnation cycles. For example, to get 5 wt% loading of Pt total of 10 impregnation cycles were carried out and for 2.5% Pt-2.5% Ru, total of 5 impregnation cycles were carried out. Considering the performance of the catalyst as well as the difficulty in preparation, the Pt-Ru based bimetallic catalysts were not pursued further.

IV.3.12.2 Pt-Pd Catalyst Promoted with Tin Oxide

The Pt – Pd catalysts were prepared by co – impregnation. The SnO_2/SiO_2 was prepared by potassium stannate route with all the drying steps carried out under vacuum at 40°C. The resulting SnO_2/SiO_2 was calcined at 600^0C for two hours. Noble metal deposition was carried out by co-impregnation of diammine dinitro Pt(II) and/or diammine dinitro Pd(II) precursor followed by drying at 100^0C for 12 hours and calcination at 500^0C for 3 hours. Bimetallic catalysts (Pt:Pd = 4:0; 0:4; 4:4; 4:2; 2:4; 2:2 (% w/w)) were prepared and tested for CO oxidation and the results are shown in Figure IV.4.

The CO activity results showed that the catalyst containing only Pt outperformed all the other catalysts. Palladium based catalyst did not show much activity (10% CO conversion). It was also observed that the addition of Pd had a negative impact on the catalytic activity. For example, addition of 2% Pd to 4% Pt catalyst reduced the catalytic activity of the Pt catalyst from 80% CO conversion to 66% CO conversion from Figure IV.4.

Formation of Pt-Pd surface species might have resulted in lower catalytic activity.

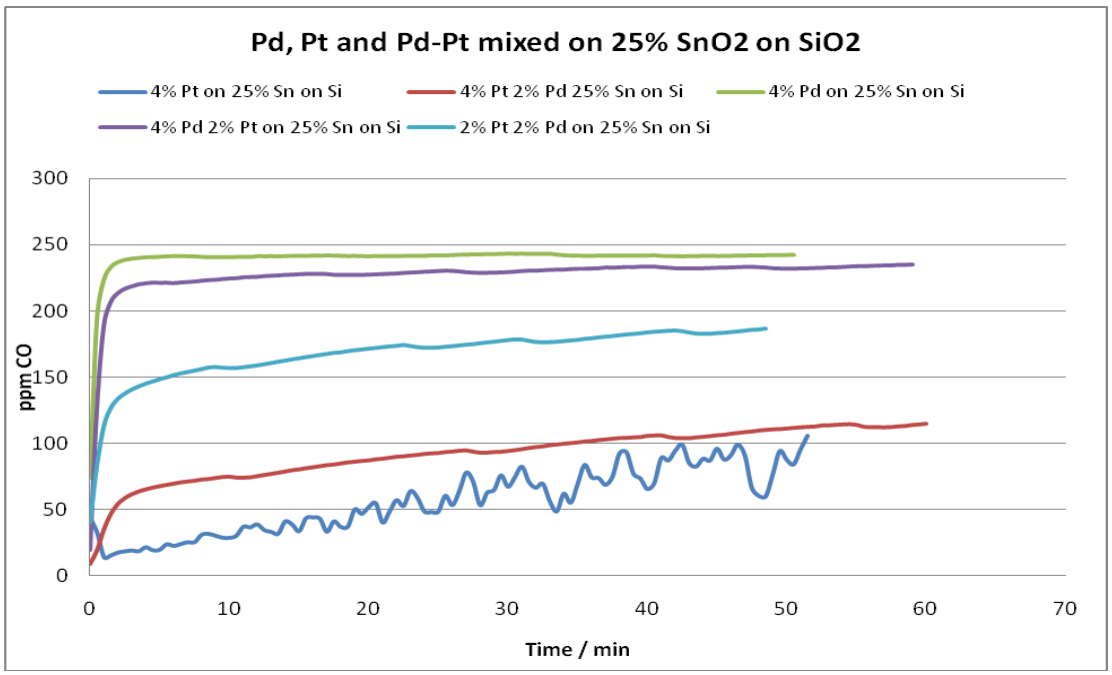

Figure IV.4. Activity of Silica Supported Pt-Pd catalysts Promoted with SnO_2

Test Conditions: Face velocity: 30 cm/sec; Humidity: 50% RH; Temperature: 25^{0}C; Particle size: 150-250µm; Reactor: 0.75" ID; Catalyst bed Ht: 2.0 mm; Inlet CO: 300ppm in air

Therefore, it was concluded that bimetallic catalysts on tin oxide/silica were not as active as the Pt based catalyst for CO oxidation at room temperature in the presence of moisture.

IV.3.13 Effect of Operating Conditions

CO oxidation reaction is a well-known example of a reaction exhibiting non – linear kinetics. Operating conditions such as temperature, water vapor content, CO concentration, and catalyst bed depth have a great impact on the catalyst activity. These effects of operating conditions on Pt – SnO_2/SiO_2 catalyst were investigated.

From the silica support selection studies it was concluded that the reaction was diffusion controlled on Pt-SnO2/SiO2 catalyst. Therefore the effect of particle size on activity was investigated.

IV.3.13.1 Particle Size Effect

In order to investigate whether CO oxidation on 5%Pt-25%SnO_2/ SiO_2 catalyst was diffusion controlled or reaction controlled, impact of catalyst particle size was studied. To minimize batch variations in catalyst preparation, catalyst was prepared with a larger particle size and the particles were crushed and sieved to obtain required particle sizes. The activity results are given in Figure IV.5.

The reaction was significantly diffusion limited, for example, when the particle size was decreased from 1000 micron to 100 micron the reaction rate increased by more than two times. The reactor was operated in integral mode in order to get non-zero reaction rates for larger particles. Since the reactor was operated in integral mode, when the change in CO conversion was 2 times, the change in actual kinetics would definitely be more than double.

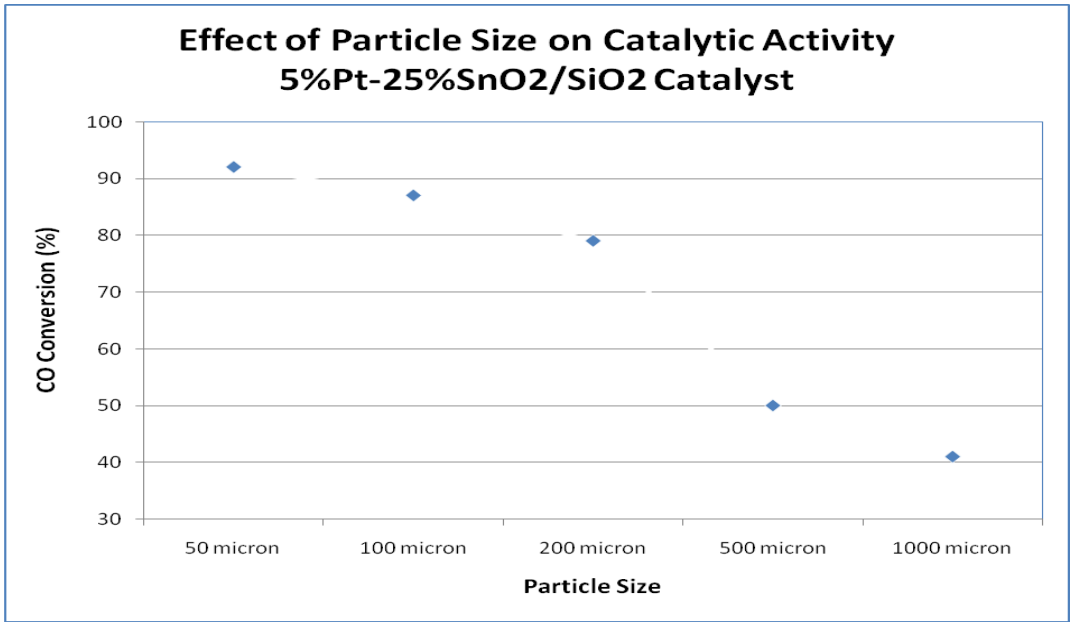

Figure IV.5. Effect of Particle Size on Catalytic Activity of 5%Pt-25%SnO_2/SiO_2 Catalyst

Test Conditions: Face velocity: 45 cm/sec; Humidity: 50% RH; Temperature: 25^{0}C; Reactor: 0.75" ID; Catalyst bed Ht: 6.0 mm; Inlet CO concentration: 750ppm

The reaction was diffusion controlled at room temperature and optimum utilization of Pt would demand use of smaller catalyst particles. However, considering the application requirement of low pressure drop, it was concluded that a particle size of 150-250 micron would be optimum from pressure drop as well as performance point of view.

IV.3.14 Effect of Catalyst Bed Depth

If a reaction is carried out in an integral reactor mode, any increase in the bed depth would correspond to increase in conversion governed by reaction kinetics, as long as the bed depth satisfies the criteria for negligible dispersion/ channeling (i.e. bed depth > 10*dp). However, in case of reactions governed by non – linear kinetics, any slight positive change in catalyst bed depth could give rise to a significant increase in conversion. The effect of bed depth on CO conversion was studied for two bed thickness of 4mm and 5mm. The results are given in Figure IV.6.

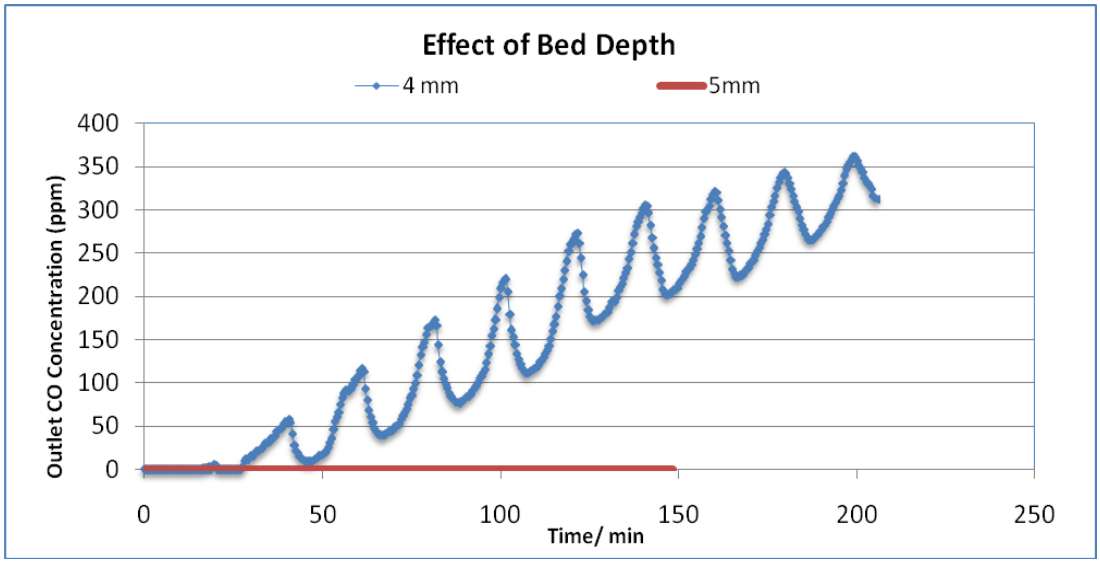

Figure IV.6. Effect of Bed Depth on Catalytic Activity – Pt-SnO_2/SiO_2 Catalyst

Test Conditions: Face velocity: 30 cm/sec; Humidity: 50% RH; Temperature: 25^{0}C; Particle size: 150-250µm; Reactor: 0.375" ID; Inlet CO concentration: 500ppm

The non – linear kinetics of CO oxidation was clearly evident from the effect of bed depth. An increase of bed depth by 25% caused the CO conversion to change from less than 50% to more than 99%. The oscillatory behavior as seen from Figure IV.6 was a common feature of the Pt-SnO_2/SiO_2 catalyst, when the catalyst was not either at the upper steady state or the lower steady state. When the catalyst bed was ignited as seen in the case of a 5mm bed, the catalyst would be in the upper steady state and would not show any oscillations, on the other hand if the catalyst was fully extinct and showing no conversion, having in the lower steady state, then the catalyst would not show oscillations. It was only when the catalyst would be in the meta-stable steady states that the catalyst would show oscillatory behavior.

The significant change in activity by a small increase in the catalyst bed thickness could not be explained by plug-flow reactor model even by using non-linear kinetic model. However, this behavior could be explained by means of possible heat and mass transfer effects in the catalyst bed. Along the length of the bed the CO concentration would go down and temperature would go up due to energy released from CO adsorption or reaction. Then heat transfer from the back of the bed to the front of the bed, in opposite direction of gas flow, would cause the entire catalyst bed to be active. If the last few particle layers were not active then the amount of heat released would be lower as the activity would be lower. Therefore the extent of the bed that would be active would also be lower.

Therefore, 5mm catalyst bed performed better in comparison with the 4mm catalyst bed.

IV.3.14.1 Effect of Face Velocity

With increase in face velocity, the heat transfer and mass transfer coefficients change resulting in a change of ignition – extinction points in non – linear reactions. This effect was investigated in the case of 5%Pt – 25% SnO_2/SiO_2 catalyst for CO oxidation. The face velocity was changed from 20-120

cm/sec at constant CO concentration (550ppm), and the results are given in Figure IV.7. Further, the effect of change of face velocity (15-60cm/sec) was also investigated for different particle sizes (100 and 200 µm) at same CO concentration (250ppm), and the results are given in Figure IV.8.

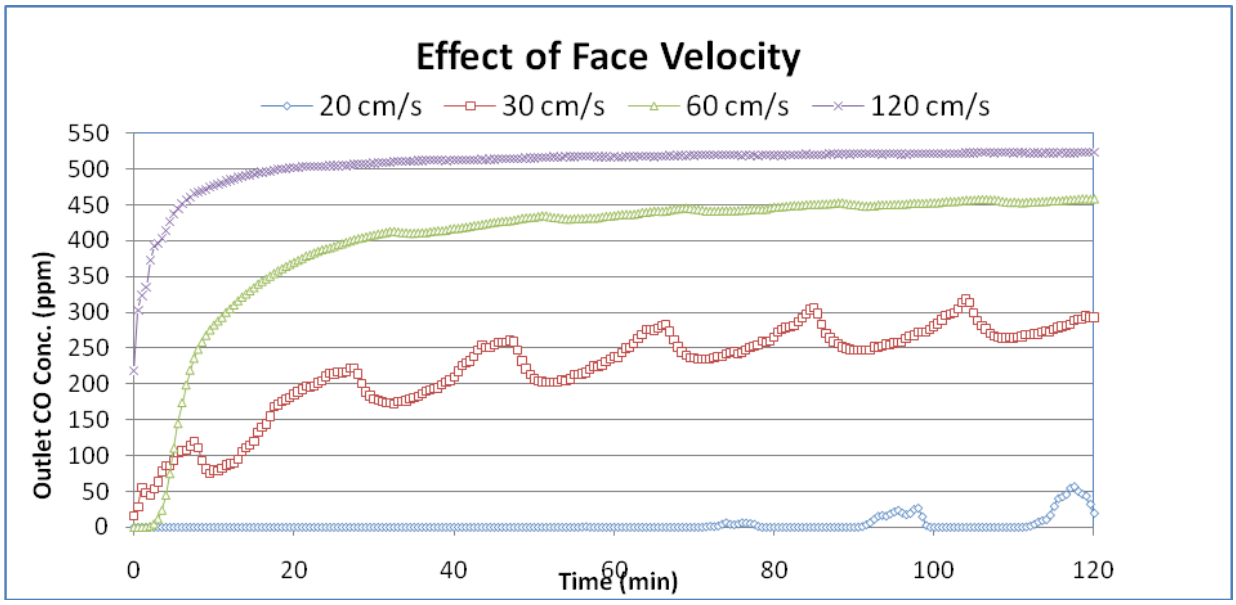

Figure IV.7. Effect of Face Velocity on Catalyst Performance

Test Conditions: Humidity: 50% RH; Temperature: 25^{0}C; Particle size: 150-250µm; Reactor: 0.375" ID; Inlet CO concentration: 550ppm; Catalyst bed depth: 3.3mm;

These results prove the non – linear behavior of the CO oxidation reaction. Further, an increase in the face velocity after a particular value caused the entire catalyst bed to get deactivated. When the face velocity was significantly higher, the end of the catalyst bed probably was unable to achieve high activity since the length of the bed was small. As the last few layers of the bed could not get ignited and achieve an upper steady state level, due to lack of heat transfer entire bed got deactivated faster. On the other hand, when the face velocity was lower, the end of the bed could maintain activity causing the entire bed to be active by thermal diffusion.

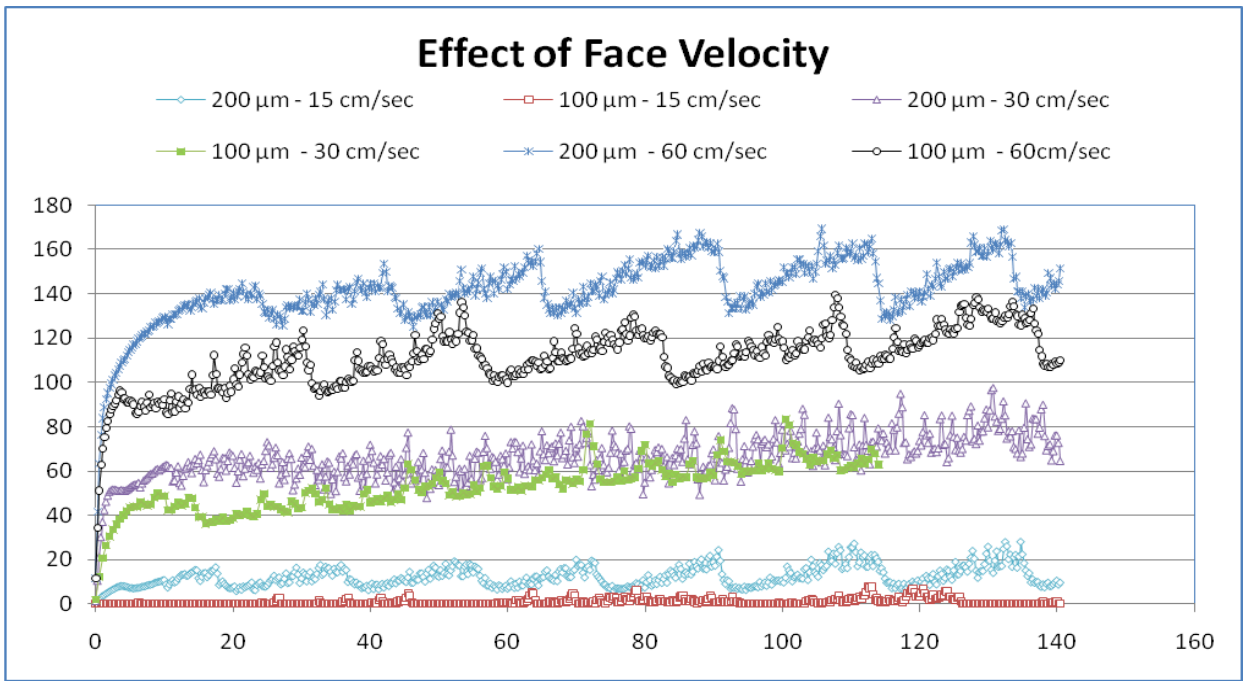

Figure IV.8. Effect of Face Velocity and Particle Size on Catalyst Performance

Test Conditions: Humidity: 50% RH; Temperature: 25^{0}C; Reactor: 0.375" ID; Inlet CO concentration: 250ppm; Catalyst bed depth: 2.0 mm;

Based on the results of these face velocity effects on the catalyst performance, it was clear that the system was non-linear in nature and there were more parameters contributing to the activity of the catalyst such as mass and heat diffusion within the bed apart from the internal diffusion within the catalyst particles and the surface reaction.

IV.3.14.2 Effect of CO Concentration

CO oxidation is believed to follow Langmuir – Hinshelwood kinetics, which is characterized by negative orders of reactions at higher CO concentrations. For low CO concentrations, the reaction follows close to first order behavior. However, if the reaction is run in an adiabatic condition, the reactions being highly exothermic would result in a significant rise in catalyst bed temperature. The rise in temperature favors kinetics; hence, the rate of reaction would go up, at higher CO concentrations. In

other words, there is a trade-off between ignition of the catalyst bed, due to adiabatic temperature rise and extinction of the catalyst bed due to CO poisoning.

Experimental results showed that the catalyst followed first order kinetics up to 500 ppm of CO and after 1000 ppm of CO the CO self-poisoning effect was dominant.

IV.3.14.3 Effect of Moisture Content

In the case of tin oxide promoted Pt catalyst, it was found out that the catalyst was stable in the presence of moisture. It was also found out that the catalyst needed presence of moisture to maintain activity. The catalyst got completely deactivated in the absence of moisture (in bone dry conditions, CO conversion: 1%). The effect of water vapor content on catalytic activity was studied by changing the relative humidity of gas from 25% to 90% RH. The results are given in Figure IV.9. Increased humidity increased catalytic activity.

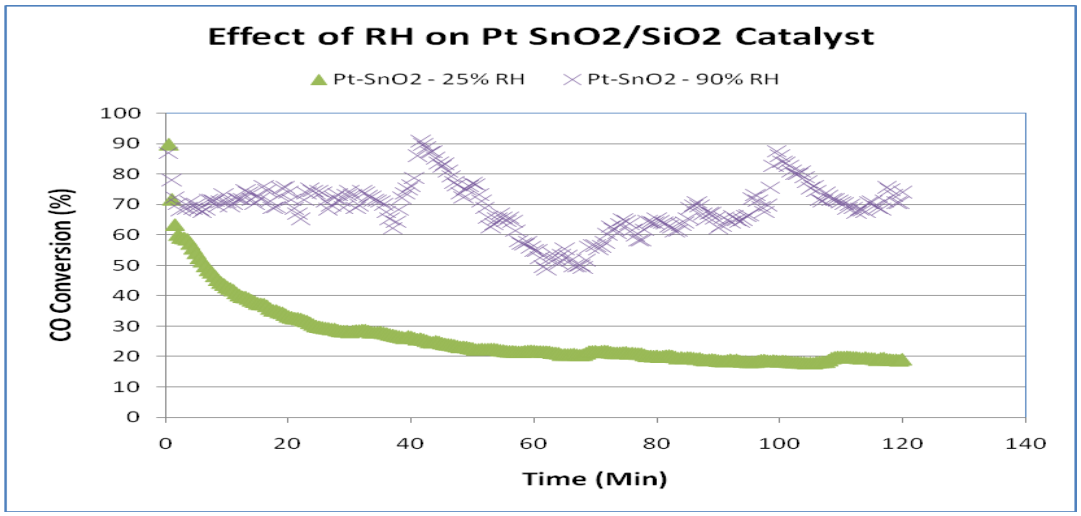

Figure IV.9. Effect of RH on the Performance of Pt-SnO2/Silica Catalyst

Test Conditions: Face velocity: 30 cm/sec; Temperature: 25^{0}C; Reactor: 0. 625" ID; Catalyst weight: 0.5gm; Particle Size: 150-250 µm; Inlet CO Concentration: 500ppm in air

Based on the activity results, it could be proposed that the CO oxidation mechanism on Pt-SnO_2/SiO_2 catalyst involved moisture (or formation of hydroxyl groups by water vapor on the surface). Also the absence of any H_2 at reactor outlet eliminated any possibility of water-gas shift reaction. Significant amount of work is needed to postulate a mechanism for the CO oxidation reaction over tin oxide promoted Pt catalyst; however, it can be said that the reaction involves hydroxyl group interaction with adsorbed CO on Pt.

IV.3.15 Activity Maintenance of the Catalyst

The activity maintenance of the 5%Pt-25% SnO_2/SiO_2 catalyst was tested at two conditions based on the application requirements: fire escape mask application (2500 ppm) and advanced filtration systems (250 ppm). The results are given in Figure IV.10.

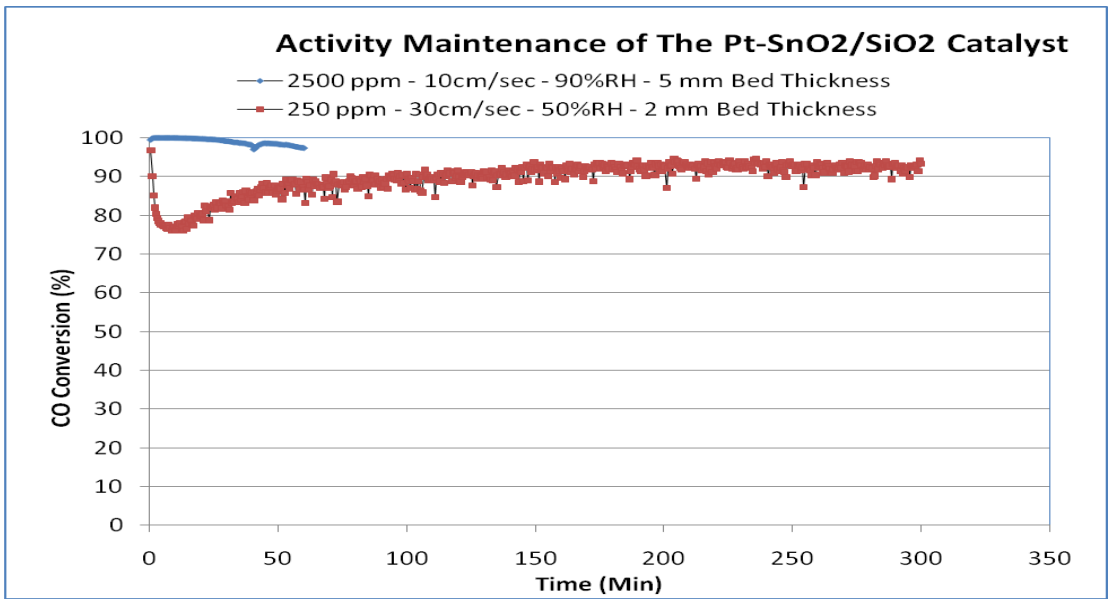

Figure IV.10. Activity Maintenance of the Pt-SnO2/SiO2 Catalyst

Test Conditions: Temperature: 25^{0}C; Reactor: 0. 625" ID; Particle Size: 150-250 µm; (a) FV: 10cm/sec; CO: 2500ppm; 90%RH; Cat.:1.2gm; (b) FV: 30cm/sec; CO: 250ppm; 50%RH; Cat.:0.5gm;

For the fire escape respirator application, the catalyst was required to maintain at least 90% conversion for at least 15 minutes. For the advanced filtration system application, the catalyst was required to maintain at least 75% conversion for four hours. From Figure IV.10, Pt-SnO_2/SiO_2 catalyst indeed met the activity requirements for both of these applications under consideration. In the case of high CO test, the catalyst maintained activity for more than 60 minutes almost four times the desired performance (90% conversion for 15 minutes). For low CO test, the catalyst maintained activity (>90% conversion for 5 hours) for more than the desired time.

IV.4 Conclusion

The Pt-SnO_2 catalyst was optimized regarding calcination and drying conditions, precursors, metal (oxide) loading and support. The catalyst recipe path finding exercise yielded good results. The reaction was found to be heavily dependent on the type of Pt precursor used, how it was dried and calcined as well as the amount of SnO_2 and Pt impregnated into the catalyst. The reaction was limited by internal diffusion.

The goal of this work was to develop a catalyst that would work at room temperature in the presence of moisture, and maintain high activity. The catalyst was completely inactive in dry environments, while maintaining excellent activity in moist conditions with humidity > 10% RH. Possibility of a water-gas shift reaction was eliminated based on absence of any H_2 at the outlet of the reactor. The catalyst required the presence of moisture for activity at room temperature.

V Development and Characterization of Ceria Promoted Pt Catalyst

V.1 Introduction

CO is harmful to humans as well as the environment. CO poisoning alone causes 3500 to 4000 deaths every year in the US [3]. Since adsorption or absorption of CO is inadequate at ambient conditions ($T \leq 50^0C$, 10-95%RH), the removal of CO by catalytic oxidation to CO_2 is the most viable option. However, CO oxidation at low temperature ($T \leq 50^0C$) is difficult because of slow surface kinetics and strong CO self-poisoning. Further, the presence of moisture can deactivate a catalyst by blocking the active sites, for example, the gold based catalysts [97]. Therefore a CO oxidation catalyst that is highly active at low temperatures ($T \leq 50^0C$) and in the presence of moisture (10-95%RH) is desired.

In the case of noble metals, water vapor could reduce the effect of catalyst CO poisoning by breaking the CO islands formed on noble metal surfaces [98]. Ceria can act as an oxygen reservoir and the presence of ceria can stabilize noble metal dispersion [38] and noble metal deposition on ceria could increase the oxygen storage capacity of the ceria [41]. Further, a study of CO oxidation using ceria supported noble metal catalysts found that CO oxidation on Pt/CeO_2 catalysts involved a transfer of lattice oxygen from ceria to adjacent Pt site [40]. Also, ceria showed a superior reducibility at nano scale compared to bulk ceria [42].

Although ceria supported metal oxide catalysts [32, 34] and noble metal catalysts [36, 38] have been investigated for CO oxidation, ceria as a support does not provide greater surface area for Pt dispersion and the superior redox properties of nano-scale ceria could not be harnessed by using ceria

as a support. Considering the superior attributes of noble metals and nano-scale ceria, the authors studied the effect of ceria as a promoter for supported Pt catalysts for CO oxidation.

Catalyst preparation variables significantly impact the catalytic activity by affecting the surface characteristics of the catalyst. A higher surface area support would result in better active metal (oxide) dispersion due to greater availability of the nucleation sites. However, the higher surface area of the support is a result of the highly tortuous narrower pores that could reduce the effective diffusivity of the reactant gases. Therefore the selection of the catalyst support is particularly important in the diffusion controlled reactions [99, 100].The type of Pt precursor (basic, acidic or neutral) used during catalyst preparation has a significant impact on activity, since the pH of the precursor and the iso-electric point (IEP) of the support determine the adsorption of the precursor on the support [89]. So, the type of precursor could determine Pt dispersion and the Pt distribution profile on the support. Precursors have shown significant impact on the activity and dispersion of noble metal catalysts [87, 101].

The precursor drying rate would dictate the active metal (oxide) distribution profile on the support (homogeneous, egg-shell, egg-white, and egg-yolk [93]). The rate of drying also affects the precursor salt crystal growth rate and in turn the crystal size [88]. Therefore, the drying conditions significantly affect metal (oxide) dispersion and distribution profile [96]. The metal distribution profile is crucial, particularly in the case of highly exothermic as well as the diffusion controlled reactions [94]. During calcination, precursor salt crystallites formed after drying are decomposed in oxidizing atmosphere to form the active metal (oxide) on the support and the gaseous by products are removed [102]. Calcination conditions could significantly impact the active metal dispersion on the support. Higher calcination temperatures could increase the rates of surface diffusion resulting in larger crystallites, whereas lower calcination temperatures could result in contamination of active sites due to the presence of decomposition by-products or un-decomposed precursor salt. Therefore, the selection

of optimum calcination temperature is crucial to the activity of the catalyst. The effect of calcination temperature on Pt dispersion has been studied extensively [103-107].

During this study, the effects of ceria deposition variables such as the type of ceria deposition method, ceria loading, and ceria precursor drying and calcination conditions on the activity were studied. The catalytic activity was correlated to the surface characteristics using $O_2 – H_2$ titration, XRD, and O_2 chemisorption on ceria. Also the Pt deposition variables such as the type of Pt precursor, Pt loading, calcination and drying conditions of the Pt precursor were investigated in detail. The catalytic activity was correlated to the surface characteristics using CO/H_2 chemisorption on Pt, TPR, TEM and BET surface area and pore size measurements. Finally, the performance and stability of the catalyst was tested at ambient temperature (25^0C).

V.2 Experimental

V.2.1 Catalyst Preparation Methods and Materials

Except for the study involving the effect of ceria deposition method, all of the catalysts were prepared by using the successive incipient wetness impregnation method (successive IN method). The steps followed were: (a) impregnation of a ceria precursor (cerium (III) nitrate hexahydrate (REacton® 99.99%, Alfa Aesar)) on a silica support (Davisil® 645, Sigma Aldrich) followed by drying overnight at 100^0 C and calcination at 300^0 C for two hours in air, and (b) impregnation of a Pt precursor (diammine dinitro platinum (DADNP) (8.2% w/w in dil. NH_4OH, Strem Chemicals)) on the ceria-silica support followed by drying for 4 hours at 125^0C and calcination at 400^0C for 3 hours in air.

In order to investigate the impact of a particular preparation parameter on activity, the parameter under investigation was varied while maintaining other parameters as uniform as possible

V.2.1.1 Ceria Deposition Method and Catalyst Support

The effects of various ceria deposition methods were studied by preparing 4%Pt-22%CeO_2/SiO_2 catalysts using three different ceria deposition methods: incipient wetness impregnation method (IN), deposition precipitation method (DP, Reddy et al [47]) and grafting method (GR, Bensalem et al. [48]). The effects of catalyst support was studied by preparing 4%Pt-22%CeO_2/support catalysts using Silica (Davisil® 645, Sigma Aldrich) and γ-Al_2O_3 (Alumina catalyst support, Alfa Aesar) supports with similar surface properties (SA: 300m^2/g; PV: 1.15 cc/g; APS: 120 - 150Å).

V.2.1.2 Silica Support Selection

The effects of the type of silica support were studied by preparing 2.5%Pt–16%CeO_2/SiO_2 catalysts using these silica supports: (Davisil® 645 + Davisil® 644), Merck® 10180, Merck® 10184, silica Grade 7734 (Sigma Aldrich) and Davisil® LC 250 (Grace Davison). The CeO_2 and Pt loadings were chosen based on the lowest PV of the selected supports (Merck 10180; PV: 0.68cc/g), and the maximum available Pt precursor concentration (5% Pt w/w), so that only one step of ceria and Pt impregnation needed to be carried out for catalyst preparation. The catalysts were prepared by the successive IN method. Other catalyst preparation conditions used were: (a) ceria precursor was dried overnight at 75^{0}C and calcined at 300^{0}C for 2 hours in air; (b) Pt precursor (DADNP) was dried in oven at 125^{0}C for 4 hours and calcined at 500^{0}C for 3 hours in air.

The surface characteristics of these supports, BET SA (m2/g), PV (cc/g) and APS(Å), were: Merck® 10180 (750, 0.68, 40); Grade 7734 (550, 0.8, 60); Merck® 10184 (330, 1.00, 100); Davisil® LC 250 (330, 1.65, 250); and mixture of Davisil® 645 and Davisil® 644 (300, 1.15, 150). The particle size for the experiments was kept uniform (125 µm). These surface characteristics were provided by the manufacturer for the bare supports.

V.2.1.3 Platinum and Ceria Loading

The effects of Pt loading on the catalytic activity were studied by preparing (1.25-10% w/w) Pt – 20% (w/w) CeO_2/SiO_2 catalysts by the successive IN method. In order to get different Pt loadings, either diluted Pt precursor solution or multiple Pt impregnation cycles were carried out. The effects of ceria loading were investigated by preparing 4%Pt (w/w)–(4-27% w/w) CeO_2/SiO_2 catalysts by the successive IN method. Different ceria loadings were obtained in one impregnation cycle using different molarities of ceria precursor.

V.2.1.4 Platinum Precursor, Drying and Calcination Conditions

The effect of the Pt precursor on Pt dispersion and catalytic activity was studied by preparing 4%Pt – 16%CeO_2/SiO_2 catalysts using four Pt precursors differing in acidity. The Pt precursors used were: (a) diammine dinitro platinum (DADNP) (8.2% w/w in dil. NH_4OH, Strem Chemicals), (b) tetraammineplatinum (II) hydroxide hydrate (TAPH) (Sigma Aldrich), (c) tetraammineplatinum (II) nitrate (TAPN) (99.99%, Sigma Aldrich) and (d) chloroplatinic acid (8wt% in H_2O, Sigma Aldrich). All of the Pt precursors were calcined at 300^0C, 400^0C, 500^0C or 600^0C for 3 hours in air.

For Pt precursor (DADNP) calcination time studies, 2%Pt– 16%CeO_2/SiO_2 catalysts were prepared by calcining the precursor at 500^0C in air for (a) one, (b) two, (c) three, and (d) four hours. For Pt precursor (DADNP) drying condition studies, 2.5%Pt– 16%CeO_2/SiO_2 catalysts were prepared by using one of the following drying conditions: (a) vacuum drying at 40^0C for 6 hours, (b) overnight drying at 75^0C, or (c) drying for 4 hours at 125^0C.

V.2.1.5 Ceria Precursor Drying and Calcination Conditions

Effect of ceria precursor drying conditions was investigated by preparing 2.5%Pt – 16%CeO_2/SiO_2 catalyst varying only the drying condition: (a) vacuum drying at 40^0C for 6 hours, (b) drying overnight at 100^0C, and (c) drying at 125^0C for 4 hours. While ceria precursor calcination studies were carried out by

preparing four 2.0%Pt – 16%CeO_2/SiO_2 catalysts, prepared by varying only the calcination temperature (200^0C, 250^0C, 300^0C, and 350^0C). The drying condition used was: vacuum dry at 40^0C for 6 hours.

V.2.2 Catalyst Characterization

Ceria crystallite sizes were estimated from powder XRD spectra obtained at 0.5 (2theta) /min. BET SAs, PVs and APS were obtained using N_2 adsorption at 77K. CO and H_2 chemisorption on Pt and O_2 chemisorption on ceria was carried out at 30^0C. Static O_2 – H_2 Titration was carried out using the protocol developed by Salasc et al [52]. Temperature Programmed Reduction (TPR) was carried out using 15sccm of 5% H_2 in Argon in the temperature range of 293 – 1023 K at heating rate of 10K/min. TEM images were obtained using a ZEISS EM 10 TEM, with 200K magnification. The rest of process and instrumentation details are given in "experimental section" chapter.

V.3 Results and Discussion

V.3.1 Catalyst Support and Ceria Deposition Method Selection

CO oxidation activity results and estimated ceria crystallite sizes (XRD and O_2 titration) for the catalysts prepared by different ceria deposition methods are given in Table V.1. The observed XRD spectra are given in Figure V.1 and the estimated ceria crystallite sizes are given in Table V.1. Ceria deposition by GR method yielded smaller ceria crystallites or better ceria dispersion compared to the IN method. The DP method could result in significant amounts of amorphous ceria, which would explain the absence of ceria peaks in the XRD spectra. Similar results were obtained by other researchers as well, for example, *Craciun et al* observed less than 30% crystalline ceria in ceria/silica samples prepared by DP method (calcined at 500ºC) and the amount of amorphous ceria increased with decreasing calcination temperature[108].

The silica supported catalyst prepared by the IN method was more active for similar Pt dispersion and lower ceria dispersion. Further, for same amount of Pt and ceria, alumina supported catalysts showed 68% Pt dispersion, yet the activity of alumina supported catalyst was poor. These observations indicated that CeO_2 SA or Pt SA did not dictate catalytic activity. Pt-ceria contact area had been shown to be responsible for the CO oxidation activity of the Pt-ceria catalysts [38]. Transfer of lattice oxygen from ceria to adjacent Pt site could explain the role of Pt-ceria contact area in catalytic activity. Also, the presence of highly mobile superoxide radicals (O_2^-) in ceria lattice and in turn the Pt-ceria interfacial area has been attributed for the activity [109].

Table V.1. Ceria Deposition Method and Support Effect on Activity, Pt and Ceria Dispersion

Catalyst	Reaction rate* (µmol/g/s)	CeO_2 SA (m^2/g)	Ceria, Pt SA (m^2/g)	Pt %D	Ceria Dp (nm)	
					XRD	O_2 tit.
4%Pt-22%CeO_2/SiO_2-DP	1.31	15.5	7.31	36	ND	10.1
4%Pt-22%CeO_2/SiO_2-GR	1.96	51.6	31.7	45	3.30	3.00
4%Pt-22%CeO_2/SiO_2-IN	5.77	23.9	20.9	42	7.30	6.60
4%Pt-22%CeO_2/Al_2O_3-IN	1.05	10.3	5.95	68	5.00	15.2
22% CeO_2/ SiO_2 – IN	NA	22.28	NA	NA	7.20	5.60
5% Pt/Al_2O_3	0.23	NA	NA	63	NA	NA
5% Pt/SiO_2	0.61	NA	NA	16	NA	NA

**Test Conditions: CO Conc.: 500 ppm CO in air, Catalyst bed depth: 3.2mm (0.25g Cat. + 66% inert silica), Face velocity: 45 cm/sec, Particle Size: 200 µm, Reactor ID: ¾", Humidity: 50% RH, Temperature: 25^{0}C.*

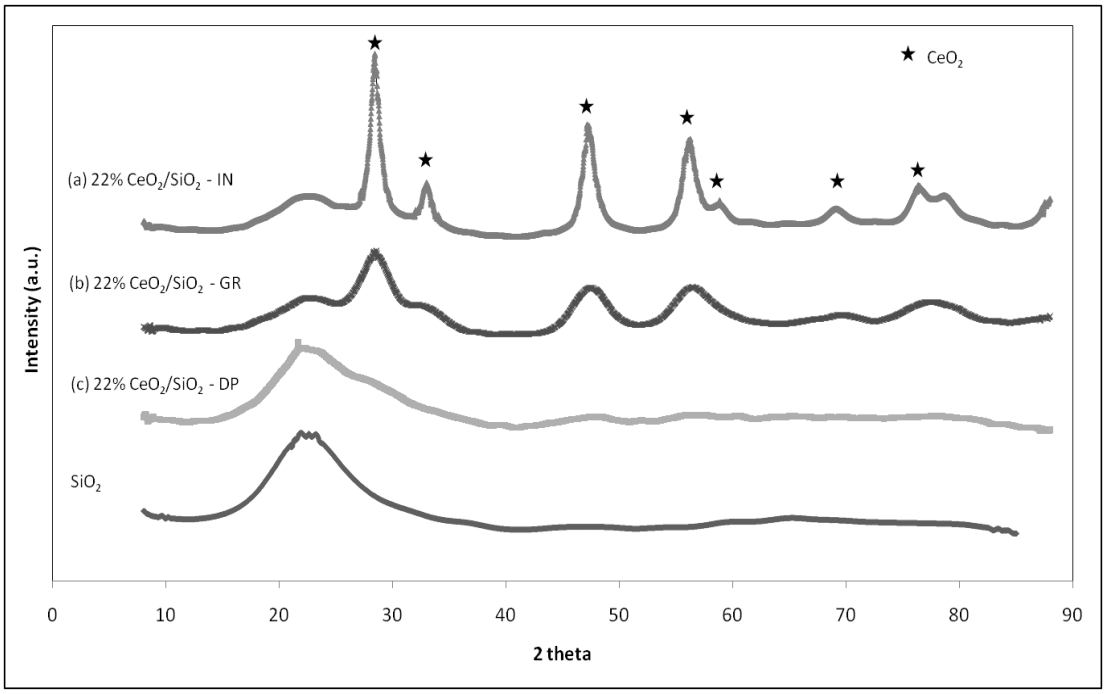

Figure V.1. Powder XRD Patterns for SiO_2 and CeO_2/SiO_2 samples prepared by IN, GR, and DP method

Pt deposition is a function of iso-electric point (IEP) of the support and pH of the precursor solution. The Pt precursor solution had a pH of 7-8, and the Pt species in the solution was neutral in charge. SiO_2 is negatively charged (IEP: 1.7-3.5) and CeO_2 is neutral (IEP: 6.8-8.6). However, the presence of NH_4^+ ions in the precursor solution would block the silica surface, so Pt precursor would be adsorbed on ceria in the case of ceria/silica. H_2 chemisorption results support this hypothesis, as the Pt dispersion improved by addition of CeO_2 on SiO_2 supported Pt catalysts (16% to 42%). Ceria could inhibit Pt metal sintering thereby improving Pt dispersion [38]. In the case of ceria/alumina, any Pt precursor would result in non-preferential deposition of Pt on γ–Al_2O_3 (IEP: 7-8) and CeO_2 (IEP: 6.8-8.6). As can be seen from the estimated Pt dispersion values (H_2 chemisorption), addition of ceria did not change Pt dispersion significantly (63% to 68%).

So addition of ceria would improve Pt dispersion on silica supported catalysts, and Pt-ceria contact area as well. However, the catalytic activity was significantly affected by the type of ceria deposition method on silica supported catalysts. To investigate the origin of the catalytic activity, O_2-H_2 titration studies were carried out using the protocol developed by *Salasc et al* [52]. By using this protocol, O_2 and H_2 uptakes during O_2/H_2 chemisorption (OC, HC) and O_2/H_2 titration (OT, HT) were estimated. The estimated values of the uptake are given in Table V.2. Using this protocol, total CeO_2 SA, Pt dispersion and the CeO_2 SA in contact with Pt (Ceria-Pt) were estimated and are given in Table V.1.

Table V.2. Effect of Ceria Deposition Method – Uptake values during O_2–H_2 Titration

Catalyst	OC µmol/g	HT µmol/g	OT µmol/g	HC µmol/g
4% Pt – 22% CeO_2/SiO_2 – DP - B	77.24	110.5	72.34	46.17
4% Pt – 22% CeO_2/SiO_2 – GR - B	160.8	242.9	135.4	57.60
4% Pt – 22% CeO_2/SiO_2 – IN - B	101.3	199.6	108.8	53.58
4% Pt – 22% CeO_2/Al_2O_3 – IN - B	107.2	254.7	120.2	86.64
22% CeO_2/ SiO_2 – IN	44.55	NA	NA	NA
5% Pt/Al_2O_3	NA	NA	NA	80.2
5% Pt/SiO_2	NA	NA	NA	20.12

The protocol was based on the H_2 spillover effect and redox reactions of ceria at room temperature. Briefly, Salasc et al found out that in a system of noble metal-ceria, H_2 reduction at 573K reduced only the noble metal and the ceria surface and bulk CeO_2 reduction required a significantly higher temperature (T>750K) [110]. Further, in the presence of noble metals, the ceria surface adjacent

to the noble metal could be reduced even at room temperature due to the spillover of H_2 to the ceria surface. Based on this surface chemistry, this protocol was developed which could be used to find out total CeO_2 SA, total Pt SA and the CeO_2 SA in contact with Pt.

In the case of Pt/Ceria catalyst, O_2-H_2 titration studies revealed that CeO_2 SA in contact with Pt was 112 m^2/g and total CeO_2 SA was 123 m^2/g [52]. So, if the entire Pt was in contact with ceria, the ratio of Ceria-Pt to the total CeO_2 SA would be close to unity. During this study, this ratio was 0.88, 0.47 and 0.6 for the catalysts prepared with ceria deposition by IN, DP, and GR method respectively. The ratio would give the extent of ceria deposited with Pt, zero being no deposition and one being all ceria deposited with Pt crystallites.

The ratio was also lower in the case of γ–Al_2O_3 supported catalysts and the estimated CeO_2 crystallite sizes from XRD and O_2-H_2 titration were not in agreement. During O_2-H_2 titration, the pre-treatment step of reduction at 300°C in H_2 would form cerium (Ce^{3+}) ions, and γ–Al_2O_3 could stabilize the Ce^{3+} ions [53]. The stabilization of the Ce^{3+} ions by the γ–Al_2O_3 would lead to lower O_2 uptake during OC and over-estimation of CeO_2 crystallites. However, the estimated ratio of Ceria-Pt to the total CeO_2 SA would not change due to the stabilization of Ce^{3+} ions.

The possibility of cerium (Ce^{3+}) ions stabilization by silica could be neglected as the estimated ceria crystallite sizes (XRD: 6.9nm; OC: 7.3nm) were in agreement for 22%CeO_2/SiO_2. Also, there was a possibility of H_2 spill over during HC. As per the O_2-H_2 titration protocol, this H_2 spill over would result in underestimation of total CeO_2 SA. From Table V.1, CeO_2 SA of 22%CeO_2/SiO_2 (22.3 m^2/g, OC, prior to Pt deposition) and total CeO_2 SA estimated for 4%Pt-22%CeO_2/SiO_2 from O_2-H_2 titration (23.9 m^2/g) were in agreement. Therefore, the O_2-H_2 titration studies over 4%Pt-22%CeO_2/SiO_2 catalyst would yield better estimates for Pt and Ceria dispersion.

During Pt precursor calcination, segregation of ceria and Pt could take place if ceria crystallites are smaller, for e.g. by grafting method. Impregnation method resulted in larger ceria crystallites, providing anchoring sites for Pt and therefore, for equivalent Pt loading, resulted in greater Pt-CeO_2 contact area. Considering the surface characteristics of silica and alumina and the impact of ceria deposition method on the Pt-ceria contact area, the deposition of ceria by incipient wetness impregnation method on silica resulted in a superior catalyst.

V.3.2 Silica Support Structure Selection

The effect of silica support structure on the catalytic activity of 2.5%Pt-16%CeO_2/SiO_2 was studied by using five different types of silica supports. The CO activity results of these catalysts along with the catalyst surface characteristics are given in Table V.3.

Table V.3. **Effect of Type of Silica Support – Catalyst Properties and Catalytic Activity**

Catalyst	**BET SA (m^2/g)**	**PV (cc/g)**	**APS (A°)**	**Reaction Rate* (µmol/g/s)**	**TOF (x100)**	**Pt (%D)**	**Ceo2 Dp (nm) XRD**	**Deff. (mm^2/s)**
Merck 10180	417	0.52	50	2.26	2.8	63.3	4.7	12.3
Grade 7734	370	0.57	61	2.45	3.6	53.3	6.8	18.1
Merck 10184	296	0.82	111	2.59	3.8	52.5	7.7	29.4
Davisil LC 250	236	1.05	179	2.82	4.5	48.6	8.3	66.2
Davisil (644+645)	259	0.91	141	2.89	5.2	43.0	7.7	42.5

**Test Conditions: Humidity: 50% RH, Temperature: 25^{0}C, Reactor ID: ¾", Particle Size: 63-200 µm, Cat. Wt: 0.25g (+ 50% inert SiO_2), Face velocity: 30 cm/sec, CO Conc.: 250ppm in air*

The support SA had a major impact on the Pt and CeO_2 dispersion, with increased Pt and CeO_2 dispersion with increased support SA, as seen from the XRD and chemisorption results. Since ceria is known to stabilize noble metals [38], it would be prudent to say that the greater surface area along with higher ceria dispersion resulted in a better Pt dispersion. As expected the final catalysts had lower BET SAs and PVs compared to the supports. The catalysts prepared from supports with greater SAs showed a greater drop in the BET SA, and PVs. The APS of the catalysts prepared using supports with narrower pore openings was greater than the bare support itself; whereas, the supports with wider pore openings showed a decrease in the APS. The increased APS was a clear indication of blocking of narrower pores in the catalyst and decreased APS could be a result of pore narrowing or a combined effect of pore narrowing and pore blocking.

However, the catalytic activity was not directly proportional to BET SA or Pt/ceria dispersions. The catalysts prepared on a support with a greater SA (Merck® 10180) fared poorly in comparison with those prepared on a support with lower surface area (Davisil® (644 + 645)). The comparison of estimated TOF revealed that Davisil® (644 + 645) supported catalyst (TOF: 0.052 s^{-1}) was almost two times more active compared to Merck® 10180 supported catalyst (TOF: 0.028s^{-1}).

If a catalyst with better Pt/CeO2 dispersion performs poorly compared to one that had lower dispersion, the number of active sites was certainly not a deciding factor. Consequently, it was not the reactivity but the transport properties that could explain this behavior. Therefore, the effective diffusivity of CO inside the porous catalyst was estimated for all of the catalysts and given in Table V.3.

Initially, the mean free path was calculated by using Equation V.1 [79]. The mean free path at room temperature for CO is: 6.5×10^{-8} (in m).

Equation V.1. Estimation of Mean Free Path

$$l = \frac{3.2\,\mu}{P}\left[\frac{RT}{2\pi M}\right]^{1/2}$$

l: Mean free path, μ: viscosity, P: pressure, M: molecular weight, T: Temperature.

Since, for ($l/d_{pore} > 10$), the diffusion is mainly Knudsen diffusion[79], for supports with APS ≤ 60 Å, the diffusion was assumed to be Knudsen diffusion. For other supports, the diffusion was assumed to be a combined bulk and Knudsen diffusion. The Knudsen diffusion coefficient was estimated using Equation V.2 [79].

Equation V.2. Estimation of Knudsen Diffusivity

$$D_K = 48.5 d_{pore}\left(\frac{T}{M}\right)^{1/2};(in\ m^2/_S)$$

$d_{pore}: average\ pore\ diameter$

Further, the effective Knudsen diffusivity was estimated from Equation V.3. Whereas, the combined bulk and Knudsen diffusivity [79] was estimated by Equation V.4.

Equation V.3. Estimation of Effective Knudsen Diffusivity

$$D_{Keff} = \frac{\varepsilon_p D_K}{\tau}$$

D_{Keff} : Effective Knudsen Diffusivity, ε_p: particle voidage, τ: tortuosity, D_K : Knudsen Diffusivity

Equation V.4. Estimation of Effective Diffusivity

$$D_{eff} = \left(\frac{1}{D_{Beff}} + \frac{1}{D_{Keff}}\right)^{-1}$$

D_{eff} : Combined Bulk and Knudsen Effective Diffusivity, D_{Beff} : Effective bulk Diffusivity, D_{Keff} : Effective Knudsen Diffusivity

The bulk diffusivity(D_B) was estimated using Chapman-Enskog kinetic theory [80], whereas, the effective bulk diffusivity was estimated along the lines of Equation V.3. Although, the tortuosity and particle porosity would be different for all of these supports, due to lack of any experimental data, a tortuosity value of three ($\tau = 3$), and a particle porosity of 0.6 ($\varepsilon_P = 0.6$) was assumed for all the catalysts.

The effective diffusivity of CO (42.5 mm^2/sec) for Davisil® (644 + 645) supported catalyst (APS: 141 Å), was almost 3.5 times that of the effective diffusivity of CO (12.3 mm^2/sec) for Merck® 10180 supported catalyst (APS: 50 Å). The Merck® 10180 supported catalyst with lower effective CO diffusivity performed poorly compared to the Davisil® (644 + 645) supported catalyst.

The catalysts with wider pore openings had greater effective diffusivity and resulted in better catalytic activity. These observations clearly indicate the effect of mass transport limitations on the rate of reaction and in turn on TOF, indicating that the reaction was a diffusion controlled reaction (DCR).

V.3.3 Ceria Precursor Drying Rate

The impact of ceria precursor drying conditions on catalytic activity was studied and the CO activity results, and XRD and O_2 chemisorption analysis results are given in Table V.4. The effect of the drying conditions on the ceria crystallite size was studied by XRD and the XRD spectra are given in Figure V.2. Surface characterization revealed that the drying rate affected the ceria dispersion and in turn catalytic activity. CeO_2 dispersion decreased with increasing drying temperature or drying rate.

The positively charged species of ceria (Ce^{3+}) in the impregnating solution would adsorb strongly on the negatively charged silica support. In the case of strong precursor-support interactions, rate of drying can affect the distribution profile only in the case of high concentration precursor solutions [96]. Faster drying rates would result in increasingly egg-shell like distribution profiles while slower drying rates would yield close to homogeneous profile. Further, greater concentration of the solute would

result in poor dispersion for distribution profiles other than the homogeneous distribution profile. Considering the ceria loading (20% w/w), the precursor concentration in the solution was higher. So, a faster drying rate (drying at 125^0C) would result in an egg – shell like profile and slower drying rate (drying at 40^0C) would result in more uniform ceria distribution profile.

Table V.4. **Effect of Ceria Precursor Drying & Calcination Condition on Activity and Ceria Dispersion**

Catalyst	Drying Condition #	Calcination Temp.	Calcination Time	Reaction Rate* (µmol/g/s)	CeO2 Dp (nm)	
					XRD	O2 Chemi.
2.5%Pt – 16%CeO_2/SiO_2	**A**	300^0C	2 Hrs	1.96 (a)	6.4	6.5
2.5%Pt – 16%CeO_2/SiO_2	**B**	300^0C	2 Hrs	1.62 (a)	6.5	6.9
2.5%Pt – 16%CeO_2/SiO_2	**C**	300^0C	2 Hrs	1.08 (a)	7.9	7.2
2.0%Pt – 20%CeO_2/SiO_2	**A**	200^0C	2 Hrs	0.24 (b)	6.4	6.2
2.0%Pt – 20%CeO_2/SiO_2	**A**	250^0C	2 Hrs	2.04 (b)	6.8	6.6
2.0%Pt – 20%CeO_2/SiO_2	**A**	300^0C	2 Hrs	2.54 (b)	7.0	6.8
2.0%Pt – 20%CeO_2/SiO_2	**A**	350^0C	2 Hrs	1.74 (b)	7.1	7.3
2.0%Pt – 20%CeO_2/SiO_2	**A**	300^0C	3 Hrs	2.26 (b)	ND	7.0
2.0%Pt – 20%CeO_2/SiO_2	**A**	300^0C	4 Hrs	1.93 (b)	ND	7.3

#(A) Vacuum Dry @ 40^0C; (B) Overnight @ 75^0C; (C) 4 hours @ 125^0C

* *Test Conditions: Humidity: 50% RH, Temperature: 25^0C, Reactor ID: 0. 75", Particle Size: 200 µm; (a) CO: 250 ppm; Face velocity: 30 cm/sec; Catalyst: 0.25 g; (b) CO: 300 ppm; Face velocity: 45 cm/sec; Catalyst: 0.2g*

Based on the activity and the characterization results, a slower drying rate was beneficial to the ceria dispersion and in turn the catalytic activity. The CeO_2 SA was crucial to activity, since CeO_2 provided

sites for Pt deposition and greater ceria dispersion improved Pt dispersion. Also, the active sites for CO oxidation, the Pt– CeO_2 interfacial area, were dependent on ceria SA as well.

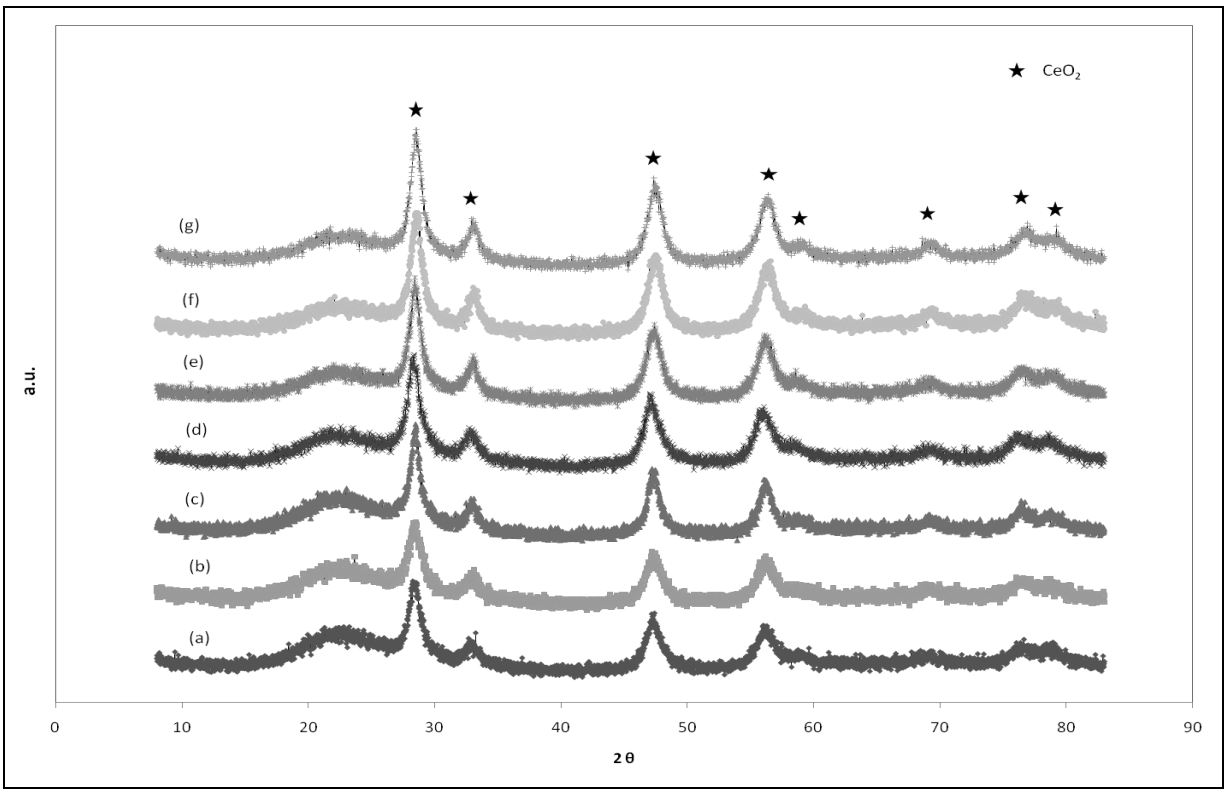

Figure V.2. XRD Spectra for CeO_2/SiO_2 samples: precursor drying and calcination temperature

Effect of ceria precursor calcination temperature on the catalytic activity was studied and the CO activity results and O_2 chemisorption and the XRD analysis results are given in Table V.4. The XRD spectra are given in Figure V.2. (A) Effect of Ceria Precursor Drying (16% CeO_2/SiO_2) – (a) vacuum dry at 40^0C, (b) overnight at 75^0C, (c) 4 hrs at 125^0C, and (B) Effect of Calcination temperature (20% CeO_2/SiO_2) – (d) calcined at 200^0C, (e) calcined at 250^0C, (f) calcined at 300^0C, and (g) calcined at 350^0C. The catalytic activity increased with increasing calcination temperature up to 300^0C and then dropped when the calcination temperature was raised to 350^0C. As expected, the CeO_2 dispersion decreased with increased

calcination temperature as shown by XRD analysis as well as O_2 chemisorption. So, the catalytic activity was not a function of the CeO_2 dispersion alone.

The volcano type of activity profile could be explained by two factors: (a) the total CeO_2 SA available for the Pt deposition, and (b) the property of the CeO_2 to decorate the Pt crystallites during the Pt precursor calcination. The total CeO_2 SA available for the Pt deposition decreased with increased calcination temperature of the CeO_2 precursor as observed from the O_2 chemisorption. During the calcination of the Pt precursor at 400^0C, due to the increased surface diffusion and sintering of the CeO_2, the Pt crystallites would be decorated by the CeO_2. So the extent of the Pt decoration would depend on the stability of the CeO_2 and in turn the CeO_2 precursor calcination temperature. The extent of decoration would decrease with increased ceria precursor calcination temperature. Although moderate amount of decoration of Pt by ceria would increase the catalytic activity by increasing the Pt-ceria contact area, significant decoration could result in lower active surface area and lower activity.

At lower ceria precursor calcination temperature, ceria SA for deposition would be greater, but significant ceria decoration of Pt would result in lower active SA. At higher calcination temperatures of ceria precursor, ceria SA for Pt deposition would be lower and the ceria decoration would also be lower resulting in lower activity. The catalytic activity increased with increased calcination temperature of ceria precursor from 200^0C to 300^0C due to decreased ceria decoration. The catalytic activity decreased when the calcination temperature was increased from 300^0C to 350^0C, because the ceria SA available for Pt dispersion was lower and the extent of Pt decoration by ceria was also lower.

The impact of ceria precursor calcination time was investigated by preparing catalysts with same composition by varying only the ceria precursor calcination time (2, 3, and 4 hours). The CO activity results and surface characterization results for these catalysts are given in Table V.4. The catalytic

activity decreased with increased calcination time. As expected, the CeO_2 dispersion decreased with increased calcination time as shown by O_2 chemisorption.

Ceria provided the anchoring sites for the Pt crystallites and improved the Pt dispersion; therefore, better ceria dispersion would in turn improve catalytic activity. Since, increased calcination time decreased ceria dispersion it had a negative impact on the activity.

V.3.4 Effect of Ceria/Silica Pre-treatment

In order to understand the impact of ceria calcination on catalytic activity, the effect of ceria – silica pretreatment prior to Pt (2.5%) deposition was investigated in detail. 16% ceria – silica samples were pretreated in air for two hours at temperatures greater than the ceria precursor calcination temperature (300^0C, 400^0C, 500^0C and 600^0C). These catalysts were tested for CO oxidation activity. The surface characteristics of ceria/silica sample calcined at 600^0C were compared with that of the untreated ceria - silica and are summarized in Table V.5.

Increase in the ceria – silica pre-treatment temperature gradually decreased the catalytic activity. The rates of reaction (μmol/g.s) were 1.57, 1.47, 1.05, and 0.99 for the catalysts with ceria/silica samples calcined at 300^0C, 400^0C, 500^0C and 600^0C respectively. The catalyst prepared without any pre-treatment was 1.5 times more active compared to the catalyst pretreated at 600^0C. The XRD results showed that ceria/silica pre-treatment at 600°C resulted in an increase of the ceria crystallites (7.5 nm) in comparison to the un-treated ceria (6.8nm).

CO chemisorption showed that the change in the Pt dispersion was not more than 4% (instrument error: ±2%). Ceria provided the anchoring sites for Pt deposition and also improved Pt dispersion. Further, during high temperature Pt precursor calcination, there was a possibility of decoration of Pt by ceria. The decoration effect of ceria would cause slight reduction in Pt dispersion

measurements; however, would yield highly active catalyst due to increased Pt-CeO_2 interfacial area. Pre-treatment of ceria/silica at a temperature greater than Pt precursor calcination temperature prior to Pt deposition had two-pronged effect: (a) lower ceria SA for Pt deposition, and (b) reduced decoration of Pt by ceria.

Table V.5. CeO_2/SiO_2 Pre-treatment - Activity, Surface Properties and CeO_2 dispersion

Analysis Results	No Pre-treatment	Calcination @ 600°C
Rate of Reaction (µmol/g.s)*	1.57	0.99
CeO2 Crystallite Size (nm) XRD	6.8	7.5
CeO2 Crystallite Size (nm) O2 Chemisorption	6.7	7.1
BET SA (m2/g)	260	251
PV (cc/g)	0.91	0.86
APS (Å)	140	137
Pt (%D) – CO Chemisorption	29	26
TOF (x100) – from CO chemisorption	4.2	3.0

**Test Conditions: Humidity: 50% RH, Temperature: 25^{0}C, Reactor ID: ¾", Particle Size: 200 µm, Catalyst wt: 0.6g, Face Velocity: 45 cm/sec, CO Conc.: 500 ppm CO in air.*

If the only effect of pre-treatment were to be reduction in ceria SA thus causing reduced Pt dispersion, then the TOF values of the catalysts should have been comparable. However, comparing the estimated TOF values, the absence of decoration effect for pre-treated sample was obvious.

This pre-treatment study of the ceria-silica qualitatively confirmed the existence of the decoration of the Pt crystallite by the ceria from the Pt dispersion results. The ceria calcination temperature affected two properties of the catalyst: (a) available ceria SA for Pt deposition; and (b) the extent of Pt decoration by ceria.

This effect enabled explanation of the existence of volcano type of activity profile for ceria precursor calcination temperature.

V.3.5 Effect of Ceria Loading

Increased ceria content could increase the Pt-ceria contact area and thereby improve the activity. The effect of CeO_2 loading on the activity of 4%Pt/SiO_2 catalyst was studied by varying the ceria promoter content (4-27% w/w). The catalytic activity tests results and chemisorption results are given in Table V.6.

Table V.6. **Effect of Ceria Content on Catalytic Activity, Pt Dispersion and TOF**

Catalyst	**Reaction rate* (µmol/g/s)**	**Pt % D – CO Chemi.**	**TOF**
SiO_2	NA	NA	NA
4% Pt - 4% CeO_2/SiO_2 – IN – B	1.05	36	0.011
4% Pt - 9% CeO_2/SiO_2 – IN – B	1.57	37	0.016
4% Pt - 15% CeO_2/SiO_2 – IN – B	2.94	42	0.028
4% Pt - 22% CeO_2/SiO_2 – IN – B	5.77	46	0.049
4% Pt - 27% CeO_2/SiO_2 – IN – B	5.46	52	0.043

**Test Conditions: CO Conc.: 500 ppm CO in air, Catalyst bed depth: 3.2mm (0.25g Cat. + 66% inert silica), Face velocity: 45 cm/sec, Particle Size: 200 µm, Reactor ID: ¾", Humidity: 50% RH, Temperature: 25^0C.*

The XRD spectra are given in Figure V.3. The results of XRD analysis and O_2 chemisorption along with BET SA, PV and APS results are given in Table V.7.

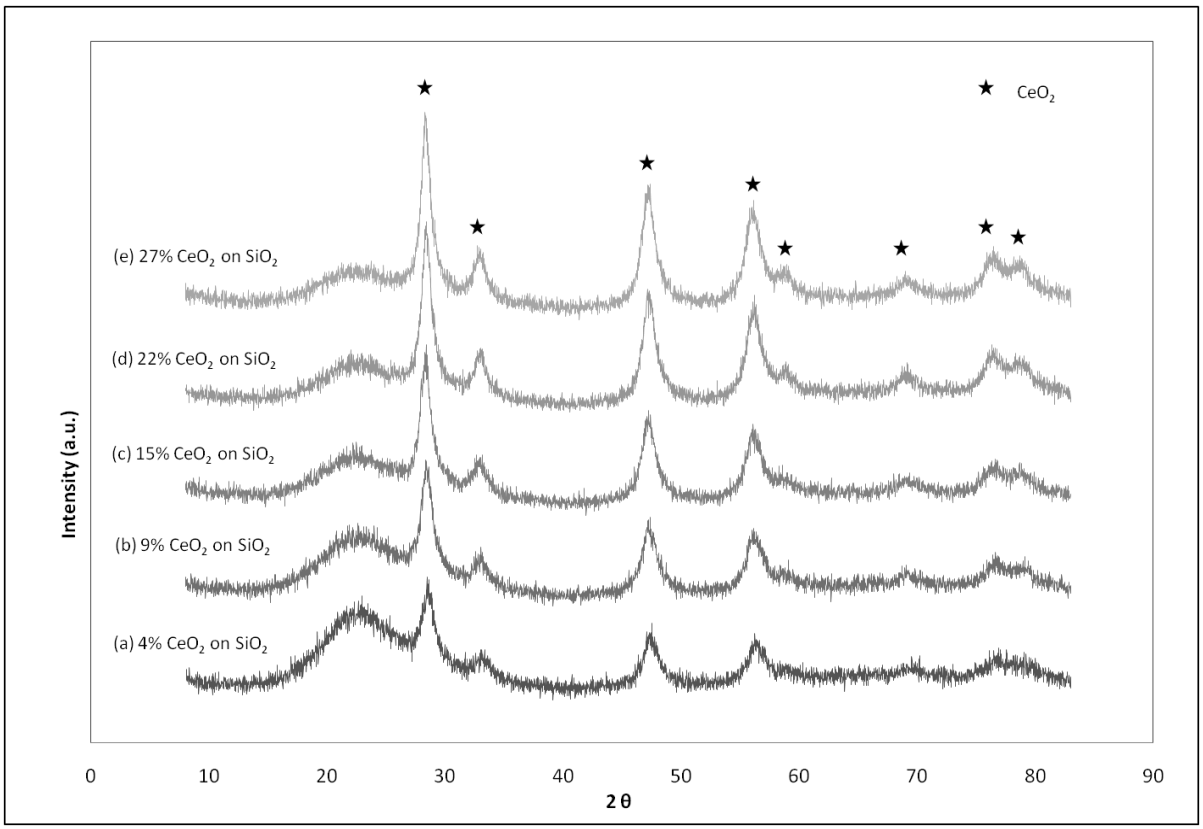

Figure V.3. Powder XRD Patterns for Ceria/silica Prepared by IN: 4%, 9%, 15%, 22%, and 27%.

The catalytic activity and Pt dispersion improved with increased CeO_2 content from 4% CeO_2 (reaction rate: 1.05 µmol/g/s; Pt %D: 36) to 22% CeO_2 (5.77 µmol/g/s; 52%). However, the TOF values increased with increased CeO_2 content indicating that Pt dispersion was not the only factor for activity improvement. Since Pt – CeO_2 contact area was deemed responsible for activity, the increased CeO_2 SA along with the increased Pt dispersion could explain the improved activity with increased CeO_2 content.

When CeO_2 content was increased from 22% CeO_2 to 27% CeO_2, the reaction rate and TOF values decreased slightly. This drop in the catalytic activity could be explained by two possible reasons:

(a) the increased CeO_2 crystallite size, resulting in lesser utilization of ceria, reduced Pt – ceria contact area, and (b) change in the catalyst porous structure due to pore blockage or pore narrowing. The changes in the porous structure were evident from the PV and APS analysis, as both of these paramters decreased with increased ceria content. CO diffusion in these catalyst pores was dominated by Knudsen diffusivity [79]. Narrow pores would result in lower effective diffusivity. In the case of diffusion controlled reactions, lower effective diffusivity would result in lower activity.

Increasing the ceria content from 22% to 27% would not only reduce ceria utilization but it would also reduce the effective diffusivity of CO resulting in lower activity. So, the optimum value of ceria loading was in the range of 15-25% (w/w).

Table V.7. **Effect of Ceria Content on Ceria Dispersion and Total SA, PV and Avg. Pore Size**

Catalyst	**CeO_2 Dp (nm)**		**BET SA (m^2/g)**	**PV (cc/g)**	**Avg. Pore Size (Å)**
	O_2 Chemi.	**XRD**			
SiO_2	NA	NA	319	1.14	143
4% Pt - 4% CeO_2/SiO_2 – IN – B	6.2	6.0	306	1.10	144
4% Pt - 9% CeO_2/SiO_2 – IN – B	6.4	6.4	293	1.03	141
4% Pt - 15% CeO_2/SiO_2 – IN – B	6.9	6.9	257	0.92	143
4% Pt - 22% CeO_2/SiO_2 – IN – B	7.0	7.3	248	0.87	140
4% Pt - 27% CeO_2/SiO_2 – IN – B	7.6	7.7	251	0.85	135

V.3.6 Platinum Precursor Selection

The effect of the type of Pt precursor was studied by comparing the Pt dispersion and CO activity of four different catalysts prepared by using different Pt precursors. The CO oxidation activity results are given in Table V.8 and the H_2 and CO chemisorption results are given in Table V.9.

Table V.8. Effect of Platinum Precursor on Catalytic Activity

(Catalyst: 4% Pt – 16% CeO_2/ SiO_2) Pt Precursor	Rate of Reaction* (µmol/g/s) Calcination Temp.			
	300°C	**400°C**	**500°C**	**600°C**
Chloroplatinic Acid#[a]	**0.28**	0.21	0.16	0.09
Tetraammine platinum hydroxide (TAPH)[b]	2.87	3.36	**3.78**	2.28
Tetraammine platinum nitrate (TAPN)[b]	0.35	0.70	**4.40**	2.94
Diammine dinitro platinum (DADNP)[b]	0.84	1.54	**9.04**	8.65

#Different test conditions used for chloroplatinic acid based catalyst to obtain non-zero reaction rates;

**Test Conditions: Humidity: 50% RH, Temperature: 25^{0}C, Reactor ID: ¾", Particle Size: 200 µm, Cat. Wt.: 0.5g, (a) Face Velocity: 45 cm/sec, CO: 300 ppm in air; (b) Face Velocity: 60 cm/sec, CO: 750 ppm in air.*

Table V.9. Effect of Platinum Precursor on Pt Dispersion and TOF

(Catalyst: 4% Pt – 16% CeO_2/ SiO_2) Pt Precursor	Platinum % D		TOF (x10^2)*
	H2 Chemi.	**CO Chemi.**	
Chloroplatinic Acid	16.0	22.2	0.9
Tetraammine platinum hydroxide (TAPH)	31.2	30.1	5.9
Tetraammine platinum nitrate (TAPN)	34.4	34.5	4.8
Diammine dinitro platinum (DADNP)	44.5	40.3	12.8

*Estimated TOF from CO chemisorption only for the best performing catalyst for each Pt precursor

TEM images were also obtained for these catalysts which are given in Figure V.4: (a) chloroplatinic acid, (b) tetra ammine platinum hydroxide (TAPH), (c) tetra ammine platinum nitrate (TAPN), and (d) diammine dinitro platinum (DADNP). Due to the closeness of the Pt crystallite sizes; an in-depth analysis using TEM was not performed. However, the TEM images showed that the chlorinated precursor resulted in larger Pt crystallites in comparison.

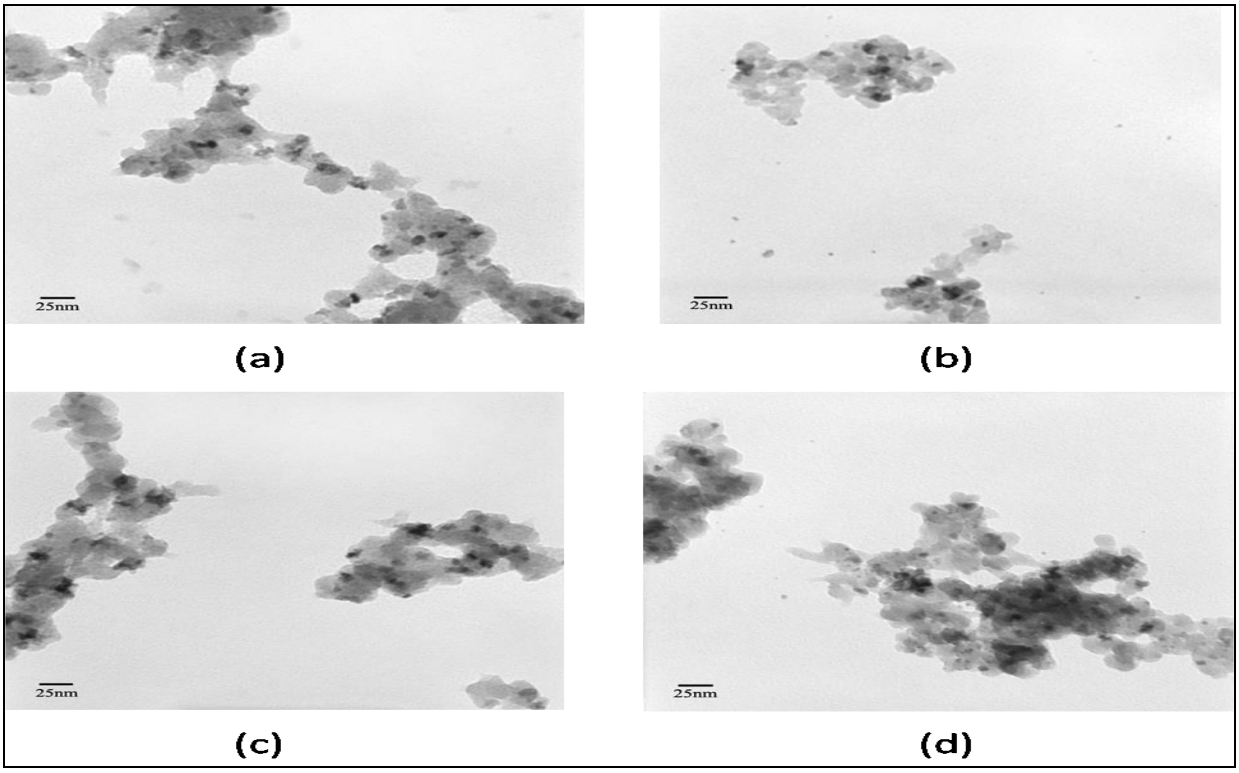

Figure V.4. TEM Images of 4%Pt – 16%CeO_2/SiO_2 catalysts prepared by different Pt precursors.

Better dispersion would explain the greater activity of the catalyst prepared with DADNP precursor. However, the TOF values indicated that catalytic activity was not directly proportional to the Pt dispersion. Pt crystallites could either be deposited directly on SiO_2 or could be deposited on CeO_2/SiO_2. Analysis by CO/H_2 chemisorption could not distinguish between these two types of Pt crystallites. So, it would be important to understand Pt dispersion as well as location of the Pt crystallites

in the catalyst. Temperature programmed reduction (TPR) studies were performed on these catalysts to try to distinguish between Pt/CeO_2 and Pt/SiO_2. The TPR profiles for these catalysts in the temperature range of 100^0C - 750^0C are given in Figure V.5: (a) 16%CeO2/SiO2; (b) 4%Pt- 16%CeO2/SiO2 – Prepared by using chloroplatinic acid; (c) 4%Pt- 16%CeO2/SiO2 – Prepared by using TAPH; (d) 4%Pt- 16%CeO2/SiO2 – Prepared by using TAPN; (e) 4%Pt- 16%CeO2/SiO2 – Prepared by using DADNP. The presence of metallic Pt in contact with CeO_2 would lead to spill over of hydrogen to the adjacent CeO2. *Salasc et al* have shown that due to this hydrogen spill over, surface CeO_2 adjacent to Pt could get reduced even at room temperature [52]. So, a H_2 consumption peak in the TPR profile corresponding to surface ceria reduction would indicate absence of Pt crystallites deposited on CeO_2/SiO_2.

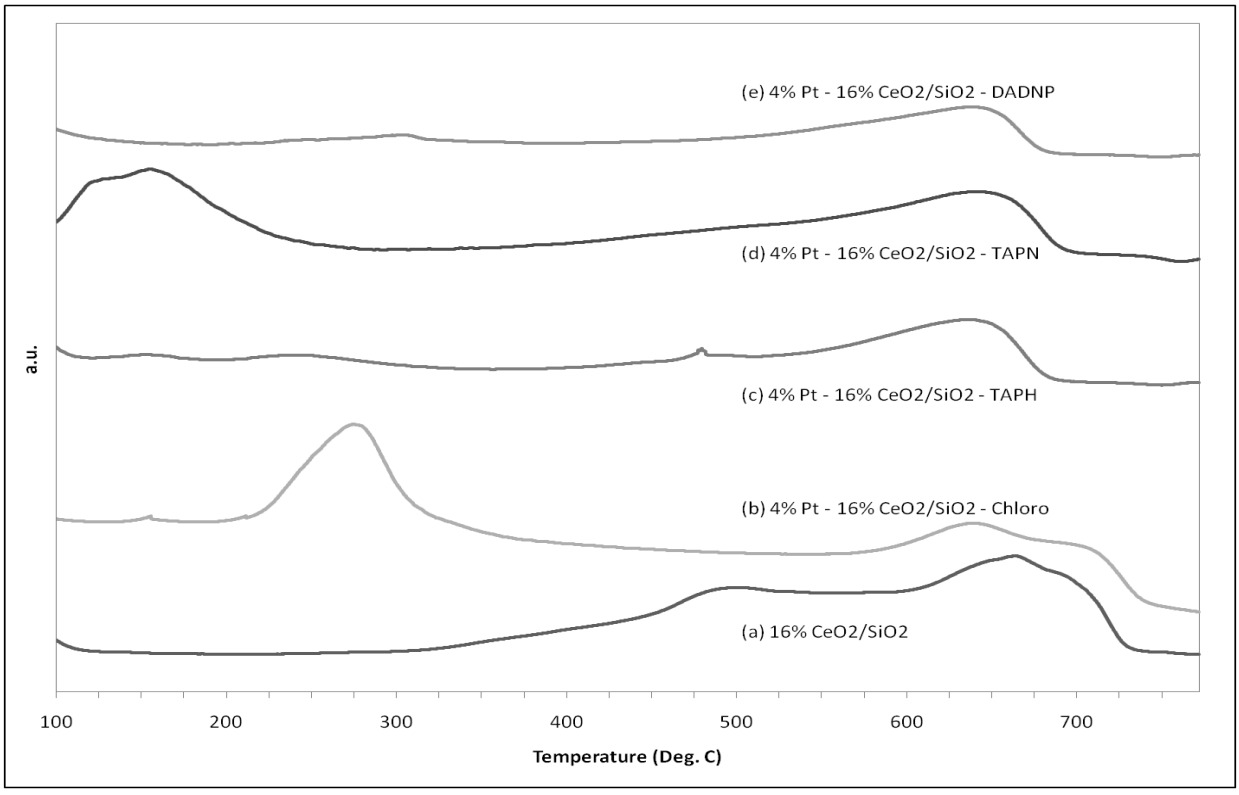

Figure V.5. TPR Profiles of Catalysts Prepared with Different Pt Precursors.

In the case of CeO_2/SiO_2 sample, two peaks for ceria reduction were obtained at 490°C (reduction of the surface of the CeO_2) and 680°C (reduction of the bulk CeO_2). All of the catalysts showed a reduction peak at 670°C corresponding to the reduction of the bulk CeO_2. A low temperature peak corresponding to the reduction of a Pt oxide species (PtO, PtO_2, PtOx or PtClxOy) was obtained at 180°C (for catalysts prepared with TAPH) and at 280°C (for catalyst prepared with chloroplatinic acid).

In the case of catalyst prepared with TAPH a narrow reduction peak at 480°C corresponding to the surface CeO_2 reduction was also obtained. The presence of this peak would mean presence of some of the ceria grains which were not in contact with Pt crystallites. The absence of a H_2 uptake peak representing the reduction of the surface of CeO_2 (for chloroplatinic acid, TAPN, and DADNP) indicated H_2 spillover from Pt to adjacent CeO_2 resulting in surface ceria reduction. However, even a small amount of Pt present in contact with ceria could lead to complete surface ceria reduction due to spill over of H_2 [52]. So, a quantitative estimation of Pt/CeO_2 would be difficult.

The IEP of the support and pH of the impregnating solution would dictate the interaction between the two and ultimately the distribution profile of the active sites. Many researchers have observed that the Pt dispersion was a function of Pt precursor used during preparation [82-84, 86]. In the case of Pt/SiO_2 catalysts, the nature of the ionic species of the Pt precursor played a crucial role in the final dispersion of Pt [86]. If the pH of the precursor solution is below the IEP of the support then the anionic species of the precursor could easily chemisorb on the support surfaces with a positive charge. In contrast, cationic species easily chemisorb on the support surfaces with a negative charge if the pH of the precursor solution is over the IEP of the support [87].

During this study, the pH of the non-chlorinated Pt precursor solutions was in the range of 7-8, and the surface of silica was negatively charged with an IEP of 1.7 – 3.5, while the surface of ceria

promoter was neutral in charge with an IEP of 6.7 – 8.6 [78]. Among the Pt precursors used, TAPH ($(NH3)_4Pt^+$) and TAPN ($(NH3)_4Pt^+$) had positively charged ionic species, and the DADNP precursor resulted in a neutral Pt species. So the Pt deposition would be greater on silica compared to that on CeO_2, in the case of TAPH and TAPN. However, as mentioned earlier, the DADNP precursor due to the neutral Pt species and the presence of NH_4^+ ions would result in greater amounts of Pt/CeO_2 in the catalyst and better dispersion.

Depending on the type of Pt precursor, the degree of Pt deposition on ceria and in turn the Pt-CeO_2 contact area would change. Since ceria could stabilize Pt and the interfacial Pt-CeO_2 area could provide the sites for CO oxidation, the Pt-CeO_2 contact area was important for the catalytic activity. The catalyst prepared using the DADNP precursor did not show any other peak apart from the bulk ceria reduction peak (at 670^0C). In other words, most of the deposited Pt was present in the metal crystallites form and all of the ceria grains were deposited with the Pt crystallites. So, the catalysts prepared by the DADNP precursor resulted in greater activity.

V.3.7 Platinum Precursor Calcination and Drying Conditions Selection

The activity results and estimated Pt dispersion values for different Pt precursor calcination temperatures are given in Table V.10. Activity increased with increased calcination temperature till 500^0C, and the activity decreased when calcination temperature was increased to 600^0C. The Pt dispersion decreased with increased calcination temperature. A reduction in the Pt dispersion should have an adverse effect on catalytic activity; however, the catalytic activity increased with calcination temperature up to 500^0C.

There could be two possible reasons for decline in the Pt dispersion: (a) metal sintering or (b) decoration of Pt crystallites by CeO_2. Pt metal sintering due to surface diffusion would lead to lower Pt

dispersion and reduced activity. However, the ceria decoration of Pt would increase the Pt-CeO_2 interfacial area leading to improved activity. Decoration of noble metal crystallites had been studied in detail, for example, *Zhang et. al.* showed that for Pt/TiO_2 catalysts, decoration of Pt by TiO_2 increased with calcination temperature resulting in lower Pt dispersion[104].

Table V.10. Effect of Platinum Precursor Calcination and Drying Conditions

Catalyst (X%Pt-16%CeO_2/SiO_2)	**Drying Condition#**	**Calc. Time**	**Calc. Temp.**	**Rxn. Rate* (µmol/g/s)**	**CO Chemi. on Pt**		**TOF (x10^2)**
					%D	**Dp (nm)**	
2.5% Pt	A	4 Hrs	400^{0}C	0.37 (a)	52.4	2.2	0.7
2.5% Pt	B	4 Hrs	400^{0}C	0.91 (a)	49.4	2.3	1.8
2.5% Pt	C	4 Hrs	400^{0}C	1.84 (a)	48.9	2.3	3.7
4.0% Pt	C	4Hrs	300^{0}C	0.84 (b)	54.1	2.1	0.76
4.0% Pt	C	4 Hrs	400^{0}C	1.54 (b)	49.4	2.3	1.55
4.0% Pt	C	4 Hrs	500^{0}C	9.04 (b)	40.3	2.8	10.9
4.0% Pt	C	4 Hrs	600^{0}C	8.65 (b)	21.9	5.2	19.3
2.0% Pt	C	1 Hr	500^{0}C	0.70 (c)	43.1	2.6	1.6
2.0% Pt	C	2 Hrs	500^{0}C	1.72 (c)	37.7	3.0	4.5
2.0% Pt	C	3 Hrs	500^{0}C	0.65 (c)	33.9	3.3	1.9
2.0% Pt	C	4 Hrs	500^{0}C	0.32 (c)	33.6	3.4	1.0

#(A) Vacuum Dry @ 40^{0}C; (B) Overnight @ 75^{0}C; (C) 4 hours @ 125^{0}C; * *Test Conditions: Humidity: 50% RH, Temperature: 25^{0}C, Reactor ID: ¾", Particle Size: 200 µm, (a) Cat. Wt.: 0.5g, Face velocity: 45 cm/sec, CO Conc.: 500ppm; (b) Cat. Wt.: 0.2g, Face velocity: 60 cm/sec, CO Conc.: 750ppm; (c) Cat. Wt.: 0.5g; Face velocity: 45 cm/sec; CO Conc.: 300ppm.*

Based on the activity and Pt dispersion results, the ceria decoration of Pt must be the main cause for reduced Pt dispersion till 500^0C and Pt metal sintering was significant above 500^0C. So, a trade-off existed between ceria decoration of Pt and Pt sintering which was optimum at around 500^0C.

The impact of calcination time on the activity was also studied and the results are summarized in Table V.10. Calcination time showed a volcano type profile for catalytic activity similar to that of the calcination temperature. Additionally, the Pt dispersion decreased with increased calcination time. The aggregation of Pt crystallites by surface diffusion and ceria decoration of Pt crystallites are functions of calcination temperature and calcination time. With increased calcination time, the crystallites would grow bigger and the extent of decoration would be greater. Analogous to the calcination temperature trend, a volcano type of correlation existed between the calcination time and the catalytic activity which in the case of the calcination temperature of 500^0C for the DADNP precursor peaked at about 2 hours.

The effect of Pt precursor drying conditions on CO activity and Pt dispersion was studied and the results are given in Table V.10. The drying condition had a significant impact on activity with faster drying rates yielding better catalysts. However, the drying condition did not affect the Pt dispersion significantly (difference in Pt %D: 4%). The drying conditions affect not only Pt dispersion but also the Pt distribution profile in catalyst. Considering that the drying condition had a minor impact on Pt dispersion of the catalyst (instrument error (%D): ±2%), the drying conditions must have played a major role in determining Pt distribution profile.

There are two important factors that affect distribution profile [96]: (a) type of precursor adsorption on support: strong or weak; and (b) drying rate: fast or slow. For weakly adsorbed precursors, greater drying rate would result in egg-shell profile and slower drying would result in homogeneous distribution profiles [96]. Weak interaction existed between ceria-silica support and

DADNP resulting in weak adsorption. So, faster drying at 125^0C could have resulted in a Pt distribution profile close to an egg-shell profile.

As observed earlier, during the study of type of silica support, CO oxidation on the Pt-CeO_2/SiO_2 catalyst was diffusion limited. In the case of diffusion limited reactions, an egg-shell Pt distribution profile would be favorable [94].

V.3.8 Effect of Platinum Loading

The effect of Pt loading was studied by varying the Pt content from 1.25% to 10% w/w. The activity and characterization results are given in Table V.11.

Table V.11. Effect of Pt Loading on Activity, Pt Dispersion and Surface Characteristics

(X%) Pt – 20% CeO2/SiO2 - IN	Reaction rate* (µmol/g/s)	Pt (%D) CO Chemi.	TOF (x100)	BET SA (m^2/g)	PV (cc/g)	Avg. Pore Size (Å)
1.25% Pt	**1.34**	76	2.8	268	0.90	134
2.50% Pt	**2.46**	51	3.8	260	0.88	135
3.75% Pt	**2.80**	40	3.6	258	0.87	136
5.00% Pt	**3.13**	39	3.1	249	0.84	136
7.50% Pt	**3.52**	31	3.0	225	0.79	140
10.0% Pt	**2.74**	27	1.9	230	0.78	136
5% Pt/SiO_2	**0.61**	23	1.1	ND	ND	ND
SiO_2	**0.00**	NA	NA	319	1.14	143

* *Test Conditions: CO Conc. : 500 ppm CO in air, Catalyst bed depth: 3.2mm (inert silica: 50-75%), Face velocity: 60 cm/sec, Particle Size: 150-250 µm, Reactor ID: ¾", Humidity: 50% RH, Temperature: 25^0C.*

Increased Pt content improved activity and reduced Pt dispersion. For example, catalyst with 5%Pt (rate: 3.13 µmol/g/s; %D: 39) and the catalyst with 1.25% Pt (1.34 µmol/g/s; 76%). However, the TOF values decreased with increased Pt content.

Since the Pt – CeO_2 interfacial area was crucial to the activity of the catalyst, the formation of larger Pt crystallites would diminish the Pt –CeO_2 interfacial area, thus resulting in the decline of the rate of reaction on per surface Pt atom basis, i.e. TOF. Further, an increase in the Pt loading after 7.5% caused a significant drop in the TOF as well as the overall rate of reaction. This could possibly be a combined effect of: (a) increased Pt crystallite size resulting in decreased Pt –CeO_2 interfacial area, and (b) changes in the porous structure of the catalyst such as pore blocking and/or pore narrowing.

The PV and APS analysis results showed decreased PVs and APS with increased Pt content. The changes in PV and APS were indicative of both pore blocking and pore narrowing. Based on these results an optimum Pt content should be in the range of 2.5 – 7.5 % Pt (w/w).

V.3.9 Effect of Other Preparation Variables

V.3.9.1 Effect of Platinum Precursor Concentration

Successive thermal treatments could be avoided using high concentration of Pt precursor; however, greater precursor concentrations could adversely affect dispersion due to limited number of exchange sites available on the support. Therefore, a trade-off exists between the number of thermal treatments and the precursor concentration. Effect of Pt precursor concentration was investigated by preparing catalysts with same composition and the activity results, estimated Pt dispersion and TOF results are tabulated in Table V.12.

There was no significant change observed in the reaction rate as well as in the Pt dispersion due to the increased Pt precursor concentration. Since up to 5% Pt can be obtained in one impregnation step by using a high concentration precursor (5 % Pt (w/w)), that precursor was used in most of the studies.

Table V.12. Effect of Platinum Precursor Concentration on Activity and Pt Dispersion

Pt Loading	Rate of Reaction (µmol/g/s)	%D	TOF
2.50%	2.46(a)	50.76	0.0378
2.5% Two Imp	2.52(a)	53.99	0.0364
5.00%	3.13(b)	39.12	0.0312
5% Two Imp	3.36(b)	41.53	0.0315

Test Conditions: Humidity: 50% RH, Temperature: 25^{0}C, Reactor ID: ¾", Particle Size: 200 µm, (a) Catalyst wt: 0.25g (inert silica: 0.25g), Face Velocity: 30 cm/sec, CO Conc.: 300 ppm CO in air; (b) Catalyst wt: 0.25g (inert silica: 0.25g), Face Velocity: 45 cm/sec, CO Conc.: 400 ppm CO in air.

V.3.9.2 Effect of Hydrogen Reduction

The last step of Pt – Ceria/Silica catalyst preparation was high temperature calcination in air. During this calcination step there was also possibility of formation of PtOx species on the surface which could be converted into Pt metal by reducing in hydrogen. Further, it has also been reported that in case of ceria – silica systems, high temperature (T>325^{0}C) redox cycles changed the ceria crystallite size and significantly improved the redox behavior of ceria crystallites [111]. However, increasing the reduction temperature to more than 573 K would improve the chances of formation of CePt5 alloy [81]. Considering these constraints, the effect of H_2 reduction on catalyst activity was investigated by reducing the catalyst in H_2 up to 250^{0}C.

After reduction for 2 hours at designated temperature, the catalysts were cooled down to room temperature in N_2 and then treated in air for one hour at 50^0C before storing. The CO oxidation activity results are shown in Figure V.6. The catalyst used was 2% Pt – 12% Ceria/Silica.

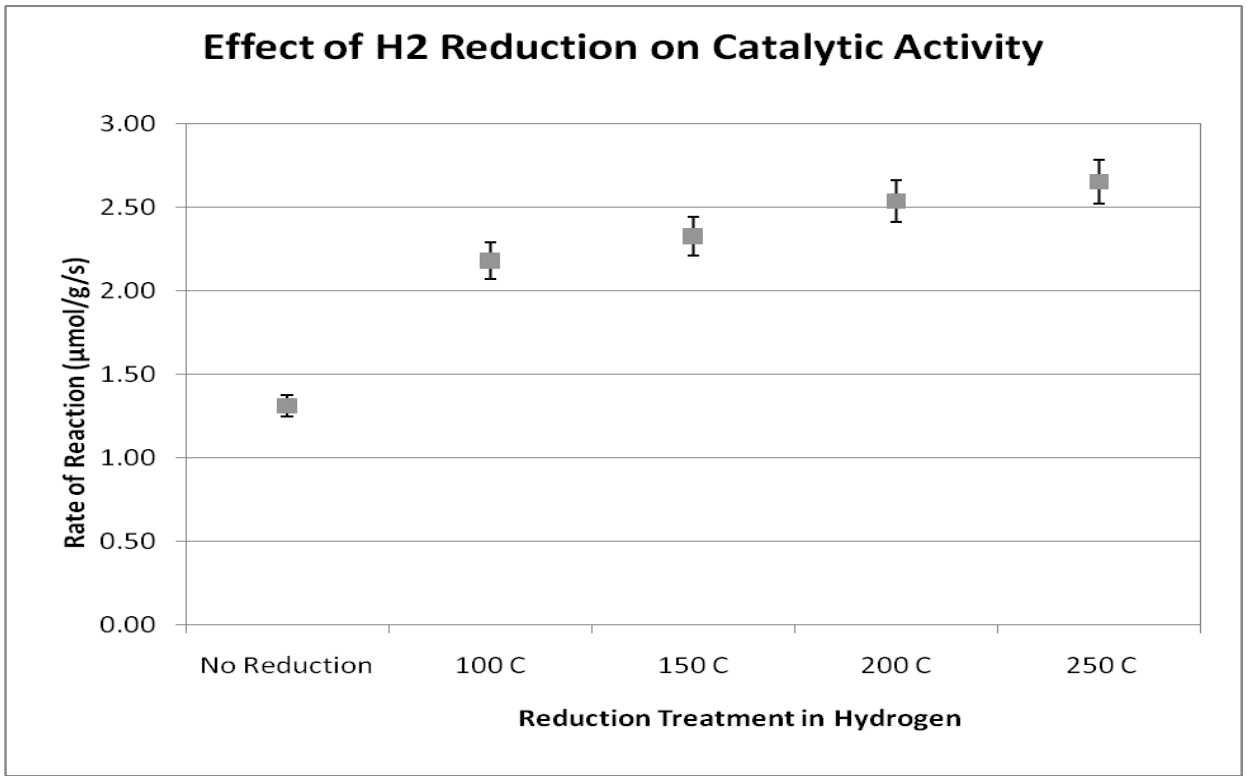

Figure V.6. Effect of H_2 reduction Treatment on Catalytic Activity

Test Conditions: Face velocity: 45 cm/sec; Humidity: 50% RH; Temperature: 25^{0}C; Reactor: 0. 75" ID; Catalyst bed depth: 3.2mm; Particle Size: 150-250 µm; Inlet CO: 300ppm in air

Reduction of the catalyst in hydrogen at 250^0C improved the catalytic activity by more than 100%; the rate of reaction increased from 1.24 µmol/g/s to 2.6 µmol/g/s. There could be two possible reasons for activity improvement after hydrogen reduction: (a) reduction of PtOx species to metal Pt species; (b) reduction of ceria to form cerium ions and oxygen vacancies, which would get reoxidized at room temperature to form superoxide ions (O_2^-) [112]. Presence of Pt decreases the reduction temperature of

ceria [52, 112]; therefore, the probability of formation of superoxide radicals would be higher. These superoxide radicals have been reported to be involved in CO oxidation reaction on Pt- Ceria/Alumina catalyst [113].

During this work, possibility of PtOx species formation during calcination and their conversion to Pt by H_2 reduction was tested by analyzing oxidation states of Pt before and after reduction. XPS spectra were obtained for the catalysts, before and after reduction to identify oxidation state of Pt; the results of XPS analysis are given in Table V.13.

Table V.13. XPS Results for Pt 4f in BE Values for Reduced and Non-Reduced Catalyst

Sample	**Pt $4f_{7/2}$ (BE in eV)**	**Pt $4f_{5/2}$ (BE in eV)**
No reduction	72.6	76.0
H_2 Reduction @ 250^{0}C	70.3	73.6
Elemental Pt	70.9	74.3

For stoichiometric PtO, BE for the $Pt4f_{7/2}$ peak is 73.5 - 74.0 eV; whereas, for PtO_2 it is 74.5 – 75.0 eV. For the non – reduced catalyst, there was a significant shift in BE (72.6 eV) in comparison to elemental Pt (70.9 eV). In other words, it was reasonable to assume that Pt existed in the form of PtOx on the surface before H_2 reduction. After reduction with hydrogen, the BE for $Pt4f_{7/2}$ peak was 70.3 eV which was in more agreement with elemental Pt (70.9 eV). From these results it could be said that non-reduced catalyst had certain PtOx species, which got converted to Pt metal after H_2 reduction. Additionally, the XPS spectra for reduced catalyst were obtained after exposing the sample to air at room temperature (RT). This indicated that re-oxidation of Pt at RT was inhibited.

V.3.9.3 Effect of Pt Precursor Calcination Atmosphere

Calcination in general refers to thermal treatment in air. During this study, it was envisioned that there might be formation of PtOx species during calcination, hence effect of calcination (or thermal treatment) atmosphere was studied in detail and the results are given in Figure V.7. The Catalyst used was 2% Pt – 12% Ceria/Silica.

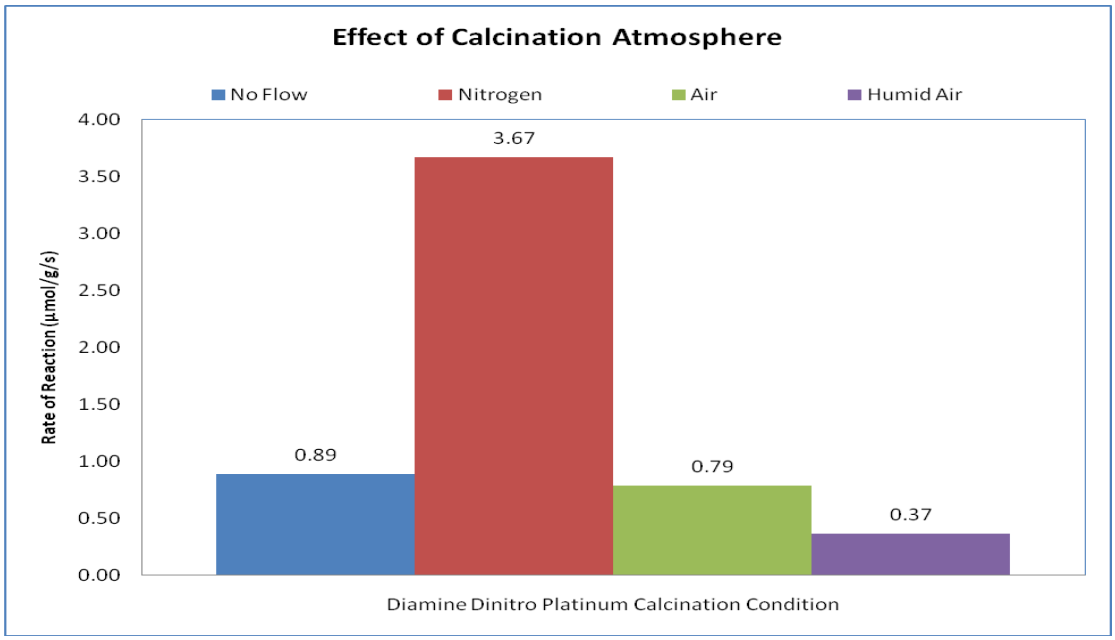

Figure V.7. Effect of Pt Precursor Calcination Atmosphere on Catalytic Activity

Test Conditions: Face velocity: 45 cm/sec; Humidity: 50% RH; Temperature: 25^{0}C; Reactor: 0. 75" ID; Catalyst bed depth: 3.2mm; Particle Size: 150-250 µm; Inlet CO: 400ppm in air

When an inert like nitrogen was used during thermal decomposition of Pt precursor, the resulting catalyst had a much better activity in comparison with the catalyst prepared by calcining in air. However, the catalyst prepared by calcining in N_2 did not show a better shelf life and the activity decreased over time. Considering the stability of the catalyst being an important issue during the development of the catalyst, the calcination was carried out in air.

V.3.10 Effect of operating Conditions

V.3.10.1 Effect of Particle Size

In order to investigate if CO oxidation on Pt–Ceria/Silica catalyst was diffusion controlled or reaction controlled the effect of particle size on activity was studied and the results are given in Figure V.8. To minimize batch variations in catalyst preparation, larger catalyst particles were crushed and sieved to obtain different particle sizes.

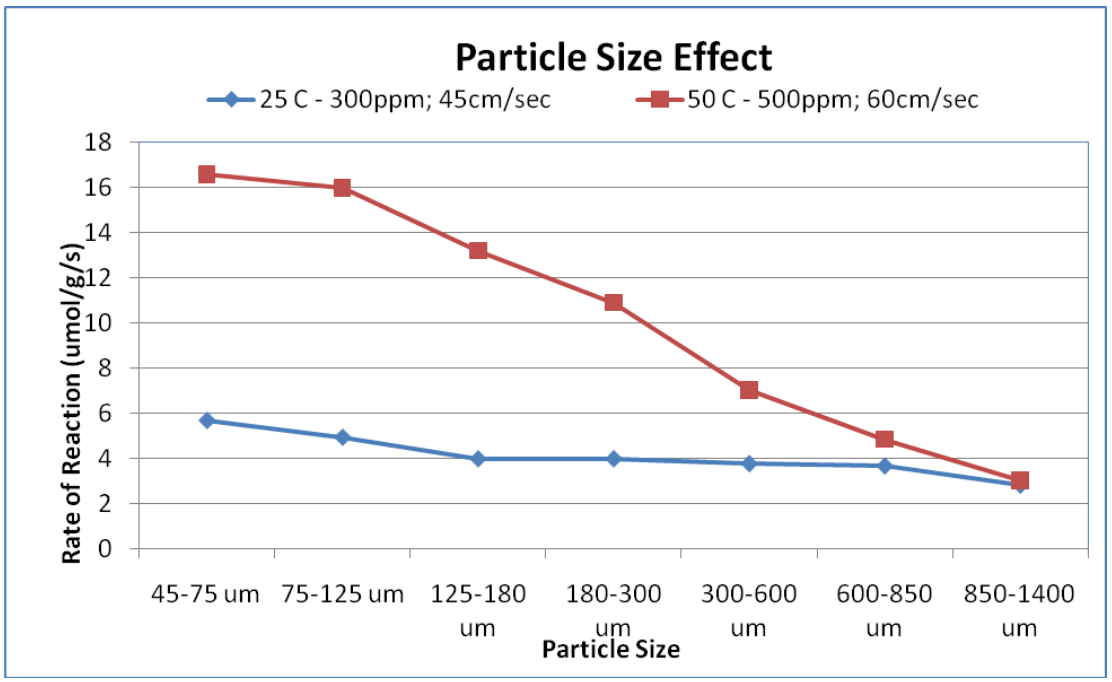

Figure V.8. Effect of Particle Size on the Activity of Pt-Ceria/Silica Catalyst

Test Conditions: Humidity: 1% H_2O, Reactor ID: ¾", Catalyst wt: 0.05g (inert silica: 0.5g)

The reaction was significantly diffusion limited. When the particle size was reduced from 0.75 mm to 0.075 mm, the change in the reaction rate was almost double at room temperature. The Weisz – Prater parameters (C_{WP}) were calculated for all the particles which are tabulated in Table V.14. C_{WP} is a ratio of actual reaction rate to that of diffusion rate. Expression [114] for C_{WP} is given in Equation V.5.

Equation V.5. Weisz – Prater parameter

$$C_{WP} = \frac{R_{obs}\rho_c R^2}{D_{eff}C_{AS}} = \frac{actual\ reaction\ rate}{a\ diffusion\ rate}$$

If $C_{WP} < 1$, the reaction is internal diffusion limited;

Where, R_{obs} : observed rate of reaction; ρ_c: catalyst density; R: radius of catalyst particle; D_{eff}: effective diffusivity; C_{AS}: concentration at surface

In order to find out if the reaction was external diffusion limited, Mears' criterion [114] was followed, the values estimated from Equation V.6 are tabulated in Table V.14.

Equation V.6. Mears' Criterion for external diffusion control

$$\frac{-r_A{}'\rho_b R\, n}{k_c C_{Ab}} < 0.15$$

Where, $-r_A{}'$: rate of reaction; ρ_b: bulk density of catalyst; *R*: particle radius; *n*: reaction order; k_c: mass transfer coefficient; C_{Ab} : bulk concentration

For estimation of k_c, correlations by wakao [79, 115] and that by Thoenes and Kramers [114, 116] were followed. From the Mears' criterion it was clear that the reaction was not external diffusion controlled. Effect of diffusion limitations was significant even at room temperature (25^0C), C_{WP} value being more than 40 for 450 µm (C_{WP} = 42.8), and more than 10 for 250 µm (C_{WP} = 12.9). At greater reaction temperature, the increase in effective diffusivity was negligible compared to increase in the reaction rate. For example, ratio of reaction rate on 725 µm particles to that of 60 µm particles was 1.72 at 25^0C and 3.4 at 50^0C.

In the case of exothermic reactions such as CO oxidation, for smaller particles the diffusivity is greater; therefore, the reaction rates are higher resulting in greater adiabatic temperature rise and improved activity. However, higher diffusivity could possibly result in greater rates of catalyst self CO-poisoning at lower temperatures, so there is a trade-off as well.

Table V.14. Estimated Weisz – Prater parameters and Mears' criteria for Particles

Particle Size (μm)	**C_{WP} at T:25^{0}C**	**C_{WP} at T:50^{0}C**	**Mears' criterion at T:25^{0}C**	**Mears' criterion at T:50^{0}C**
600 – 850	96.96	88.17	0.149	0.135
300 – 600	42.79	49.27	0.084	0.096
180 – 300	12.85	21.74	0.034	0.058
125 – 180	5.59	10.63	0.019	0.036
75 – 125	2.76	5.54	0.011	0.023
45 – 75	1.14	2.07	0.006	0.011

V.3.10.2 Effect of Temperature

The effect of temperature was studied on 100 micron particles and the results are plotted in Figure V.9. Further, effective diffusivities and C_{WP} values were estimated at different temperatures and are given in Table V.15. Higher reaction rates at elevated temperatures made it impossible to run the

reactor in a differential mode at low CO and lower face velocities. Therefore, different CO flux values were used for different temperatures and the dilution of catalyst bed with silica was kept uniform.

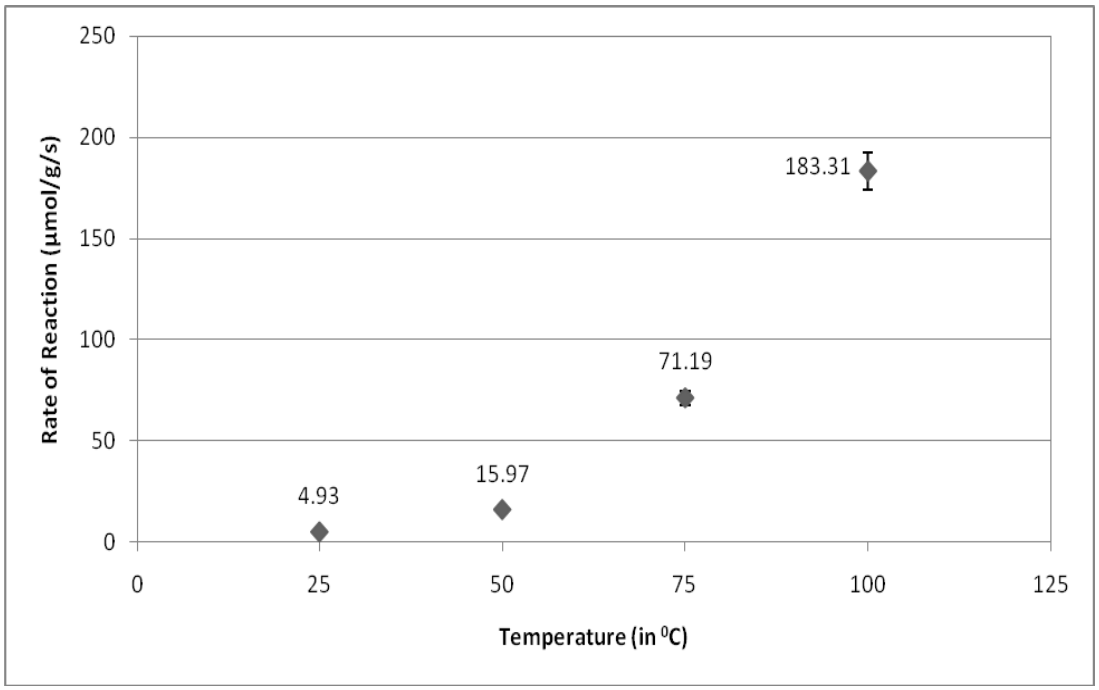

Figure V.9. Effect of Temperature on Catalytic Activity (Particle Size: 100 micron)

Test Conditions: Water Vapor: 2%; Reactor: 0. 75" ID; Catalyst bed: 3.2mm (50mg catalyst + inert); (300, 500, 700, 1000 ppm CO respectively for T: 25^{0}C to T: 100^{0}C); Face velocity: (45, 60, 60, 60 cm/sec respectively for T: 25^{0}C to T: 100^{0}C.).

Increase in effective diffusivity was negligible because the diffusion was dominated by Knudsen diffusion for this catalyst (where l/d_{pore}: 5). For example, the increase in effective diffusivity going from 25^{0}C to 100^{0}C was only 15%. On the other hand, the change in reaction rates was significant, the increase in temperature from 25^{0}C to 100^{0}C had increased the observed reaction rate almost by a factor of 40. The C_{WP} had gone up from 2.76 (at 25^{0}C) to 33.5 (at 100^{0}C).

Table V.15. Estimated C_{WP} and Effective Diffusivity at Different Temperatures

Temperature (in K)	Observed Reaction Rate (µmol/g/s)	Effective Diffusivity D_{eff} (in cm^2/sec)	C_{WP} (Weisz-Prater parameter)
298	4.93	4.25E-03	2.76
323	15.97	4.47E-03	5.52
348	71.19	4.68E-03	23.29
373	183.31	4.88E-03	33.52

With increasing temperatures, the CO adsorption equilibrium would shift resulting in lower adsorbate on the Pt surface, for example, during CO chemisorption on Pt-CeO_2/SiO_2 catalyst CO uptake was 49.9 µmol/g at 30^0C, and 43.3 µmol/g at 40^0C. The ability of CO to form islands on Pt surface is greater at lower temperatures causing catalyst poisoning, while the probability of forming islands at higher temperatures is lower due to shift in CO adsorption equilibrium. So, reduced CO poisoning and improved kinetics would results in greater catalytic activity.

Even for 100 micron particles the reaction was severely diffusion controlled at temperatures above 50^0C. By looking at the C_{WP} values in Table V.15 for 100 micron particles, the reaction probably wouldn't be diffusion controlled for 25 micron particles at 25^0C. However, at higher temperatures, the reaction kinetics improved by orders of magnitude and diffusional rates were slightly improved. So, it was speculated that the reaction would be diffusion limited even for 10 micron particles at T >75^0C.

At higher temperatures, improved kinetics, reduced poisoning and greater ceria redox rates significantly improve the catalytic activity.

V.3.10.3 Effect of Humidity on Catalytic Activity

The effect of water vapor content on catalytic activity was studied by changing the relative humidity of gas from 0% (dry) to 90% RH. The results are given in Figure V.10. The catalytic activity improved with increased moisture content. The catalyst deactivate in dry conditions.

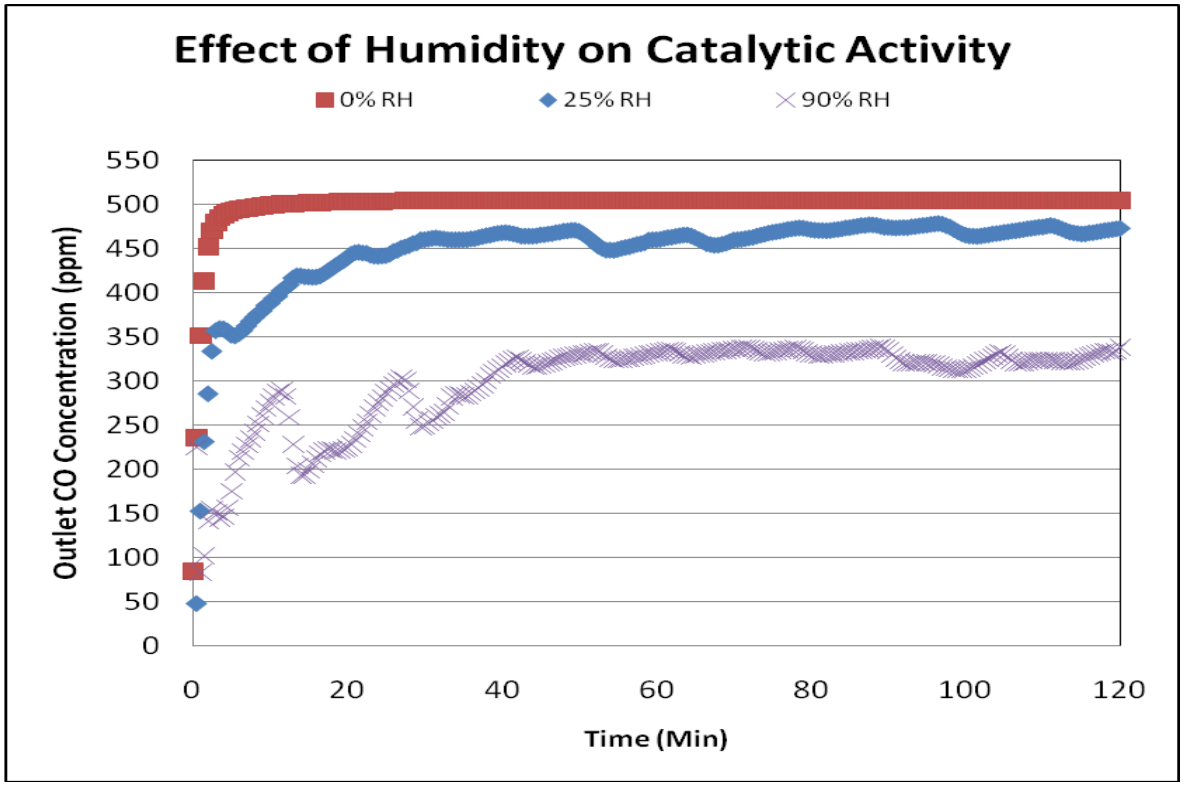

Figure V.10. Effect of Moisture Content on Catalytic Activity

Test Conditions: Inlet CO: 500 ppm; Reactor: 0.75" ID; Temperature: 25^{0}C; Catalyst wt: 0.2gm; Particle Size: 200 µm; Face Velocity: 30cm/sec; Catalyst used: 5%Pt-20%Ceria/Silica.

Activity improved with humidity and the presence of moisture helped maintain activity.

V.3.11 Activity Maintenance of the Catalyst

The activity and stability of 4%Pt-22%CeO_2/SiO_2 catalyst for CO oxidation at ambient conditions was tested and the results are given in Figure V.11: (A) CO: 250 ppm; SV: 360,000 hr-1; (B) CO: 2500 ppm; SV: 90,000 hr-1; (C) CO: 10000 ppm; SV: 72,000 hr-1.

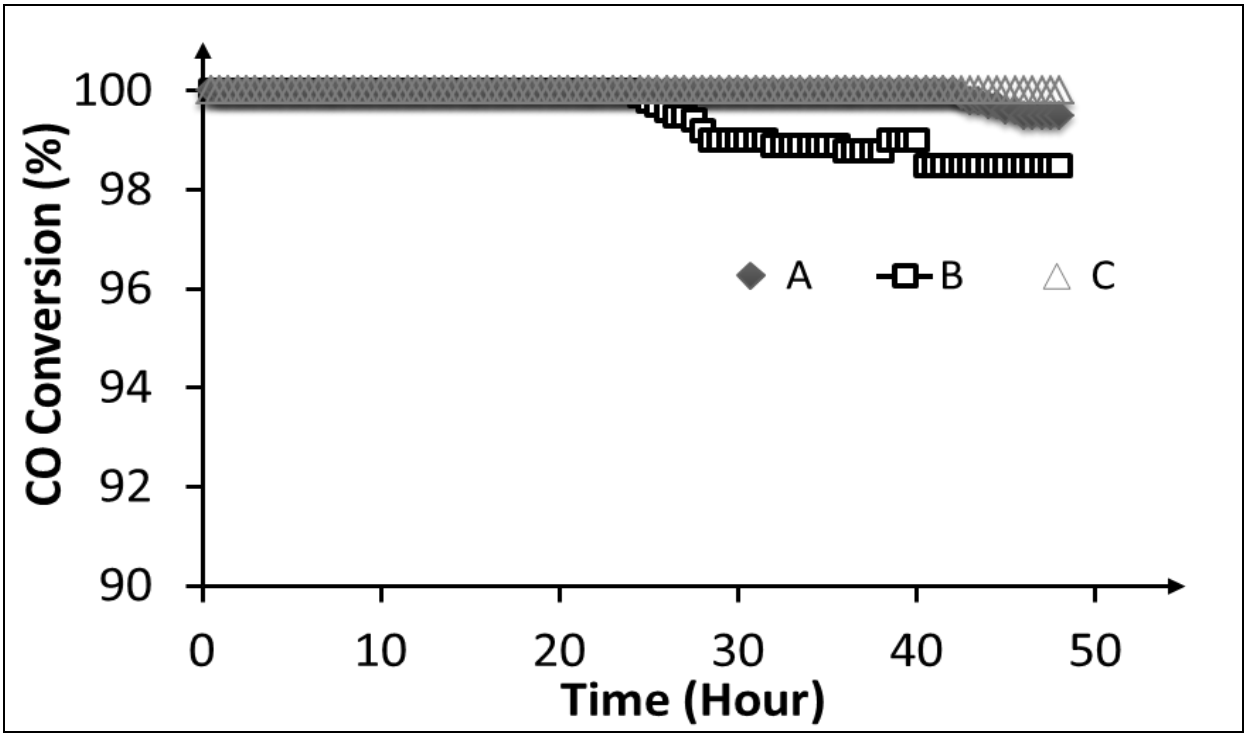

Figure V.11. Activity of 4%Pt-16%CeO_2/SiO_2 catalyst (200 *μm)* at 25^{0}C and 50% RH

The catalyst was highly active (conv. >98%) over a wide range of CO concentrations at ambient conditions (CO: 250-10000 ppm; 50% RH, 25^{0}C). Also, the catalyst maintained activity for more than 50 hours.

V.4 Conclusion

The ceria promoted Pt catalysts were most active for CO oxidation in humid air, wherein the ceria deposition method and type of support played an important role in the catalytic activity. The Pt – CeO_2

interfacial area was crucial to the activity of the catalyst, as determined by O_2-H_2 titration. Further, the deposition of ceria using the incipient wetness impregnation method resulted in the highest Pt – CeO_2 interfacial area and subsequently the most active catalyst. Use of DADNP precursor yielded better dispersion and activity due to the interaction between the precursor and the ceria promoter. The (2.5-7.5%) Pt – (20-25%) CeO_2/SiO_2 catalyst was highly active at room temperature at low and high CO concentrations in the presence of moisture. Also, catalyst preparation parameters played a crucial role in determining the activity of the catalyst. The reaction being diffusion controlled, the silica supports with wider pore openings were favored. The drying and calcination conditions of both the ceria and Pt precursors were crucial in determining the dispersion as well as the distribution profile of the active sites within the catalyst.

VI Comparison with Commercial Catalysts

VI.1 Introduction

CO even in trace amounts is harmful to humans as well as the environment [1, 2, 4]. Low temperature CO removal from air finds applications in many areas ranging from emission control to breathing air purification [117]. Therefore, catalytic CO oxidation at ambient or room temperature(RT) has been an active area of research for more than 4-5 decades now [118]. Slow surface kinetics at RT makes the CO oxidation difficult at RT. However, the high heat of the CO oxidation reaction ($-\Delta H_R$ = 284KJ/mol) may improve the surface kinetics due to its adiabatic temperature rise (approx. $\Delta T_{ad} = 1^0C$ per 100 ppm CO reacted). Further, CO is known to act as a reaction inhibitor during CO oxidation on noble metal catalysts and islands of strongly adsorbed CO were formed on active metal sites during CO oxidation [119]. Therefore, the interplay of these two opposing factors namely, surface oxidation kinetics versus CO self-poisoning dictate the catalytic activity at ambient temperature.

The presence of water vapor has a significant impact on activity at ambient conditions. Water vapor can act as an activity enhancer, activity suppressant or as an inert depending on the type of catalyst and the reaction mechanism. The presence of water vapor can disrupt the formation of CO islands on the noble metal surfaces thereby enhancing the catalytic activity [98]. Also, the presence of water vapor can rapidly replenish the surface hydroxyl groups thereby improving surface kinetics as observed in the case of tin oxide promoted Pt catalysts [120]. However, water vapor may also compete

with CO for active sites and cause decreased activity. Further, water vapor can block the active sites for CO oxidation and make the catalyst inactive in the presence of moisture [7].

Operating conditions also have a significant impact on oxidation activity. The high exothermicity of the reaction and CO self-poisoning give rise to multiple steady states and transient instabilities leading to oscillatory behavior [121, 122]. Instabilities in surface reaction kinetics and the non-linear kinetics of CO oxidation (Langmuir-Hinshelwood dual site mechanism) are the main reasons for hysteresis effect [123]. Hysteresis has been reported during CO oxidation [119, 123, 124] and the sequence of CO introduction to the reactor, CO flux, catalyst bed depth, and variations in temperature or CO concentration play a crucial role in determining observed activity. Further, the presence of kinetic vs. diffusion coupled instabilities in the case of catalyst particles with lower effectiveness factor and the presence of local patches of active and inactive catalysts in the reactor could also give rise to oscillations [125]. Therefore, the reactor parameters such as catalyst particle size, flow distribution in the reactor and catalyst packing are also crucial to the observed oxidation activity.

CO oxidation activity is affected by four major variables: (a) temperature, (b) water vapor content, (c) CO concentration, and (d) operating conditions. Figure VI.1 illustrates the general behavior of catalysts under different test conditions. Activity improves with increased temperature due to increased surface reaction kinetics and reduced CO self-poisoning. CO oxidation is often characterized by a Langmuir Hinshelwood dual site mechanism (Equation VI.1); therefore, at low CO concentrations (typically CO < 500ppm) the activity is low due to slow surface kinetics and the activity is also low at higher CO concentrations (typically CO > 2500ppm) due to significant CO self-poisoning. Depending on the type of the catalyst, water vapor may act as activity enhancer/suppressant as shown in Figure VI.1. At room temperature, two test variables (CO and H_2O vapor concentration) can have major impact on catalytic activity.

$$-R_A = \frac{k * C_A}{(1 + K_A * C_A)^2}$$

Equation VI.1. Rate Expression for Langmuir-Hinshelwood Dual Site Mechanism for CO oxidation in Air

C_A: CO Conc., *k*: rate constant; K_A: CO adsorption equilibrium constant; and ($-R_A$): rate of reaction

The two extremes of these variables, namely: low CO concentration versus high CO and low RH versus high RH profoundly influence observed activity. There are a number of ambient temperature CO removal applications that require CO oxidation in one or more of the above noted regimes. For example, CO removal from cathode air for PEM fuel cells (CO<250ppm, RH>50%) and respiratory protection equipment (CO: 25-10000 ppm; RH>50%).

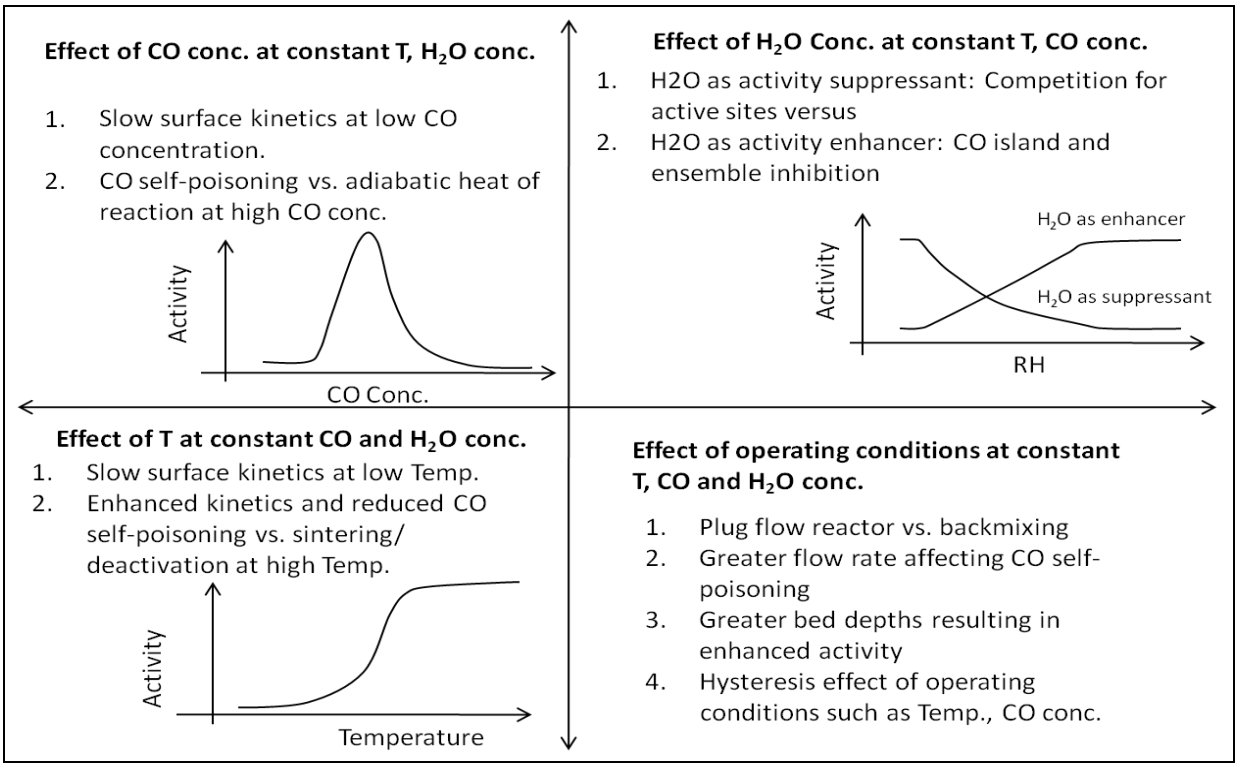

Figure VI.1. General Activity Trends for CO Oxidation Catalysts under Different Testing Conditions

A number of catalyst formulations have been studied for CO oxidation. These catalysts can be broadly classified into three present categories: (a) Pt group metal based catalysts – with or without promoters [68, 69, 126], (b) transition metal oxide based (TM) catalysts, which are often used due to cost advantages [10, 32, 34], and (c) nano-gold based catalysts – discovered by Haruta et al [12, 13]. All of these catalysts have relevant applications niches but behave differently with respect to temperature, CO concentration and water vapor content.

The aim of this study was to identify regions of activity for the gold-based, Pt-based and TM catalysts. These catalysts were tested for CO activity varying the test conditions such as CO concentration, temperature, humidity and CO flux.

VI.2 Experimental Details

VI.2.1 Catalyst Evaluation

VI.2.1.1 Catalyst Selection

As mentioned earlier, CO oxidation catalysts can be broadly categorized in three groups: (a) Pt group metal based (PGM) catalysts, (b) TM catalysts, and (c) nano-gold catalysts. For catalyst evaluation purposes, commercially available catalysts that represented each group were selected. STC catalyst, a tin oxide promoted Pt catalyst supported on silica [127] was selected to represent PGM catalysts. Carulite®, a hopcalite type of catalyst (mixture of CuOx and MnOx) was selected as a representative of TM catalyst. And, in the case of nano-gold catalysts, two commercial catalysts namely AUROlite® and 3M's NanAuCat™ were selected. AUROlite® is a 1%Au/TiO_2 catalyst and 3M's NanAuCat™ is a Au/TiO_2/Carbon catalyst, wherein the gold nanoparticles and TiO_2 particles are deposited via physical vapor deposition [128].

Earlier studies on low temperature CO oxidation had revealed that Pt-SnO_2/SiO_2 and Pt-CeO_2/SiO_2 catalysts were highly active for low temperature CO oxidation [129]. Therefore, in addition to the commercial catalysts, these two promoted Pt catalysts were also chosen for catalyst evaluation studies. The detailed optimization studies and performance of these two novel catalysts is given in Chapter IV, and Chapter V.

VI.2.1.2 Catalyst Testing

The challenge gas used for the experiments was 250-2500 ppm of CO in air (RH: 0-90%). Rest fof the experimental testing details with schematic of the set up are given in Chapter II.

The CO removal applications demand lower reactor footprint and minimal pressure drop which are related to volume and in turn to the weight of the catalyst. Packing densities of the catalysts under consideration were similar (approx. 0.7-0.8 g/cc). Therefore, the basis for catalyst comparison was chosen as the catalyst bed depth.

VI.2.1.3 Catalyst Preparation Methods and Materials

Commercial catalysts used during this study were obtained from their respective suppliers: AUROlite (Strem chemicals), Carulite® (courtesy of Carus Chem), STC catalyst (courtesy of STC catalysts Inc.) and NanAuCat (courtesy of 3M).

The preparation method for 5%Pt-25%SnO_2/SiO_2 catalyst in detail has been given in Chapter IV. The optimized method of preparation was used with potassium stannate route and all the drying steps were vacuum drying at 40°C. Resulting SnO2/SiO2 was calcined at 600 ^oC for two hours followed by Pt deposition with DADNP precursor which was dried overnight at 75^oC and calcined at 500 ^oC in air for 2 h.

4%Pt-16%CeO_2/SiO_2 catalyst was prepared by successive incipient wetness impregnation method as optimized and given in detail in Chapter V. Briefly, silica (Davisil® 645) was impregnated with cerium nitrate solution followed by drying in vacuum at 40^0C for six hours and calcination at 300^0C for

two hours in air. Pt deposition was carried out using DADNP precursor which was dried at 125^0C for four hours and calcined at 500^0C for two hours in air.

VI.2.2 Catalyst Characterization

Surface characterization techniques and processes are outlined in Chapter II. BET SA, PV, APS were estimated for all the commercial catalysts. These surface characteristics and particle sizes used during this study are given in Table VI.1. Since the gold based catalysts were sensitive to grinding due to their method of preparation, physical vapor deposition resulting in egg-shell distribution of active gold nanoparticles [128], except for the gold based catalysts, all the other commercial catalysts were ground and sieved to get the desired particle size (150-250 µm).

Table VI.1. Catalyst Characterization Data – Commercial Catalysts and Novel Catalysts

Catalyst	**Composition**	**BET SA (m2/g)**	**PV (cc/g)**	**APS (Å)**	**Particle Size**	**Estimated %D**
3M's NanAuCat	Au/TiO_2/Carbon	988	0.52	21	1.2 – 2.0 mm	ND
AUROlite	1% Au/TiO_2	48	0.17	141	1.2 – 2.0 mm	ND
STC Catalyst	Pt-SnO_2/SiO_2	155	0.36	94	150-250 µm	ND
Carulite	CuOx-MnOx mixture	250	0.18	28	150-250 µm	NA
Pt-CeO_2/SiO_2	4%Pt-16%CeO_2/SiO_2	246	0.81	136	150-250 µm	Pt %D: 40%
Pt-SnO_2/Silica	5%Pt-25%SnO_2/SiO_2	212	0.75	140	150-250 µm	Pt %D: 22%

*ND: not determined; NA: not applicable

VI.3 Results and Discussion

VI.3.1 Catalytic Activity Comparison

The ambient temperature catalyst evaluation was done at the various extremes of the test matrix: (a) low CO: with and without moisture; and (b) high CO: with and without moisture. These conditions were chosen based on the application requirements such as respiratory protection equipment and advanced filtration units for PEM fuel cell cathode and clean room facilities and the like.

VI.3.1.1 Activity Comparisons at Low CO Concentration

The absence of a significant adiabatic temperature rise and slow CO removal kinetics versus CO self-poisoning is the major challenge for CO oxidation at room temperature and low CO concentration (CO<0.05%). These catalysts were compared at low CO and room temperature with (50%RH) and without moisture and the results are given in Figure VI.2 and Figure VI.3.

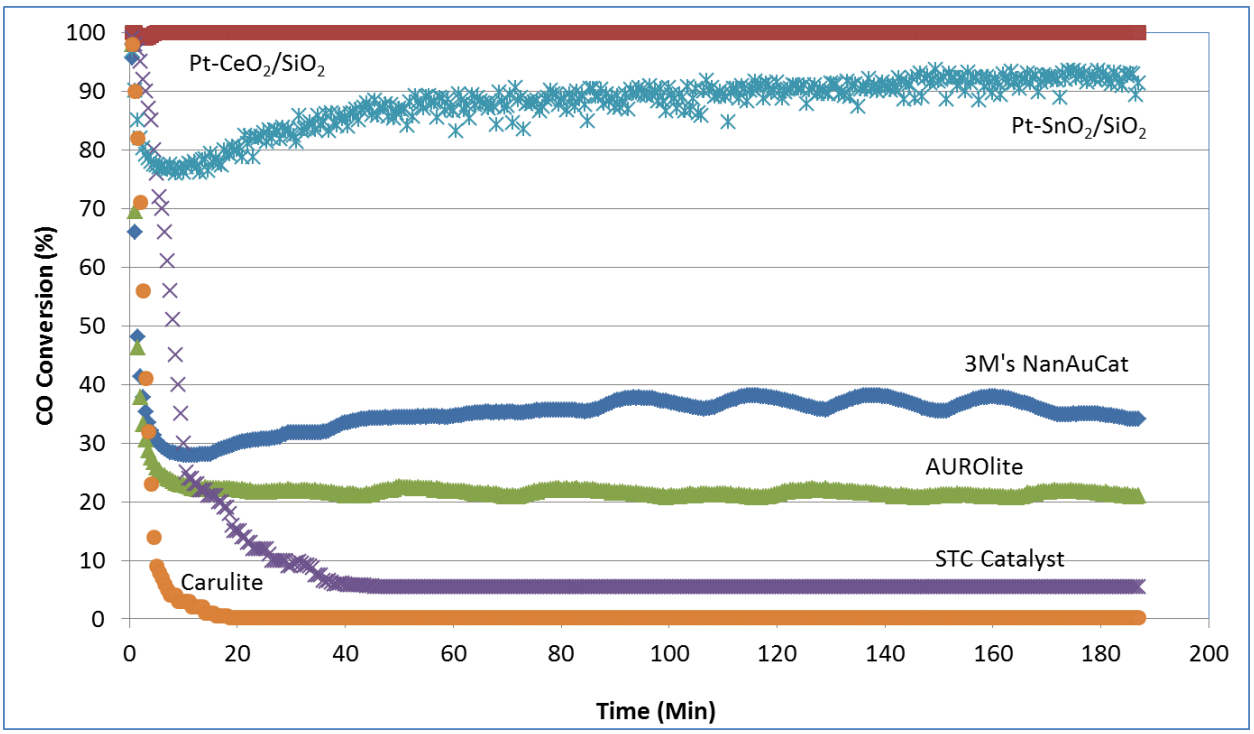

Figure VI.2. Catalyst Comparison at Low CO (250ppm) – 50% RH and 25^{0}C; SV: 540000 hr^{-1}

The TM catalyst (Carulite) was inactive while the STC catalyst showed very low activity. The promoted Pt catalysts were highly active (>90%CO conversion) and showed excellent stability over time. In the presence of moisture, activity trend was: Pt based catalysts > nano-gold catalysts > TM catalysts.

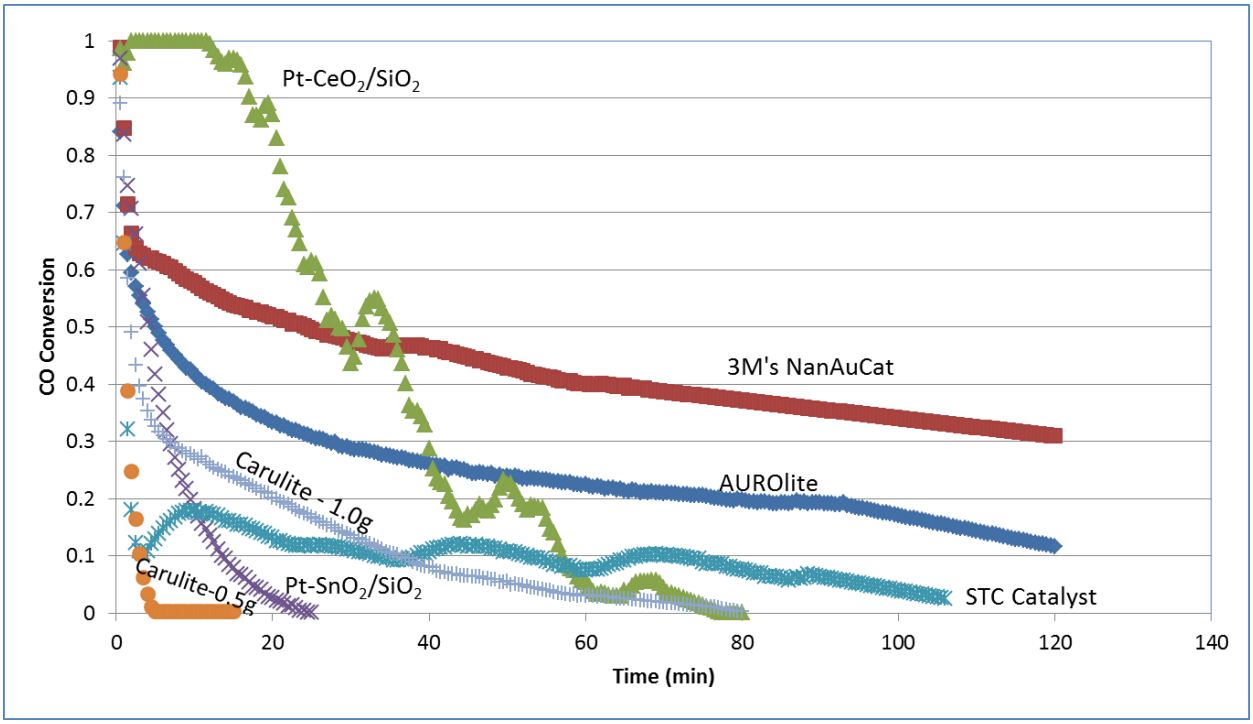

Figure VI.3. Catalyst Comparison at Low CO (250ppm) – 0% RH and 25^{0}C; SV: 540000 hr^{-1}

The Pt based catalysts (STC, Pt-CeO_2/SiO_2 and Pt-SnO_2/SiO_2) rapidly deactivated in the absence of moisture. Also, gold based catalysts showed deactivation over time and were found to have low activity Further, Carulite was inactive and showed very low activity (CO conversion <10%) even at double catalyst loading (1.0gm). In dry conditions, the activity trend was: gold catalysts > TM or Pt catalysts.

The gold based catalysts showed poor activity, although these catalysts have shown activity at even 0°C at high CO concentration. Certainly the absence of heat of reaction decreased the activity of gold based catalysts. Pt based catalysts required the presence of moisture whereas the TM catalysts showed some activity in the absence of moisture. Also, comparing the activity of gold catalysts for CO

oxidation with and without moisture, the effect of water as activity suppressant was evident. In the absence of moisture, the decline in the activity of the gold catalysts was gradual and in the presence of moisture the activity drop was instant.

VI.3.1.2 Activity Comparison at High CO Concentration

The catalysts were compared at 2500ppm at 25^{0}C with (90%RH) and without water vapor and results are given in Figure VI.4 and Figure VI.5.

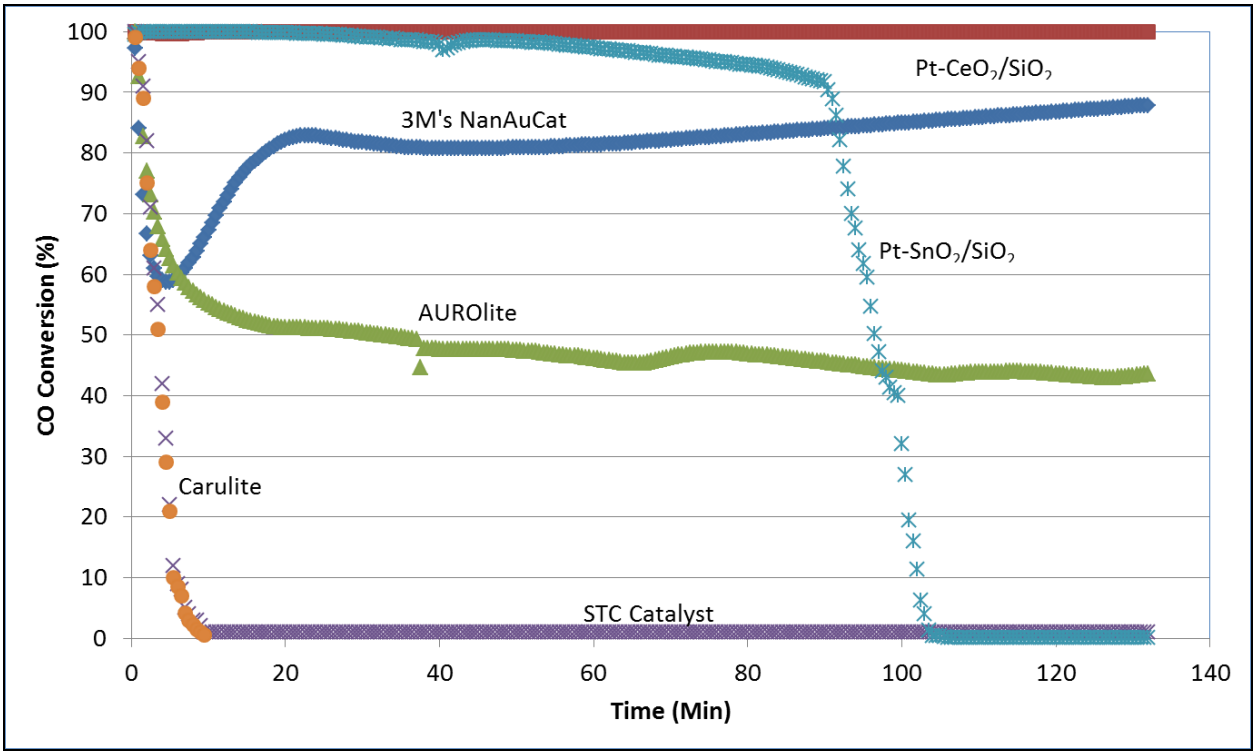

Figure VI.4. Catalyst Comparison at High CO (2500ppm) – 90% RH and 25^{0}C; SV: 90000 hr^{-1}

At high CO concentration and in the presence of moisture, the Pt-CeO_2/SiO_2 catalyst (conv.>99%) outperformed other catalysts. Pt-SnO_2/SiO_2 catalyst was highly active (conv.>95%); however, the activity gradually declined and the catalyst was completely inactive after 110 minutes (no. of reactions per Pt atom (TON) before deactivation ≈2000). Carulite and STC catalysts showed no activity

under test conditions. Gold based catalysts were also active (3M: conv.>85%; AUROlite: conv.>40%). The activity trend was: Pt catalyst > gold catalysts > TM catalysts.

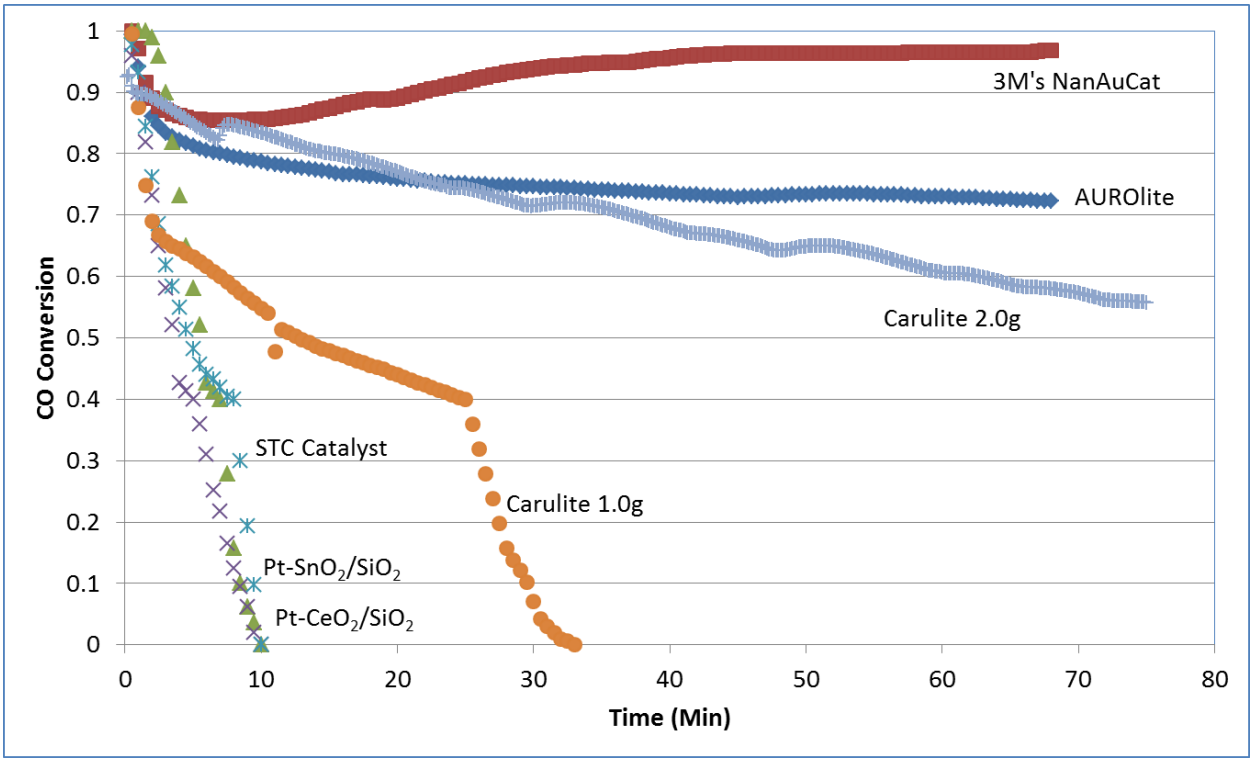

Figure VI.5. Catalyst Comparison at High CO (2500ppm) – 0% RH and 25^{0}C; SV: 90000 hr^{-1}

At high CO concentrations and in the absence of moisture, 3M's NanAuCat outperformed other catalysts (conv. > 95%). AUROlite showed more than 70% CO conversion and maintained activity. TM catalysts are known to be active at high CO in dry conditions [6]; therefore, the high activity of Carulite (2.0g) was not surprising. The Pt based catalysts deactivated immediately (TON before deactivation < 10). The activity trend was: gold catalysts > TM catalysts >Pt catalysts.

At high CO concentrations (CO > 2500ppm), the interplay of the two opposing effects namely, the high heat of reaction of CO oxidation and the CO self-poisoning of the catalyst, would decide the catalytic activity at low temperatures. Also, water vapor could act as an activity suppressant by forming a passivation layer over the active sites, in the case of TM catalysts [7] or compete with CO for active

sites, as reported by *Bollinger et al* in the case of 1%Au/TiO_2 [97].Water vapor could also act as an activity enhancer by disrupting the formation of CO ensembles, similar to observations made in the case of Pt/alumina catalysts [98].

Gold based catalysts and Carulite showed greater activity at high CO (2500ppm) by exploiting the high exothermicity of the reaction (at 2500ppm CO, ΔT_{ad} = 25^0C @ 100% conversion). When the activity of the gold based catalysts and Carulite with and without water was compared, the effect of water as an activity suppressant was evident. Further, the activity profile of 3M's NanAuCat in the presence of moisture would also explain the interplay of temperature, CO concentration and water vapor. NanAuCat catalyst initially showed low activity (Figure VI.4, conv. < 60% after 5 minutes); however, its activity improved over time (Figure VI.4, conv. > 85% after 120 minutes). The presence of moisture certainly lowered the activity of the catalyst; however, due to the adiabatic temperature rise, the impact of moisture on activity decreased over time and the activity improved with increased temperature.

3M's NanAuCat is made by physical vapor deposition method [128], which would yield the active site distribution profile closer to an egg-shell profile (active sites close to external particle surface). Catalytic activity is dictated by the type of reaction regime and active sites distribution profile in the catalyst [130]. CO oxidation reaction at room temperature (25^0C) was diffusion controlled (Section: V.3.10.1 Effect of Particle Size). For diffusion controlled reactions, an egg-shell profile is favored [102]. This might explain why NanAuCat was able to exploit exothermicity of the reaction and showed activity at high CO in the presence of moisture.

Pt based catalysts certainly required the presence of water vapor to maintain activity at low temperature (25^0C). Water vapor probably minimized CO self-poisoning by disrupting CO island formation on Pt active sites.

VI.3.2 Impact of Water Vapor Content on Activity

Impact of water vapor concentration on nano-gold catalysts and promoted Pt catalysts was investigated and the results are given in Figure VI.6 and for these catalysts.

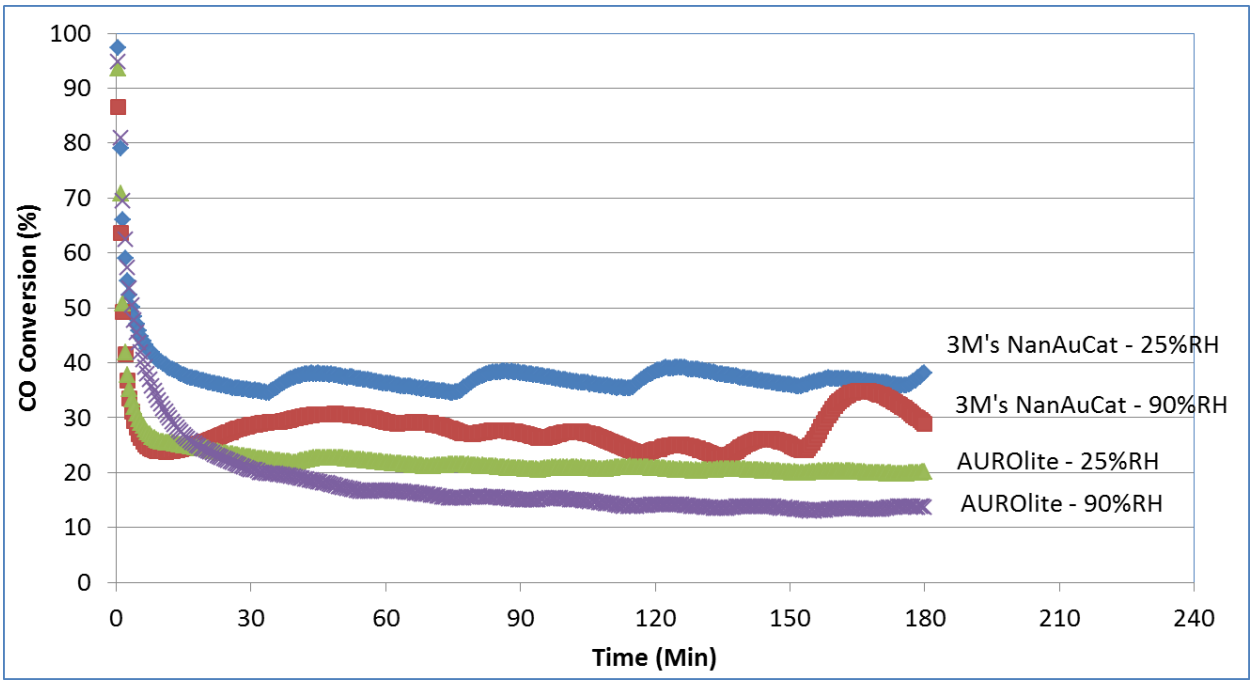

Figure VI.6. Effect of Humidity on Gold Catalysts: 500 ppm CO; 250C; SV: 540000 hr^{-1}

For both of the nano-gold catalysts, increased moisture content from 25% RH to 90% RH resulted in decreased catalytic activity. These results confirm the earlier observations made regarding the gold catalysts that the water vapor acts as an activity suppressant. However, activity suppression at high CO was significant (conv. ≈ 70% (0% RH); conv. ≈ 40% (90% RH)) compared to that at 500 ppm CO. This could be explained based on the availability of active sites for CO oxidation and the higher activity at high CO.

For Pt-CeO_2/SiO_2 catalyst, the SV was increased by two times to study the impact of humidity since its activity at lower SV was quite high at both 25% RH and 90% RH. In the case of promoted Pt catalysts, increased moisture content improved CO conversion.

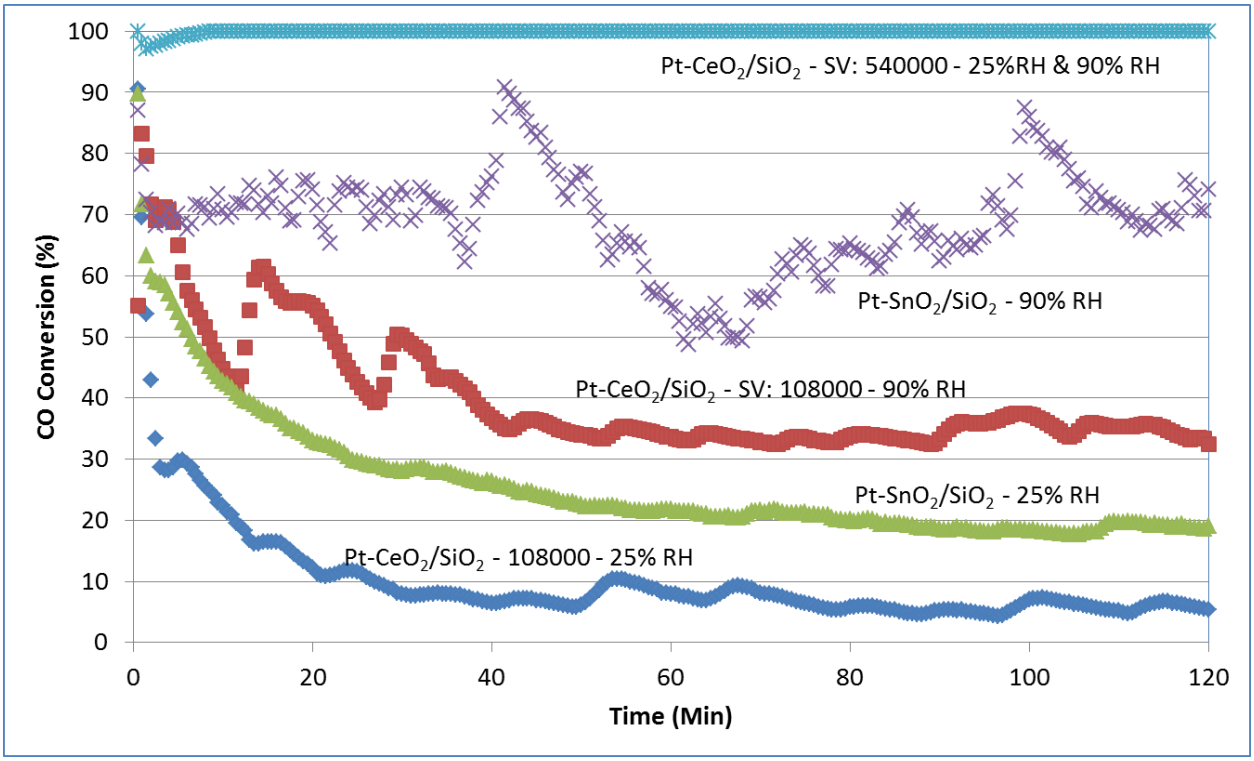

Figure VI.7 Effect of Humidity on Pt Catalysts: 500 ppm CO; 25^{0}C; SV: 540000 hr^{-1} & 1080000 hr^{-1}

For both of these Pt based catalysts (Pt-CeO_2/SiO_2 and Pt-SnO_2/SiO_2), the integral reactor howed significant oscillations. The oscillations were not periodic but chaotic in nature. The oscillatory behavior of CO oxidation reaction has been studied extensively [121, 131, 132] and it has been attributed to either the presence of multiple steady states [122] or the existence of local patches of active and inactive catalysts in the reactor bed [125]. If the water vapor disrupted the formation of CO islands on Pt active sites, as observed by other researchers, for example in the case of Pt/Alumina catalyst [98], there was a possibility of local patches of active and inactive catalysts within the catalyst bed. This could be one of the possible reasons for the oscillatory behavior.

VI.3.3 Hysteresis Effect of Catalyst Testing Conditions

Due to the non-linear CO oxidation surface kinetics often described by the LH mechanism, any fluctuation in surface CO concentration, water vapor concentration or temperature could give rise to significant instabilities in the surface reaction kinetics. These instabilities in surface reaction kinetics may exhibit hysteresis effect. During this study, the effects of variations in operating conditions such as water vapor content, temperature, CO concentration, and CO flux on nano-gold catalysts (3M's NanAuCat and AUROlite) as well as Pt-CeO_2/SiO_2 catalyst were investigated.

VI.3.3.1 Hysteresis Effect of Humidity and CO Flux

These catalysts were subjected to variations in water vapor content and CO flux and the activity results are given in Table VI.2 and Table VI.3.

Table VI.2. Impact of Water Vapor Content Variation on Activity: 500ppm; 25°C; SV: 540000 hr^{-1}

RH	NanAuCat – CO Conv. (%)		AUROlite – CO Conv. (%)		Pt-CeO_2/SiO_2 – CO Conv. (%)	
	Increasing RH	Decreasing RH	Increasing RH	Decreasing RH	Increasing RH	Decreasing RH
0%	30	28	30	29	9	5
25%	17	10	26	25	32	99
50%	8	7	20	18	98	99
75%	6	5	15	13	99	99
90%	4	4	8	8	99	99

The effect of water vapor content was completely reversible and no hysteresis effect was observed. For example, in the case Pt-CeO_2/SiO_2 catalyst when the water vapor content was increased from 0% RH to 90% RH the activity improved from less than 5% CO conversion to more than 99% CO

conversion; however, when the water vapor content was decreased from 90% RH to 0% RH, the activity dropped to less than 5% CO conversion.

Table VI.3. Impact of CO Flux on Activity – Transient Test Conditions

Gas Face Velocity (FV) (cm/sec)	NanAuCat – CO Conv. (%)*		AUROlite – CO Conv. (%)*		Pt-CeO_2/SiO_2 – CO Conv. (%)	
	Increasing FV	Decreasing FV	Increasing FV	Decreasing FV	Increasing FV	Decreasing FV
30	33	38	30	29	99	99
45	17	21	24	22	99	99
60	8	12	10	11	99	99
75	0.4	0.4	5	5	99	97
90	0.2	0.2	1	1	47	47

*500 ppm CO in air, Catalyst wt.: 0.5g, 25^0C, Humidity: 50% RH

The effect of CO flux was also completely reversible and no hysteresis effect was observed. For example, in the case of 3M's NanAuCat catalyst, when the gas face velocity was increased from 30 cm/sec to 90 cm/sec, the conversion decreased from 33% to 0.2%; however, when the gas face velocity was decreased from 90 cm/sec to 30 cm/sec, the conversion was back to 38%.

VI.3.3.2 Hysteresis Effect of CO Concentration

During this study, the effect of variations of CO concentration on nano-gold catalysts (3M's NanAuCat and AUROlite) and Pt-CeO_2/SiO_2 catalyst was studied at ambient temperature in the presence of water vapor content and the activity results in terms of CO conversion are given in Figure VI.8. The CO concentration was increased in a step-wise manner. At an interval of 20 minutes, CO concentration was changed by 250 ppm. The conversion values were taken at 15 minutes from the step-change.

In the case of AUROlite catalyst, no hysteresis effect of CO concentration was observed. The hysteresis effect was clearly visible in the case of 3M's NanAuCat catalyst. For example, CO conversion

was 63% during CO increasing cycle and 92% during CO decreasing cycle at 1000 ppm of CO. The increased activity could be attributed to the high exothermicity of the reaction and the ability of the catalyst to maintain the higher state of activity during the decreasing CO concentration cycle. Also, the observations made earlier about the gold based catalysts that they showed greater activity at high CO concentrations by exploiting the exothermicity of the reaction was confirmed from Figure VII.6.

Pt-CeO_2/SiO_2 catalyst showed a significant hysteresis effect of CO concentration. The catalyst showed greater activities at low CO; however, when the CO concentration was increased to CO>1500ppm, the CO conversion dropped to less than 5% at 2500 ppm. The CO inhibition effect was clearly visible at 2500 ppm of CO. When the CO concentration was decreased to 250ppm of CO, the catalyst yielded 10% CO conversion whereas during the CO increasing cycle the CO conversion was more than 99%, thus exhibiting a hysteresis effect of CO concentration.

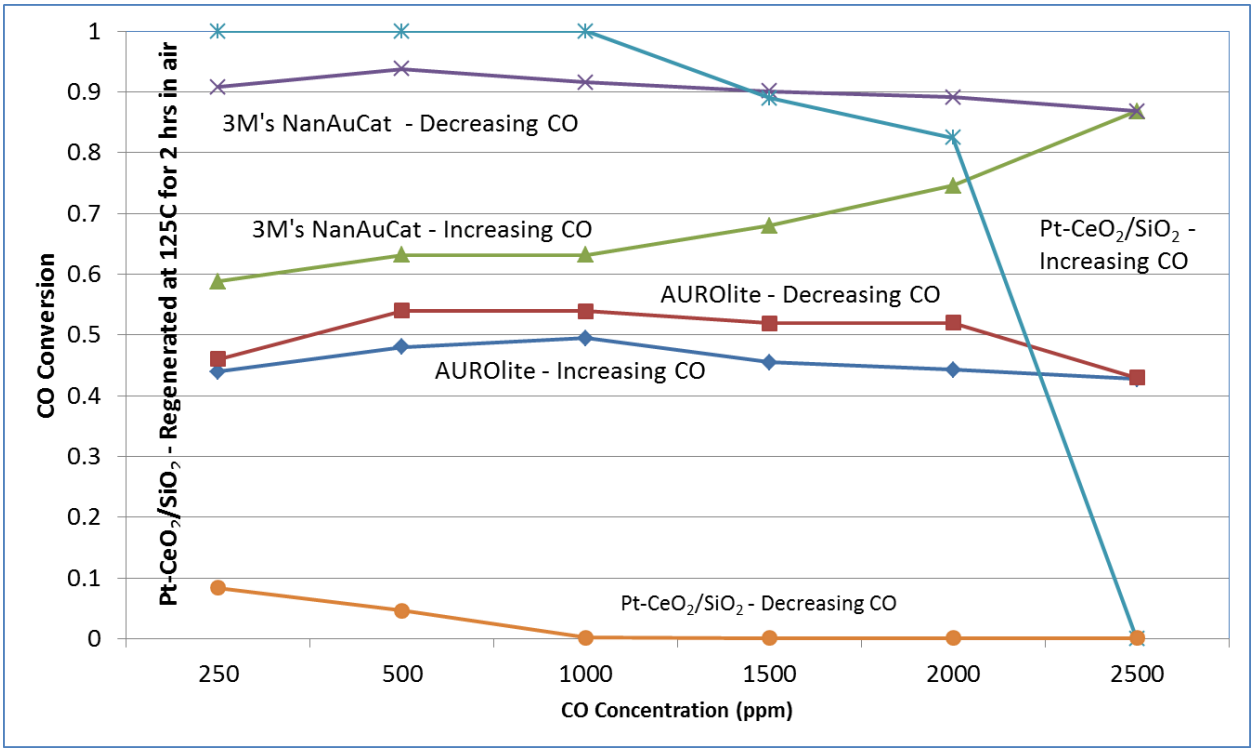

Figure VI.8. CO Concentration – Hysteresis Effect; *25^0C; 50%RH; SV: 120000 hr^{-1}.*

When this poisoned Pt-CeO_2/SiO_2 catalyst was subjected to a high temperature (125^{0}C) treatment in air for two hours, the catalyst regained activity and yielded more than 99% CO conversion at 250ppm. The ability of the Pt-CeO_2/SiO_2 catalyst to regain activity after high temperature treatment proved that the declined activity at high CO concentration was a result of CO poisoning alone.

VI.3.3.3 Hysteresis Effect of Temperature

The effect of temperature variations (from 25^{0}C to 150^{0}C) on gold catalysts and Pt-CeO_2/SiO_2 catalyst was investigated and the activity results are given in Figure VI.9. For this analysis, the temperature of the reactor was change by 10C every 30 minutes. The system was given 5 minutes to reach the set temperature, and then next 20 minutes to reach steady state and the conversion values were obtained by taking a mean of the CO outlet values measured during the last 5 minutes before next temperature change.

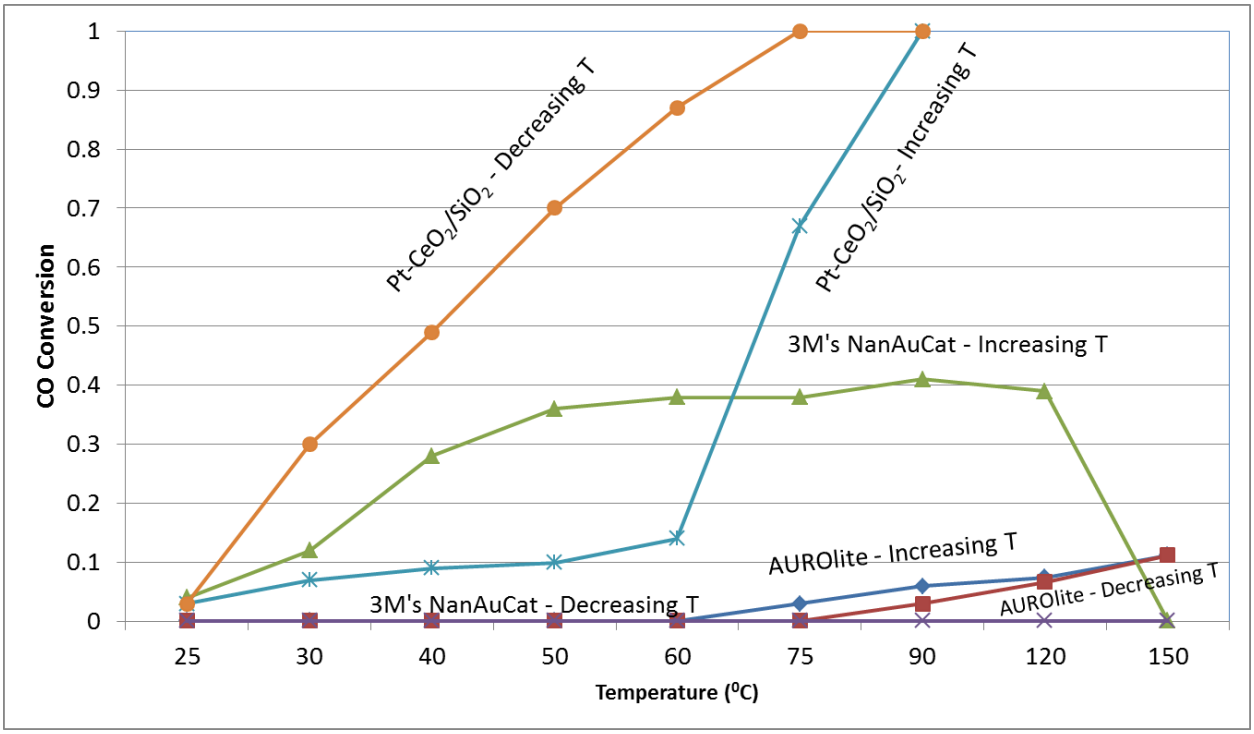

Figure VI.9. Temperature Hysteresis Effect; CO: 1500 ppm; 1% H2O (v/v); SV: 540000 hr^{-1}

CO oxidation over Pt-CeO_2/SiO_2 catalyst was sensitive to temperature and the activity significantly improved with increased temperature. The catalyst showed substantial activity improvement due to thermal cycling and significant hysteresis effect of temperature was observed.

In the case of AUROlite, activity did not improve much with increased temperature, yielding 5% CO conversion at 90^0C and 10% CO conversion at 150^0C. Also, no hysteresis effect of temperature was observed. The presence of moisture and high CO concentration might have caused catalyst poisoning initially at 25^0C, and increased temperature probably failed to regenerate the catalyst in the presence of moisture.

The activity of the NanAuCat catalyst showed an unexpected behavior with regards to temperature. Initial increase in temperature did improve the catalytic activity; however, further increase in temperature from 50^0C to 120^0C had no effect on activity. When the temperature was increased from 120^0C to 150^0C; however, the conversion dropped from 42% to 1%. During the reducing temperature cycle, the catalyst did not gain activity and showed no CO oxidation activity.

One of the reasons for this activity decline could be the sintering of gold nano-crystals at high temperature (at 150^0C), thereby causing decreased activity. The nano-gold catalysts have been found to be susceptible to metal sintering or support sintering at higher temperatures [133-136]. Experimental studies have shown that the melting point of 2-3 nm gold particles was close to 75-125^0C [137]. Sintering of supported metallic particles is faster closer to the melting point [138] and the onset temperature for metal sintering has been shown to be 0.3/0.5 times the melting point depending on the crystal structure [138]. Additionally, the presence of O_2 or H_2O could increase the rate of metal sintering [138]. Considering that the NanAuCat catalyst was prepared by physical vapor deposition [128], sintering of the nano-gold particles might be responsible for decreased activity at higher temperatures (T>120°C).

The nano-gold sintering hypothesis for the NanAuCat catalyst was investigated further. A sample of the NanAuCat catalyst was treated at 125^0C overnight in air and the sample was then tested for CO oxidation activity at 2500 ppm CO at 25^0C in 0% RH. The high temperature treated sample showed poor activity (conversion < 10%) compared to un-treated sample (conversion > 90%, from Figure VI.5). Although this study by no means would confirm the hypothesis of nano-gold sintering at higher temperatures; however, the stability of nano-gold catalysts at higher temperatures was questionable and needs further investigation.

VI.4 Conclusion

Based on the catalyst evaluation study, following conclusions could be drawn. (A) The transition metal oxides based (TM) catalysts (for example, Carulite) were active only in the absence of water vapor and at high CO concentration. (B) The activity of nano-gold based catalysts (3M's NanAuCat and AUROlite) decreased in the presence of water vapor and the activity improved with CO concentration due to high exothermicity of the reaction. (C) Promoted Pt catalysts (Pt-CeO_2/SiO_2 and Pt-SnO_2/SiO_2) were active for CO oxidation in humid air over a wide range of CO concentrations; however, these Pt based catalysts were inactive in the absence of moisture. (D) Both gold based catalysts and promoted Pt catalysts showed hysteresis effect of operating conditions such as CO concentration and temperature

CO oxidation at ambient temperature was affected by CO concentration as well as water vapor content and a single catalyst formulation that was highly active under all the testing conditions could not be found; therefore, the selection of a catalyst should be done judiciously based on CO removal application requirements. The stability of nano-gold based catalysts (particularly 3M's NanAuCat) was found to be questionable at higher temperatures (T>125^0C) and would require further investigation to determine the cause of decreased activity.

VII Reactor Modeling

VII.1 Introduction

From the experimental observations it was established that the Pt-Ceria/Silica catalyst outperformed all the other catalysts for CO oxidation at low temperature in the presence of moisture. It was important to develop a model that would enable the designing of the catalytic applications. It was important to develop a reactor model that would fit the experimental data as well as predict the catalyst performance at desired conditions with significant accuracy.

VII.2 Reactor Model Details

VII.2.1 Types of Reactor Models

The catalytic reactor models are broadly divided into two categories, namely: steady state and transient models [139]. Based on the assumptions for external mass and heat transfer, the models can be further categorized as heterogeneous or pseudo-homogeneous [139]. Also, with the assumptions made towards the thermal behavior of the reactor, the reactor models can be further termed as isothermal or non-isothermal reactor models [114]. The reactor models may or may not include mass and thermal dispersion in the bed [139]. Finally, the reactor models are categorized based on the number of dimensions used for modeling such as one-dimensional or two-dimensional models. There have been a significant number of attempts to model the non-isothermal CO oxidation reaction [140-142].

VII.2.2 System Description and Model Simplifications

The CO oxidation reaction is highly exothermic, therefore the reactor model needed to capture the heat effects within the reactor. Further, from the experimental results it was observed that the effects of mass and heat dispersion were prominent within the reactor, therefore the model needed to capture these effects as well. Furthermore, the model needed to be transient to capture the evolution of catalytic activity with respect to time.

During this study, considering the computing resources required for two-dimensional modeling, during this study one-dimensional model was used. Based on the experimental set-up (reactor ID < 1”), the radial symmetry could be assumed. Further, Mear’s criterion indicated that the reaction was not externally diffusion controlled [114]. Therefore, a pseudo-homogeneous model can be assumed. Further simplification of the reactor model came from the way the kinetic data was collected. The apparent kinetic data was collected for 200 micron particles and the rate law parameters were estimated. So, the internal diffusion resistance in the catalyst particles can be assumed negligible. With these assumptions a transient, non-isothermal, one-dimensional, pseudo-homogeneous reactor model with axial mass and heat dispersion was used.

VII.2.3 Reactor Model Selection

Two different types of reactor models were considered. The first reactor model did not include any CO poisoning of the catalyst. The rate law is given in Equation VII.1. The reactor model used is given in Equation VII.2 and Equation VII.3. Danckwert’s boundary conditions were used [143], the initial and boundary conditions are given in Equation VII.4.

$$-R_C = \frac{k0e^{-\frac{E_a}{RT}}C_{CO}}{(1+K_A C_{CO})^2}$$

Equation VII.1. Rate Law for Langmuir – Hinshelwood Dual Site Mechanism

$$\varepsilon\frac{\partial C}{\partial t} = -u\frac{\partial C}{\partial z} + Dax\frac{\partial^2 C}{\partial z^2} - (1-\varepsilon)R_C$$

Equation VII.2. One – dimensional Pseudo-homogeneous Transient model for Concentration

$$\varepsilon\frac{\partial T}{\partial t} = -u\frac{\partial T}{\partial z} + \lambda\frac{\partial^2 T}{\partial z^2} - (1-\varepsilon)\frac{\Delta H}{\rho C_p}R_C$$

Equation VII.3. One – dimensional Pseudo-homogeneous Transient model for Temperature

Inlet BC $\quad uC|_{z=0^-} = \left|uC - Dax\frac{\partial C}{\partial z}\right|_{z=0^+}$; $\quad \rho C_p T|_{z=0^-} = \left|\rho C_p T - \lambda\frac{\partial T}{\partial z}\right|_{z=0^+}$

Outlet BC $\quad \left.\frac{dC}{dz}\right|_{z=L} = 0$; $\quad \left.\frac{dT}{dz}\right|_{z=L} = 0$

Initial conditions: C = 0 at all z at t=0; T= T_R at all z at t=0; where, T_R = room temperature

Equation VII.4. Initial and Boundary Conditions

At higher CO concentration (> 1000 ppm), CO self-poisoning of the catalyst was dominant. Also, the CO poisoning was reversible and the poisoned catalyst fully regained activity with increased temperature. CO poisoning at low temperature is caused by CO island formation on active Pt sites [144]. The CO islands could be broken to re-activate the occupied Pt sites by reducing the equilibrium constant with increased temperature [119]. To account for this reversible catalyst poisoning, a model with an apparent poisoning term was developed.

The model equations are given in Equation VII.5, Equation VII.6, Equation VII.7, Equation VII.8, and the initial and boundary conditions are given in Equation VII.9. The external mass transfer was assumed negligible (km = 1000 s^{-1}). The reversible catalyst poisoning was implemented by incorporating a surface coverage dependent activation energy term, β. The value of β increased with CO concentration (β = 0 (CO: 1-750 ppm); β = 1 (CO: 1000 ppm); β = 2 (CO: 1500 ppm); β = 3 (CO: 2000 ppm); β = 4 (CO: 2500 ppm), and interpolated β values for other CO values.

$$\varepsilon\frac{\partial C}{\partial t} = -u\frac{\partial C}{\partial z} + Dax\frac{\partial^2 C}{\partial z^2} - km(1-\varepsilon)(C-CS)$$

Equation VII.5. One – dimensional Transient model for Concentration

$$\varepsilon\frac{\partial T}{\partial t} = -u\frac{\partial T}{\partial z} + \lambda\frac{\partial^2 T}{\partial z^2} - (1-\varepsilon)\frac{\Delta H}{\rho C_p}R_{CS}$$

Equation VII.6. One – dimensional Pseudo-homogeneous Transient model for Temperature

$$\frac{\partial CS}{\partial t} = km(C-CS) - R_{CS}$$

Equation VII.7. Transient model for Surface Concentration

$$-R_{CS} = \frac{k0e^{-\frac{(E_a+\beta\theta)}{RT}}C_{CS}}{(1+K_A C_{CS})^2}$$

Equation VII.8. Rate Equation for Surface Concentration

Inlet BC $$uC|_{z=0^-} = \left|uC - Dax\frac{\partial C}{\partial z}\right|_{z=0^+}; \quad \rho C_p T|_{z=0^-} = \left|\rho C_p T - \lambda\frac{\partial T}{\partial z}\right|_{z=0^+}$$

Outlet BC $\left.\frac{dC}{dz}\right|_{z=L} = 0;$ $\left.\frac{dT}{dz}\right|_{z=L} = 0$

Initial conditions: C = 0 at all z at t=0; CS = 0 at all z at t=0; T= T_R at all z at t=0;

Equation VII.9. Initial and Boundary Conditions

VII.2.3.1 Nomenclature

C: concentration (mol/m^3)

C_{CO}: CO concentration (mol/m^3)

C_S: surface concentration (mol/m^3)

C_{IN}: inlet concentration (mol/m^3)

C_P: heat capacity (J/kg.K)

Dax: axial dispersion coefficient (m^2/s)

Ea: activation energy (kJ/mol)

K: thermal conductivity (W/m.K)

k_r: reaction rate constant (m^3/kg.s)

K_A: equilibrium constant

k0: pre-exponential factor (m^3/kg.s)

km: mass transfer coefficient (1/s)

L: length of reactor (m)

R: universal gas constant

R_{CO}: rate of CO oxidation reaction (mol/kg.s)

R_C: rate of reaction (mol/kg.s)

R_{CS}: rate of reaction – surface concentration (mol/kg.s)

T: temperature (K)

T_R : room temperature (K)

t: time (s)

u: superficial velocity (m/s)

z: axial dimension (m)

ε: bed voidage

λ: thermal diffusivity (m^2/s) = $k/\rho C_P$

ΔH: Heat of reaction (kJ/mol)

ρ: density (kg/m^3)

β: surface poisoning dependent activation energy (kJ/mol);

β=0 (<750 ppm); β=1 (1000 ppm); β=2 (1500 ppm); β=3 (2000 ppm); β=4 (2500 ppm)

θ: surface poisoning = C_S/C_{IN};

VII.2.4 Solution Method

These partial differential equations (PDEs) were solved by using commercial software COMSOL® multiphysics. The method used by COMSOL® for solving these coupled PDEs was finite element method.

VII.3 Results and Discussion

VII.3.1 Kinetic Parameter Estimation

VII.3.1.1 Reaction Mechanism – Data Fitting

The first step during the model development was to use the experimental data to find out the reaction mechanism. It is important to note that since the catalyst activity was heavily dependent upon the catalyst bed thickness, the experimental data used for the reaction parameter estimation was from the integral reactor. The experimental data used is given in Table VII.1. Two different types of reaction mechanisms were deemed fit for data fitting, namely: Langmuir-Hinshelwood dual site mechanism (LH), and different active sites mechanism.

The rate law for the LH dual site mechanism is given in Equation VII.10. This rate law predicts first order behavior of reaction rate at lower concentrations and exhibits negative order at higher concentrations. The reaction mechanism assumed that two adjacent active sites take part in the reaction. The assumption is that these two active sites are similar in nature and both of the active sites adsorb one reactant each and each of the active site can adsorb any of the reactant.

$$-R_C = \frac{k0e^{-\frac{E_a}{RT}}C_{CO}}{(1+K_A C_{CO})^2}$$

Equation VII.10. Langmuir Hinshelwood Dual Site Mechanism Rate Law

The mechanism called as different active sites mechanism assumes that the reaction takes place between two adjacent sites; however, both of these sites adsorb different reactants. So, CO gets adsorbed on Pt metal and O_2 gets adsorbed on Ceria active sites and a reaction between the adsorbed CO and O atom on adjacent catalytic active sites yield the product CO_2. The rate law is given in Equation VII.11.

$$(-R_G) = k*C_A*C_B/((1+K_A*C_A)*(1+K_B*C_B))$$

Equation VII.11. Rate Law for the Different Active Site Mechanism

Table VII.1. Experimental Data used for Reaction Rate Parameter Estimation

CA (ppm)	CA (mol/m3)	FV (cm/s)	FA0 (mol/s)	Cat. Wt. (kg)	CONV (X)	OBS Rx* (mol/kg.s)	OBS Rx (µmol/g/s)
10	4.09E-04	100	1.16E-07	2.50E-04	0.70	3.26E-04	3.26E-01
25	1.02E-03	100	2.91E-07	2.00E-04	0.60	8.74E-04	8.74E-01
50	2.04E-03	60	3.49E-07	2.00E-04	0.70	1.22E-03	1.22E+00
100	4.09E-03	60	6.99E-07	2.00E-04	0.65	2.27E-03	2.27E+00
150	6.13E-03	45	7.86E-07	2.50E-04	0.80	2.52E-03	2.52E+00
250	1.02E-02	30	8.74E-07	4.00E-04	0.99	2.16E-03	2.16E+00
250	1.02E-02	60	1.75E-06	3.50E-04	0.70	3.49E-03	3.49E+00
500	2.04E-02	30	1.75E-06	3.75E-04	0.87	4.05E-03	4.05E+00
750	3.07E-02	30	2.62E-06	5.00E-04	0.85	4.46E-03	4.46E+00
1000	4.09E-02	15	1.75E-06	5.00E-04	0.90	3.15E-03	3.15E+00
1500	6.13E-02	15	2.62E-06	7.50E-04	0.80	2.80E-03	2.80E+00
2000	8.17E-02	10	2.33E-06	8.00E-04	0.90	2.62E-03	2.62E+00

**Temperature: 25^{0}C; Catalyst Particles: 200 µm; Humidity: 50%RH; Reactor ID: ¾"; CO in air.*

However, the reaction was carried out in air, so the oxygen was present in excess and the concentration of oxygen would not change due to reaction. Also the ceria could be assumed to be saturated with C_B (or O_2). Based on these assumptions, the modified rate law for the different active site mechanism is given in **Equation VII.12**.

$$(-R_G) = k*C_A/(1+K_A*C_A)$$

Equation VII.12. Rate Law for Different Active Site Mechanism – CO Oxidation in Air

Using commercial software Polymath® the regression analysis was performed. Considering the fact that this data was obtained from Integral reactor, the analysis was not straight-forward and involved non-linear regression and estimation of weight of the catalyst from the available data. The equation used in Polymath for LH dual site mechanism data fitting is given in Equation VII.13.

$$W=F_{A0}*((-1)*\ln(1-X))/(K*C_{A0})+2*F_{A0}*K_A*X/K+F_{A0}*K_A\text{^}2*C_{A0}*X/K-F_{A0}*K_A\text{^}2*C_{A0}*X\text{^}2/K/2$$

Equation VII.13. Polymath Equation used - LH Dual Site Mechanism

Where, K and K_A are reaction rate constant and equilibrium constant respectively.

The analysis results obtained from Polymath are given in Table VII.2.

Table VII.2. Non-Linear Regression Results from Polymath for LH-Dual Site Mechanism

No.	Parameter	Value
1	K	1.449
2	KA	87.96
3	R^2	0.969

The equation used for the non-linear regression for the different active site mechanism used in POLYMATH is given in Equation VII.14.

$$W = F_{A0}*((-1)*\ln(1-X)/(k*C_{A0}) + K_A*X/k)$$

Equation VII.14. Polymath Equation used – Modified Different Active Sites Mechanism

Where, K and K_A are reaction rate constant and equilibrium constant respectively.

The analysis results obtained from Polymath are given in Table VII.3.

Table VII.3. Regression Results from Polymath for Different Active Site Mechanism

No.	Parameter	Value
1	K	734.9
2	KA	2.52E+05
3	R^2	0.8593

From the non-linear regression results, LH dual site mechanism showed a very good fit (R^2>0.95) for the experimental data.

VII.3.1.2 Reaction Rate Parameter Estimation

Using the LH dual site mechanism the kinetic parameters were estimated at room temperature from non-linear regression. Considering that the LH dual site mechanism would hold true for the temperature range studied (25-100^{0}C), the effect of temperature on reaction rate constant (k) and equilibrium constant (KA) and in other words the effect of temperature on rate of reaction was investigated.

The Van't Hoff equation gives the relation of equilibrium constant as a function of temperature. The Van't Hoff equation is given in Equation VII.15 [79].

$$Ln(K) = (-\Delta Had/(R*T))$$

Equation VII.15. Van't Hoff's Equation for Equilibrium Constant as Function of Temperature

Where, (-ΔHad): heat of adsorption; R: universal gas constant; T: temperature in K

From the literature survey, it was found out that the heat of adsorption of CO on Pt has been estimated to be in the range of 85-130 KJ/mol [145]. For this study, the heat of adsorption was assumed to be 100 KJ/mol. Using this heat of adsorption ($-\Delta H_{ad}$ = 100KJ/mol) in the Van't Hoff's equation, estimated values of K_A (eq. constant) are given in Table VII.4. Experiments were carried out different temperatures (25, 50, 75, 100^0C); the experimental results are given in Table VII.4. Using these experimental results obtained at different temperatures, the reaction rate constants were estimated using the equilibrium constants so obtained from van't hoff equation and the estimated rate constants are given in Table VII.4.

The reaction rate constants thus obtained were fitted to the Arrhenius Equation [114], and the activation energy and the pre-exponential factors were estimated. In order to fit the data, the natural log of rate constant was plotted against the reciprocal of absolute temperature. From the slope of the line, activation energy was estimated and from the intercept, the pre-exponential was estimated. The plot of ln(k) vs reciprocal of absolute temperature is shown in Figure VII.1. From the plot of natural log of rate constant vs reciprocal of absolute temperature, following information was obtained: (a) slope: -2092.1, (b) intercept: 7.2366, and (c) R^2: 0.9219. The pre-exponential factor and the activation energy were estimated from the intercept and the slope respectively. The results are given in Table VII.5.

Table VII.4. Experimental Data & Estimated Reaction Rate Parameters at Different Temperatures

CA (ppm)	Temp (^{0}C)	CA0 (mol/m3)	FA0 (mol/sec)	Cat. Wt (g)	Conv. (X)	Rate* (µmol/g.s)	KA Eq. Constant	Kr Rate Constant
300	25	1.23E-02	1.57266E-06	0.05	0.1	2.99	87.96	1.45
500	50	1.89E-02	2.41833E-06	0.04	0.40	24.2	3.881	1.75
700	75	2.45E-02	4.19008E-06	0.035	0.50	59.9	0.2681	3.11
1090	100	3.56E-02	6.08743E-06	0.03	0.65	132	0.0265	5.90

** Particles: 200 micron; Humidity: 1%H_2O; Reactor ID: ¾"; catalyst diluted in 0.25g inert silica.*

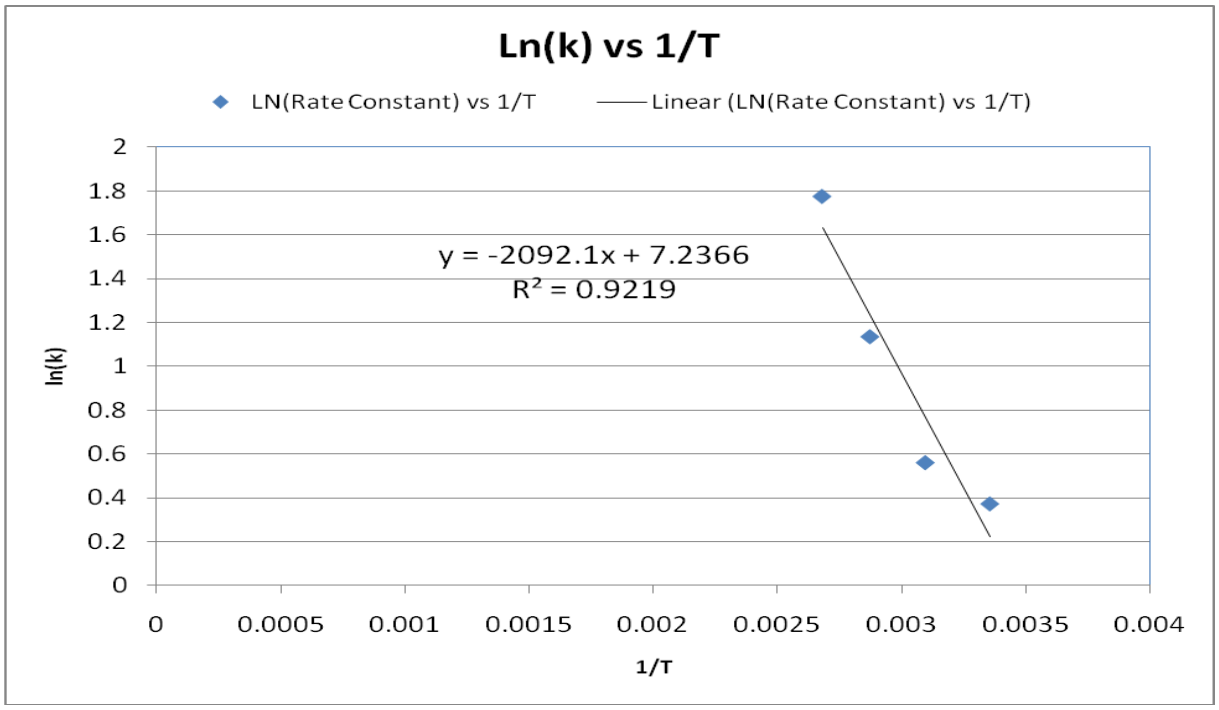

Figure VII.1. Kinetic Parameters Estimation from Experimental Data

Table VII.5. Reaction Rate Parameters Estimated from Experimental Data

No.	Parameter	Equation	Constant (1)	Constant (2)
1	KA – Eq. Constant	Ln(K)=(-ΔHad/(R*(T))	ΔHad = 100KJ/mol	--
2	k –rate constant	k = k0*exp(-Ea/(R*T))	k0 = 1389.4	Ea = 17.4 KJ/mol

The parameters so estimated from the experimental data (Table VII.5) were used for the reactor modeling. As noted above, the model used was transient 1-D pseudo-homogeneous reactor model.

VII.3.2 Model Validation

Once the reaction rate parameters were established, it was important to validate the reactor model by comparing with the experimental data. Two reactor models were solved by COMSOL® Multiphysics and the comparison of simulation results with the experimental results is given in Figure VII.2. The reactor model without CO poisoning, over-predicted the CO conversion and the difference was greater at high CO concentration.

The reactor model with CO poisoning; however, reasonably predicted the CO conversion. The error in the simulation and experimental results was less than 10%. The kinetic parameters were estimated by solving a plug flow reactor (PFR) model in isothermal conditions; whereas, the model captured the non-isothermal behavior as well. So, the model over-predicted the reaction rates. However, data-fitting in non-isothermal conditions was challenging, computationally intensive and failed to give a good data fit for experimental results over the wide range of CO concentrations and temperatures.

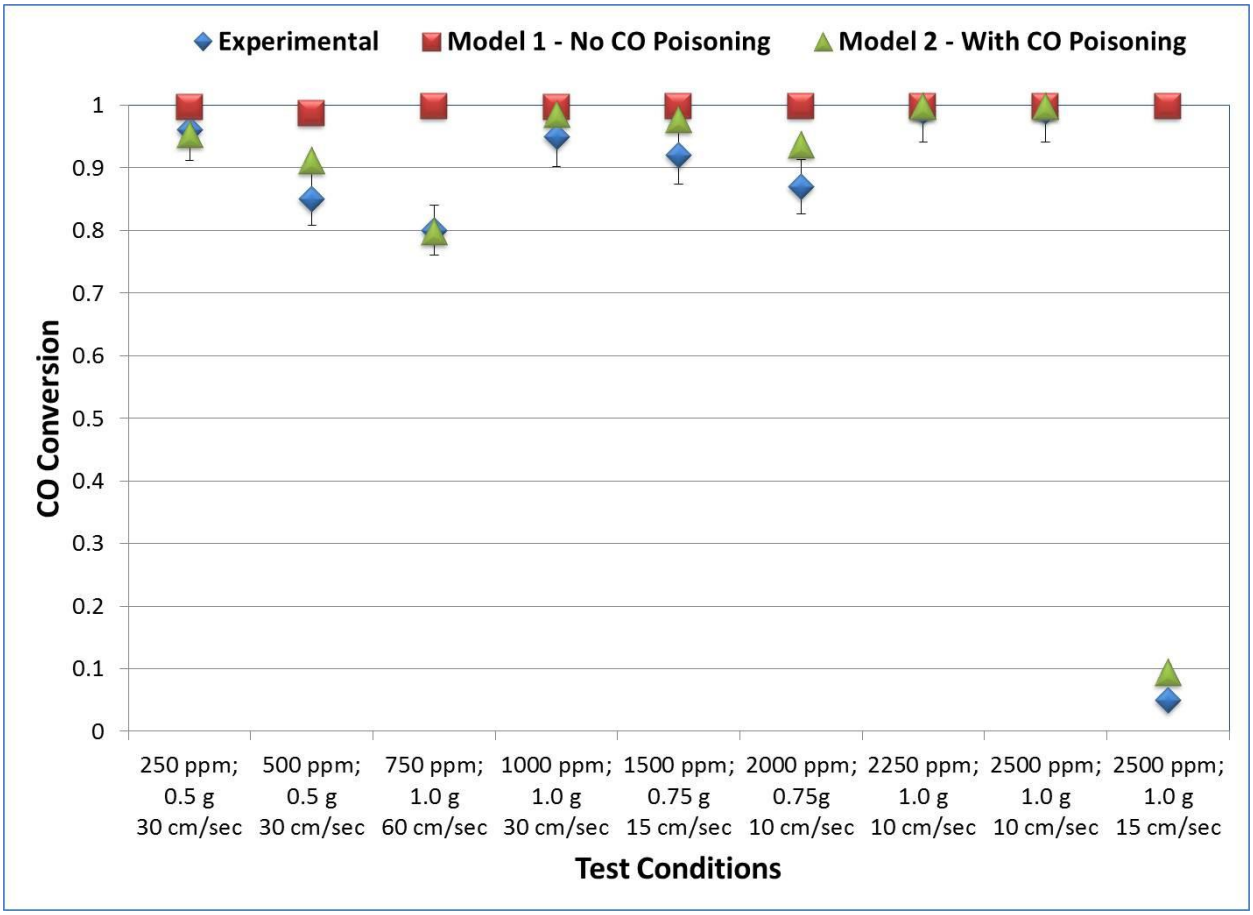

Figure VII.2. Reactor Model Validation Results – Comparison of Two models with Reactor Data

VII.3.3 Progression of Reaction in Catalyst Bed

VII.3.3.1 Experimental Observations – Effect of Catalyst Bed Depth

During this study, it was observed that the reactor performance was significantly dependent on the length (depth) of catalyst bed. Based on the integral plug flow reactor (PFR) model, increase in bed depth would result in lower rates of reaction per gram of catalyst. Reactor performance results for different catalyst bed depths are given in Figure VII.3 and the estimated reaction rates are given in Table VII.6. Using PFR model, the observed decline in the reaction rates when the catalyst bed depth was increased from 3.5 mm to 4.0 mm could be explained. However, the observed increase in the reaction

rate when the catalyst bed depth was increased from 3.0 mm (conv. ≈65%) to 3.5 mm (conv. ≈98%) could not be explained by the PFR model.

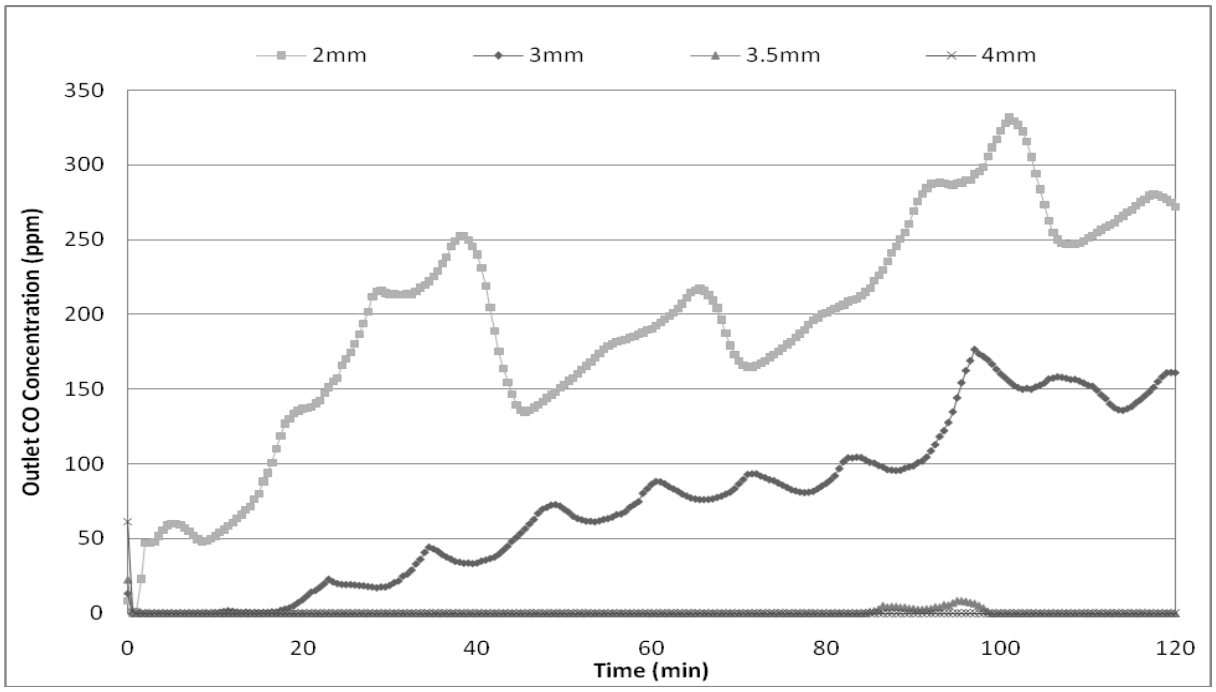

Figure VII.3. Effect of Catalyst Bed Depth on Activity at Low CO Concentration

Table VII.6. Reaction rate for different catalyst bed depths

Catalyst Bed Depth	Conversion (%)	Reaction Rate (µmol/g/s)*
2.0 mm	35.0	1.36
3.0 mm	65.0	1.69
3.5 mm	98.0	2.18
4.0 mm	99.8	1.94

* *Test Conditions: 50%RH; Reactor ID: 0.375"; 500 ppm CO; 25^{0}C; FV: 30 cm/sec; Particle: 200 µm*

Tests were conducted at higher CO concentrations (2500 ppm CO), with varying catalyst bed depths, the results are plotted in Figure VII.4.

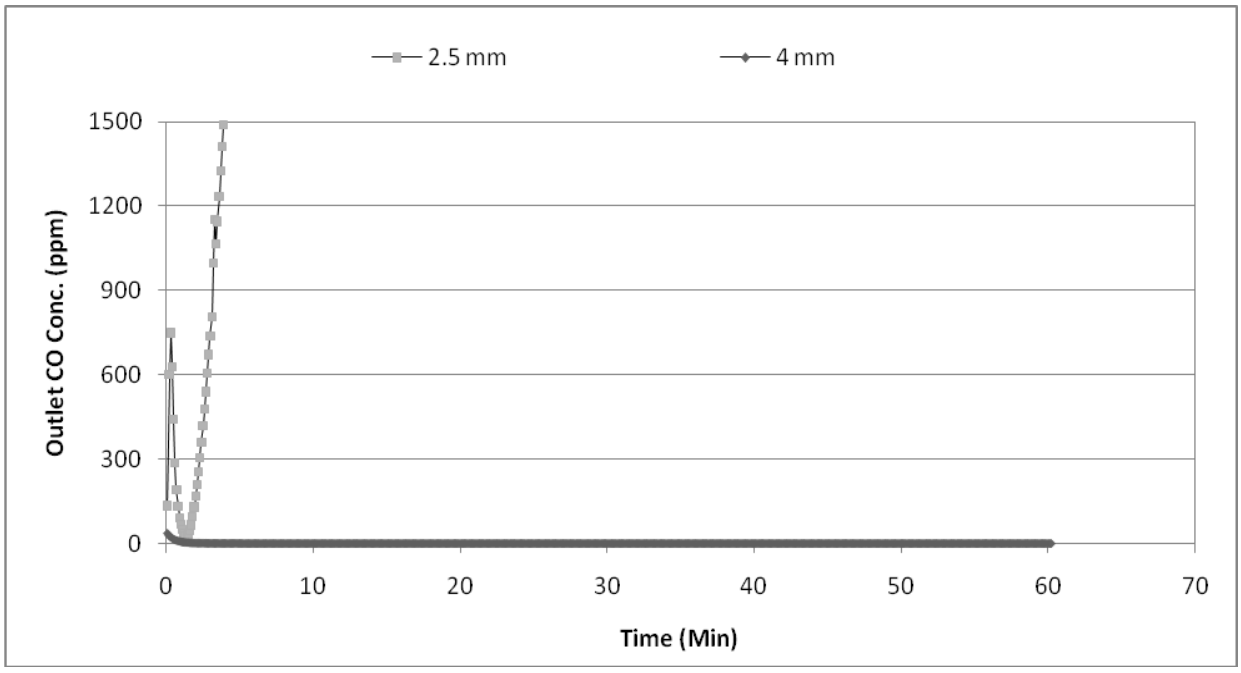

Figure VII.4. Effect of Catalyst Bed Depth on Activity at High CO Concentration

Test Conditions: Humidity: 90%RH; Reactor: 0.75" ID; CO Concentration: 2500 ppm; Temperature: 25^{0}C; Face velocity: 10 cm/sec; Particle Size: 200 µm

When a 2.5 mm catalyst bed was used, the catalyst yielded less than 5% conversion. When the catalyst loading was increased to have a 4.0 mm catalyst bed, the catalyst exhibited more than 99.9% conversion. This behavior could not be explained by the PFR model.

VII.3.3.2 Experimental Observations – Effect of Face Velocity

If the reaction is not externally diffusion controlled, the rate of reaction would be independent of gas face velocity. However, it was observed that the rate of reaction was a function of face velocity. The reactor performance results obtained at four different gas face velocities are given in Figure VII.5.

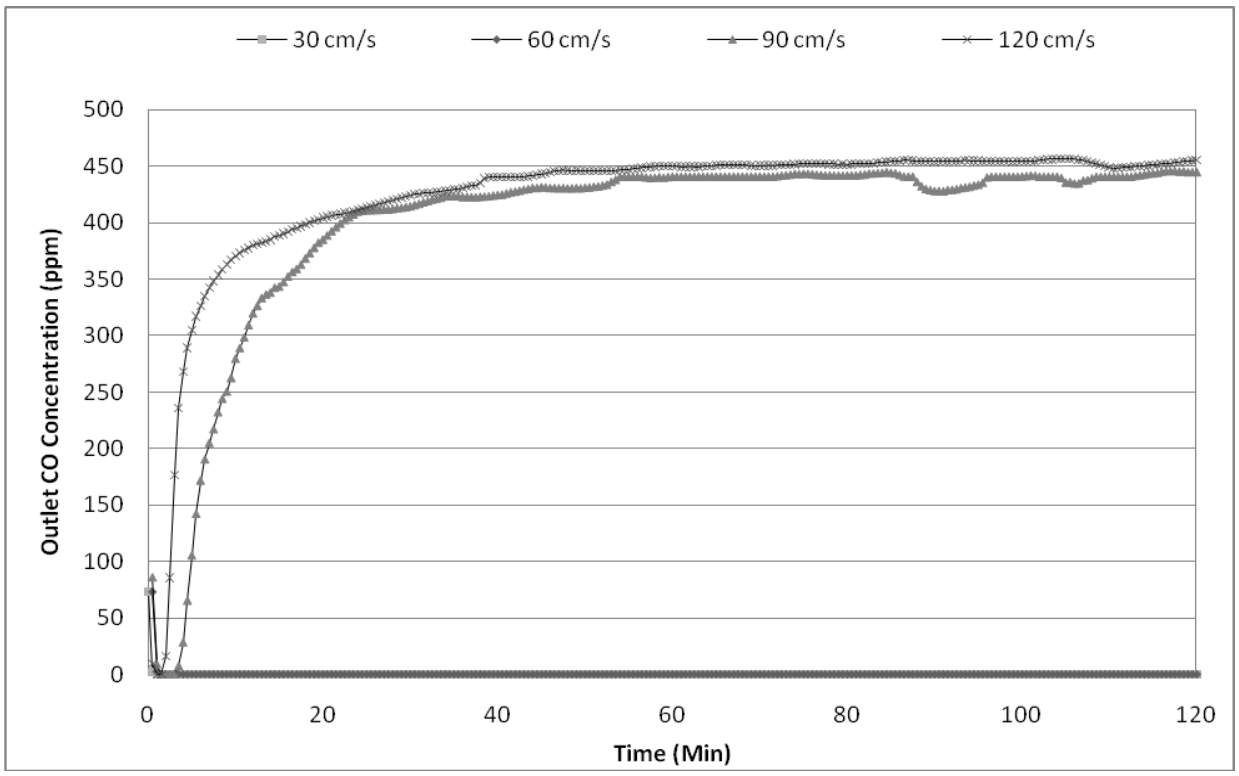

Figure VII.5. Effect of CO Flux on Catalytic Activity at Low CO Concentration

Table VII.7. Effect of Face Velocity on Activity and Convective Heat Transfer Coefficient

Face Velocity (cm/sec)	Residence Time (ms)	Conversion (%)	Reaction Rate* (µmol/g/s)	Mears' Criterion	Convective HTC (J/Sec.K)
30	11.7	99.5	2.32	0.037	0.08
60	5.83	99.5	4.66	0.058	0.13
90	3.89	12.0	0.837	0.009	0.17
120	2.92	10.0	0.935	0.009	0.21

* *Test Conditions: 50%RH; Reactor: 0.75" ID; 500 ppm CO; 25^{0}C; Bed depth: 3.5 mm; Particles: 100 µm*

Mears' criteria and convective heat transfer coefficients (HTC) were estimated and given in Table VII.7. Increase in face velocity from 60 cm/sec to 90 cm/sec significantly changed the reaction rate. Although, the Mears' criterion for external diffusion was satisfied in all the cases studied, change in face velocity had a major impact on the rate of reaction.

VII.3.3.3 Effect of CO Concentration

During this study, the effect of CO concentration on the catalytic activity of a thin bed was studied and the results are given in Figure VII.6.

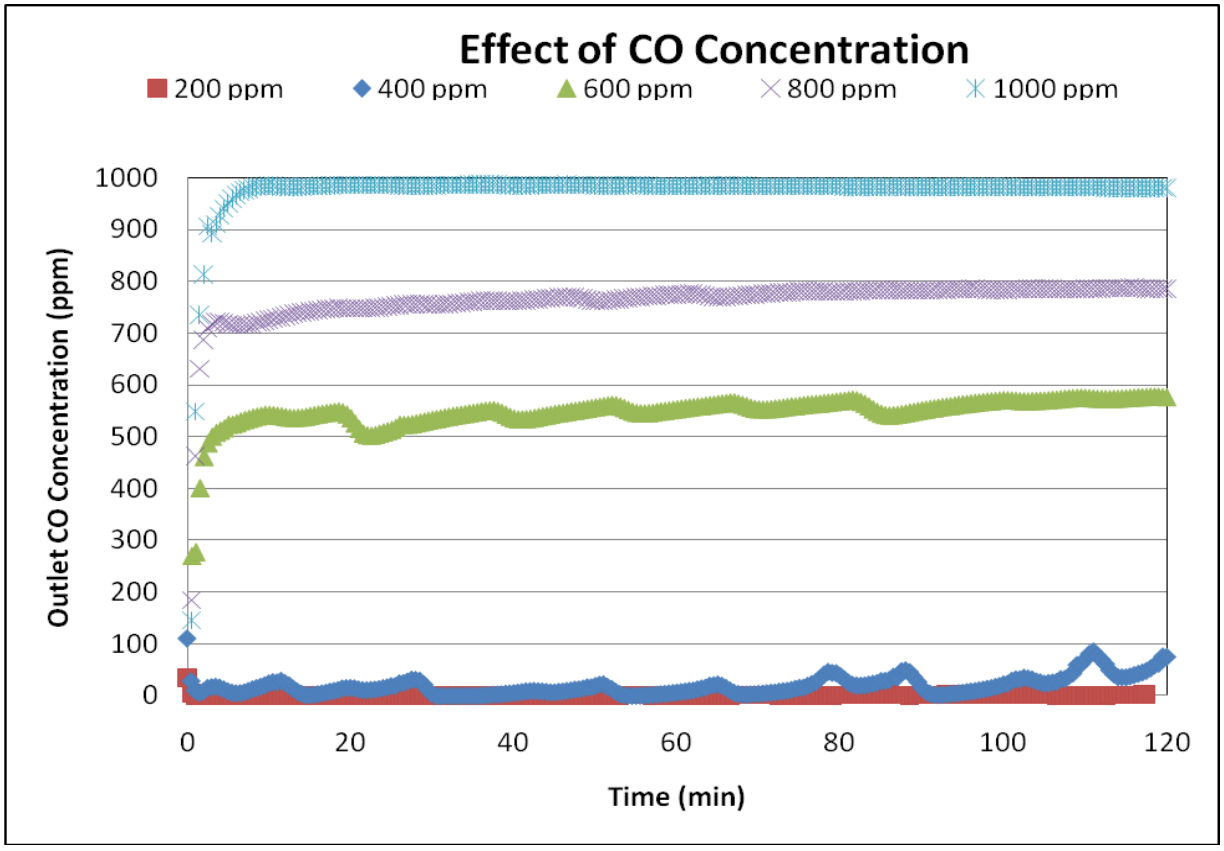

Figure VII.6. Effect of CO Concentration on Catalytic Activity

Test Conditions: Humidity: 50%RH; Reactor: 0.75" ID; Temperature: 25^{0}C; Catalyst wt: 0.2gm; Particle Size: 100 µm; Face Velocity: 30cm/sec; Catalyst used: 4%Pt-16%Ceria/Silica

The catalyst yielded almost 99% conversion at 200 ppm, also the catalyst yielded more than 80% conversion at 400 ppm. However, the catalyst yielded less than 10% conversion for 600 ppm CO and had no activity at 800ppm and 1000 ppm.

A similar behavior to that of the catalyst bed depth study and face velocity study was shown even by the CO concentration effect study. The catalyst had significant activity at 200 ppm and 400 ppm; however, the catalyst completely deactivated when the CO concentration was increased slightly. This behavior could not be explained by the LH dual site mechanism.

VII.3.3.4 Hypothesis

The effect of catalyst bed depth, face velocity and CO concentration could be explained on the basis of the propagation of the reaction in the reactor. A hypothesis has been proposed to explain this behavior: it was postulated that initially, the front of the bed was exposed to total bulk concentration; however, as more and more CO was either adsorbed or reacted, CO concentration decreased along the length of bed; therefore, the end of the catalyst bed was exposed to the least CO concentration. Moreover, at lower temperatures, the impact of CO self-poisoning was higher; therefore, initial few layers of catalyst possibly acted as sacrificial layers, only adsorbing CO. After the initial few catalyst layers, number of active sites being more than the poisoned sites, there would be some CO adsorption accompanied by reaction. Further down the length of catalyst bed, decrease in CO concentration would eventually decrease the poisoning probability for catalyst. Additionally, a smaller reaction rate in the front/mid of the bed would also result in some release of heat, heat of CO adsorption would get carried over by the gas. This exothermicity would increase the reaction kinetics and lower the CO poisoning probability for catalyst particles down flow. Additionally, at lower CO concentrations, there would be significant amount of active sites still available for reaction on particles near the end of the bed.

Further, once the back of the catalyst bed was active, there was a transfer of heat amongst the catalyst particles, which would eventually make the entire bed active. If the catalyst particles at the front of the bed were highly active, particles down flow would get heat from convection as well as conduction. However, in this case, the heat transfer was mostly via conduction or thermal diffusion in the opposite direction of the flow. A schematic representation of the proposed hypothesis is given in **Error! Reference source not found.**.

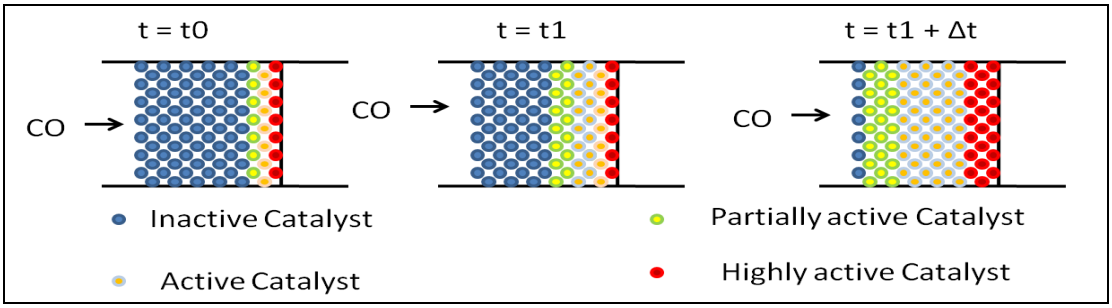

Figure VII.7. Proposed Hypothesis for the Propagation of Reaction

The steps during reaction propagation: (a) CO adsorption by front of the bed, so the end of the bed would see low CO concentration, (b) heat of adsorption (and reaction if any) carried to the end of the bed, (c) low CO and high temperature resulting in highly active end of the bed, (d) transfer of heat from end of the bed to the front of the bed by thermal diffusion opposite to the gas flow, and finally (e) in this fashion, the whole bed would get ignited.

VII.3.3.5 Experimental Testing of the Hypothesis

This hypothesis was tested by designing the catalyst bed in such a way that the layers of the catalyst particles were separated from each other by a medium different from the catalyst particles. Mediums with different thermal conductivity were used for separation of the catalyst layers. The

schematic of the catalyst bed for these tests is shown in Figure VII.8. The activity results are given in Figure VII.9 .

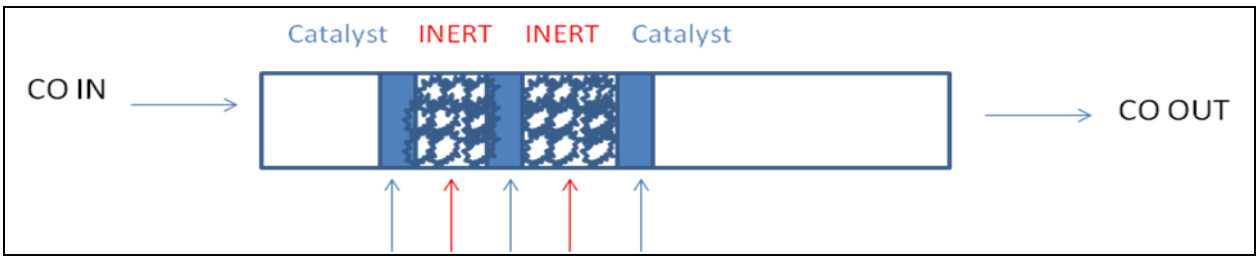

Figure VII.8. Reactor Design to Study the Propagation of the Reaction in the Reactor

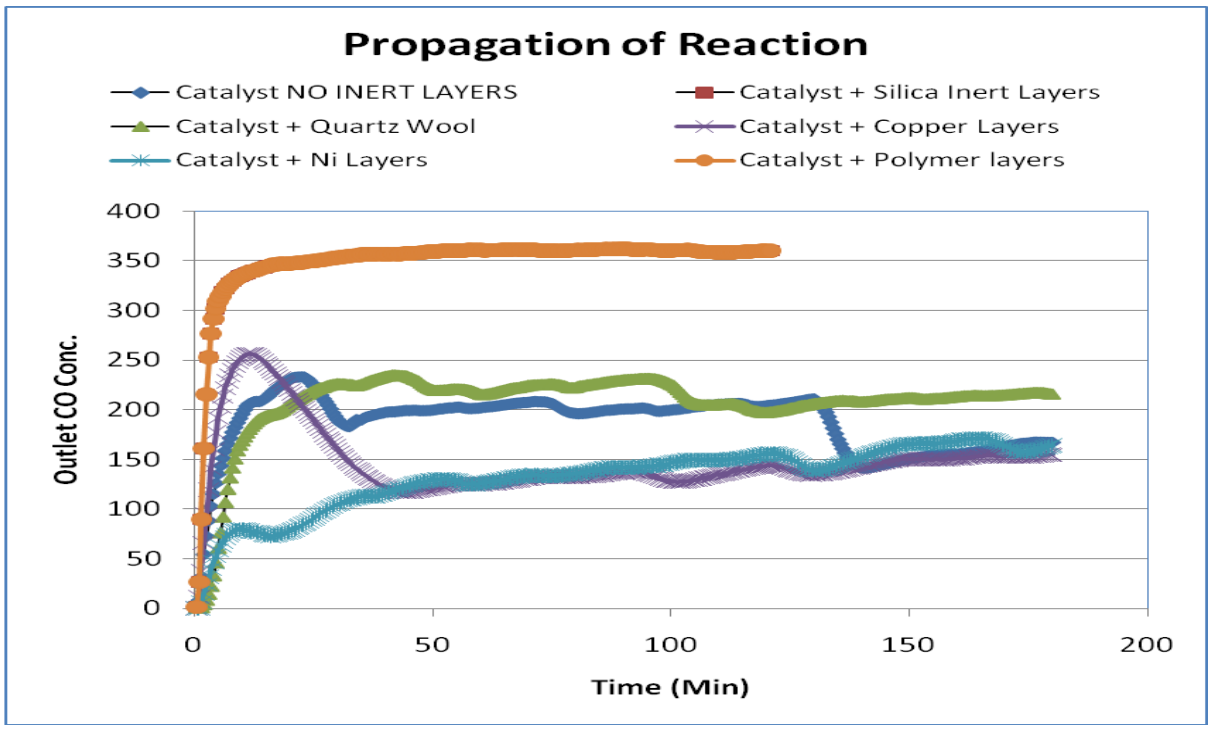

Figure VII.9. Impact of Catalyst Layers Separation by Inert Media on the Reactor Performance

375ppm CO; FV: 30cm/sec; Reactor ID: 3/4"; 25°C; 50% RH; 200µm; Cat. Wt.: 0.5gm-divided in three layers; Separation layers used: (a) Sintered Cu media (12 µm fibers); (b) Sintered Ni media (12 µm fibers); (c) Polymer media (13 µm fibers); (d) quartz wool: 12 micron fibers; (e) silica particles of 200 microns.

The total amount of catalyst was segregated in three layers separated by inert layers of 2mm thickness each. Five different mediums were used as inert for the separation of the catalyst layers, namely: (a) sintered copper fibrous media, (b) sintered nickel fibrous media, (c) quartz wool, (d) polymer fiber media, and (e) silica powder. The test conditions were kept the same and care was taken that the catalyst layers were of the same size in all the configurations tested. (*Catalyst: 4%Pt-16%Ceria/Silica)*

Separation of the catalyst layers by poorly conductive media such as silica and polymer layers resulted in decreased reactor performance. When the catalyst layers were separated by metallic inert layers such as the Cu or Ni sintered fiber layers, the performance of the reactor bed improved initially and later on the activity was close to that of the catalyst without any separation layers.

Therefore, it could be said that the separation of catalyst layers with a highly thermally diffusive media helped the catalyst to transfer heat faster within the catalyst bed and thereby performing better. Thermal diffusion within the bed was important and from the results obtained during this study, the catalyst layers were thermally connected to each other. Also, when the catalyst layers were separated by thermally insulating layers, the performance of the catalyst declined because the thermal connection between the layers of the catalyst was destroyed or significantly reduced.

This study qualitatively proved the hypothesis that the reaction initially started at the back of the bed and then due to the heat transfer to the front of the bed, the front of the bed regained activity and finally the entire bed became active.

VII.3.3.6 Hypothesis Validation by Reactor Model

In order to check the first part of the hypothesis that the reaction mainly took place at the end of the bed, two simulations were carried out wherein except for the length of the bed all the other simulation conditions were kept the same. So, if the proposed hypothesis were to be right, then the

reactor with greater bed length should show significantly greater activity in comparison with the reactor with lower catalyst loading or smaller bed length. The simulation results are plotted in Figure VII.10.

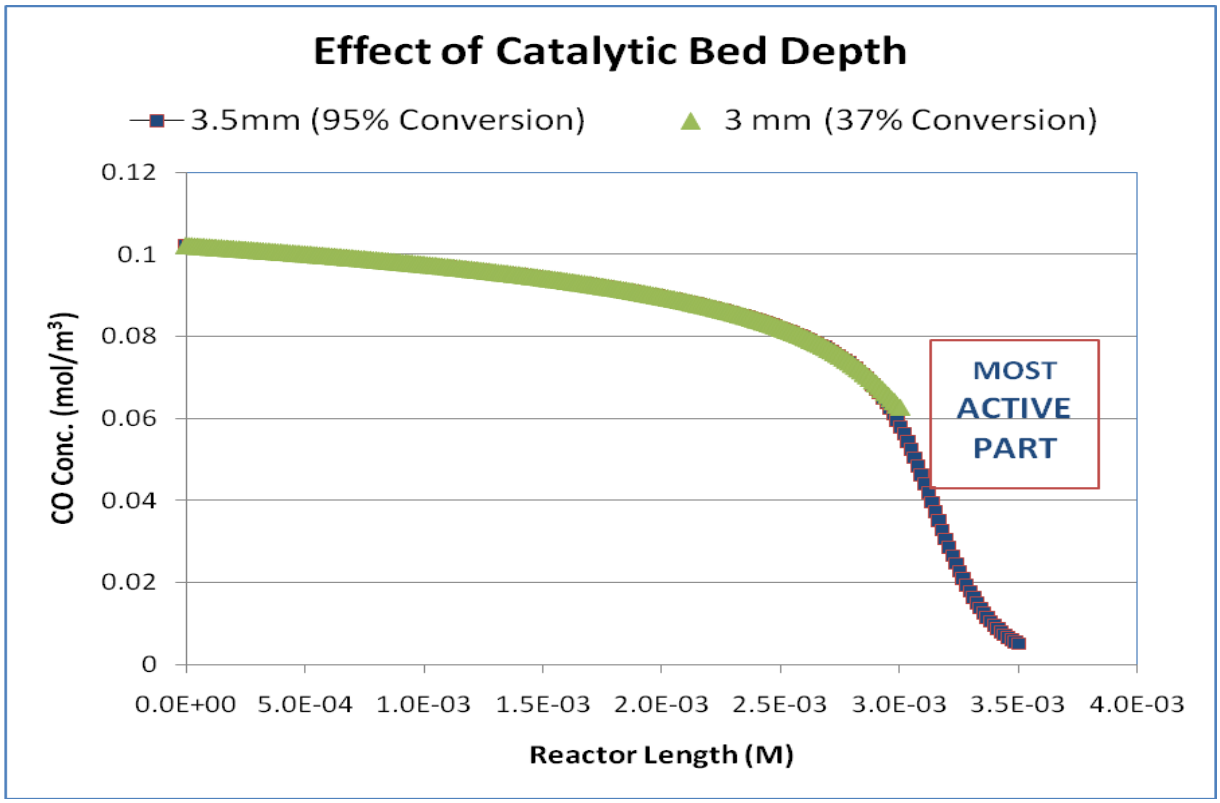

Figure VII.10. Simulation Results – Impact of Catalyst bed Depth on Activity at High CO

Simulation Conditions: Temperature: 25^{0}C; Challenge gas: 2500 ppm CO; Face Velocity: 30cm/sec; Thermal diffusivity: Ka

From the simulation results it was observed that increasing the bed depth by less than 20% (from 3mm to 3.5mm) increased the CO conversion from 37% to 95%. So, the last few layers of the catalyst bed was the most active part of the catalyst bed.

These simulation results prove the first part of the hypothesis that it would be the end of the bed which would be highly active due to low CO and high temperature.

The second part of the hypothesis which was quite crucial to the whole theory, that the heat transfer from the end of the bed to the front of the bed would make the entire bed active over a period of time. The mode of heat transfer from the end of the bed to the front of the bed was proposed to be thermal diffusion.

Therefore, the reactor model in its current form was used to simulate the transient reactor performance at high CO. The simulation results are given in Figure VII.11.

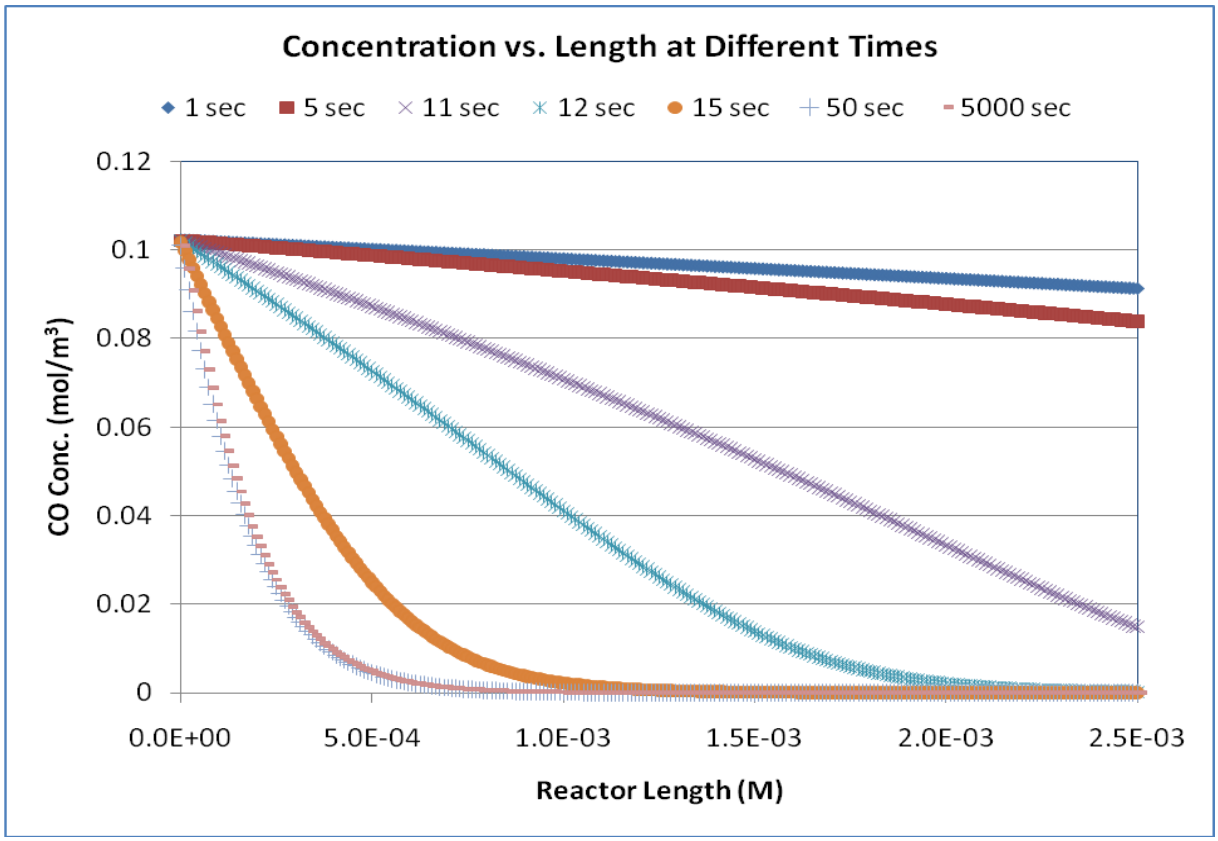

Figure VII.11. Simulation Results: Progression of Reaction – CO vs. Length at Different Times

Simulation Conditions: Temperature: 25^{0}C; Challenge gas: 2500 ppm CO.

From the simulation results, CO conversion in the reactor changed with respect to time. During the first 10 seconds, the temperature at the back of the bed was higher. Due to thermal diffusion, heat

was transferred to the middle of the bed and then to the front of the bed. Due to the heat transfer, the entire bed got ignited and then at around 15 seconds the reactor reached steady state of higher activity and maintained the higher state of activity for 5000 seconds.

From Figure VII.10 and Figure VII.11 the two parts of the hypothesis, namely: (a) reaction started at the end of the bed, and (b) thermal diffusion resulted in ignition of the catalyst bed were validated.

VII.3.3.7 Explanation of the Experimental Observation based on Reaction Propagation

In the case of the catalyst bed depth experiments, if the catalyst bed depth in not sufficient enough such that the end of the bed could achieve ignited state, then the entire catalyst bed would get poisoned. Since the end of the bed would not be active, there would not be any heat transfer, resulting in complete deactivation of the bed. For example, the results from Figure VII.3, a 3 mm bed did not have sufficient catalyst layers to have the last few layers reach ignited state whereas the 3.5 mm layer which due to addition of just the last couple of particle layers resulted in greater activity.

Similarly, when the face velocity was increased, if the catalyst bed depth was not sufficient enough such that the end of the bed could achieve higher activity, then the entire catalyst bed would get deactivated. From Figure VII.5, it could be seen that when the face velocity was increased from 30 cm/sec to 60 cm/sec the catalyst bed depth was sufficient to handle the increased CO flux and maintained close to 99% CO conversion. However, increased CO flux beyond 60 cm/sec face velocity resulted in a situation wherein the catalyst bed depth was insufficient to achieve higher activity.

Similar explanation was applicable to the CO concentration study, Figure VII.6. There would be a value of CO concentration up to which the thin catalyst bed could remain active. However, increased CO concentration beyond a threshold point, in this case 400 ppm, resulted in the catalyst layers even at the end of the bed being poisoned which resulted in poor observed reactor performance.

VII.4 Conclusion

From the reactor modeling study, the following conclusions were drawn: (a) the proposed hypothesis for the progression of the reaction in the catalyst bed that the reaction initially occurred at the back of the bed and due to the heat transfer to the front of the bed, the entire bed became active was verified.

Also, a reactor model with a concentration and temperature dependent catalyst CO self-poisoning term showed a greater fit for the observed experimental results. A 1-D pseudo-homogeneous, non-isothermal, transient model was sufficient to explain most of the observed experimental behavior qualitatively and quantitatively.

VIII Microfibrous Entrapped Catalysts

VIII.1 Introduction

CO oxidation at ambient temperature is difficult due to slow surface kinetics and CO self – poisoning of the catalyst. In the presence of moisture, the reaction becomes more difficult as the water vapor also competes with CO for active sites. A number of catalyst formulations, both commercial and those reported in scientific literature, were screened for this application (Chapter III). However, none of the catalysts were found to be highly active for CO oxidation under ambient conditions (25^0C and 50-90% RH) over a wide range of CO concentrations. So, a number of novel catalyst formulations were developed and screened. A silica supported Pt catalyst with ceria as a promoter was found to be highly active for CO oxidation at ambient conditions yielding more than 99% conversion at low (<500ppm) as well as high (2500ppm) CO concentrations (Chapter V).

Further, the reaction was found to be diffusion controlled at ambient conditions (Section: V.3.10.1). Therefore, use of small catalyst particles (<500 micron) was imperative to maximize Pt utilization and reduce footprint of the system. However, a conventional packed bed (PB) of smaller catalyst particles (dia. < 500 μm) is prone to cluster formation which results in channeled flow, flow maldistribution and local bypass of the catalyst [46, 146]. Further, a packed bed of small particles can get unsettled due to change in orientations or exposure to vibrations which may result in lower activity. In order to improve performance and lower costs, a catalyst carrier was needed for this application.

Catalyst carriers mainly affect the heat and mass transport properties of the reactor. Use of entrapment or wash-coat techniques minimizes the gas-solid heat/mass transfer resistance by enabling the use of smaller catalyst particles. Further, mass dispersion and thermal diffusivity of the system would change due to the presence of monolith/foams or fiber matrix that carries the catalyst particles. A packed bed can be viewed as a series of main voids interconnected by smaller voids or channels. The eddy or molecular diffusion causes appreciable mixing in the main voids resulting in dispersion [147]. Axial dispersion reduces the conversion per pass, as the concentration seen by the catalyst is lower than predicted [148]. Catalyst carriers with greater voidage could minimize dispersion and improve performance. Packed beds are poor conductors of heat and introduction of a catalyst carrier with better heat transport properties would certainly improve performance for exothermic systems. For example, *Visconti et. al.* have shown that use of a high thermal conductivity monolith improved activity and yield in Fischer-Tropsch synthesis [149]. Also, metallic foams have been pursued in applications demanding higher thermal conductivities [150, 151].

Catalyst washcoated monoliths are one of the solutions for applications that prefer small catalyst particles for greater contacting efficiency. For example, environmental applications involving gas phase catalytic reactions use monoliths [152, 153]. However, monoliths suffer from many disadvantages such as lower volumetric catalyst loading (maximum catalyst loading: 10-15% v/v) and excess inert thermal mass [154]. The CO oxidation reaction at ambient conditions is mainly driven by the temperature rise in the reactor owing to the high exothermicity of the reaction ($-\Delta H_R$ = 284 KJ/mol). In the case of monoliths, addition of inert thermal mass would result in lower temperature rise in the reactor causing reduced activity. So, monoliths were considered inappropriate for this application.

Catalyst carrier that would exhibit greater contacting efficiency and higher heat and mass transport rates while maintaining greater catalyst loading (v/v) was required. With this goal in mind,

microfibrous entrapped catalysts or sorbent (MFECs/MFESs) have been developed [43, 155]. These MFECs typically entrap 50 to 300 µm particles in a 3-dimensional network of 2-20 µm fibers (polymer, ceramic or metal fibers). MFECs can be made more open (voidage: ε = 0.45 - 0.8) and can be made out of metallic fibers thereby increasing heat transfer within the reactor [156]. MFECs with their open and uniform reduce peaking flows, minimize flow maldistribution, reduce axial dispersion, and offer lower pressure drop [146]. MFECs are flexible and pleatable, so the packaging issues with small particles could be eliminated. A typical micrograph of MFEC is shown in Figure VIII.1 and an image of rolled MFECs is shown in Figure VIII.2. Use of these MFECs/MFESs has shown significant performance improvements in a number of applications [45, 157].

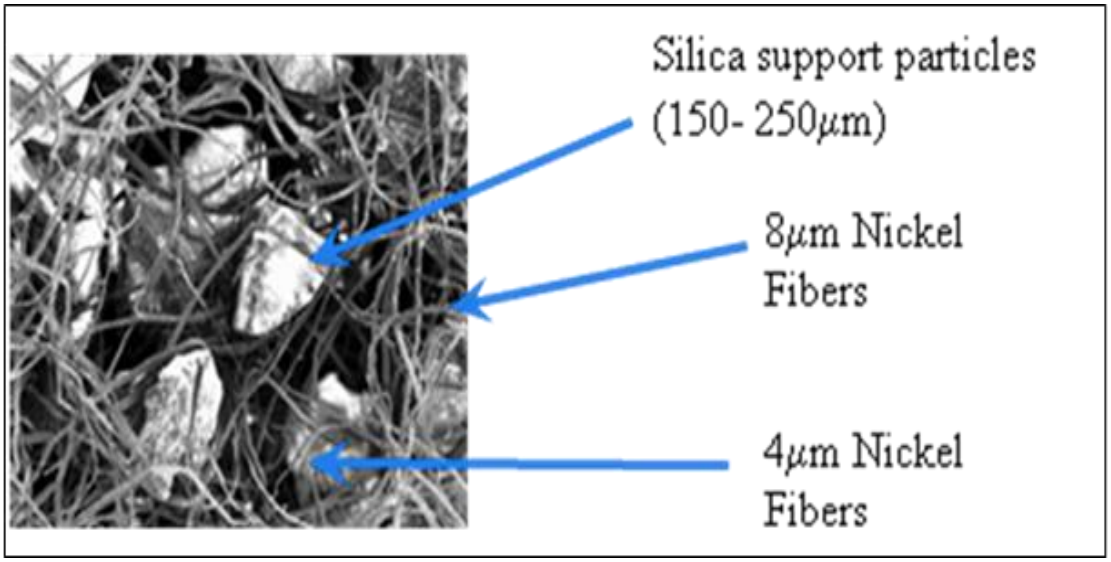

Figure VIII.1. SEM Micrograph of MFEC

During this study, impact of intra-particle diffusion on the activity of Pt-CeO_2/SiO_2 catalyst was studied. The use of Ni fibers entrapped Pt-CeO_2/SiO_2 catalyst for CO oxidation was investigated in detail. Further, the impact of axial mass dispersion and thermal diffusivity on activity was studied by changing

these reactor properties by catalyst dilution. The catalyst bed was diluted with silica, nickel or copper powders and these diluted PBs were evaluated for CO oxidation activity.

Figure VIII.2. Image of Rolled MFEC

The relative impacts of reactor properties such as mass dispersion, thermal diffusivity and heat capacity were analyzed using the reactor model. The reactor model was solved by COMSOL® Multiphysics.

Finally, the stability and performance of the Ni microfibers entrapped Pt-CeO_2/SiO_2 catalyst was investigated and compared against conventional packed bed.

VIII.2 Experimental Details

VIII.2.1 Preparation Methods and Materials

The catalysts were prepared by using successive incipient wetness impregnation method on a silica (Davisil® 645, Sigma Aldrich) support. The steps followed during catalyst preparation were: (a)

impregnation of a ceria precursor (cerium (III) nitrate hexahydrate (REacton® 99.99%, Alfa Aesar)) on the silica support followed by drying under vacuum at 40^0 C for six hours and calcination at 300^0 C for two hours in air, and (b) impregnation of a Pt precursor (diammine dinitro platinum (DADNP) (8.2% w/w in dil. NH_4OH, Strem Chemicals)) on the ceria-silica support followed by drying at 125^0C for four hours and calcination at 500^0C for 2 hours.

The microfibrous media were prepared using nickel fibers (4 – 8 μm; Intramicron Inc.), cellulose fibers (13 – 19 μm; Intramicron Inc.) and silica support. MFEC preparation process is described in detail by Tatarchuk et. al. [156, 158]. Briefly, the MFEC preparation method has four steps: (a) pre-form preparation, (b) pre-oxidation, (c) sintering, and (d) active metal/promoter deposition. Pre-forms were prepared by wet-lay method. A suspension of nickel and cellulose fibers was prepared using a blender, which was then added to a head box followed by addition of silica. A uniform mix of particles and fibers was obtained in the head box by continuous stirring. Finally the excess water was drained and a uniform media that entrapped particles in the mesh of metal and cellulose fibers was obtained. These pre-forms were then dried in oven at 100^0C overnight to get rid of excess water.

During the pre-oxidation step of the MFEC preparation, the dried pre-forms were cut to the desired sizes and the cellulose fibers in the pre-forms were burned at 450^0C for 45 minutes in air diluted with N_2. During sintering step for MFEC preparation, the pre-oxidized sheets were sintered in diluted hydrogen atmospheres at about 900-1000^0C for 30 minutes. During sintering, the metal microfibers bond with each other and form a sinter-locked mesh of fibers that entraps the catalyst particles. The deposition of Pt/Ceria on the entrapped silica was carried out using the same process given above.

VIII.2.2 Catalyst Testing

The challenge gas used for the experiments was 250-2500 ppm of CO in air (RH: 10-90%). Air and CO (5% CO in Nitrogen, from Airgas) streams were controlled using mass flow controllers. These streams were mixed and passed through a water saturator to get the desired RH of the resulting stream. The RH was measured using a RH detector. The CO concentration in the challenge gas was measured using an Agilant® gas chromatogram (GC). Outlet CO concentration was measured using an electrochemical sensor (detection limit: 0.1 ppmv CO). A tubular pyrex reactor with a glass-frit support for the catalyst powder was used for the experiments. In order to get a uniform flow in the catalyst bed, a thin layer of quartz wool was used before the catalyst bed.

VIII.2.3 Catalyst Characterization

Brunauer-Emmet-Teller surface area (BET SA) were obtained using a Quantachrome AS1 surface area and pore size analyzer using N_2 adsorption at 77K. BET surface area analysis employed a five point method. Static CO chemisorption was performed to estimate Pt dispersion using the same Quantachrome AS1 instrument. A stoichiometry of (1:1) was assumed for (CO: Pt) for chemisorption at 30^0C. In order to get reproducible isotherms of CO chemisorption on Pt, the samples were pre-treated. The pre-treatment sequence followed was: (a) cleaning (200^0C, 1 hr, He), (b) evacuation (200^0C, 2hr, vacuum), (c) reduction (300^0C, 1 hr, H_2) and (d) adsorbed H_2 removal (300^0C, 2 hr, vacuum). In the case of MFECs, to obtain reproducible results for BET SA and CO chemisorption, the catalyst particles from MFECs were dislodged mechanically and were then analyzed in a powder form.

VIII.2.4 Reactor Model Details

Reactor model with apparent CO poisoning term was used. The reactor model is given in Chapter VII. Reactor Modeling. The model was solved by COMSOL® multiphysics.

VIII.3 Results and Discussion

VIII.3.1 MFECs as a Solution to Intra-Particle Diffusion Problem

Effect of particle size on activity of the 4%Pt – 16%CeO_2 /SiO_2 catalyst was studied at 25^{0}C and 50^{0}C and the results are given in Figure VIII.3. When the particle size was reduced from 750µm to 75µm, the reaction rate almost doubled at 25^{0}C. At 50^{0}C, the rate of reaction of 60 micron particles was almost 6 times that of the 1200 micron particles. The reaction was significantly reactant diffusion limited, so to optimize the Pt utilization use of the small catalyst particles was imperative.

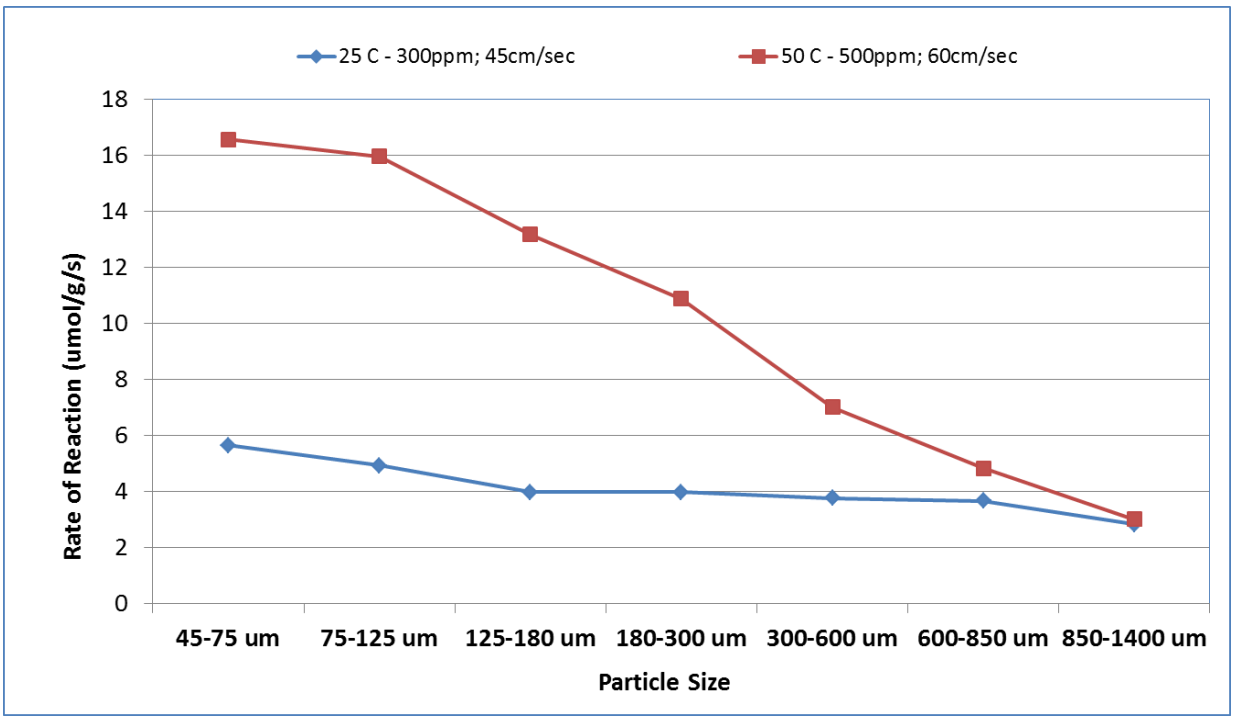

Figure VIII.3. Effect of Particle Size on Catalytic Activity of Pt-Ceria/Silica Catalyst

Test Conditions: Humidity: 1% H_2O (v/v), Reactor ID: ¾", Catalyst wt: 0.05g (inert silica: 0.5g)

Nickel microfibers entrapped Pt-CeO_2/SiO_2 catalysts (MFECs) were tested for CO oxidation and activity comparison results with packed bed (PB) are given in Figure VIII.4. The surface characteristic

properties, such as BET SA and Pt dispersion, for both of these catalysts are given in Table VIII.1. In the case of MFEC, high temperature sintering at 950^0C had a negative impact on the SA (10% less than powder catalyst). Also, Pt dispersion was lower in the case of MFEC (Pt crystallites ≈ 10% bigger than powder catalyst). In Figure VIII.4 (A) 250 ppm CO; Face Velocity: 30 cm/sec; Catalyst: 0.5 g; (B) 750 ppm CO; Face Velocity: 30 cm/sec; Catalyst: 0.75 g; (C) 2500 ppm CO; Face Velocity: 10 cm/sec; Catalyst: 1.0 g. As seen from the figure, the MFEC (CO Conversion (X_{CO}) > 99%) outperformed PB (X_{CO} ≈ 90%) for the same amount of catalyst loading, despite lower SA and poor Pt dispersion.

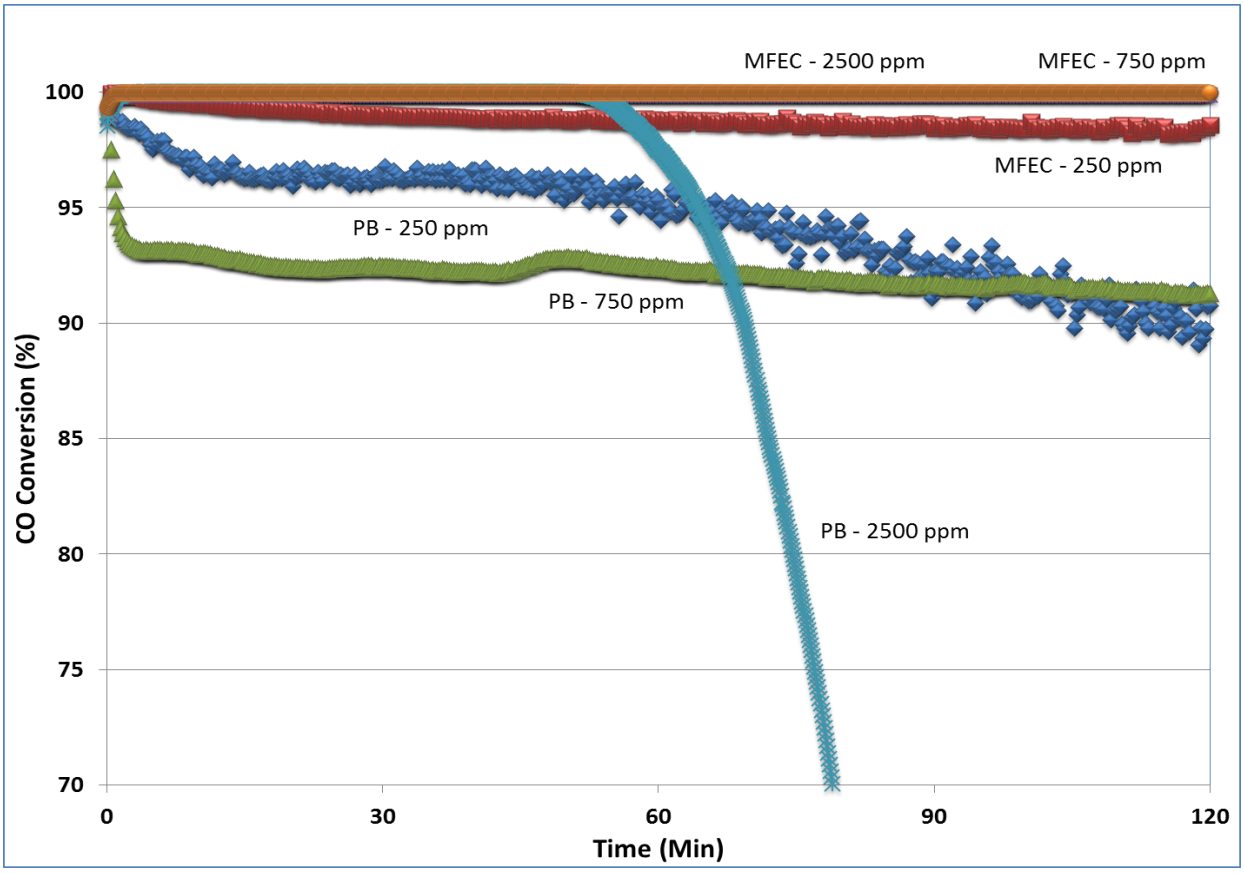

Figure VIII.4. PB - MFEC Comparison - 25°C; 50% RH; Dp: 200µm; Reactor ID: 0.75"

Greater activity of the MFECs could be attributed to either greater voidage (ε > 0.6) which could reduce mass dispersion or presence of Ni fibers that would improve thermal conductivity. The impact of

heat and mass transport properties on the activity were studied experimentally, to understand reasons behind the greater activity of MFECs. The impact of axial dispersion on activity was investigated by catalyst dilution with inert silica powder. In order to study the impact of thermal properties on the activity, the catalyst bed was diluted with copper or nickel powder.

Table VIII.1. Characterization Results for Powder & Ni MF Entrapped 4% Pt-16%Ceria/Silica

Catalyst	BET SA (m^2/g)	Pt Dispersion (%D)	Pt Crystallite Size (nm)
Powder Catalyst	184.5	27.83	4.07
MFEC	171.4	25.74	4.40

VIII.3.2 Effect of Axial Dispersion on Reactor Performance

Axial dispersion in PB is known to reduce overall conversion. Further, smaller particles (dia. < 500 μm) in a PB have a tendency to form clusters which could result in local – bypass of the catalyst resulting in lower activity. However, the axial dispersion can be minimized by catalyst dilution [159]. The effect of catalyst dilution was investigated by diluting the catalyst PB with inert silica of same size to get 30% and 20% catalyst loading (v/v) in a diluted PB. Activity of these diluted PBs was compared against PB and the results are given in Figure VIII.5. At lower CO concentration (375 ppm), dilution with silica improved the overall activity (CO conversion: 50%, 80%, 85% for PB, dil. PB (30% v/v) and dil. PB (20% v/v) resp.). However, at higher CO concentration (2500 ppm), dilution with silica significantly decreased activity (CO conversion: 99%, 10%, 5% for PB, dil. PB (30% v/v) and dil. PB (20% v/v) resp.).

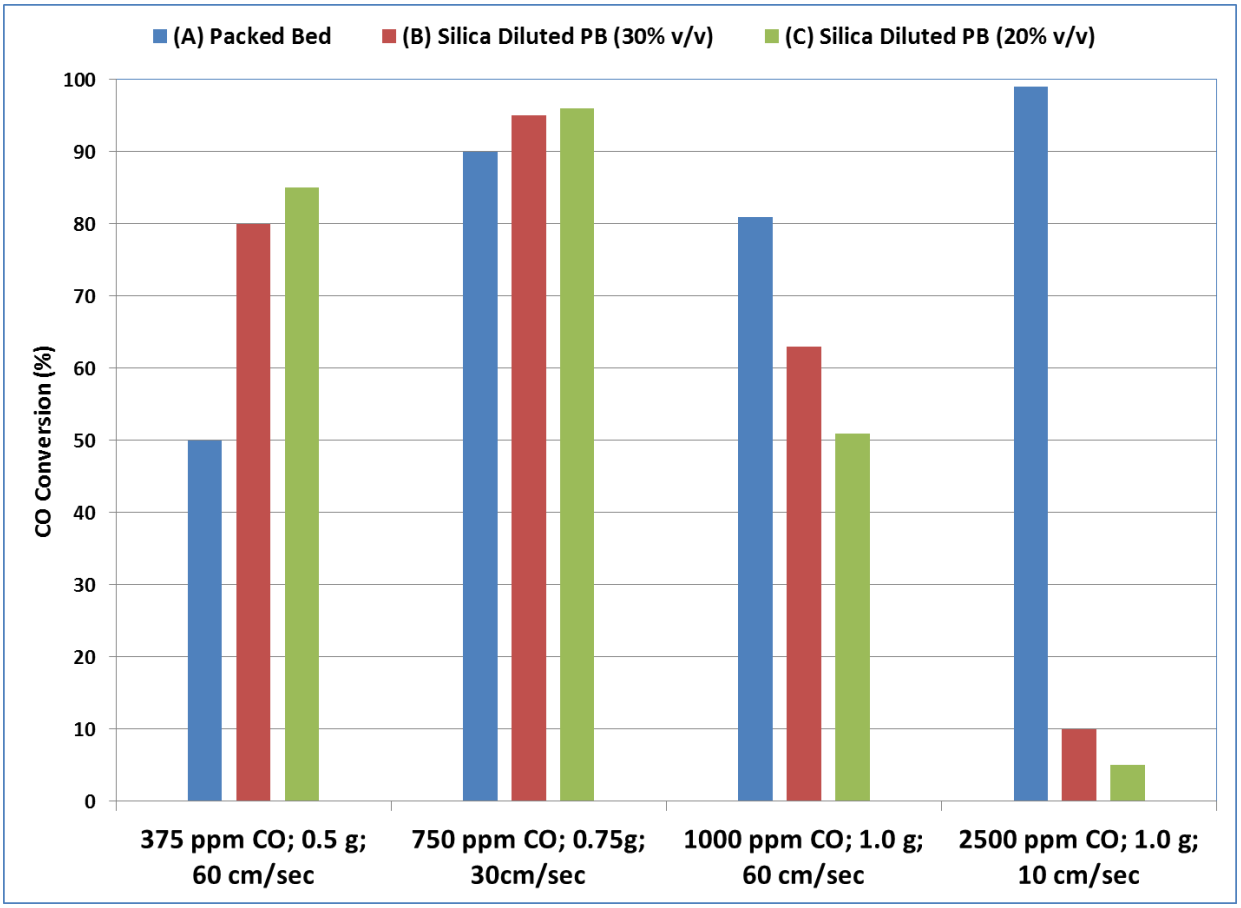

Figure VIII.5. Packed Bed Dilution Study: 25^{0}C & 50% RH, Particle Size: 200 µm; Reactor ID: 0.75"

CO oxidation reaction on Pt-CeO_2/SiO_2 catalyst followed Langmuir-Hinsherlwood (LH) type dual site mechanism and was therefore first order w.r.t CO concentrations at lower CO concentrations (<500 ppm) Therefore, axial dispersion would certainly diminish the catalytic activity at lower CO concentrations. At higher CO concentrations (≥1000 ppm), due to the CO self-poisoning effect inherent of the LH mechanism, increased axial dispersion would be beneficial to the activity; therefore, catalyst dilution which minimizes axial dispersion would have a negative impact on the activity. Results from Figure VIII.5 indicate the expected trend of increased activity with dilution at lower CO concentrations and decreased activity with dilution at higher CO concentrations.

Comparing the results from Figure VIII.4 and Figure VIII.5, it could be seen that MFECs with 30% catalyst loading (v/v) (hence reduced axial dispersion) outperformed PB at low as well as high CO concentration. MFECs could have benefited from reduced axial dispersion at low CO; however, the greater activity of MFECs at high CO could not be explained by reduced axial dispersion.

VIII.3.3 Effect of Thermal Properties on the Reactor Performance

The impact of thermal properties on the activity was studied by comparing performance of catalyst beds diluted with silica, Cu and Ni powder. PB and these diluted PBs (catalyst (30% v/v); void (40% v/v); diluents (30% v/v): silica, Cu powder, Ni powder) were tested for CO oxidation and the results are given in Figure VIII.6. Effective k for these diluted PBs were estimated by the equation for composite PBs (equation 8) given by Kulkarni et al [160]. The estimated effective k and thermal diffusivity (λ) values for these diluted PBs are given in Table VIII.2.

Table VIII.2. Estimated Effective K and Thermal Diffusivities of Different Bed Configurations

Composition	Keff (W/m.K)	ρ (Kg/m^3)	Cp (J/Kg.K)	λ (cm^2/s)	Ratio of Cp w/PB
Catalyst Powder	0.08	875	703	0.13	1.00
Cat + SiO_2 Powder	0.08	690	703	0.16	1.55
Cat + Ni Powder	1.20	3110	481	0.80	4.86
Cat + Cu Powder	1.70	3120	429	1.27	4.35
Ni MFEC	3.77	656	617	9.31	1.32

Addition of Cu/Ni powder improved effective k by a factor of 21/15 and increased λ of the reactor by a factor of 9/7. However, the addition of silica, Cu or Ni powder certainly increased the total heat capacity of the reactor by a factor of 1.6, 4.4 and 4.9 respectively.

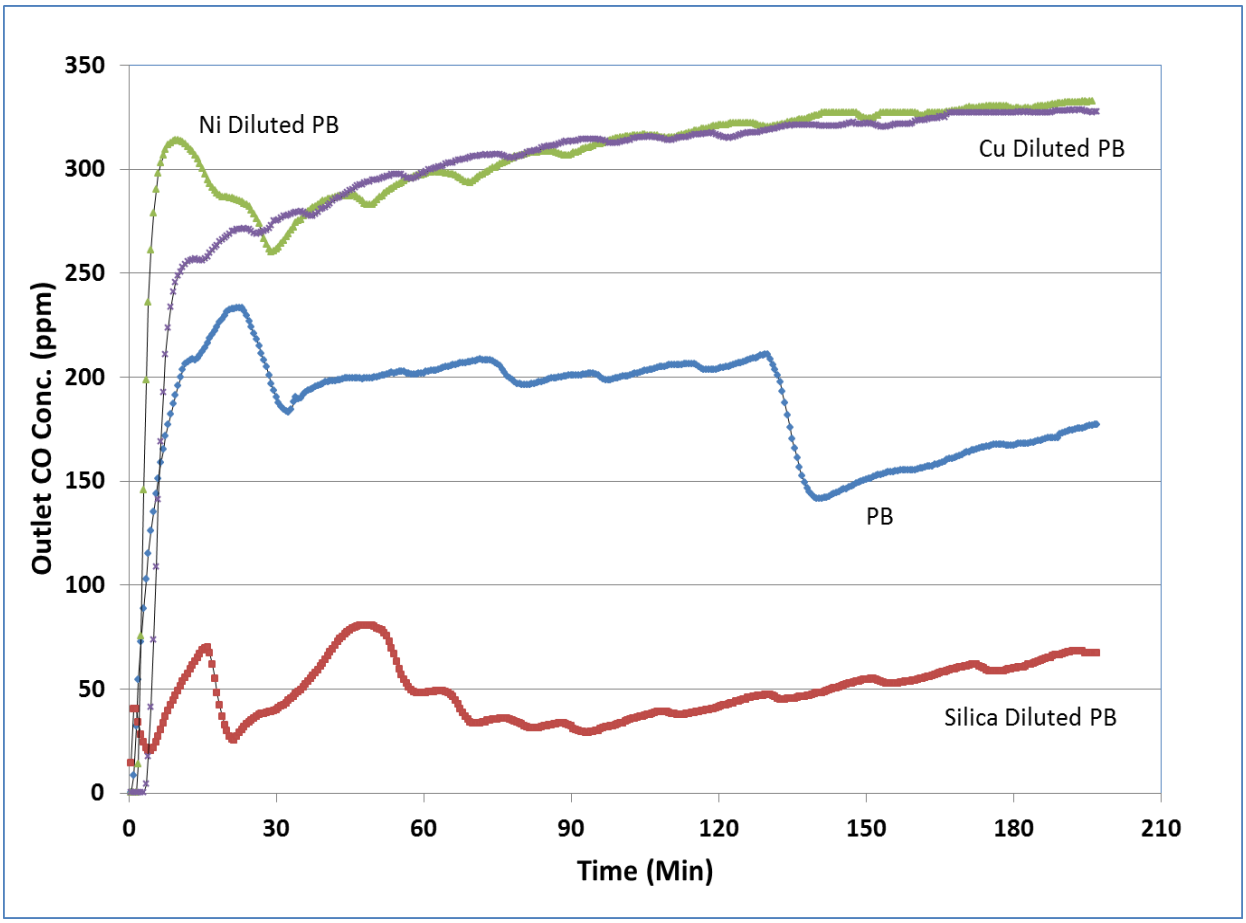

Figure VIII.6. Diluents Effect on Activity - 25°C; 50% RH; Dp: 200µm; Reactor ID: 0.75"; CO: 375 ppm

At low CO (≤ 750 ppm), catalyst dilution with silica improved activity as expected due to reduced axial dispersion. Cu/Ni powder diluted PBs performed poorly in comparison with PB or silica diluted PBs. The diluents certainly affected both heat and mass transfer even at low CO concentration (375 ppm CO; maximum $\Delta T_{AD} = 3.75^{0}C$). At high CO (≥ 1000 ppm), all of the diluted PBs performed poorly compared to PBs and this significant activity decline could only be described by the thermal effects in the bed. The

heat transfer within the bed has two aspects: heat capacity and thermal diffusivity. The thermal diffusivities of the diluted PBs (Cu/Ni) were greater than PBs. Therefore, the excess thermal mass in the case of metallic powders (Cu/Ni) must have significantly reduced the reactor activity.

Catalytic CO oxidation at low temperature is a delicate balance between CO self-poisoning and improved kinetics due to heat of reaction. The CO self-poisoning is reversible and elevated temperatures in the reactor decrease the extent of CO self-poisoning of the catalyst. Therefore, the heat transfer within the reactor was crucial to the activity. Improved thermal diffusivity would increase the reactor temperature faster, thereby improve kinetics and lower CO poisoning which would ignite the entire catalyst bed faster resulting in improved activity. In contrast, excess thermal mass would diminish the overall temperature rise in the bed, minimize local temperature gradients within the bed thereby decreasing the activity.

The impact of excess thermal mass would be profound during the transient state of operation, such as the start of reaction or the rapid progression of activity front within the reactor. If the temperature rise in the bed is slower, then CO self-poisoning would take over making the entire bed inactive. CO poisoning of the catalyst at ambient temperature takes place by formation of CO islands on active Pt sites and breaking of these CO islands to fully regain activity requires elevated temperatures.

In the case of Cu or Ni powder diluted PBs, CO poisoning was evident as seen from the performance of these diluted PBs over a wide range of CO concentrations. Similarly in the case of silica diluted PBs, at high CO (2500 ppm), the increased heat capacity served as an obstruction to the heat transfer resulting in lower activity.

MFECs on the other hand performed better than the PB over a wide range of CO concentration, as seen from Figure VIII.4. The effective “k” for MFEC was estimated by the method developed by *Sheng et.*

al. [161] and is given in Table VIII.2. MFEC had improved "k" and improved λ (factor of 72, compared to PB). MFECs although increased the overall heat capacity, due to addition of Ni fibers, the excess thermal mass was lower (MFEC m*Cp: PB m*Cp = 1.3). During transient CO oxidation reaction, the temperature rise within MFEC would be faster (due to lower heat capacity) and the rate of heat transfer would be significantly higher (due to higher thermal diffusivity). The superior heat transport properties of the MFEC could explain the better performance results of the MFEC seen in Figure VIII.4.

The results in Figure VIII.6 also support the basis for the exclusion of washcoated monoliths and ceramic foams as potential candidates for this application. Addition of inert thermal mass in monoliths or foams would diminish ΔT in the reactor and would result in lower overall activity.

VIII.3.4 Reactor Modeling Results

Reactor model was solved by COMSOL® Multiphysics. It is difficult to study the impact of heat and mass transfer parameters independent of each other in an experimental set up. For example, change in thermal diffusivity would affect the heat capacity as well. During this study, the reactor model with CO poisoning was used to study the effects of heat capacity, axial mass dispersion and thermal diffusivity on the activity independent of each other.

VIII.3.4.1 Effect of Axial Mass Dispersion

The reactor model was used to analyze the effect of axial mass dispersion on the reactor performance at low (250 ppm) and high (2500 ppm) CO concentrations. The results are given in Figure VIII.7. Reduced axial dispersion improved activity at low CO concentrations (CO conversion: 75% (Dax/50) and 74.6% (Dax*50)); however, the activity improvement was not significant. At high CO concentration, activity improved with increased dispersion, yet the activity improvement was insignificant.

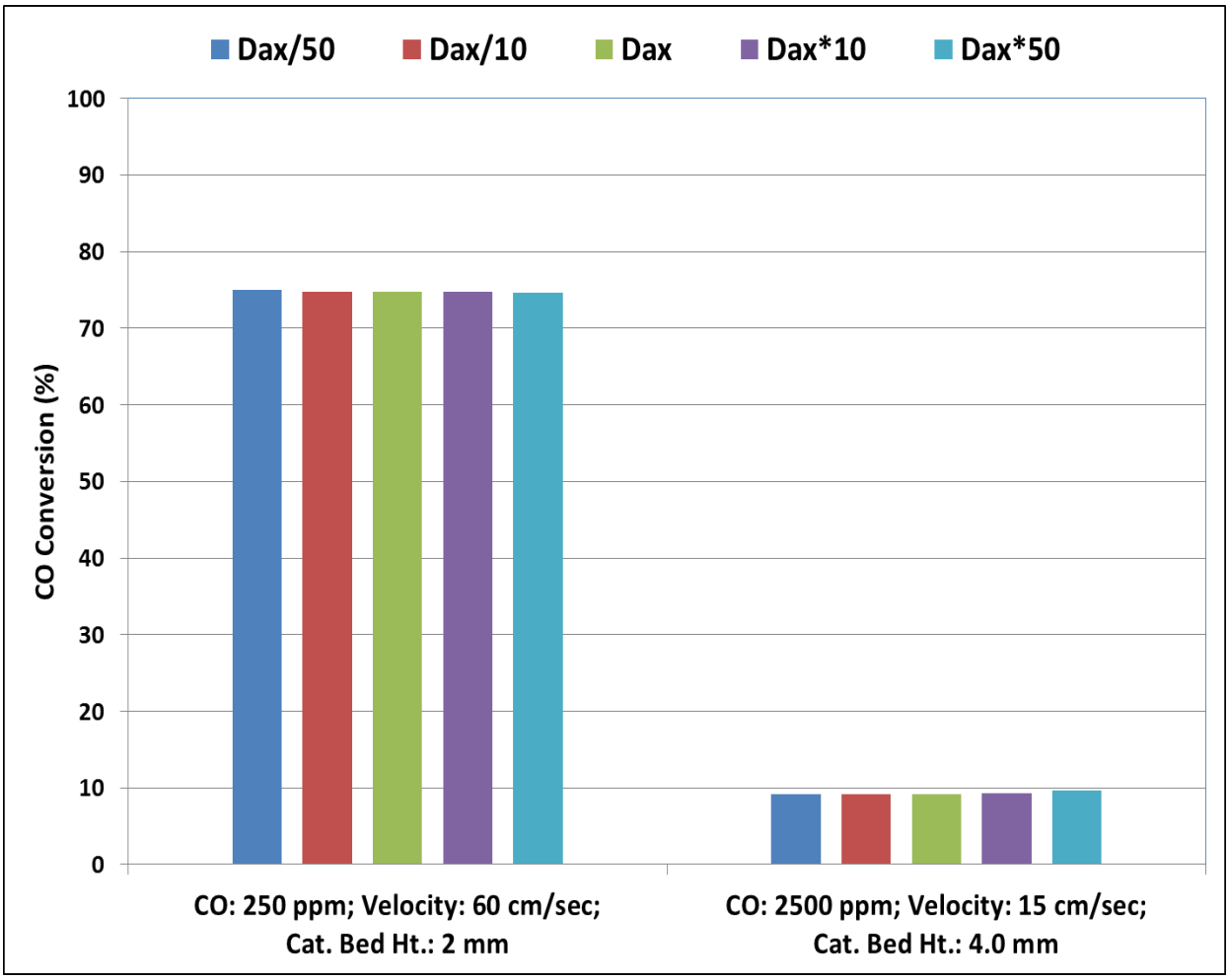

Figure VIII.7. Axial Mass Dispersion Effect on Reactor Activity at 25^{0}C: Simulation Results

The simulation results showed that the axial mass dispersion change hardly improved any activity, Figure VIII.7. From Figure VIII.5, silica diluted PB performed better than PB at CO < 750ppm, even with greater overall heat capacity. So, the catalyst dilution must have reduced cluster formation and thereby reducing bed channeling, flow maldistributions and local by-pass of the catalyst.

VIII.3.4.2 Effect of Thermal Diffusivity (λ) on Reactor Performance

The impact of λ on the reactor performance was investigated using the reactor model and the results for low (250 ppm) as well as high CO (2500 ppm) concentration are given in Figure VIII.8. At low

CO concentration, increased λ slightly improved the reactor performance. For example, increasing the λ by 100 times improved CO conversion from 74% to 77%. At higher CO concentrations (2500 ppm), the λ had a significant impact on the reactor performance. Increasing λ by 25 times improved the CO conversion from 19.2% (λ) to 99.9% (25*λ).

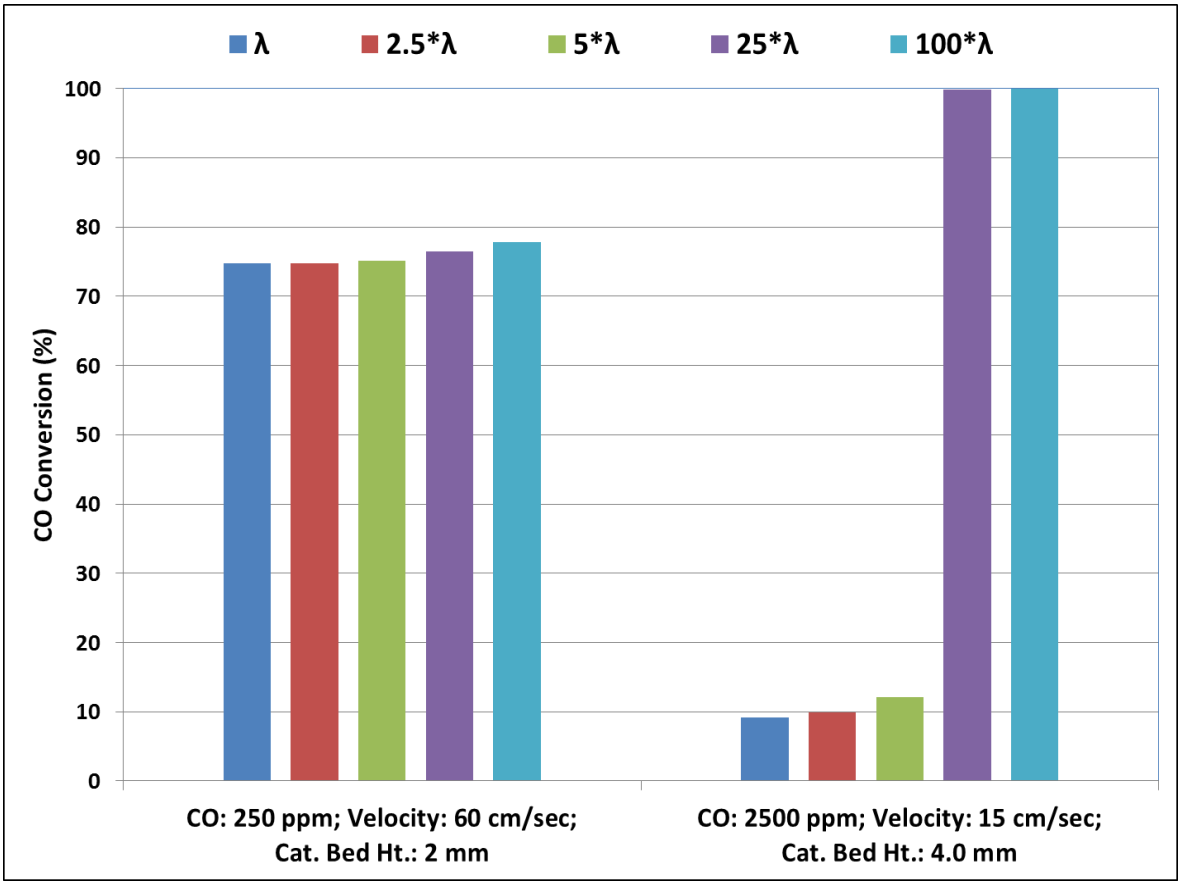

Figure VIII.8. Thermal Diffusivity Effect on Reactor Activity at 25^{0}C: Simulation Results

In the case of Ni MFECs, the thermal conductivity (λ) was greater by a factor of 70 compared to PB, which would explain the performance improvement shown by MFEC at high CO concentrations.

VIII.3.4.3 Effect of Thermal Mass on Reactor Performance

The impact of thermal mass on the activity was simulated with the reactor model and the results for low (250 ppm) and high CO (2500 ppm) are given in Figure VIII.9.

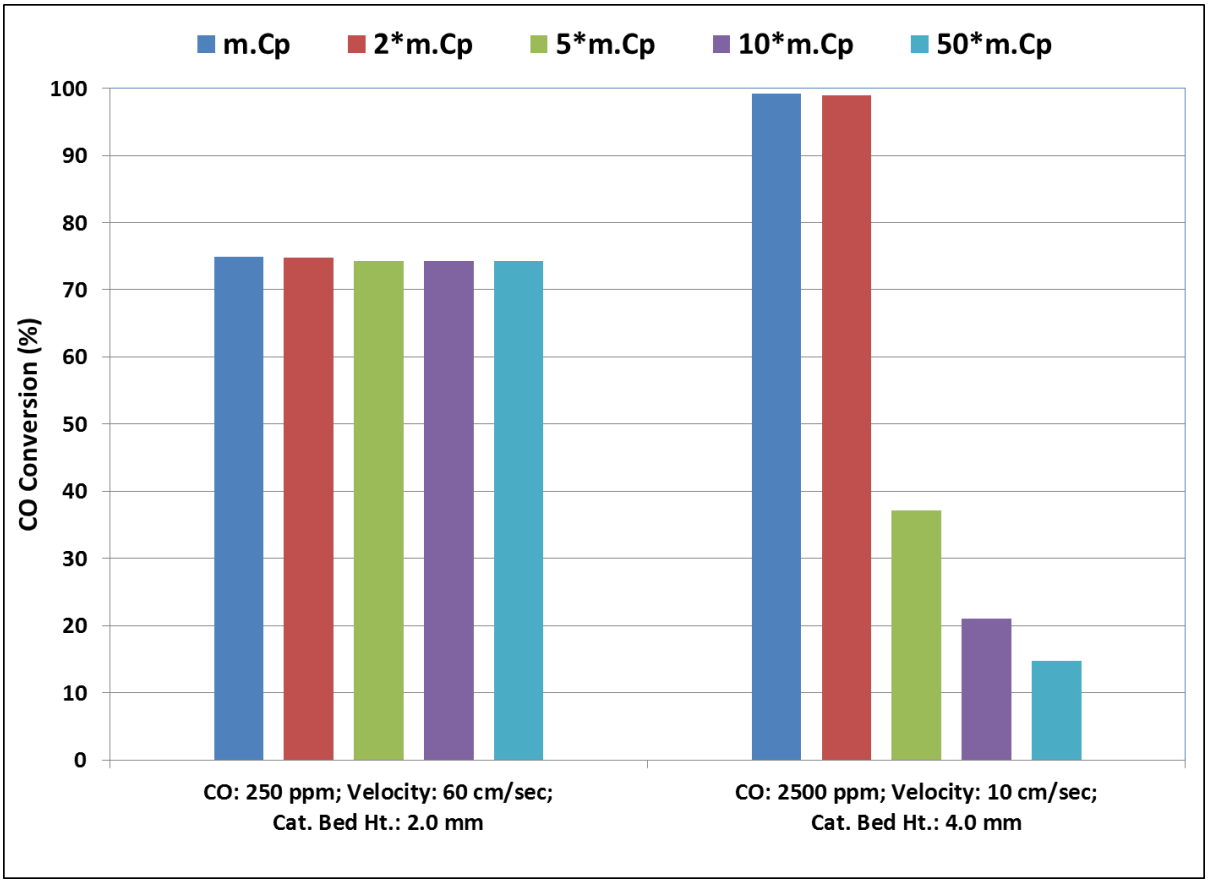

Figure VIII.9. Effect of Reactor Heat Capacity on Overall Activity at 25^{0}C: Simulation Results

At low CO (250 ppm), increased thermal mass (mCp) slightly lowered the activity (CO conv.: 74.9% (mCp); 74.2% (50*mCp)). At higher CO concentration (2500 ppm), the thermal mass had a significant impact on the reactor performance. Increasing the mCp by 5 times lowered the CO conversion from 99% (mCp) to 37% (5*mCp). Thermal mass had major impact on activity. The increased thermal mass lowered the temperature rise in the reactor resulting in greater CO self-poisoning of the catalyst and lower activity. Experimentally, similar results were observed for Cu or Ni diluted PBs.

Different bed architectures were also simulated using the reactor model and the comparison of simulation results with experimental results is given in Figure VIII.10.

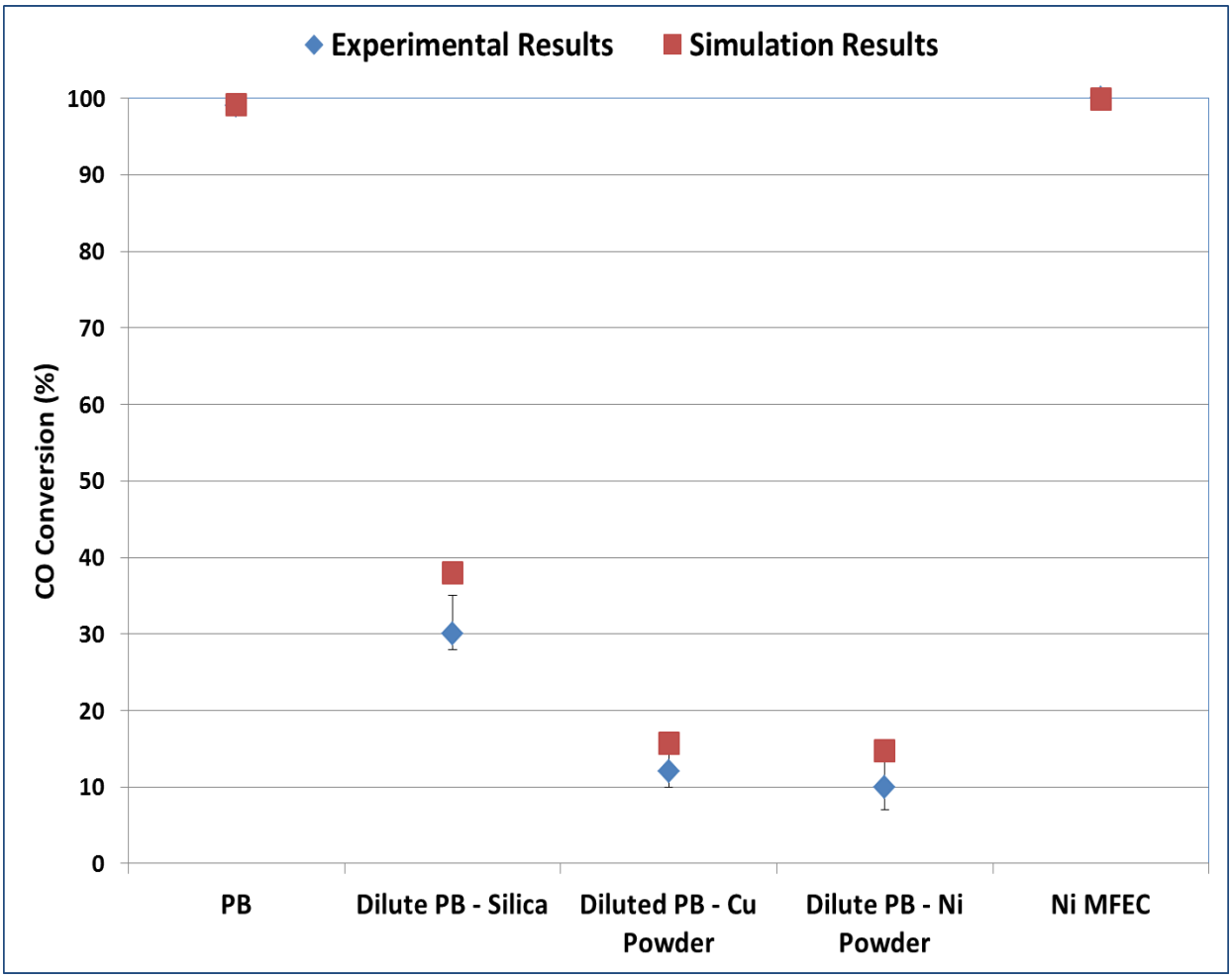

Figure VIII.10. Impact of Catalytic Bed Architecture on Activity –Simulation vs. Experimental Results

Test Conditions: CO: 2500ppm; Velocity: 10 cm/sec; 25°C; 90% RH; Particle Size: 200µm; Reactor ID: 0.75"; Catalyst Wt.: 1.0 g

The reactor model reasonably predicted the experimental results. The negative effect of excess heat capacity in the case of copper and nickel powder diluted beds outweighed the benefits of improved thermal diffusivity.

VIII.3.5 Improved Activity and Stability of MFECs

The possibility of using lower amount of catalyst in the MFECs was explored. MFEC with lower catalyst loading was evaluated against PB and the results are given in Figure VIII.11.

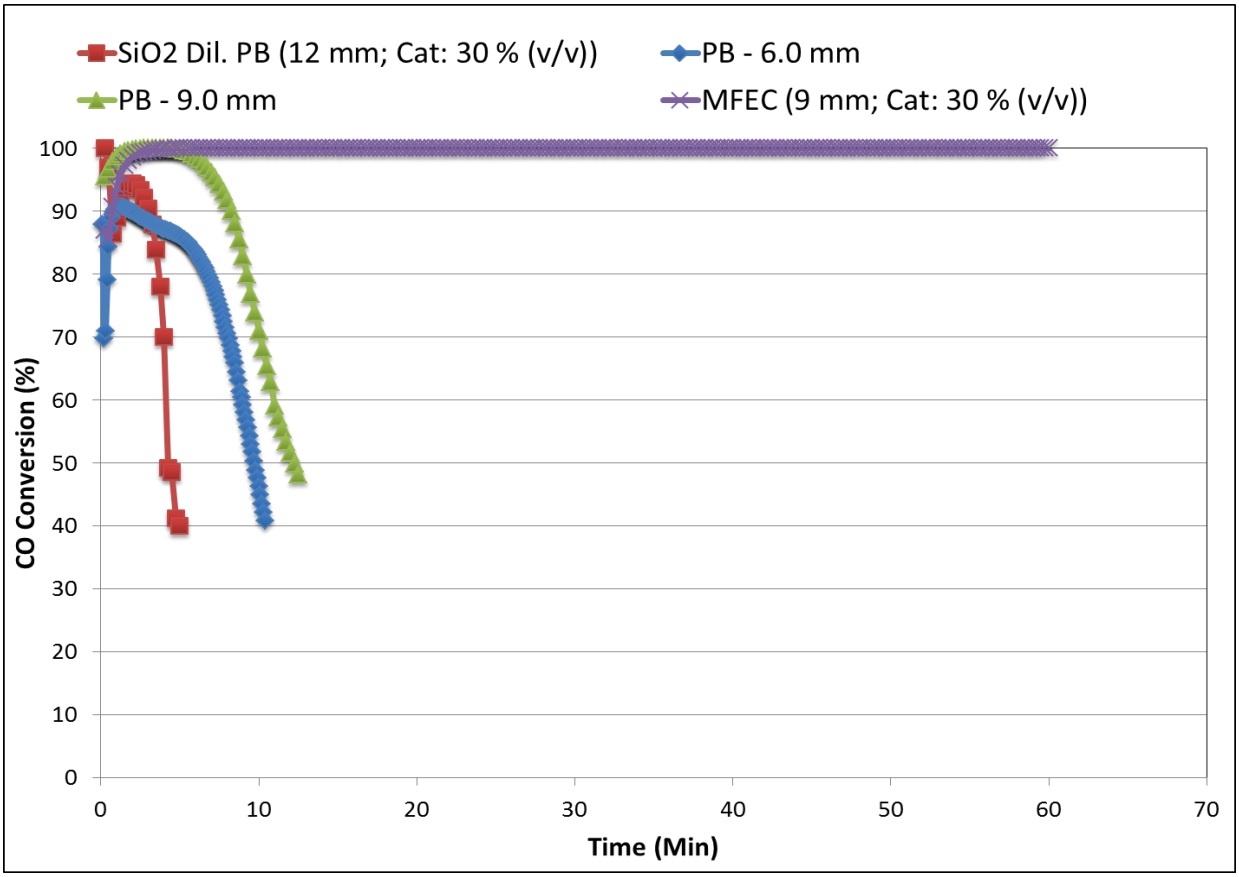

Figure VIII.11. Activity Improvement by MFECs

Test Conditions: CO: 2500ppm; Face Velocity: 15 cm/sec; 25°C; 90% RH; Particle Size: 200µm; Reactor ID: 0.75"; Catalyst: PB (6mm): 1.5g; PB (9mm): 2.25 g; Silica Dil. PB (12mm): 1.5g; MFEC (9mm): 1.125g

PB (6 mm) deactivated quickly and the diluted PB (silica diluents) deactivated faster than the PB itself. Although, a PB with higher loading (9 mm) was active, the PB was unstable and lost activity after 10 minutes. MFEC maintained higher activity (CO Conversion > 99%) for more than 300 minutes.

VIII.4 Conclusion

Experimental results showed catalyst bed dilution with silica significantly improved activity at low CO concentrations; whereas the simulation results predicted minimal improvement by dilution. So, the bed dilution must have reduced cluster formation thereby minimizing bed channeling, reducing flow maldistributions and reduce local bypass of the catalyst. Increased thermal diffusivity was predicted to improve performance and increased thermal mass was predicted to diminish activity. Experimental results showed that Cu/Ni powder diluted catalyst bed performed poorly in comparison with packed bed. Therefore, the excess thermal mass had more impact than increased thermal diffusivity on activity. Ni microfibers entrapped catalysts (MFECs – Pt-CeO_2/SiO_2) improved thermal diffusivity of the reactor by a factor of 70 (compared to packed bed) while adding minimal excess thermal mass. MFECs with their open and uniform structure minimized axial dispersion and reduced cluster formation.

MFECs were highly effective and stable CO oxidation catalysts over a wide range of CO concentrations at ambient conditions. These MFECs would be potential candidates for low temperature CO oxidation applications such as fire escape mask, cathode air filter, advanced filtration and the like.

IX Conclusions and Recommendations for Future Work

IX.1 Conclusions

Conclusions for various studies carried out during this work have been given at the end of each chapter. Overviews of all the achievements during this work are presented here. The notable achievements are:

1. A significant number of catalyst formulations including commercially available catalysts were tested for CO oxidation.

2. A couple of novel promoted Pt catalysts, Pt-SnO_2/SiO_2 and Pt-CeO_2/SiO_2 catalysts have been developed for low temperature CO oxidation in humid air.

3. These novel catalysts were developed and characterized for catalyst compositions as well as catalyst preparation variables.

4. A method of entrapment of Pt-CeO_2/SiO_2 catalyst in Ni microfibers has been developed and has been shown to significantly improve the catalytic activity.

5. The effect of catalyst testing conditions such as temperature, water vapor content, CO concentration and effect of reactor parameters such as face velocity, bed depth, axial and thermal dispersion on overall performance was investigated in detail.

6. Basic one-dimensional pseudo-homogeneous model was developed that described the reactor performance and enabled the confirmation of observed experimental results such as progression of reaction and mass and thermal dispersion

7. Finally a highly active entrapped catalytic media that could be used in CO oxidation at ambient temperature and humidity such as respiratory protection equipments, advanced filtration units, and the like has been successfully developed.

The comparison of Pt-CeO_2/SiO_2 catalyst with the commercially available catalysts revealed that the novel catalyst so developed showed significantly better performance at ambient conditions. Further, entrapment in metal microfibers improved the activity of the catalyst by reducing axial dispersion, minimizing bed channeling and flow maldistributions in the bed as well as by enhancing heat transfer within the reactor bed due to significantly greater thermal diffusivity.

IX.2 Recommendations for Future Work

IX.2.1 Optimization of Catalyst Recipe

A lot of work was done during this study to optimize the catalyst recipe. The catalyst composition of Pt-CeO_2/SiO_2 catalyst as well as the precursors used and their drying and calcination conditions were also optimized. Additionally, a lot of characterization data was also obtained to support the conclusions drawn from the optimization study. However, there are a few preparation variables that could be investigated further to achieve enhanced catalytic activity.

For example, during this study it was observed that the contact area between Pt and ceria was crucial to the activity of the catalyst and the use of a neutral precursor was beneficial. It would be interesting to see the effect of using a non-chlorinated acidic precursor for Pt deposition. Since under the conditions of impregnation the silica support would be negatively charged, the use of acidic

precursor would mostly result in greater deposition of Pt on ceria promoter, thereby increasing the activity of the catalyst. Additionally, the effect of preferentially masking the silica surface during Pt precursor impregnation so that Pt would get preferentially deposited on ceria surface could also be investigated.

Additionally, during the study of effect of calcination conditions on Pt precursor, it was found that the calcination in inert atmosphere (N_2) yielded highly active catalyst, almost three times active that of catalyst calcined in air. However, the activity was not reproducible; therefore, the Pt precursor was calcined in air during this study. It would be interesting to see the effect of Pt precursor calcination in inert atmosphere as well as attempts should be made to improve the reproducibility of activity. Further, hydrogen reduction of the air calcined catalyst was found to be beneficial for the catalytic activity. It would be interesting to see the effect of reduction-oxidation cycles on surface properties of the surface and ultimately on the catalytic activity.

IX.2.2 Optimization of Catalyst Loading

From the studies involving the change of bed depth showed that overall reactor performance was a function of catalyst loading. The proposed hypothesis for this observation was that initial few layers of the catalyst bed acted like CO adsorbent and later on the reaction started at back of catalyst bed and due to heat transfer within reactor, the entire bed was activated. This hypothesis was confirmed from reactor modeling and it was observed that rate of reaction at the end of catalytic bed was significantly higher due to decreased CO concentration and increased temperature, due to exothermicity of the reaction. Additionally, from the experiments involving separation of the catalyst layers by inert media layers also confirmed the hypothesis and showed that the heat effects within reactor made the entire bed active.

Keeping these observations in mind, a system could be designed that would enable optimization of catalyst loading at higher CO concentrations as well as at low CO concentrations and higher face velocities. A system has been proposed here, which could help optimize the catalyst loading and in other words, the cost of catalytic application system. A schematic of the proposed system is given in Figure IX.1.

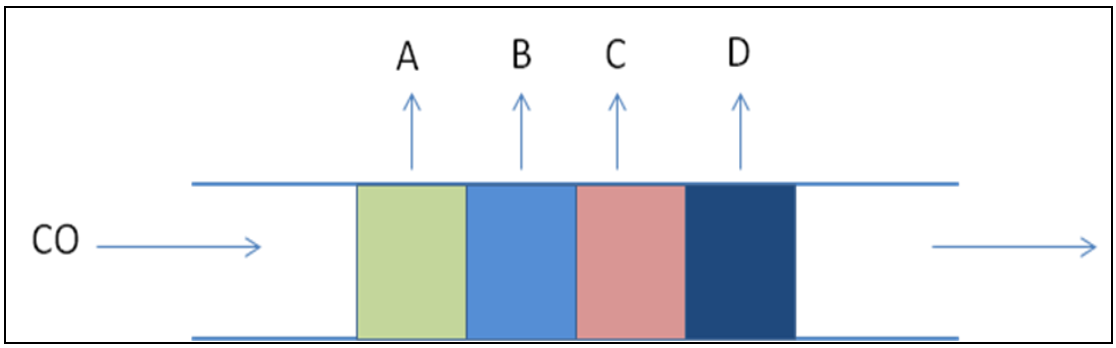

Figure IX.1. Proposed Catalyst Packing System

In the proposed system, as shown in Figure IX.1, the reactor could be packed in layered packed bed format with different catalysts/adsorbents denoted in Figure IX.1 by A, B, C, and D. Since it has been established that the initial layers of catalyst bed act as CO adsorbent; therefore, it would be interesting to see the effect of using CO adsorbent as an initial layer, layer 'A' in Figure IX.1, on catalytic activity. This study could also enable investigating the feasibility of minimizing the noble metal catalyst loading for an application under consideration. Further, the catalyst layers A, B, C and D shown in Figure IX.1, could be made out of the same catalysts differing only in Pt loading to optimize the use of noble metal. Further, the layers could be made out of different particle sizes to exploit the exothermicity of the CO oxidation reaction as well as enable optimization of the pressure drop offered by the catalyst bed.

Further, the comparison with commercial catalysts also revealed that the gold based catalysts were active in the absence of water vapor whereas the Pt based catalysts were highly active in the presence of moisture. Further, it was also observed that the effect of water vapor was almost

completely reversible in both types of catalysts. Using these experimental observations, a system (as shown in Figure IX.1) could be designed by making a layered bed out of gold and Pt based catalysts, so that the resulting packed bed would be highly active in both dry as well as humid conditions.

IX.2.3 Optimization of Microfibrous Entrapped Catalysts (MFECs)

From the experimental results, it was observed that the metal microfibers entrapped Pt-CeO_2/SiO_2 catalysts were highly active in comparison with the packed bed of powder catalyst. Further, the improved activity was attributed to the improved thermal diffusivity of the bed architecture as well as the reduced axial dispersion and minimized bed channeling in the MFECs. Additionally, it was seen from the reactor modeling results that the effect of improved thermal diffusivity of MFECs was significantly greater than reduced axial dispersion or reduced bed channeling.

In order to utilize the MFECs to their full potential it is important to find out the effective thermal conductivity of the MFECs and thus the thermal diffusivity of the MFECs. Further, addition of excess thermal mass to the reactor was found to have a negative impact on overall performance of the reactor. Therefore, a MFEC that would have minimum amount of fiber loading as well as significantly higher thermal diffusivity needs to be designed to improve the performance of MFECs. Min Sheng et al have experimentally measured values of effective thermal conductivities of MFECs [162]. However, a lot work is needed to develop a model to predict the effective thermal conductivity of MFECs made with varying fiber loading, fiber diameter as well as different voidage. The model development would require determining effective K of MFECs experimentally.

An attempt has been made here to estimate the effective thermal conductivity of MFECs. For this proposed model to predict effective K of MFECs, experimental data from Min Sheng et al (personal communication) [162] has been used.

The proposed model for prediction of effective K of MFECs is as follows:

a. Estimate the effective K for MFECs using Equation IX.1.

b. Estimate K_{St} from Equation IX.2 [160], however, the K_f or thermal conductivity of fluid in the case of the MFECs was estimated in the following manner.

c. Assume that the fluid phase & fibers together form the voidage (or the fluid phase in the packed bed terminology).

d. Calculate the "Kf" for this fluid phase (fibers + gas) using Equation IX.4 and Equation IX.5 [163], however, for this estimation the voidage should be taken as follows: for 2 vol % loading of fibers in MFECs, voidage = 0.98, and so on.

e. Using this Kf, estimate "δ" from the chart for δ vs. (Kf/Ks) given by Kulkarni et al [160]; β: obtained from voidage of the MFECs

f. Use the formula for the packed bed, Equation IX.2, to estimate the effective K_{st} for the MFEC

g. Using the experimentally obtained data, use Equation IX.3 to determine the value of α. For estimation of α, the value of Kf used was the one (Ke) that was estimated from Equation IX.4.

h. Using Kst from Equation IX.2 and Kd from Equation IX.3 calculate the effective K for MFEC by using Equation IX.1.

The equations used for the determination of effective K for MFECs are given below. The effective K of sintered metal fibers from Equation IX.4, was used as the fluid phase thermal conductivity of MFEC in Equation IX.2 as well as Equation IX.3.

Equation IX.1. Effective K for MFECs – Sum of Static and Dynamic Thermal Conductivity

$$K_{eff} = K_{St} + K_d$$

Where, K_{eff}= Effective thermal conductivity of the bed; K_{St}= Static conductivity of the bed; K_d= Dynamic contribution

Equation IX.2. Determination of Static Thermal Conductivity of MFECs

$$\frac{K_{St}}{K_f} = \varepsilon_b + (1 - \varepsilon_b) * \left(\frac{\beta}{\delta + \frac{2 * K_f}{3 * K_s}} \right)$$

Where, K_{St}= Static conductivity of the bed; ε_b = void fraction; β = distance between two particles; δ = stagnant fluid thickness; K_f= thermal conductivity of fluid; K_s= Thermal conductivity of solid.

Equation IX.3. Estimation of Dynamic Contribution to Effective K for MFECs

$$\frac{K_b^d}{K_f} = \alpha\beta(N_{Re}N_{Pr})^{0.7}$$

Where, N_{Re} = Reynold's Number; N_{Pr} = Prandtl Number; α = constant – dependent on the microfibrous material used; β = distance between two particles.

Equation IX.4. Estimation of Effective Thermal Conductivity of Sintered Metal Fibers

Ke/Ks = 1 + ε/((1-ε)/M) + Ks/(Kf-Ks))

Where, M is given by Equation IX.5.

Equation IX.5. Estimation of M from Fiber Properties and Voidage

$M = (1.2 – 29(d/l)) * (0.81 – \varepsilon)^2$

Where, ε = voidage; Ks: metal fiber conductivity; Kf: gas conductivity; d=fiber dia; l=fiber length; Ke: effective thermal conductivity of sintered metal fibers

Using this proposed formula, effective K for some of the MFECs were estimated and were compared with experimentally obtained values of effective K given by Min Sheng et al [162]. The estimated and the experimental values along with the estimated errors are given in Table IX.1.

Further, using the experimental data obtained by Min Sheng et al [162], the dynamic contribution of MFECs was also estimated and the average value of α for two different MFECs was estimated. Additionally, the overall effective thermal conductivity of MFECs were estimated by Equation IX.1 and the experimental values obtained by Min Sheng et al [162] were compared with the estimated values and errors were estimated. The estimated and the experimental values as well as the estimated errors are given in Table IX.1.

Table IX.1. Estimated and Experimental Values of Static Thermal Conductivity of MFECs

Configuration	**Materials**	**Keff (W/m.K)**		**% Error**
		Experimental	Estimated	
Packed Bed	Alumina	0.164	0.163	0.35%
SS MFEC	5.7% SS + 18.2% Alumina	1.09	1.12	-3.1%
Ni MFEC	4.9% Ni + 18.2% Alumina	3.77	3.45	8.5%
Cu MFEC	7.4% Cu + 29.4% Alumina	9.05	9.87	-9.0%

As can be seen from Table IX.1, the estimated values of static thermal conductivity were in close agreement with the experimentally measured values. Average error was estimated to be in the range of 5-10%. As can be seen from Table IX.2, the estimated and the experimental values of effective K for copper fibers entrapped alumina MFECs were in close agreement.

Table IX.2. **Estimated and Experimental Effective K for Cu Entrapped Alumina**

For Cu – Alumina MFEC; α = 3.23				
No.	**FV (m/s)**	**Estimated K_{eff}**	**Expt. K_{eff}**	**Error**
1	0.05	21.06	21.98	4.2%
2	0.10	28.57	27.99	-2.1%
3	0.18	38.50	39.45	2.4%
4	0.27	48.17	45.08	-6.8%

Further, the average error was estimated to be not more than 5%. The estimated value of α in the case of Cu entrapped alumina was estimated to be 3.23.

Table IX.3. Estimated and Experimental Effective K for Ni Entrapped Alumina

For Ni – Alumina MFEC; α = 5.67				
No.	**FV (m/s)**	**Estimated K_{eff}**	**Expt. K_{eff}**	**Error**
1	0.05	7.74	8.02	3.5%
2	0.10	10.23	9.29	-10.0%
3	0.18	13.51	12.63	-7.0%
4	0.27	16.71	18.89	11.5%

As can be seen from Table IX.3, the estimated and the experimental values of effective K for Ni entrapped alumina MFECs were in close agreement. Further, the average error was estimated to be not more than 5%. Further, the estimated value of α in the case of Ni entrapped alumina was estimated to be 5.67.

Considering the accuracy of these proposed formulae, additional experiments should be carried out to verify or modify the proposed model for the estimation of effective K for MFECs.

The main use of this model would be to estimate the thermal diffusivity of MFECs and then judiciously select the metal fiber diameter as well as metal fiber loading for MFECs to optimize the cost as well as performance. Since the micron sized metal fibers are expensive, the optimization of metal fiber loading is crucial from cost point of view.

IX.2.4 Catalyst Application System Design

The MFECs were found to be significantly active for CO oxidation at low temperature in humid conditions. There are a lot many applications for CO removal at ambient conditions. Here a few of the applications and the approach for designing a catalytic media for these applications is mentioned. It would serve as a guideline for someone who would like to design CO filter media for these applications.

1. MFECs for Fire Escape mask

This research work would involve designing a MFEC filter which can be integrated in an emergency escape mask. The work would require studying following: (a) Tests under EN 403 conditions; Tests under ANSI standards; (b) Pleating effect; (c) Effect of catalyst volume % loading in MFEC; (d) Pressure drop studies on MFEC, MFEC thickness; (e) Optimize Pt loading; (f) Full size filter tests.

Pleating should reduce pressure drop and the decrease in face velocity should help in optimizing MFEC thickness. Pt loading is also crucial from cost point of view.

2. MFECs for Advanced Filtration Units

This research work would involve designing a filter which can be used for low concentration CO removal applications at higher face velocities. During this work, following tasks should be carried out: (a) Selection of suitable particle size; (b) Pressure drop through MFEC and MFEC thickness optimization; (c) Pleating effect; (d) Optimization of Pt loading; (e) Full size filter tests.

During this study, it could also be established if such a filter can be used in HVAC filtration systems. Additionally, applicability of such a filter for removal of small amounts of CO from a stream containing mainly air and CO_2 should be verified.

References

[1] P.G. Flachsbart, Chemosphere - Global Change Science 1 (1999) 301-329.

[2] A. Ernst, J.D. Zibrak, The New England Journal of Medicine 339 (1998) 1603-1608.

[3] J. Rucker, J.A. Fisher, K.A. Richard, Md, S.S. Arthur, Md, V.M. Ranieri, Md, T. Jukka, Md, T. Antoni, Md, Clinical Critical Care Medicine (First Edition), Mosby, Philadelphia, 2006, pp. 679-683.

[4] O. Badr, S.D. Probert, Applied Energy 50 (1995) 339-372.

[5] M.V. Twigg, Catalysis Today 117 (2006) 407-418.

[6] A.B. Lamb, W.C. Bray, J.C. Frazer, Industrial Engineering Chemistry 12 (1920) 213-221.

[7] A.B. Lamb, W.E. Vail, Journal of the American Chemical Society 47 (1925) 123-142.

[8] S. Veprek, D.L. Cocke, S. Kehl, H.R. Oswald, Journal of Catalysis 100 (1986) 250-263.

[9] Y.F.Y. Yao, The oxidation of hydrocarbons and CO over metal oxides. III. Co 3 O 4, 1974, pp. 108–122.

[10] J. Jansson, A.E.C. Palmqvist, E. Fridell, M. Skoglundh, L. Oesterlund, P. Thormaehlen, V. Langer, Journal of Catalysis 211 (2002) 387-397.

[11] J. Jansson, M. Skoglundh, E. Fridell, P. Thormahlen, Topics in Catalysis 16/17 (2001) 385-389.

[12] M. Haruta, N. Yamada, T. Kobayashi, S. Iijima, Journal of Catalysis 115 (1989) 301-309.

[13] M. Haruta, Catalysis Today 36 (1997) 153-166.

[14] G.R. Bamwenda, S. Tsubota, T. Nakamura, M. Haruta, Catalysis Letters 44 (1997) 83-87.

[15] S.-J. Lee, A. Gavriilidis, Journal of Catalysis 206 (2002) 305-313.

[16] R.C. Shishu, L.S. Kowalczyk, Platinum Metals Review 18 (1974) 58-64.

[17] H.-I. Lee, J.M. White, Journal of Catalysis 63 (1980) 261-264.

[18] D.W. Goodman, C.H.F. Pedent, Journal of Physical Chemistry 90 (1986) 4839-4843.

[19] N.W. Cant, P.C. Hicks, B.S. Lennon, Journal of Catalysis 54 (1978) 372-383.

[20] E.C. Akubuiro, X.E. Verykios, L. Lesnick, Applied Catalysis 14 (1985) 215-227.

[21] A. Boulahouache, G. Kons, H.G. Lintz, P. Schulz, Applied Catalysis, A: General 91 (1992) 115-123.

[22] C. Hardacre, R.M. Ormerod, R.M. Lambert, The Journal of Physical Chemistry 98 (1994) 10901-10905.

[23] P. Thormählen, M. Skoglundh, E. Fridell, B. Andersson, Journal of Catalysis 188 (1999) 300-310.

[24] Y.J. Mergler, A. van Aalst, J. van Delft, B.E. Nieuwenhuys, Applied Catalysis, B: Environmental 10 (1996) 245-261.

[25] X. Liu, O. Korotkikh, R. Farrauto, Applied Catalysis, A: General 226 (2002) 293-303.

[26] P.G. Harrison, C. Bailey, W. Azelee, Journal of Catalysis 186 (1999) 147-159.

[27] K. Sekizawa, H. Widjaja, S. Maeda, Y. Ozawa, K. Eguchi, Applied Catalysis A: General 200 (2000) 211-217.

[28] K. Eguchi, H. Arai, Applied Catalysis A: General 222 (2001) 359-367.

[29] L.S. Sun, S.Y. Li, B.L. Li, Reaction Kinetics and Catalysis Letters 62 (1997) 151-156.

[30] K. Grass, H.G. Lintz, Journal of Catalysis 172 (1997) 446-452.

[31] A.N. AkIn, G. Kilaz, A.I. Isli, Z.I. Önsan, Chemical Engineering Science 56 (2001) 881-888.

[32] X.-D. Hou, Y.-Z. Wang, Y.-X. Zhao, Catalysis Letters 123 (2008) 321-326.

[33] R. Lin, M.-F. Luo, Y.-J. Zhong, Z.-L. Yan, G.-Y. Liu, W.-P. Liu, Applied Catalysis, A: General 255 (2003) 331-336.

[34] S.-P. Wang, X.-Y. Wang, X.-C. Zheng, S.-R. Wang, S.-M. Zhang, W.-P. Huang, S.-H. Wu, Reaction Kinetics and Catalysis Letters 89 (2006) 37-44.

[35] M.-F. Luo, J.-M. Ma, J.-Q. Lu, Y.-P. Song, Y.-J. Wang, Journal of Catalysis 246 (2007) 52-59.

[36] A.I. Boronin, E.M. Slavinskaya, I.G. Danilova, R.V. Gulyaev, Y.I. Amosov, P.A. Kuznetsov, I.A. Polukhina, S.V. Koscheev, V.I. Zaikovskii, A.S. Noskov, Catalysis Today 144 (2009) 201-211.

[37] X.-Y. Wang, S.-P. Wang, S.-R. Wang, Y.-Q. Zhao, J. Huang, S.-M. Zhang, W.-P. Huang, S.-H. Wu, Catalysis Letters 112 (2006) 115-119.

[38] A. Holmgren, B. Andersson, D. Duprez, Applied Catalysis, B: Environmental 22 (1999) 215-230.

[39] X.-S. Huang, H. Sun, L.-C. Wang, Y.-M. Liu, K.-N. Fan, Y. Cao, Applied Catalysis B: Environmental 90 (2009) 224-232.

[40] T. Bunluesin, E.S. Putna, R.J. Gorte, Catalysis Letters 41 (1996) 1-5.

[41] A. Trovarelli, M. Boaro, E. Rocchini, C. de Leitenburg, G. Dolcetti, Journal of Alloys and Compounds 323-324 (2001) 584-591.

[42] D.R. Modeshia, C.S. Wright, J.L. Payne, G. Sankar, S.G. Fiddy, R.I. Walton, The Journal of Physical Chemistry C 111 (2007) 14035-14039.

[43] M.F.R. B.J. Tatarchuk, A. Krishnagopalan, J.N. Zabasajja, D. Kohler, US Patent 5080963, Auburn University, USA, 1992.

[44] D.R. Cahela, B.J. Tatarchuk, Catalysis Today 69 (2001) 33-39.

[45] B.-K. Chang, Y. Lu, B.J. Tatarchuk, Chemical Engineering Journal 115 (2006) 195-202.

[46] R.R. Kalluri, D.R. Cahela, B.J. Tatarchuk, Separation and Purification Technology 62 (2008) 304-316.

[47] B.M. Reddy, A. Khan, Y. Yamada, T. Kobayashi, S. Loridant, J.-C. Volta, Journal of Physical Chemistry B 106 (2002) 10964-10972.

[48] A. Bensalem, F. Bozon-Verduraz, M. Delamar, G. Bugli, Applied Catalysis, A: General 121 (1995) 81-93.

[49] B.M.W. Trapnell, Chemisorption, Academic Press, New York, 1955.

[50] O. Beeck, V.I.K.a.E.K.R. W.G. Frankenburg, Advances in Catalysis, Academic Press, 1950, pp. 151-195.

[51] I.E. Wachs, Characterization of catalytic materials, Butterworth-Heinemann, 1992.

[52] S. Salasc, V. Perrichon, M. Primet, M. Chevrier, N. Mouaddib-Moral, Journal of Catalysis 189 (2000) 401-409.

[53] S. Salasc, V. Perrichon, M. Primet, M. Chevrier, F. Mathis, N. Moral, Catalysis Today 50 (1999) 227-235.

[54] E. Rocchini, M. Vicario, J. Llorca, C. de Leitenburg, G. Dolcetti, A. Trovarelli, Journal of Catalysis 211 (2002) 407-421.

[55] P.W. Park, J.S. Ledford, Applied Catalysis, B: Environmental 15 (1998) 221-231.

[56] J. Huang, S. Wang, Y. Zhao, X. Wang, S. Wang, S. Wu, S. Zhang, W. Huang, Catalysis Communications 7 (2006) 1029-1034.

[57] Y. Teng, H. Sakurai, A. Ueda, T. Kobayashi, International Journal of Hydrogen Energy 24 (1999) 355-358.

[58] A. Tschope, W. Liu, M. Flytzanistephanopoulos, J.Y. Ying, Journal of Catalysis 157 (1995) 42-50.

[59] X.-C. Zheng, S.-H. Wu, S.-P. Wang, S.-R. Wang, S.-M. Zhang, W.-P. Huang, Applied Catalysis A: General 283 (2005) 217-223.

[60] Z. Qu, M. Cheng, C. Shi, X. Bao, Journal of Molecular Catalysis A: Chemical 239 (2005) 22-31.

[61] L. Kundakovic, M. Flytzani-Stephanopoulos, Journal of Catalysis 179 (1998) 203-221.

[62] Y.-Z. Wang, Y.-X. Zhao, C.-G. Gao, D.-S. Liu, Catalysis Letters 125 (2008) 134-138.

[63] M. Wojciechowska, M. Zielinski, A. Malczewska, W. Przystajko, M. Pietrowski, Applied Catalysis A: General 298 (2006) 225-231.

[64] J. Shao, P. Zhang, X. Tang, B. Zhang, W. Song, Y. Xu, W. Shen, Chinese Journal of Catalysis 28 (2007) 163-169.

[65] M. Kang, M. Song, K. Kim, Reaction Kinetics and Catalysis Letters 79 (2003) 3-10.

[66] J.-Y. Luo, M. Meng, X. Li, X.-G. Li, Y.-Q. Zha, T.-D. Hu, Y.-N. Xie, J. Zhang, Journal of Catalysis 254 (2008) 310-324.

[67] P.T. Fanson, W.N. Delgass, J. Lauterbach, Journal of Catalysis 204 (2001) 35-52.

[68] Y.J. Mergler, A. van Aalst, J. van Delft, B.E. Nieuwenhuys, Applied Catalysis B: Environmental 10 (1996) 245-261.

[69] B. Grbic, N. Radic, B. Markovic, P. Stefanov, D. Stoychev, T. Marinova, Applied Catalysis B: Environmental 64 (2006) 51-56.

[70] J.L. Ayastuy, M.P. González-Marcos, J.R. González-Velasco, M.A. Gutiérrez-Ortiz, Applied Catalysis B: Environmental 70 (2007) 532-541.

[71] D. Schryer, B. Upchurch, B. Sidney, K. Brown, G. Hoflund, R. Herz, 130 (1991) 314-317.

[72] M.M.V.M. Souza, N.F.P. Ribeiro, M. Schmal, International Journal of Hydrogen Energy 32 (2007) 425-429.

[73] I.J. Dijs, J.W. Geus, L.W. Jenneskens, Journal of Physical Chemistry B 107 (2003) 13403-13413.

[74] J.G. Seo, M.H. Youn, I.K. Song, Journal of Power Sources 168 (2007) 251-257.

[75] O. Pozdnyakova-Tellinger, D. Teschner, J. Kroehnert, F.C. Jentoft, A. Knop-Gericke, R. Schloegl, A. Wootsch, Journal of Physical Chemistry C 111 (2007) 5426-5431.

[76] S.D. Gardner, G.B. Hoflund, D.R. Schryer, J. Schryer, B.T. Upchurch, E.J. Kielin, Langmuir 7 (2002) 2135-2139.

[77] B. Upchurch, US 4855274, in: USPTO (Ed.), NASA, USA, 1989.

[78] M. Kosmulski, Chemical properties of material surfaces, Mercel Dekker, New York, 2001.

[79] R.H. Perry, D.W. Green, J.O. Maloney, Perry's handbook of chemical engineering, Seventh ed., Mc Graw-Hill, New York, 1997.

[80] R.B. Bird, W.E. Stewart, E.N. Lightfoot, Transport Phenomena, Second ed., John Wiley & Sons, Inc., New York, 2002.

[81] M. Abid, G. Ehret, R. Touroude, Applied Catalysis A: General 217 (2001) 219-229.

[82] L. Hu, K.A. Boateng, J.M. Hill, Journal of Molecular Catalysis A: Chemical 259 (2006) 51-60.

[83] H. Iida, K. Kondo, A. Igarashi, Catalysis Communications 7 (2006) 240-244.

[84] T. Lopez, P. Bosch, M. Moran, R. Gomez, The Journal of Physical Chemistry 97 (1993) 1671-1677.

[85] D. Nazimek, W. Cwikla-Bundyra, Catalysis Today 90 (2004) 39-42.

[86] W. Zou, R.D. Gonzalez, T. Lopez, R. Gomez, Materials Letters 24 (1995) 35-39.

[87] M. Morbidelli, A. Gavriilidis, A. Varma, Catalyst design, Cambridge University Press, 2001.

[88] J.F. Le Page, Applied heterogeneous catalysis: design, manufacture, use of solid catalysts, Editions Technip, Paris, 1987.

[89] V.B. Fenelonov, A.V. Neimark, L.I. Kheifets, A.A. Samakhov, Analysis of Steps of Impregnation and Drying in Preparation of Supported Catalysts, Elsevier, New York, 1979, p. 233.

[90] A.V. Neimark, L.I. Kheifez, V.B. Fenelonov, Theory of preparation of supported catalysts, 1981, pp. 439–450.

[91] D. Berger, D.C.T. Pei, International Journal of Heat and Mass Transfer 16 (1973) 293-302.

[92] S.-Y. Lee, R. Aris, Catalysis Reviews 27 (1985) 207 - 340.

[93] Y.-S. Shyr, W.R. Ernst, Journal of Catalysis 63 (1980) 425-432.

[94] M. Komiyama, Catalysis Reviews 27 (1985) 341 - 372.

[95] N. Santhanam, T.A. Conforti, W. Spieker, J.R. Regalbuto, Catalysis Today 21 (1994) 141-156.

[96] A. Lekhal, B.J. Glasser, J.G. Khinast, Chemical Engineering Science 56 (2001) 4473-4487.

[97] M.A. Bollinger, M.A. Vannice, Applied Catalysis B: Environmental 8 (1996) 417-443.

[98] H. Muraki, S.-I. Matunaga, H. Shinjoh, M.S. Wainwright, D.L. Trimm, Journal of Chemical Technology & Biotechnology 52 (1991) 415-424.

[99] Y.W. Rhee, J.A. Guin, C.W. Curtis, Energy & Fuels 3 (1989) 391-397.

[100] X.M. Liao, W. Chu, Y. Li, F.D. Zhou, S.Z. Luo, Chinese Chemical Letters 20 (2009) 344-347.

[101] N. Mahata, V. Vishwanathan, Journal of Catalysis 196 (2000) 262-270.

[102] F. Pinna, Catalysis Today 41 (1998) 129-137.

[103] L.R. Raddi de Araujo, M. Schmal, Applied Catalysis A: General 203 (2000) 275-284.

[104] M. Zhang, Z. Jin, J. Zhang, Z. Zhang, H. Dang, Journal of Molecular Catalysis A: Chemical 225 (2005) 59-63.

[105] J.T. Miller, M. Schreier, A.J. Kropf, J.R. Regalbuto, Journal of Catalysis 225 (2004) 203-212.

[106] G. Larsen, L.M. Petkovic, Applied Catalysis A: General 148 (1996) 155-166.

[107] M.G. Falco, S.A. Canavese, N.S. Fígoli, Catalysis Communications 2 (2001) 207-211.

[108] R. Craciun, Solid State Ionics 110 (1998) 83-93.

[109] A. Aboukais, E.A. Zhilinskaya, J.-F. Lamonier, I.N. Filimonov, Colloids and Surfaces, A: Physicochemical and Engineering Aspects 260 (2005) 199-207.

[110] E. Rogemond, N. Essayem, R. Fréty, V. Perrichon, M. Primet, M. Chevrier, C. Gauthier, F. Mathis, Catalysis Today 29 (1996) 83-87.

[111] E. Rocchini, A. Trovarelli, J. Llorca, G.W. Graham, W.H. Weber, M. Maciejewski, A. Baiker, Journal of Catalysis 194 (2000) 461-478.

[112] A. Martinez-Arias, J.M. Coronado, R. Cataluna, J.C. Conesa, J. Soria, The Journal of Physical Chemistry B 102 (1998) 4357-4365.

[113] J. Soria, A. Martínez-Arias, J.M. Coronado, J.C. Conesa, Colloids and Surfaces A: Physicochemical and Engineering Aspects 115 (1996) 215-221.

[114] H.S. Fogler, Elements of chemical reaction engineering, Third ed., Prentice-Hall Englewood Cliffs, NJ, 1999.

[115] N. Wakao, T. Funazkri, Chemical Engineering Science 33 (1978) 1375-1384.

[116] D. Thoenes, H. Kramers, Chemical Engineering Science 8 (1958) 271-283.

[117] S. Cypes, A. Hagemeyer, Z. Hogan, A. Lesik, G. Streukens, A.F. Volpe, Jr., W.H. Weinberg, K. Yaccato, Combinatorial Chemistry & High Throughput Screening 10 (2007) 25-35.

[118] X.C. Zheng, S.H. Wu, S.P. Wang, S.R. Wang, S.M. Zhang, W.P. Huang, Applied Catalysis, A: General 283 (2005) 217-223.

[119] D.M. Haaland, F.L. Williams, Journal of Catalysis 76 (1982) 450-465.

[120] D. Schryer, B. Upchurch, B. Sidney, K. Brown, G. Hoflund, R. Herz, A proposed mechanism for Pt/SnO (x)-catalyzed CO oxidation, 1991, pp. 314-317.

[121] G. Ertl, P.R. Norton, J. Rüstig, Physical Review Letters 49 (1982) 177-180.

[122] L. Lous, AIChE Journal 23 (1977) 632-642.

[123] S. Wehner, F. Baumann, J. Küppers, Chemical Physics Letters 370 (2003) 126-131.

[124] A. Jaree, R.R. Hudgins, H.M. Budman, P.L. Silveston, V.Z. Yakhnin, M. Menzinger, Industrial & Engineering Chemistry Research 42 (2003) 1662-1673.

[125] C.C. Chen, E.E. Wolf, H.C. Chang, The Journal of Physical Chemistry 97 (2002) 1055-1064.

[126] J.T. Kummer, The Journal of Physical Chemistry 90 (1986) 4747-4752.

[127] B.T. Upchurch, I.M. Miller, D.R. Brown, P.P. Davis, D.R. Schryer, K.G. Brown, J.D. Van Norman, US Patent 4991181, NASA, USA, 1991.

[128] Brey; Larry A., Wood; Thomas E., Buccellato; Gina M., Jones; Marvin E., Chamberlain; Craig S. , S.A. R., US Patent 7989384, 3M Innovative Properties Company, USA, 2011.

[129] S. S. Punde, B.J. Tatarchuk, Low Temperature CO Oxidation Using Platinum-Ceria On Silica Catalyst, AIChE Annual Meeting, Nashville, TN, 2009.

[130] A.V. Neimark, L.I. Kheifets, V.B. Fenelonov, Industrial & Engineering Chemistry Product Research and Development 20 (1981) 439-450.

[131] R.E. Lagos, B.C. Sales, H. Suhl, Surface Science 82 (1979) 525-539.

[132] R. Imbihl, G. Ertl, Chemical Reviews 95 (1995) 697-733.

[133] L. Wen, J.-K. Fu, P.-Y. Gu, B.-X. Yao, Z.-H. Lin, J.-Z. Zhou, Applied Catalysis B: Environmental 79 (2008) 402-409.

[134] R. Liu, C. Zhang, J. Ma, Journal of Rare Earths 28 376-382.

[135] N.A. Hodge, C.J. Kiely, R. Whyman, M.R.H. Siddiqui, G.J. Hutchings, Q.A. Pankhurst, F.E. Wagner, R.R. Rajaram, S.E. Golunski, Catalysis Today 72 (2002) 133-144.

[136] X. Zhang, H. Wang, B.-Q. Xu, The Journal of Physical Chemistry B 109 (2005) 9678-9683.

[137] P. Buffat, J.P. Borel, Physical Review A 13 (1976) 2287.

[138] J.A. Moulijn, A.E. van Diepen, F. Kapteijn, Applied Catalysis A: General 212 (2001) 3-16.

[139] A.A. Iordanidis, Mathematical Modeling of Catalytic Fixed Bed Reactors, University of Twente, University of Twente, 2002.

[140] X. Ouyang, R.S. Besser, Journal of Power Sources 141 (2005) 39-46.

[141] D.J. Kaul, R. Sant, E.E. Wolf, Chemical Engineering Science 42 (1987) 1399-1411.

[142] R.H. Venderbosch, W. Prins, W.P.M. van Swaaij, Chemical Engineering Science 53 (1998) 3355-3366.

[143] H.H. Lee, Heterogeneous Reactor Design, Butterworth, London, 1985.

[144] K. Arnby, A. Törncrona, B. Andersson, M. Skoglundh, Journal of Catalysis 221 (2004) 252-261.

[145] C. Lu, I.C. Lee, R.I. Masel, A. Wieckowski, C. Rice, The Journal of Physical Chemistry A 106 (2002) 3084-3091.

[146] R.K. Duggirala, C.J. Roy, S.M. Saeidi, J.M. Khodadadi, D.R. Cahela, B.J. Tatarchuk, Journal of Fluids Engineering 130 (2008) 071302-071313.

[147] S.F. Miller, C.J. King, AIChE Journal 12 (1966) 767-773.

[148] J.J. Carberry, R.H. Bretton, AIChE Journal 4 (1958) 367-375.

[149] C.G. Visconti, E. Tronconi, G. Groppi, L. Lietti, M. Iovane, S. Rossini, R. Zennaro, Chemical Engineering Journal 171 1294-1307.

[150] M.V. Twigg, J.T. Richardson, Chemical Engineering Research and Design 80 (2002) 183-189.

[151] L.C. Almeida, O. González, O. Sanz, A. Paul, M.A. Centeno, J.A. Odriozola, M. Montes, M.S.a.E.F.S.-A. Fábio Bellot Noronha, Studies in Surface Science and Catalysis, Elsevier, 2007, pp. 79-84.

[152] A. Cybulski, J.A. Moulijn, Catalysis Reviews 36 (1994) 179-270.

[153] R.M. Heck, S. Gulati, R.J. Farrauto, Chemical Engineering Journal 82 (2001) 149-156.

[154] A. Cybulski, J.A. Moulijn, Chemical Engineering Science 49 (1994) 19-27.

[155] M.F.R. B.J. Tatarchuk, A. Krishnagopalan, US Patent 5102745, Auburn University, USA, 1992.

[156] D.K. Harris, D.R. Cahela, B.J. Tatarchuk, Composites Part A: Applied Science and Manufacturing 32 (2001) 1117-1126.

[157] H. Yang, Y. Lu, B.J. Tatarchuk, Journal of Power Sources 174 (2007) 302-311.

[158] M.W. Meffert, Preparation and Characterization of Sintered Metal Microfiber-based Composite Materials for Heterogeneous Catalyst Applications, Chemical Engineering, Auburn University, Auburn, 1998, p. 220.

[159] T.C. Ho, B.S. White, Chemical Engineering Science 46 (1991) 1861-1863.

[160] B.D. Kulkarni, L.K. Doraiswamy, Catalysis Reviews 22 (1980) 431-483.

[161] M. Sheng, H. Yang, D.R. Cahela, B.J. Tatarchuk, Journal of Catalysis 281 (2011) 254-262.

[162] M. Sheng, H. Yang, D.R. Cahela, B.J. Tatarchuk, Journal of Catalysis 281 254-262.

[163] W.J. Mantle, W.S. Chang, Effective thermal conductivity of sintered metal fibers [for heat pipes], Energy Conversion Engineering Conference, 1989. IECEC-89., Proceedings of the 24th Intersociety, 1989, pp. 1871-1877 vol.1874.